INFORMATION TO USERS

This manuscript has been reproduced from the microfilm master. UMI films the text directly from the original or copy submitted. Thus, some thesis and dissertation copies are in typewriter face, while others may be from any type of computer printer.

The quality of this reproduction is dependent upon the quality of the copy submitted. Broken or indistinct print, colored or poor quality illustrations and photographs, print bleedthrough, substandard margins, and improper alignment can adversely affect reproduction.

In the unlikely event that the author did not send UMI a complete manuscript and there are missing pages, these will be noted. Also, if unauthorized copyright material had to be removed, a note will indicate the deletion.

Oversize materials (e.g., maps, drawings, charts) are reproduced by sectioning the original, beginning at the upper left-hand corner and continuing from left to right in equal sections with small overlaps.

ProQuest Information and Learning
300 North Zeeb Road, Ann Arbor, MI 48106-1346 USA
800-521-0600

PARTITIONING THE ELECTRON NUMBER, PAIR AND TRANSITION DENSITIES OF SILANES: AN ATOMS IN MOLECULES STUDY OF THE PROPERTIES OF SILICON COMPOUNDS

By

F. DAVID BAYLES, B.Sc.

A Thesis

Submitted to the School of Graduate Studies

in Partial Fulfillment of the Requirements

for the Degree

Doctor of Philosophy

McMaster University

PARTITIONING THE ELECTRON, PAIR AND TRANSITION DENSITIES OF SILANES

DOCTOR OF PHILOSOPHY (2000)
(Chemistry)

McMaster University
Hamilton, Ontario

TITLE: Partitioning the Electron Number, Pair and Transition Densities of Silanes: An Atoms in Molecules Study of the Properties of Silicon Compounds

AUTHOR: David Bayles, B.Sc. (McMaster University)

SUPERVISOR: Professor R. F. W. Bader

NUMBER OF PAGES: xxi, 280

Acknowledgements

I would like to thank the following people for their invaluable assistance:

- My family, who gave me life and the desire to learn all that I can.
- Dr. Richard Bader, supervisor, mentor and friend, without whom my life and career would not be progressing the way it is.
- Dr. George Heard, who provided invaluable assistance in developing the transition density software, and was incredibly patient with me during those critical development stages.
- Dr. Jesus Trujillo, who acted as a sounding board for ideas and problems, and added much to the atmosphere of the lab.
- Dr. Michael Brook and Dr. Ronald Childs, my Ph.D. committee, for pushing me in the right directions, and making sure my thesis was all it could be.
- Maggie Austen, Fernando Martin and Cherif Matta, who engaged me in numerous discussions on theory, and provided much needed support.
- McMaster University Chemistry Department, for taking me on despite my faults, and giving my future a head start.
- NSERC and OGS, for providing the much-needed funding to keep body and soul together.

ABSTRACT

The field of silicon chemistry has proven to be an ever-expanding subject of interest in both the academic and industrial fields. A large portion of this work involves computational and theoretical studies of electronic structure. These studies use Molecular Orbital theory to obtain results which closely correspond with experiment. It is not enough, however, to know the properties of the molecule as a whole, frequently, important insights can be gained by understanding the contribution of an atom in that molecule to those total properties. While invaluable for computing the properties of an entire molecule, molecular orbitals contain no information about individual atoms, requiring the development of arbitrary mathematical treatments that partition the molecular orbitals according to their basis function expansions. The theory of Atoms in Molecules removes the need for arbitrary models by partitioning the molecular properties on the basis of the topology of the electron density, a method based on established quantum mechanical principles.

This work began with a detailed analysis of the bonding and atomic properties of simple compounds containing silicon, with the analogous carbon compounds used as a comparison. This initial study illustrated why silicon species react the way they do, and how the electronic differences between silicon and carbon species result in differences in chemical properties. This work also studied the localization of electron density in silicon compounds using the pair density to further illustrate the nature of silicon's electronic structure. The focus of the study then shifted to oligosilanes, known to undergo strong electronic excitations that experience a bathochromic shift with increased chain length. Attempts to determine the nature of this so-called σ-conjugation made use of the electron and pair density properties, and finally the transition density, which allows one to partition the probability of excitation into its atomic contributions.

TABLE OF CONTENTS

LIST OF FIGURES

LIST OF TABLES

1 Introduction

Much research work, both experimental and theoretical, has been devoted to the study and understanding of silicon and its chemistry. The majority of theoretical research in this field employs sophisticated models and computational techniques, all based on molecular orbital theory. The calculations performed to obtain molecular properties usually correspond closely with experimental results, helping theoretical researchers better understand the mechanistic aspects of silane reactions. Frequently, however, valuable information can be obtained not only from the properties of a molecule in its entirety, but also from the properties of an atom within that molecule. This information helps the researcher better understand the specific role an atom, i.e. silicon, plays in that molecule's chemistry. The concept of studying a molecule's properties based on the properties of an individual atom or group within that molecule is one of the cornerstones of chemistry. The methods used to obtain the properties of a part of a molecule are many and varied, and often give conflicting results. The reason for this is because they are based on methods that apply arbitrary conditions to the partitioning of the molecular wavefunction. When such arbitrary methods are used, researchers have no way to test the validity of the results obtained. This thesis will provide new insights into the chemistry of silicon by looking at the chemistry of silicon from a different perspective, namely that of the theory of Atoms in Molecules. This approach enables one to partition a molecular property into its atomic contributions in a non-arbitrary manner, based on the physics of an open system. These principles can then be used by researchers to interpret observed chemical behavior based on the individual atomic contributions. In this thesis, the molecular properties of various silane species will be studied, specifically those properties related to the electron number density, such as charge and energy, and delocalization, a property related to the pair density. In addition, a new property will be examined: the transition probability, and its partitioning in oligosilanes, which will provide a more concrete understanding of the novel spectroscopic properties of these compounds. The above properties will be compared to those of the equivalent carbon-based compounds, to provide a clearer understanding of

the differences between carbon and silicon, and also to results obtained from Molecular Orbital, (MO), studies, to provide contrast between the two techniques.

1.1 Bonding Properties of Silicon and Carbon

1.1.1 Geometries and Bonding

The most obvious difference between carbon and silicon compounds is in geometry. Being a 3rd-row element, silicon is about 50% larger than carbon[1]; this has a dramatic effect on the structures of relative species[2]. Overall, the Si-X bond is much longer than the C-X bond, sometimes by as much as 0.4 Å, (the references to the data in Table 1 are given in parathenses).

Table 1: Experimental Bond Lengths (in angstroms) of H_3M-X

Atom X	M = C	M = Si	Δr
H	1.0919 (3)	1.474 (4)	0.382
CH_3	1.534 (5a)	1.885 (6a)	0.351
NH_2	1.474 (7)	1.706 (6a)	0.232
OH	1.414 (8)	1.626 (4)	0.212
F	1.383 (9)	1.594 (10)	0.211
PH_2	1.863 (11)	2.249 (12)	0.386
SH	1.819 (13)	2.136 (14)	0.317
Cl	1.781 (15)	2.048 (10)	0.267

A more striking difference lies in those compounds where silicon is bonded to nitrogen, oxygen or fluorine. In all three cases, the bonds formed between silicon and these elements are shorter than that predicted by covalent radii, indicating some fundamental difference in the bonding, as compared to the straightforward single bonds formed with carbon. These species also exhibit other unusual structural characteristics. Unlike the carbon-based species, where the bonded nitrogen has the pyramidal structure expected by VSEPR theory, the nitrogen in a silylamine is nearly planar[16]. Other experimental work confirms this near planarity, showing the nitrogen lone pair to be far less donating than a carbamine[17], more in keeping with an sp^2-like structure. For oxygen, a classic example of unusual geometry is silicone, a polymer with alternating silicon and oxygen atoms making up the backbone: the Si-O-Si bond angle of these species averages 145°[18]. This angle is much larger than that of a carbon ether bond angle (about 115°), again indicating something other than a classic VSEPR structure. Silyl fluorides also show unusual behavior, exhibiting strong intermolecular interactions not seen in carbon-based fluorides[19].

The bond formed between silicon and a given element X shows significant differences from the bond between carbon and the same element X, other than length. As silicon has an electronegativity of 1.8, as opposed to 2.5 for carbon, most elements that bond to silicon are considerably more electronegative. When this is combined with silicon's greater size and the more diffuse and loosely held valence electron density, most silicon-element bonds are strongly polarized, with the negative end of the dipole on the bonded atom[20].

For double bonds the pattern of length as a function of electronegativity changes somewhat. Examples of simple Si-X double-bonded species are impossible to synthesize and isolate, because of their extreme reactivity. They can only be isolated if the substituent groups are bulky, effectively blocking out potential reactants. Most calculations to date show a well-defined decrease in bond length in the C-X double bond as X becomes more electronegative, but this trend is not seen in the Si-X double bond[21]. Comparison of the C-C double bond with the C-N and C-O double bonds shows a surprisingly constant decrease in bond length[22], as does the C-Si double bond with the C-P and C-S double bonds. This pattern is not seen when silicon is substituted for carbon. The decrease of the bond length is much larger on a whole, and is larger for Si=C versus Si=N, and Si=P versus Si=S than for Si=N versus Si=O and Si=Si versus Si=P. This result implies that for the 2nd-row elements, a dramatic change in the bond density occurs from Si=C to Si=N, such as a possible change in the bond density structure. This change, having already occurred for the more electronegative nitrogen, will not cause another significant change for Si=O. This fundamental change in the bonding structure occurs in the 3rd-row elements as well, only it is the transition from phosphorus to sulphur that causes this change.

1.1.2 Co-ordination

In terms of the structures formed by silicon compounds, one finds that the co-ordination states formed have little in common with carbon. Carbon can easily form multiple bonds in low co-ordination states, and is rarely found in a state of co-ordination higher than four. The opposite is true for silicon; much of the research in the synthesis of silicon species involves creating inherently unstable and reactive low co-ordinate species, while co-ordination states of four and higher can be quite stable. These high co-ordinate states themselves exhibit interesting chemistry.

In general, extraco-ordinate silicon species are formed most easily when the ligands being added are electronegative, such as with fluorides or alkoxy groups[23] (Figure 1).

Figure 1: Pentafluorosilicate Anion

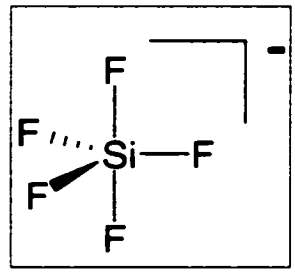

Extraco-ordinate silicon has a tendency to be more reactive when subjected to nucleophilic attack than the equivalent tetraco-ordinate silane. For example, the rate of formation of a hexaco-ordinate species from pentaco-ordinate is faster than that of the formation of the pentaco-ordinate species itself. Further, the ligands attached to an extraco-ordinate silane are themselves more nucleophilic, reacting with other species more quickly than if they were attached to tetraco-ordinate silanes. Extraco-ordination can often be an important consideration when nucleophilic substitution occurs[24]. When a nucleophilic attack occurs with retention of the stereochemistry, the nucleophile can attack from a variety of directions. The key to the reaction, however, is that the leaving group be in the apical position, which results in a longer, weaker bond, facilitating the loss of that leaving group. If the nucleophile attacks in such a way as to place the leaving group in the equatorial position, pseudorotation usually occurs to place the leaving group in the best possible position for leaving. Pseudorotation shows that the ligands are much more labile than in a tetraco-ordinate species; this is supported by the fact that extraco-ordination usually occurs when the ligands are electronegative, implying bonds with higher ionic character.

1.1.3 Bond Energy

Much work has been done to quantify the bond energies of silyl species, experimentally and theoretically[3]. The overall trend when looking at the energies of C-X and Si-X bonds, where X are various increasingly electronegative elements, is as follows: as the element X increases in electronegativity, the Si-X bond energy increases steadily and at a much faster rate than the C-X bond energy. The higher strengths of longer Si-X bonds, compared to equivalent C-X bonds, are the subject of considerable speculation. A

variety of theories have been postulated, from the unexpected shortness of the Si-X bond with elements N, O, and F, to the idea that it is the C-X bonds that are unusual. This latter reasoning suggests that the smaller bond lengths compared to Si-X actually weaken the C-X bond, possibly through some kind of repulsion[25], (Table 2, references in parathenses).

Table 2: Bond Energies (kcal/mol) for C-X and Si-X Bonds

Atom X	C-X	Si-X	ΔE
H	92 (26)	90.3 (27)	-1.7
C	90.4 (27)	82.1 (27)	-8.3
N	84.9 (27)	98.7 (3)	13.8
O	92.3 (27)	128.0 (28)	35.7
F	109.9 (27)	135.0 (28)	25.1
Si	82.1	80.5 (29)	-1.6
P	63.0 (30)	88.3 (31)	25.3
S	74.0 (27)	70.0 (32)	-4.0
Cl	80.0 (33)	113.0 (28)	33.0

These bond energies are strongly affected by other substituents attached to the central atom. Methyl groups will weaken a C-H bond, but have no real effect on an Si-H bond. This weakening effect is instead seen when silyl groups are added to the silicon.

The greater length and high degree of polarity of the Si-X double bond makes it considerably weaker than the C-X double bond. For example, calculations gauge the C-C π-bond to be 105 kcal/mol more stable than the Si-Si π-bond[34]: this is supported by emission spectra experiments[35]. Another measure of π-bond strength is bond rotation energy, which requires the breaking of the π-bond to succeed. Ethylene has had its rotational barrier measured at 65 kcal/mol[36]: the C-Si double bond has been measured at 40 kcal/mol, and the Si-Si double bond at about 25 kcal/mol[37]. Overall, the Si-X double bond energy is much lower than the C-X double bond energy, from about 60 kcal/mol lower in the case of X being carbon, to 33 kcal/mol lower when X is oxygen[34]. This intriguing downward trend in energy difference is likely because of increased polarity of the carbon double bond. Polar double bonds tend to be more reactive, as the π-bond is also polarized. The additional build-up of electron density at the more electronegative end of the bond makes the π-bond much more attractive to electrophilic attack.

1.2 Chemical Reactivity

With the unusual bonding properties of silyl species come novel reactions that they can undergo. The differences between silicon- and carbon-based species becomes very apparent, as the silicon and carbon based analogues of similar molecules undergo very different reactions.

The most common reaction seen in silicon chemistry is that of substitution. Such reactions will have very different results when carbon is substituted for silicon. One example is the C-H and Si-H bonds. The C-H bond is relatively unreactive, since the electronegativities of hydrogen and carbon are very similar. Breaking the C-H bond usually requires relatively strong reagents, such as halogens or very strong bases. The Si-H bond, on the other hand, is considerably more polar and thus more reactive. A variety of reagents are capable of breaking the Si-H bond, including:

- halogens; no light is required to activate this process,
- hydroiodic acid, which creates a silyl iodide,
- strong bases, which in the case of alkyllithium, for example, usually create the corresponding alkyl silanes rather than cause deprotonation,

With these Si-H cleavage reactions, a clear pattern emerges. While the C-H bond reacts in a variety of different ways, depending on the reagent used, the Si-H bond usually undergoes S_N2 nucleophilic substitution, even with relatively weak nucleophiles. This provides further evidence for the strong polarity of the Si-H bond. This makes sense, given the fact that the hydrogen in Si-H can act as a reducing agent, via a hydride.

When looking at the Si-Cl and C-Cl bonds, one sees far more similarity, both in the reactions that can cleave these bonds, and their reaction mechanisms. For most reagents, both the Si-Cl and C-Cl bonds undergo nucleophilic substitution. The most notable difference between these two sets of substitution reactions is their relative speed and vigor. Water will react with the C-Cl bond, creating an alcohol, but this reaction is very slow. Chlorosilanes are another matter entirely; great care must be taken when adding water to chlorosilanes, as this reaction can be explosive if the water is not added slowly. In general, nucleophiles react with the Si-Cl bond much faster than the C-Cl bond, reflecting the higher polarity of the Si-Cl bond, as well as its greater lability.

Nucleophilic substitution of silanes has itself been the subject of considerable study. The reason for this is the fact that unlike the classic S_N2 reaction with carbon-centered species, there is the possibility that when a silane undergoes nucleophilic substitution, a reactive hyperco-ordinate intermediate will form rather than a transition state[24]. This makes sense, considering that silicon proves quite stable as an extraco-ordinate species, unlike carbon. In addition, the stereochemistry of nucleophilic substitution of silanes is not nearly as straightforward as it is with carbon. With carbon, the substitution reaction usually results in an inversion of the stereocenter. Silanes, however, exhibit considerably different behavior. Depending on the leaving group involved, one can often get either inversion or retention of the stereocenter, and in many cases, racemization. In general, the trend seen in these reactions tends to be the following; the more easily displaceable the leaving group is, the more likely the reaction will proceed with inversion, while strongly bound leaving groups will be substituted with retention[38]. The reason for this is believed to involve the counterion that accompanies the nucleophile in the reaction. Strongly bound leaving groups will usually be assisted by this counterion, which binds to the already partially polarized leaving group, stabilizing it as it leaves[39]. If this counterion is also tightly bound to its nucleophile, an interesting structure develops[40] (Figure 2).

Figure 2: Silyl Nucleophilic Substitution with Retention

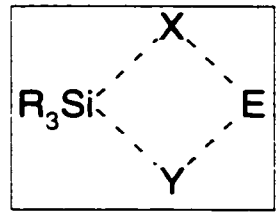

When R_3SiX is attacked by some species EY, a four-membered ring can form while X is substituted for Y, forcing retention of stereochemistry. Such a reaction does not usually happen with R_3CX, as the only easily accessible face of attack on this molecule is opposite the leaving group X. The conditions that can effect this structure are many. As one example, the solvent can have a major effect on forcing or disrupting this structure, depending on the solvent's polarity. If the solvent is very polar, and binds the counterion E, then the counterion cannot participate in the reaction, and substitution proceeds with inversion, with the solvent itself assisting the leaving group. The other ligands attached to silicon can also control the

stereochemistry, a classic example of this being silacyclobutanes[41]. These compounds usually undergo substitution with retention, because the four-membered ring effectively blocks any attack from the back of the silane, and makes inversion of the stereocenter difficult. As this ring is expanded to five and six members, the reaction occurs with racemization, as the possibility for inversion becomes greater.

1.2.1 Polysilanes and Photochemistry

There are a large number of other fascinating chemical properties exhibited by silicon-based compounds, far more than can be discussed in this thesis. One of the most intriguing class of silanes, from a chemical perspective, is polysilane, a long chain saturated polymer with a backbone consisting solely of silicon atoms, with a geometric structure similar to that of an equivalent hydrocarbon. At first glance, it would suggest that because silicon is of the same periodic group as carbon, the chemistry of polysilanes and hydrocarbons would be similar, but such is not the case. There are numerous differences between these two classes of molecules, the first being reactivity. Polysilanes are highly reactive, undergoing a variety of chemical changes even under mild conditions[42]. It is common practice, in fact, to place large, bulky substituents on the polysilane backbone, in order to reduce that reactivity. For example, the base polysilane, Si_nH_{2n+2}, has only been successfully synthesized and purified up to n = 5, and must be handled with extreme care[43]. Hydrocarbons, by contrast, are relatively unreactive, and can only be altered with strong reagents, regardless of molecular weight. The second and more important difference is in the photochemistry of these species. Hydrocarbons are by nature unreactive to light; any long-chain hydrocarbon will only undergo electronic excitation in the deep UV region, and the wavelength of excitation varies only slightly with chain length. Polysilanes, on the other hand, are very reactive to UV and visible light[44]. As the number of silicon atoms increases in the polysilane backbone, one observes a steady decrease in absorption wavelength, (known as a bathochromic shift)[45], even to the point of long-chain polysilanes being colored[46]. These photolytic properties put polysilanes in high demand in the microchip manufacturing industry[47]. When a polysilane is exposed to strong light, it has a tendency to rapidly break down, making it valuable as a photoresist; a layer of polysilane is first placed over some substrate, then exposed to UV light through a pattern. Those areas of the polysilane layer that are exposed break down, leaving the substrate exposed to etching, usually by a superacid[48]. Considerable study has been devoted to

the products of polysilane photoreactions[49,50], with the principle reactions being: silylene extrusion[46], homolytic backbone scission to produce radicals[46], and a 1,1-reductive elimination that produces a radical plus a shorter chain length polysilane[51]. The most common mechanism observed is the first, that of silylene extrusion. This reaction has been extensively studied, using trisilanes as models[52,53].

While a great deal is understood about the photochemistry of polysilanes, the reason why these species should be so reactive to light while hydrocarbons are not is not as obvious. Clearly, the electronic structure of these species is considerably different from that of hydrocarbons; the fact that the valence density is so much more diffuse than that of carbon may explain this difference. Most research looks at the backbone of polysilanes, citing a form of delocalization known as σ-conjugation as a possible explanation. While experimentation speculates on the nature of this phenomenon, it is the theoretician that must derive the mechanism to explain the behavior, usually in terms of a model.

1.3 Delocalization in Silicon and Carbon

The idea of delocalization of electronic charge is one that has been used to explain a variety of observations in chemistry. Electron delocalization is usually invoked to explain electronic excitation[54]. When observing the UV spectra of conjugated species, the absorption bands are invariably at longer wavelengths than found in the corresponding unconjugated systems, and the intensity of the absorption is also much stronger. The chemical reactivity of conjugated species also changes substantially. A conjugated alkene is much more reactive to nucleophilic substitution than an unconjugated alkene, indicating a fundamental change in the molecular properties. Even substituent effects change when conjugated systems are involved. In general, substituent effects on the molecular properties are stronger and have a much longer range of effect than a molecule that contains conjugation[55]. Clearly these systems do not behave as a series of isolated bonds, as some form of 'coupling' is occurring: the electron density of these bonds communicate any perturbation they experience to the rest of the molecule. Understanding why this happens is the task of the theoretical chemist, who applies various models of electronic behavior to hopefully describe and reproduce the effects observed.

1.3.1 Delocalization in Conjugated Carbon Species

The most commonly observed examples of electron delocalization are those that are seen in molecules containing conjugated C-C double bonds. These alternating single and double bonds consist of σ-bonds between sp^2 hybridized atoms which make up the framework of the molecule, plus π-bonds which use the remaining p-orbitals. It is the interaction of these π-bonds with each other that result in the conjugation. Numerous models have been developed to better understand the electronic structure of conjugated species.

Most models of electronic structure are based on MO theory. The reason that such a method is employed is quite simple, when one considers the Hamiltonian used for the electronic structure of molecules:

$$\hat{H} = \left(-\hbar^2/2m\right) \sum_i \nabla_i^2 - e^2 \sum_v \sum_i \frac{Z_v}{r_{vi}} + e^2 \sum_i \sum_{<j} \frac{1}{r_{ij}} \qquad (1)$$

The first and second sums represent the kinetic energy of each electron and the Coulombic attraction between each electron and each nucleus respectively, which are one-electron terms. The final sum, however, represents the electron-electron repulsions. This is a two-electron term, which makes the Schrödinger wave equation very difficult to solve for many-electron systems. In order to simplify the calculation, approximations to the Hamiltonian operator can be introduced. The easiest approach is to ignore the final sum, effectively eliminating electron-electron interactions from the system and transforming the total equation into a set of one-electron problems. This reduces the complexity of the calculation and results in the total wavefunction being expressed as a product of one-electron wavefunctions, and the energy as a sum of one-electron energies:

$$\begin{aligned} &\textit{if} \quad \hat{H} = \sum_i \hat{h}_i \\ &\textit{then} \quad \Psi = \prod_i \psi_i(i) \quad \textit{and} \quad E = \sum_i \varepsilon_i \\ &\textit{with each} \quad \psi_i(i) \quad \textit{satisfying} \quad \hat{h}_i \psi_i = \varepsilon_i \psi_i \end{aligned} \qquad (2)$$

These one-electron wavefunctions are known as orbitals, and give MO theory its name, each MO being expressed in terms of a set of atomic centered basis functions[56]. The application of this model of electronic

structure to conjugated hydrocarbons leads to Hückel theory, developed in 1931, wherein each ψ_i is expressed in terms of a Linear Combination of p π-like Atomic Orbitals, (LCAO)[57]. The σ-bond electrons are treated as an average field, and are not explicitly calculated. When these approximations are made, the Hamiltonian operator which acts on the wavefunction can be treated as a sum of 'effective' Hamiltonian operators, which do not contain any electron-electron interaction other than the average effect of the σ-bond electrons.

$$\hat{H} = -\frac{\hbar^2}{2m}\sum_i \nabla_i^2 + V \cong -\frac{\hbar^2}{2m}\sum_i \nabla_i^2 + \sum_i v(i) = \sum_i \hat{H}_{eff}(i) \tag{3}$$

This approach also excludes any electron-electron repulsion or correlation between the π-bond electrons being considered. An effective Hamiltonian can operate on an orbital, yielding the energy of that orbital.

$$\hat{H}_{eff}\psi_i = \varepsilon_i\psi_i \tag{4}$$

The energy of the molecule is thus the sum of the calculated energies of the occupied orbitals. The next question then becomes how to describe these one-electron orbitals. The LCAO model expresses each molecular orbital as a linear combination of all the p-orbitals in the molecule,

$$\psi_i = \sum_r c_{ir}\varphi_r \tag{5}$$

where φ_r represents the p-orbital centered on each atom r in the molecule, and c_{ir} the linear coefficients of all r p-orbitals that represent molecular orbital i. The coefficients are determined through the variation method, so as to give the optimal orbital energies. When this method is applied, it results in a series of secular equations, which must then be solved. A common practice is to simplify these equations by assuming certain constants:

$$\begin{aligned}
&\alpha = \int \varphi_r^* \; H_{eff} \; \varphi_r \; d\tau \\
&\beta = \int \varphi_r^* \; H_{eff} \; \varphi_s \; d\tau \quad \textit{when atoms r and s are bonded.} \\
&\beta = 0 \quad \textit{when atoms r and s are not bonded.} \\
&S_{rs} = \int \varphi_r \varphi_s \; d\tau = \delta_{rs}
\end{aligned} \tag{6}$$

The α term, known as the Coulomb integral, is considered constant for every atom in the molecule, and represents the effective energy of an electron bound to the p-orbital centered on atom *r*. The β term is also constant, and is known as a resonance integral[58]. It is only invoked when basis functions *r* and *s* are centered on bonded atoms, and is otherwise considered to be zero. Because these p-orbitals are usually normalized, the overlap integral S_{rs} equals one when *r* equals *s*, and is otherwise zero. Based on these assumptions, the secular equations can be represented as a secular determinant.

$$\begin{array}{c|ccccc} & c_1 & c_2 & c_3 & \cdots & c_N \\ \text{atom } 1 & \alpha - E_1 & \beta & 0 & \cdots & 0 \\ \text{atom } 2 & \beta & \alpha - E_2 & \beta & \cdots & 0 \\ \text{atom } 3 & 0 & \beta & \alpha - E_3 & \cdots & 0 \\ \cdots & \cdots & \cdots & \cdots & \cdots & \cdots \\ \text{atom } N & 0 & 0 & 0 & \cdots & \alpha - E_N \end{array} = 0 \qquad (7)$$

The determinants are first solved for the roots E_i to determine the energy of each orbital, followed by the coefficients c_i by including in the secular equations a normalization condition, in which the sum of the squares of all the coefficients must equal unity. The total energy of the molecule simply becomes the sum of each orbital energy E_i times the number of electrons occupying orbital *i*. Such a molecular system is considered delocalized because each orbital contains basis functions that span the entire molecule. By solving for the coefficients, one obtains expressions of the molecular orbitals themselves. The magnitudes of these coefficients can provide insight into the degree of interaction between the basis functions: the larger the value, the greater the interaction between a given set of basis functions within an orbital. These coefficients can also provide other information about the molecule, such as charge and bond order. Integrating the terms of orbital *i* over all the atomic centers *r* yields the equation

$$\int \psi_i^* \psi_i \; d\tau = c_{ir} c_{ir} \int \varphi_r^* \varphi_r d\tau = \sum_r |c_{ir}|^2 = 1 \qquad (8)$$

where the product $|c_{ir}|^2$ is the partial electron density of the p-orbital centred on atom *r* due to one electron in the *i*th molecular orbital, (assuming all coefficients are real, and there is no overlap with other atomic orbitals). The total electron population of atom *r* can thus be expressed as

$$q_r = \sum_i v_i \left| c_{ir} \right|^2 \tag{9}$$

where v_i is the occupation number of each orbital i. The bond order between two atoms r and s can be expressed in a similar fashion[59].

$$p_{rs} = \sum_i v_i \; c_{ir} c_{is} \tag{10}$$

It must be noted again that all σ-bonds and their electrons are ignored in these calculations. Thus the 'charge' is only the number of π-electrons associated with a given sp^2-hybridized atom in the molecule, and the 'bond order' will range from zero for a singly-bonded species, (no π-bond character), to one for a true double bond such as that found in ethylene, for example.

1.3.2 Beyond the Hückel Model

Clearly the Hückel model is limited in that far too many assumptions must be made, and the values obtained will be inaccurate when compared to experiment. With the increasing computational power available, far fewer approximations need be made, and all-electron calculations are now routine. What is required for these all-electron calculations is a method to account for the electron-electron repulsion, which will provide a more accurate description of the wavefunction. The first factor to be considered is the electron-electron repulsion term, which is ignored in the Hückel model. To correct for this, the following concept was proposed by Hartree. Instead of trying to calculate all the electron-electron interactions at once, treat each electron individually by subjecting it to the average field of all the other electrons. However, this does not take into account electron spin as required by the Pauli exclusion principle, even if one limits the orbital occupation to two electrons. The means of including spin was developed by Fock, who proposed the following. Rather than have a simple product of orbitals, the wavefunction is expressed instead as an antisymmetrized sum of products of spin orbitals, that is, a Slater determinant of spin orbitals. This corrects for the electron correlation due to the Pauli principle, which states that a many-electron wavefunction must be antisymmetric with respect to the interchange of space and spin co-ordinates for every pair of electrons. Expressing the wave function as a Slater determinant and incorporating the average field approximation for the treatment of electron-electron repulsion results in the so-called Hartree-Fock

approximation. When the complete Hamiltonian as given in Equation 1.1 is averaged over a Slater determinant of spin orbitals and the energy is minimized with respect to a variation of the individual orbitals, one obtains the Hartree-Fock equation for each of the spin orbitals. This equation is again expressible in the form of an effective Hamiltonian acting on an individual orbital ψ_i:

$$\hat{H}_{eff}(1)\psi_i(1) = \varepsilon_i\psi_i(1) \tag{11}$$

where (1) denotes the coordinates of electron 1. For a closed-shell molecule, $\hat{H}_{eff}(1)$ for all ψ_i is given by

$$\hat{H}_{eff}(1) = -\tfrac{1}{2}\nabla_1^2 - \sum_{\alpha}\frac{Z_\alpha}{r_{1\alpha}} + \sum_{j=1}^{N}\left[2\hat{J}_j(1) - \hat{K}_j(1)\right] \tag{12}$$

where the Coulomb operator $\hat{J}_i$ and the exchange operator $\hat{K}_i$ are given by

$$\begin{aligned}\hat{J}_j(1)\psi_i(1) &= \psi_i(1)\int|\psi_j(2)|^2\frac{1}{r_{12}}d\tau_2 \\ \hat{K}_j(1)\psi_i(1) &= \psi_j(1)\int\frac{\psi_j^*(2)\psi_i(2)}{r_{12}}d\tau_2\end{aligned} \tag{13}$$

One notes that the determination of the orbital $\psi_i(1)$ requires a knowledge of the remaining orbitals through the Coulomb and exchange operators. This is accomplished through the Self-Consistent Field method. A starting set of orbitals is chosen and the equations solved for this set. The orbitals obtained by this procedure will, in general, differ from the set used to generate them and this new set is used to generate another set of orbitals for the next iteration. This procedure is continued until the set of orbitals generated in a given iteration is identical to the set used to obtain them – that is, the field used to generate the orbitals is identical to the field they predict, thus yielding a self-consistent set of orbitals. Hence the method is known as the Self-Consistent Field, (SCF), method.

The Hartree-Fock equations are too difficult to solve analytically except for the case of an atom. To obtain solutions for a molecular system one uses the method of Roothaan[40], wherein each ψ_i is expanded in terms of a set of basis functions, usually composed of atomic centered Slater or Gaussian type functions f_j:

$$\psi_i = \sum_j c_{ij} f_{ij} \tag{14}$$

If the expansion in Equation (1.14) was infinite, or complete, one would obtain the exact solutions to the Hartree-Fock equations. However, the use of a finite size basis set yields only approximations to the true orbitals, the quality of the approximation increasing with the size of the basis set.

The Hartree-Fock method is the principle method used to obtain the wavefunctions, energies and densities discussed in this thesis. It is also the method that is used as the starting point in cases where it is necessary to go beyond this approximation to obtain a better description of the correlation between the motions of electrons. The so-called Configuration Interaction Singles, (CIS), method described in Chapter 3 of this thesis is an example of such a case.

1.3.3 Delocalization in Polysilanes

From the chemical observations mentioned earlier, one could say that polysilanes, though structurally similar to saturated hydrocarbons, have more in common with polyenes. It is these photolytic properties that are by far the most interesting, especially to theoreticians. The idea of a saturated system having the capacity for electronic delocalization has led to the development of many models that try to explain and predict this behavior[61,62]. The following are the most widely accepted models in use to describe σ-conjugation.

The simplest model that can explain σ-conjugation requires a return to the simple Hückel model, (Figure 3), as applied to π-conjugated polyenes[63]. This same model can be applied to a saturated system as well, providing similar Coulomb and resonance integrals, through a redefinition of the integral terms.

Figure 3: Hückel Model for σ-conjugation

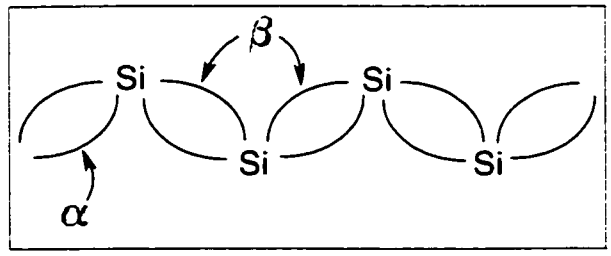

In this case, the α term represents the energy of an electron bound to one Si-Si bond. The β term represents the interaction between a pair of adjacent Si-Si bonds. When applied to a secular determinant, the orbital energies for a system containing *n* silicon atoms can be described by Equation (1.15).[64]

$$E_j = \alpha + 2\beta \cos\left(\pi j/n\right) \qquad j = 1, 2, \cdots n-1 \tag{15}$$

where j orbitals are produced and the orbital energies are symmetric about α. The β term controls the size of the gaps between orbital energies, and is an indication of the quality of bond interaction. The larger β is, the poorer the interaction is, and the larger the orbital transition energies become. With higher values of n, the transition energy between orbitals decreases, as is expected of a system containing increased conjugation. Unfortunately, as simple and intuitive as this model is, it correlates very poorly with experiment. A far more sophisticated model can be found through the work of Sandorfy[95]. These systems, known as the Sandorfy 'C' and Sandorfy 'H' models, use a different approach in describing the energy terms of a molecular system. Rather than breaking down the molecular orbitals into bond contributions, they are broken down into hybridized atomic orbitals. Each silicon has four sp^3 hybridized orbitals associated with it, and these are the basis of a linear combination system (Figure 4).

Figure 4: Sandorfy Model for σ-conjugation

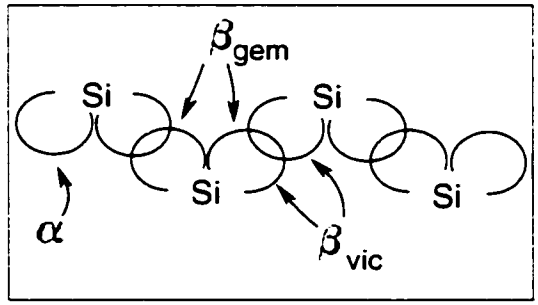

When considering only those sp^3 orbitals involved in the backbone, (Sandorfy model 'C'), one uses the same secular determinant system as is used for π-conjugated systems. The α term describes the energy of each sp^3 orbital, and the β term describes the interaction energy between sp^3 orbitals. In this case, as seen above, there are now two kinds of interactions: the expected interaction between sp^3 orbitals on adjacent silicons, (the vicinal overlap), and the interaction between sp^3 orbitals on the same silicon, (the geminal overlap). While the α term is assumed to be constant for all the silicons, one ends up with two β terms, β_{vic} for the vicinal overlap, and β_{gem} for the geminal overlap. A great deal of work has been done using this

model, and most researchers have concurred about the values of α, β_{vic}, and β_{gem} for a variety of molecular systems, based on experimental ionization potentials and transition energies to obtain the best possible fit for these terms. An added bonus to using this method is the alternative data one can obtain. For example, the ratio β_{gem}/β_{vic} is often used to describe the extent of delocalization in the system under study. A value of zero for this ratio means that the bonds in the polysilane are completely localized, i.e. there is no interaction between the geminal sp^3 orbitals. A value of one means perfect delocalization, with the interaction between geminal sp^3 orbitals on the same silicon being of the same magnitude as the interaction between the sp^3 orbitals between the silicons that form the Si-Si bonds. Accepted values for Si_nH_{2n+2} systems are: α = -8.6 eV, β_{vic} = -1.9 eV, and β_{gem} = -1.67 eV, with β_{gem}/β_{vic} = 0.87. These values take the effect of the hydrogen into account implicitly, which means, however, that this model will not work with polysilanes bearing other ligands. A more sophisticated model, (Sandorfy model 'H'), is then required. All four sp^3 orbitals associated with each silicon are employed in this case, as are the orbitals involved in the silicon-substituent bond. This results in two α values. One also generates two sets of β_{vic} values, one for the Si-Si interaction, and one for the Si-ligand interaction, as well as two β_{gem} terms. One β_{gem} term is for the two sp^3 orbitals on the one silicon involved in the backbone, while the other is for the two sp^3 orbitals involved with the two substituents bonded to the same silicon, (a β_{gem} term for the sp3-ligand/sp3-backbone interaction is usually ignored). Michl describes the effects of using this model in polysilanes very thoroughly in several articles[50,66]. In terms of the orbital energies, the inclusion of substituent terms has the following effect: the occupied orbitals are brought closer together in energy, while the unoccupied orbital energy differences widen. The Highest Occupied Molecular Orbital, (HOMO), energy remains about the same when this happens, and the lower energy orbitals are increasingly stabilized relative to it. The energy of the highest unoccupied orbital also remains about the same, and all the unoccupied orbitals below that are stabilized relative to it. This means that while the HOMO energy remains largely unchanged, the Lowest Unoccupied Molecular Orbital, (LUMO), drops in energy considerably. This is an important consideration, as it has been shown experimentally that the substituent has a marked electronic effect on the transition energy of a polysilane.

This model works well only for polysilanes with an all-anti conformation, which is what the Sandorfy models assume. To account for other geometries, a new β term was introduced, the $\beta_{1,4}$ term[67]:

Figure 5: Ladder Model for σ-conjugation

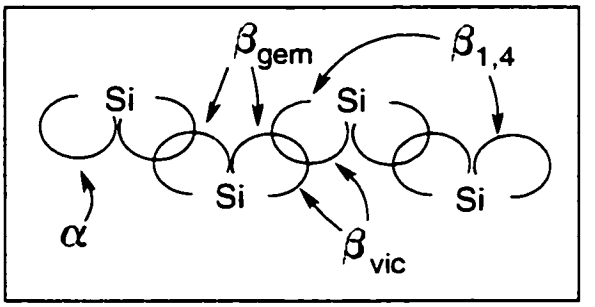

This term has the effect of accounting for sp^3 orbital interactions, whose function is dependent on the bond dihedral angle, and the overall system is called the Ladder model[68]. When added to the system, the orbital energies become corrected accordingly.

1.4 Models Based on a Molecular Orbital Model

Molecular orbital theory is the basis upon which all computational chemistry is derived. The question remains, however, whether it is valid to apply molecular orbital theory to localized groups or phenomena within a molecule. Each MO extends across the entire molecular system, and as such contains no implicit definition of individual atoms. To overcome this drawback, use is made of the expansion of each MO in terms of the atomic centred basis functions. These functions are used to partition the MOs with respect to the atomic centres. As there is no physical definition of an atom within an MO, a variety of models have been developed that partition the basis functions amongst the atomic centres within the molecule by employing various mathematical treatments and definitions. Very often these treatments lead to the development, in turn, of other models that attempt to explain the results of these treatments in terms of observed chemical behavior. The following are some examples of the theoretical work based on MO theory, and the models for silicon chemistry that have resulted.

1.4.1 Population Analysis

1.4.1.1 Mulliken Analysis

The most widely used system of separating molecular charges into atomic contributions was first proposed by Mulliken in 1949. In a series of articles[69,70], he described ways to improve upon the population analyses used at that time. He suggested the following approach to describe molecular orbitals: a given MO ψ_i can be expressed as a linear combination of 'atomic orbitals', (which are actually atom-centered basis functions), each on different atoms.

$$\psi_i = c_{ir} f_r + c_{is} f_s \tag{16}$$

The population of MO ψ_i by N electrons, (one or two), can be broken down into the following terms:

$$N = N c_{ir}^2 + 2N c_{ir} c_{is} S_{rs} + N c_{is}^2 \tag{17}$$

where the Nc_{ir}^2 and Nc_{is}^2 terms represent the net atomic populations on each atom involved in the MO and the central term represents the overlap population, with S_{rs} being the overlap integral between the two atomic orbitals in the MO. It should be noted that this an improvement in comparison to a Hückel analysis, wherein the overlap term is neglected. For the case where the total atomic populations are desired, Mulliken proposed equal divisions of this overlap population between each atom, based on orbital symmetry arguments. This overlap term also proved useful for calculating bond orders[71]. Using the same terms described above, the measure of bond order between two atoms in a given MO ψ_i is described by

$$p(r,s) = N c_{ir} c_{is} \Big/ \left(c_{ir}^2 + c_{is}^2\right) \tag{18}$$

The denominator is included to preserve the units of bond order during the calculation, i.e., single bond with a bond order of one, etc..

Practical use of this method, however, raises some important objections. The principle concern is the arbitrary nature in which overlap integrals are divided between atoms. Equal division of the overlap population applied to each atom is not entirely sensible as the resultant will not necessarily represent the actual shape of the electronic structure. For example, a polarized bond between two atoms would have more valence density on the more electronegative atom. This method completely ignores this possibility

when the overlap integral is divided in half. Secondly, there are cases where a Mulliken population can yield negative populations within MOs[72]. This of course makes no sense, as the population of an MO, and its atomic contributions, by definition and common sense must be greater than zero. A third problem is the sensitivity of Mulliken populations to the basis set being used. Studies of this dependency[73] showed considerable change in the atomic populations of hydrogen fluoride, when different basis functions of similar quality were used. Such a change in basis set should not, and did not, have any appreciable effect on the overall molecular properties, indicating this to be a direct result of the population analysis technique used. The final problem lies in the values obtained themselves, especially for systems where there is considerable bond polarization and ionic character between atoms. Inr the case of lithium fluoride, the Mulliken method predicts a charge on lithium of only +0.64 e with a 6-31*G basis set[74]. This value is unacceptably low for an ionic pair, even when taking into consideration the unusually high electronegativity of lithium with respect to other alkali cations. This same problem arises with calculations performed on silane species[75]. Examining the chemistry of these silanes shows quite clearly a strong polarization of the bonds, and significant charge separation between atoms, which allows the products to be formed. The previously referenced paper describes SiH_3F as having a computed charge of +0.993 on silicon, -0.514 on fluorine, and -0.160 on hydrogen; SiH_4 is further computed to have a charge of +0.545 on silicon and -0.136 on hydrogen. Such theoretical values do not correlate with experimental observations. SiH_4 is known to be incredibly reactive in water, undergoing vigorous nucleophilic attack. Given the extreme difference in electronegativity between silicon and fluorine, it is highly doubtful that silicon could retain almost half of fluorine's negative charge as suggested and yet still undergo facile nucleophilic substitution. Mulliken himself eventually disowned the concept of a population analysis[76], stating that it bore no relation to the charge distribution, and that "it should be possible to avoid such inconsistent and unsatisfactory results by computing atomic charges directly from the molecular charge distribution."

1.4.1.2 Natural Population Analysis

An alternative method of calculating atomic populations is the Natural Populations method developed by Reed, Weinstock and Weinhold[77]. This method takes any arbitrarily chosen basis set for a system and

converts them into natural atomic orbitals. Natural atomic orbitals are not the same as the natural orbitals introduced by Lowdin[78], which result from transformation of all the basis functions into orthonormal orbitals of maximal occupancy; such orbitals are delocalized over the entire molecule. Natural atomic orbitals result from transformation of all the basis functions centered on one atom, to maximal occupancy. This method in essence diagonalizes the one-electron matrix in terms of the atomic bases, minimizing interatomic overlap. The electron population of a given atom then becomes the sum of the occupation numbers of the natural atomic orbitals on a given atom. This method is a considerable improvement over Mulliken, as it no longer arbitrarily divides overlap equally between bonded atoms. However, this method still contains some flaws. Creating natural atomic orbitals does make sense when applied to the core electrons, as they are localized on one atomic center. Localizing valence density on atomic centers by this method, however, is riskier, especially in systems where the valence density is known to be highly delocalized. Thus, such a system does not accurately represent the structure of the valence electrons, which are by nature delocalized between at least two atomic centers.

1.4.1.3 Integrated Projection Population

The final method to be considered is the Integrated Projection Population method introduced by Streitwieser[74]. This method, rather than partitioning a molecule in terms of its MOs, uses the electron density function instead. A function ρ, expressed in terms of Cartesian co-ordinates, forms the basis of a projection function that represents a plane:

$$P(x,\ z) = \int_{-\infty}^{\infty} \rho(x,\ y,\ z)\,dy \tag{19}$$

The function P(x,z) is then fully integrated over x, creating a function P′(z). This function is then in turn integrated over z, from negative infinity to z_0, where z_0 is a minimum in P′(z). This method, while considerably superior to either Mulliken or Natural populations in terms of experimentally sensible results[79], still has an inherent flaw. The method limits the definition of an atom's boundaries as planar, an assumption that may or may not be valid even in systems containing homoatomic bonds, much less heteroatomic systems. Further, the choice of z_0 is still arbitrary, as no physical or quantum mechanical

arguments are made to validate this value, something that is crucial for any population analysis technique. Without sound roots in quantum mechanics, the choice of z_0 has no more validity than any other value, beyond the fact that it is a minimum in P'(z).

1.4.2 d – p Backbonding

As has just been discussed, there is some controversy concerning the results that are obtained when population analyses are performed on silicon species. Problems also exist with structural results, and their interpretation, as such problems develop as a result of experimental data being interpreted in the context of poor theoretical data, such as population analyses. These interpretations then become accepted models for these systems, which prove very difficult to dismiss, despite powerful evidence that refutes them. A classic example of such an interpretation is d-p backbonding.

Early researchers were at a loss to explain certain properties observed in silicon compounds. For example, the Si-F and Si-O bond are shorter than expected by theoreticians and experimentalists[80], because they are shorter than the sum of the covalent radii for each atom[20]. Covalent radii were used, because population analyses indicated that the charge differences between silicon and these electronegative atoms were quite small; therefore, the bond was presumed to be covalent. This line of thinking was supported by such data as the Si-F bond energy[28], which is much higher than that of the C-F bond[27], which led to a bond that was unusually short, and strong. There were other phenomena that defied explanation. In silicones, the Si-O-Si bond angle is abnormally large, about 145° [18], versus the C-O-C bond angle of about 110° [31]. Silanols are unusually acidic, when compared to their alcohol counterparts[82]. Silyl amines undergo pyramidal inversion of the nitrogen far more easily than carbamines, indicating more sp^2 character than expected[83]. All of these effects required some kind of explanation, and it was made through d-p backbonding[84]. This model uses the idea that the d-orbitals of silicon interact with the p-orbitals on the bonded atom: electron density in this p-orbital 'leaks back' into the empty d-orbital, forming a stronger, more stable bond.

Figure 6: d-p Backbonding Model

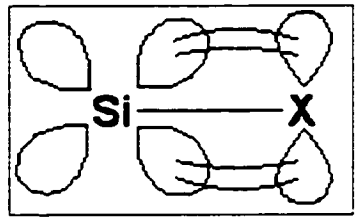

This model can quite adequately explain all of the above phenomena. Bonds formed will be shorter, and much stronger, and the increased double bond character in X makes silanols more acidic[85], and silyl amines flatter.

Numerous experiments and calculations have proved unequivocally that for 3rd-row main group elements, the d-orbitals are far too high in energy to contribute to any bonding mechanism[86,87]. Thus, this model, while convenient, has no experimental or theoretical support. The question that still remains is how to interpret these effects without d-p backbonding as a model. If one starts by questioning the idea that a silicon-atom bond is covalent, then a relatively simple conclusion can be drawn. If Si-F bonds are assigned a great deal of ionic character, then one can gauge the bond distance in terms of ionic radii, which will give a shorter bond length. Treating the Si-X bond as more ionic corrects all of the aforementioned problems. The Si-O-Si angle, having more ionic character, assumes more linearity than the C-O-C angle[88]. A silanol with a more ionic Si-O bond would put more charge on oxygen, polarizing in turn the O-H bond, making the hydrogen more acidic. An ionic Si-N bond would give the nitrogen more sp^2 character, and thus lower inversion energy.

Unfortunately, even presuming these more accurate alternatives, the p-d backbonding model is still regularly cited in computational studies[89,90]. Finally, one should note the text central to p-d backbonding principles, Linus Pauling's 'The Nature of the Chemical Bond'[20]. On the subject of d-orbitals in main-group element bonding, he himself refutes the idea of employing 3d orbitals to explain systems which contain more than 4 bonds to the central atom:

"The existence of compounds such as PF_5, PF_3Cl_2, PCl_5, PF_6^-, and SF_6 suggests that one or two 3d orbitals are here being used together with the 3s and three 3p orbitals (all hybridized to bond orbitals) for bond formation. It seems probable, however, that the completely covalent structures such as (a) are of little significance, and that the molecules instead resonate mainly among structures such as (b), etc., involving at most four covalent bonds."

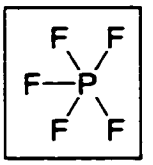

(a)

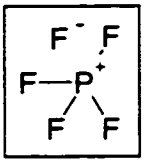

(b)

In chapter 7 of this same text, Pauling addresses the issue of the short bonds found in $SiCl_4$ using a similar resonance model as above that contains forms with four and fewer bonds to silicon, and forms with five and six bonds to silicon. He felt that these latter forms "require that one or more of the relatively unstable 3d orbitals also be drafted into service. It is probable for this reason that the structures of the first class, (with four and fewer bonds to silicon), make larger contributions than those of the second class, (with five and six bonds to silicon), the silicon atom acquiring in this way a small resultant positive charge, and the chlorine atoms corresponding negative charges." The brackets are used by this author to clarify the membership of each class. Clearly it was never Pauling's intent to involve d-orbitals as part of the electronic structure of 3rd-row main group compounds, for he knew they were too high in energy to be viable for bonding. This is a clear case where Pauling's statements have been misinterpreted, and the resulting model has managed to survive because noone has bothered to question the source that they cited.

1.4.3 Sigma Conjugation and Models

Silicon-based photochemistry has been extensively explored[49]. Despite this, and the large amount of theoretical work devoted to this subject[91], the calculations used to describe this behavior are based on relatively simple empirical models, which make use of experimental data fitted to the model parameters. As has been stated previously, the models developed only provide good results for very limited and special cases, such as all-trans oligosilanes. When these models fail to accurately describe the behavior observed in experiment, e.g. conformational dependence, more terms must be incorporated to make the models work.

The simplest example of a polysilane series is Si_nH_{2n+2}. The electronically simple nature of these compounds make them amenable to computation[86]. Unfortunately, these compounds are also highly reactive, and there are few quantitative experimental results available for substantiation of the computational values[43,92,93]. The majority of experimental work comes from spectra obtained from permethylated oligosilanes, which are considerably more stable and easy to work with[94]. For short chains up to n = 6, the models tend to slightly overestimate the excitation energy; such deviation is usually attributed to computational error, and is not considered a serious problem. Beyond this point, however, predicted excitation energies tend to become lower in value than what is actually observed. There are also cases where polysilanes with bulky alkyl substituents show abnormally low excitation energies, which cannot be explained electronically[95]. Experimentalists have proposed that it was twists in the silicon backbone that were the cause of this behavior, 'shortening' the effective length of the silicon chain with respect to excitation[96]. The fact that the model values did not correlate with experiment seemed to indicate that the conformation of the molecule was too important a factor to ignore[97]. The models have failed because the Hückel, and thus the Sandorfy models, are not equipped to deal with conformation, e.g. π-conjugated systems tend to be rigid, so such considerations are not necessary. This is the reason that the Ladder model was developed, so as to incorporate conformational dependence into the system to correct the computational results: studies have even attempted to further refine these conformationally-dependent terms through experiments[98].

There are still several cases where even these 'improved' models fail to predict experiment. One such case is that of cyclic oligosilanes, which show a trend in excitation not predicted by the model systems[99]. Another case where the models fail is with branched polysilanes. In general, all models underestimate both the excitation energies and ionization potentials of branched oligosilanes[100].

The final problem with these methods is the fact that they are based on empirical MO models, specifically the Hückel model. When models of increasing complexity are employed to predict the excitation energies of polysilanes, one obtains values that approach experiment. The parameters used to determine these excitation energies can come from a variety of sources, such as calculated ground state HOMO-LUMO gaps, or experimental vertical ionization energies[67]. Through this approach, one removes

any ability to distinguish between the ground state and excited state; these models themselves contain no information on whether the properties they are modeling are based on one or the other state. Without this information, one cannot know whether these systems are delocalized in the ground state or excited state, or even the context by which delocalization and 'σ-conjugation' can be applied. In order to obtain unambiguous information about whether a system is delocalized, one must establish whether the property one is studying is a ground state or excited state property, and determine the extent of localization or delocalization of this property, all within physical principles.

1.5 The Problem

The development of Molecular Orbital theory has made possible good approximations to the Schrödinger equation for molecular systems of chemical interest, enabling one to calculate molecular properties and understand their electronic structure. However, there is a fundamental concept of chemistry that MO theory cannot account for, that of the functional group. From the work of Dalton to the present day, it has been well established through experimental observation that molecules consist of atoms, and that these atoms and functional groupings of atoms exhibit characteristic and measurable properties. The concept of a functional group is the cornerstone of chemistry, and forms the basis for all research. One can describe the properties of a known molecule in terms of its functional group properties, and conversely, predict the presence of functional groups in an unknown molecule through observation of characteristic properties associated with those functional groups.

These same molecular properties can be calculated through MO theory, but only for the entire molecule, not an individual atom or functional group. The reason for this is, in terms of their spatial components, MOs are delocalized over the entire molecule and there is no quantum mechanical justification for dividing a MO into smaller components in real space. Molecular orbitals are mathematical functions that are based in abstract Hilbert space, and as such have no real form. The methods of population analysis described previously, which make use of the atomic-centred basis functions that form the MO, ignore the fact that these basis functions are chosen arbitrarily during the calculation of the wavefunction. They are not 'atomic orbitals', and are nothing more than mathematical functions used in the MO expansions[73]. Mulliken himself disowned the concept of population analysis based on the partitioning of

MOs, based on these facts[76].

The idea of delocalization within a molecule, and its calculation, is an extension of these same problems. Not only are delocalization studies based on the arbitrary partitioning of MOs in terms of their basis sets, but the very definition of delocalization is based on the MOs themselves. Electrons are considered delocalized if the MOs they reside in are themselves delocalized over the entire molecule. This argument is invalid, because a given wavefunction does not consist of a unique set of MOs. Any set of MOs that are used to generate a wavefunction that predicts a given set of molecular properties can be re-expressed through a unitary transformation to create a completely different set of MOs. The overall properties predicted by the wavefunction will not change, but the MOs will. They can be made to be maximally localized over certain atomic centres, or delocalized over the entire molecular framework. The Natural Population analysis technique takes advantage of this, by localizing MOs onto single atomic centers so as to assign their populations to individual atoms. Clearly, the definition of delocalization needs to be reconsidered, in order to resolve this conflict of ideas.

To address these problems, one must reconsider the extent to which MO theory can be used in quantum mechanics. As long as the MOs that make up a wavefunction are used only for certain properties such as ionization potentials, and are used to calculate properties for the entire molecule, then there is no conflict between theory and experimental observation. The question then becomes: how does one successfully partition a molecular wavefunction in such a way as to reproduce the chemical concept of atoms and functional groups, without resorting to arbitrary mathematical methods? The answer to this lies in the theory of Atoms in Molecules. The molecular wavefunction can be used to generate a density function that is measurable experimentally, and as such can be compared with theory or used directly. Such a density function can be partitioned into smaller regions within the molecular framework. These subsets of the overall space will correspond to a chemical definition of atoms in a molecule, provided that the conditions applied to form these subsets are derived from quantum mechanical principles. The measurement of delocalization within a molecule simply becomes another molecular property that can be partitioned into atomic contributions, be it electron delocalization calculated through the partitioning of the pair density, or the delocalization associated with electronic excitation, calculated through the partitioning

of the electronic excitation probability. When this method is applied to any molecular system, including those containing silicon, one obtains results that are not only non-arbitrary in their definition and calculation, but reproduce one of the most important features of chemistry, that of the atom, or in the case of this thesis, the silicon atom.

2 Theoretical

Much research in theoretical chemistry describes methods for obtaining approximate solutions to Schrödinger's equation so as to predict and understand the properties of some particular system. In most cases, chemists are interested in more than the energy, geometry and other properties of the molecule that can be obtained directly from such calculations. They also require answers couched in the conceptual language of chemistry, a language that evolved from our attempts to understand, classify and predict the observations of experiments. The initial attempts to relate this language to quantum mechanics went through the orbital model that underlies the valence bond and molecular orbital methods employed to obtain the approximate solutions to Schrödinger's equation. The one-electron model, as embodied in the molecular orbital theory, is the method for classifying and predicting the electronic structure of any system. The orbital classification of electronic states, in conjunction with perturbation theory, is a powerful tool in relating a system's chemical reactivity and its response to external fields to its electronic structure and its symmetry. The conceptual basis of chemistry is, however, a consequence of structure that is evident in real space.

The spatial distribution of electronic charge in the field of the nuclei and its flow in the presence of external fields are the physical manifestations of the forces operative in matter, and they determine the form of matter in real space. The charge distribution serves as the carrier of physical information, the topology of the charge density reflecting and encoding the concepts of atoms, bonds, structure and structural stability. The charge density is the expectation value of a quantum observable and its use in a theory of atoms in molecules will enable one to link the language of chemistry with that of physics. This field is the physical property of a system that Schrödinger stated should be used to understand the electrical properties of matter, while at the same time specifically warning against the use of the wave function in this regard, because of its unphysical nature[101].

Chemistry is presently in transition between the methods used to gather chemical insight from a calculated wave function. Orbital models relate atomic and bond contributions to the basis functions,

(incorrectly referred to in the older literature as atomic orbitals), used in the expansion of the orbitals. Increasingly, however, researchers now employ the theory of atoms in molecules in the analysis of a wave function[102]. It is important to understand that the use of this theory does not, however, represent an alternative way of obtaining chemical information from the wave function, using the electron density in place of orbitals. Rather, it represents the extension of quantum mechanics to an atom in a molecule, the charge distribution being the vehicle of its expression. Thus, the theory predicts the properties of an atom in a molecule in addition to providing a physical basis for understanding the properties.

2.1 Topology of the Electron Density

Each topological feature of the electron density function $\rho(\mathbf{r})$, whether it be a maximum, a minimum or a saddle, has associated with it a critical point, a point denoted by the coordinate $\mathbf{r}_c$ where $\nabla\rho(\mathbf{r}_c) = 0$. Such points are evident, for example, in the relief maps of the electron density given in Figure 7 for two planes of the diborane molecule.

Figure 7: Contour and Relief Maps of Diborane

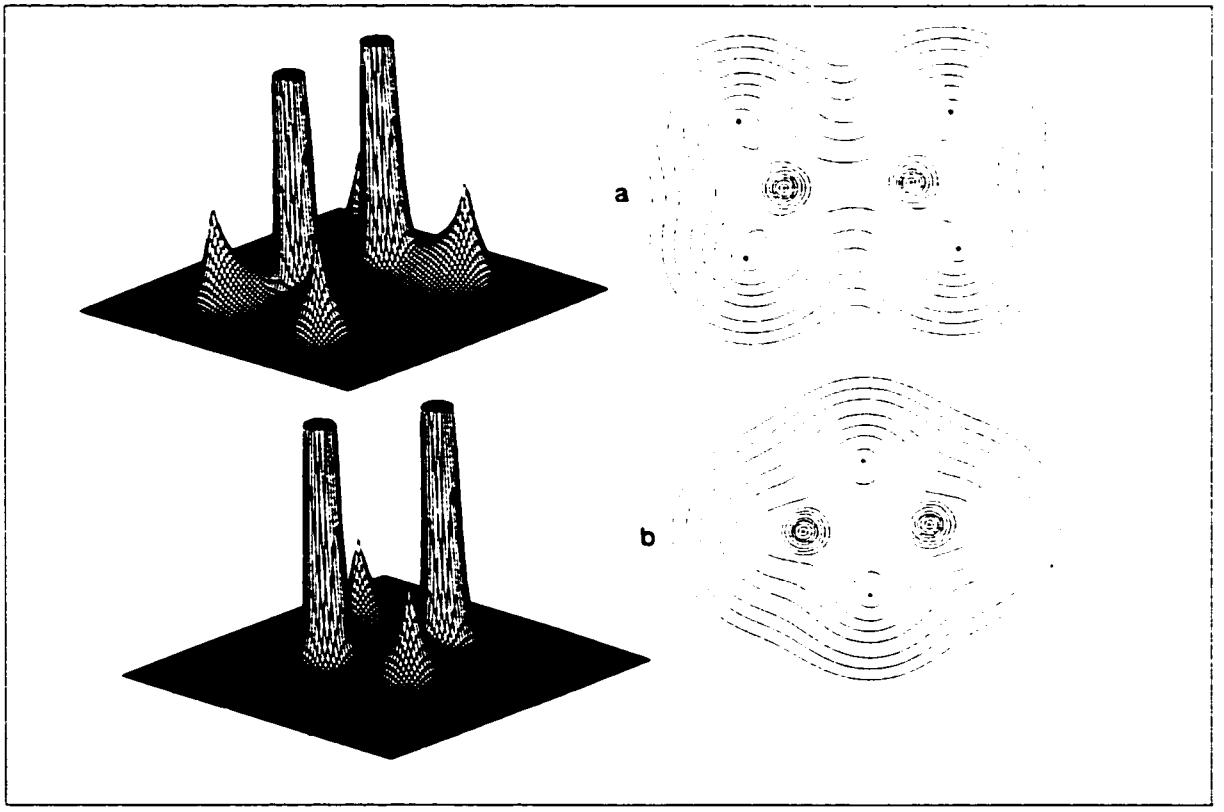

The behavior of the density in the neighborhood of a critical point is obtained via a Taylor series expansion of $\rho(\mathbf{r})$ about $\mathbf{r}_c$, retaining only the second-order terms. The collection of nine second derivatives of $\rho(\mathbf{r}_c)$, the Hessian matrix of ρ, is real and symmetric and may be diagonalized to yield a set of eigenvalues and associated eigenvectors. The former correspond to the three principle curvatures of $\rho(\mathbf{r})$ at the critical point, the latter to their associated axes, i.e., directions in space. A curvature may be a maximum, the second derivative of $\rho(\mathbf{r})$ being negative, or a minimum, the second derivative being positive. The rank of a critical point, denoted by ω, is the number of non-zero curvatures, and its signature, denoted by σ, is the sum of their algebraic signs. The critical point is labeled by assigning the denoted values with the notation (ω,σ).

With relatively few exceptions, the critical points of charge distributions for molecules at or in the neighborhood of energetically stable nuclear configurations are all of rank three. The near ubiquitous occurrence of critical points with $\omega = 3$ in such cases is a general observation regarding the topological behavior of $\rho(\mathbf{r})$ and it is in terms of such critical points that the elements of molecular structure are defined. There are just four possible critical points of rank three. They are:

- (3,-3): All curvatures of $\rho(\mathbf{r})$ at the critical point are negative and $\rho(\mathbf{r})$ is a local maximum at $\mathbf{r}_c$.
- (3,-1): Two curvatures are negative and $\rho(\mathbf{r})$ is a maximum at $\mathbf{r}_c$ in the plane defined by the two associated axes. The third curvature is positive and $\rho(\mathbf{r})$ is a minimum at $\mathbf{r}_c$ along the axis perpendicular to this plane.
- (3,+1): Two curvatures are positive and $\rho(\mathbf{r})$ is a minimum at $\mathbf{r}_c$ in the plane defined by the two associated axes. The third curvature is negative and $\rho(\mathbf{r})$ is a maximum at $\mathbf{r}_c$ along the axis perpendicular to this plane.
- (3,+3): All curvatures are positive and $\rho(\mathbf{r})$ is a local minimum at $\mathbf{r}_c$.

The boron nuclei are present in both planes shown in Figure 7 and the density is seen to exhibit a maximum at their positions in each plane. This is true for any plane containing the nuclei, since all three curvatures of $\rho(\mathbf{r}_c)$ are negative. The presence of such a 'local maximum' or (3,-3) critical point at the position of a nucleus is the dominant topological feature of an electronic charge distribution, a feature that is in turn a reflection of the dominance of the nuclear-electron attractive force. A nuclear maximum in $\rho(\mathbf{r})$

is not a true critical point, since $\nabla\rho$ is discontinuous there. However, this is not a problem of practical import and the nuclear positions behave as do (3,-3) critical points in $\rho(\mathbf{r})$ and they will be referred to as such.

The density in the plane of the terminal protons, Figure 7a, exhibits a saddle point between a boron nucleus and its two neighboring protons, as well as between the two boron nuclei. These are (2,0) critical points in two-dimensions, the curvature along the internuclear axis being positive and the other negative. In the plane of the bridging hydrogens, Figure 7b, the central critical point appears as a minimum, a (2,+2) critical point. Thus the third curvature of this critical point, the curvature along the axis between the two bridging protons, is positive and the central extremum in $\rho(\mathbf{r})$ is a (3,+1) critical point. This figure contains the unique plane wherein this critical point has the appearance of a local minimum, that is, of a (2,+2) critical point. The critical points between the boron nuclei and each of the bridging protons are again (2,0) critical points. However, the third curvature at the B-H (2,0) critical points in both planes is negative and they are (3,-1) critical points. Thus, both (3,-1) and (3,+1) critical points appear as saddles when viewed in either one of two planes containing one negative and one positive eigenvalue, but the former is a maximum and the latter a minimum in the third unique plane.

A (3,-1) critical point has the important property of accumulating electron density at the critical point in the plane perpendicular to the internuclear axis, as illustrated in Figure 8 for the (3,-1) critical point between a pair of carbon nuclei in ethene. This plane coincides with a symmetry plane in this molecule and in it, the critical point has the appearance of a local maximum, that is, of a (2,-2) critical point. A (3,-1) critical point is found between every pair of nuclei which, on chemical considerations, are considered to be "bonded" to one another. Figure 8 makes clear the accumulation of electron density that will occur all along the line linking the nuclei that is associated with the positive curvature of ρ at the critical point.

Figure 8: Contour and Relief Map of Ethene, Plane Perpendicular to Internuclear Axis

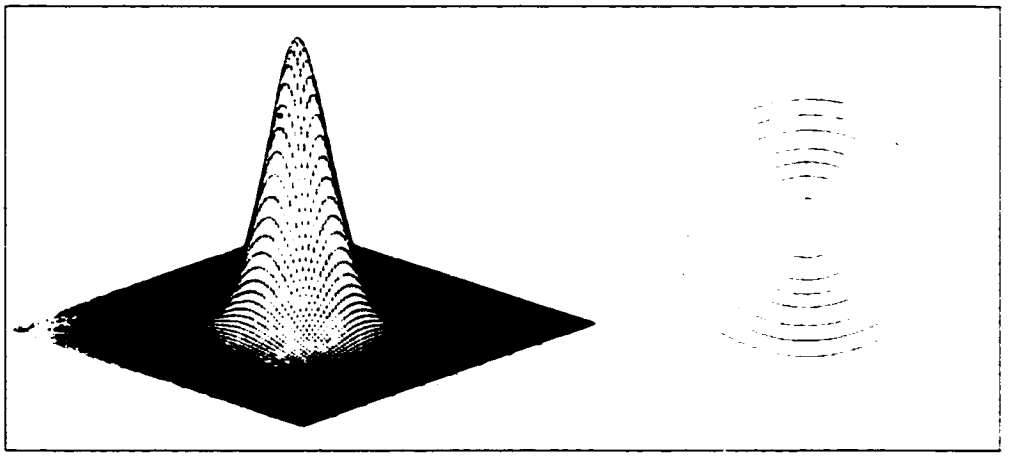

A (3,+1) critical point occurs in the interior of a bonded ring of atoms as formed by the bridging protons in diborane. The fourth and final type of stable critical point is a (3,+3) critical point, a local minimum in $\rho(r)$, as found in the interior of a cage.

These qualitative associations of topological features of the electron density with elements of molecular structure can be replaced with a rigorous theory through the use of its associated gradient vector field. The electron density is obtained for a fixed nuclear configuration, the set of nuclear coordinates being denoted collectively by $\mathbf{X}$, and the parametric dependence denoted by $\rho(\mathbf{r};\mathbf{X})$. The changes in the electron density and in its associated gradient vector field induced by changes in the molecular geometry, form the basis for a theory of molecular structure and structural stability.

2.2 Gradient Vector Field of the Electron Density

The gradient vector field of the electron density is represented through a display of the trajectories traced out by the vector $\nabla\rho(\mathbf{r};\mathbf{X})$ for a given $\mathbf{X}$, i.e., for a given molecular geometry. A trajectory of $\nabla\rho$, also referred to as a gradient path, is obtained by initially calculating the gradient vector of ρ at some arbitrary point $\mathbf{r}_0$. The components of the resulting vector $\nabla\rho(\mathbf{r}_0)$ are determined by the derivatives of $\rho(\mathbf{r}_0)$ along the x, y and z coordinates and the vector points in the direction of maximum increase in $\rho(\mathbf{r}_0)$. A trajectory of $\nabla\rho$ is generated by moving a small distance Δr away from the point $\mathbf{r}_0$ in the direction of the

vector $\nabla\rho(\mathbf{r}_0)$ and repeating the procedure until the path terminates. Every trajectory originates and terminates at a critical point where $\nabla\rho = 0$. The vector $\nabla\rho(\mathbf{r})$ is tangent to its trajectory at each point $\mathbf{r}$.

The flow of the trajectories in the neighborhood of a critical point generates what is called its phase portrait. The pair of eigenvectors associated with the two negative eigenvalues of a (3,-1) critical point span a two-dimensional manifold and generate a set of trajectories which terminate at the critical point and define a surface. The surface beyond the immediate neighborhood of a (3,-1) critical point will, in general, be curved unless the critical point lies in a symmetry plane. The unique pair of trajectories generated by the eigenvector associated with the single positive eigenvalue of a (3,-1) critical point, originate there and define a line in space. The electron density is a maximum at $\mathbf{r}_c$ in the surface manifold defined by the eigenvectors associated with the negative eigenvalues and a minimum at r_c along the axis defined by the remaining eigenvector, which is locally perpendicular to the surface. The phase portrait of a (3,+1) critical point is obtained by reversing the directions of the arrows on the trajectories for the (3,-1) case.

2.3 Elements of Molecular Structure

2.3.1 Definition of an Atom and Its Surface

The gradient vector field of the electron density of ethene is illustrated in Figure 9.

Figure 9: Gradient Vector Maps of Ethene

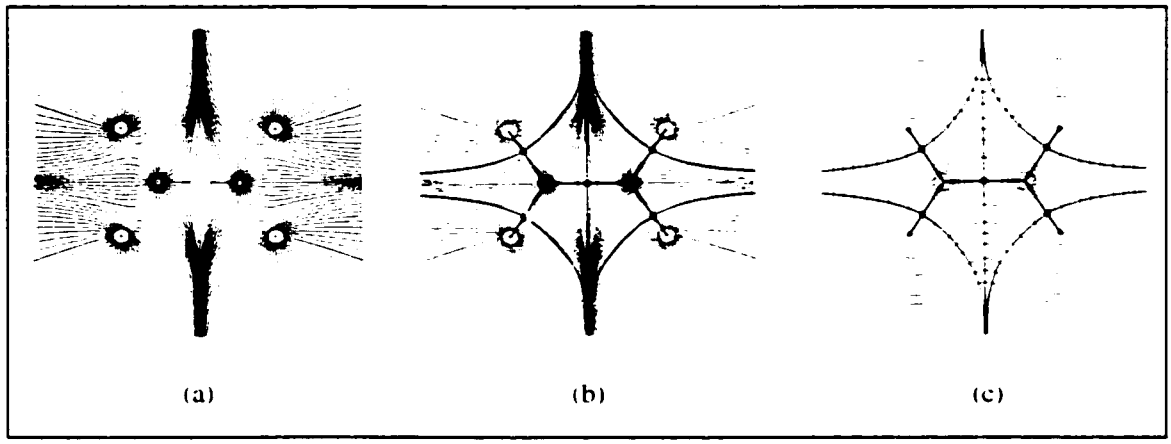

The trajectory diagram shown in Figure 9a omits the paths associated with the (3,-1) critical points between the carbon and hydrogen nuclei and they are considered first. All of the gradient paths in these diagrams terminate at one of the nuclei that behave as (3,-3) critical points. Consequently, a nucleus is seen to serve

as the terminus of all the paths starting from and contained in some neighborhood of the critical point and it thus behaves as a point attractor in the gradient vector field of $\rho(\mathbf{r})$. The basin of the attractor is defined as the region of space traversed by all of the trajectories of $\nabla\rho$ that terminate at the attractor or nucleus. Since (3,-3) critical points in a many-electron system are generally found at the positions of the nuclei, the nuclei act as the attractors of the field $\nabla\rho(\mathbf{r};\mathbf{X})$. The result of this identification is that the space of any molecular charge distribution, in real space, is partitioned into disjoint regions, or basins, each of which contains one point attractor or nucleus. Figure 9a illustrates this partitioning of space into the basins associated with the carbon and hydrogen nuclei. Because a nucleus acts as a point attractor in three-dimensional space, the partitioning so clearly indicated for these two planes extends throughout space. An atom, free or bound, is defined as the union of an attractor and its associated basin. Though the majority of (3,-3) critical points are found at the positions of nuclei, this is not to say that are only found at nuclear positions. It has been shown that non-nuclear attractors can be found in metal clusters[103], and that they are properties of the charge distribution, rather than an artifact of computation[104].

Alternatively, an atom can be defined in terms of its boundary. The basin of the nuclear attractor in an isolated atom covers the entire three-dimensional space R^3. For an atom in a molecule the atomic basin is an open subset of R^3. It is separated from neighboring atoms by interatomic surfaces. The existence of an interatomic surface S_{AB} denotes the presence of a (3,-1) critical point between neighboring nuclei A and B. The trajectory map of Figure 9b includes gradient paths that originate and terminate at the (3,-1) critical points, trajectories shown in bold. The presence of such a critical point between certain pairs of nuclei was noted above as being a general topological property of molecular charge distributions. Their presence now appears to provide the boundaries between basins of neighboring atoms. As discussed above and illustrated in Figure 9c, the trajectories which terminate at a (3,-1) critical point define a surface, the interatomic surface S_{AB}.

For the symmetry planes appearing in Figure 9c, only a single pair, (shown in bold), of the complete set of trajectories that terminate at a (3,-1) critical point appear in each plane. Each pair defines the intersection of the corresponding interatomic surface with the plane. The (3,-1) critical point between the

carbon nuclei of ethene, illustrated in Figure 9b and c, lies in the symmetry plane perpendicular to the C-C axis. The accompanying phase portrait illustrates the set of trajectories that terminate at this critical point and define the C-C interatomic surface. Because the density is a maximum at the critical point in the plane containing the interatomic surface, the critical point behaves as a (2,-2) point attractor in this plane and its phase portrait is indistinguishable from that for a nuclear attractor.

In summary, the atomic surface of atom A is defined as the boundary of its basin. Generally, this boundary comprises the union of a number of interatomic surfaces separating two neighboring basins, and some portions which may be infinitely distant from the attractor. The atomic surface of a boron atom in diborane for example, consists of two surfaces shared with neighboring terminal hydrogens and two more with the bridging hydrogen atoms. It does not share a surface with the second boron. Instead, as described in more detail below, the interatomic surfaces between each boron and the bridging hydrogens all intersect on the unique axis of the central (3,+1) cp.

Since an interatomic surface is defined by a set of trajectories of $\nabla\rho$ that terminate at a critical point, and since trajectories never cross, an interatomic surface $S(\mathbf{r})$ is one of local zero-flux in the gradient vector field of the electron density, that is, it is not traversed by any trajectories of $\nabla\rho$. The zero-flux property is expressed in terms of $\mathbf{n}(\mathbf{r})$, the unit vector normal to the surface at $\mathbf{r}$. Since $\nabla\rho(\mathbf{r})$ is tangent to its gradient path at every point $\mathbf{r}$, it is perpendicular to $\mathbf{n}(\mathbf{r})$ and their dot product vanishes.

$$\nabla\rho(\mathbf{r})\cdot\mathbf{n}(\mathbf{r}) = 0 \quad \text{for every point on the surface } S(\mathbf{r}) \tag{20}$$

The so-called "zero-flux" surface condition stated in Equation 20 is the boundary condition for the definition of a proper open system whose properties are defined by quantum mechanics, as described later.

2.3.2 Bond Path and Molecular Graph

Figure 9c also shows in bold the pairs of trajectories that originate at each (3,-1) critical point and terminate at the neighboring attractors. Thus the nuclei of every pair of neighboring atoms, those which share a common interatomic surface, are linked by a unique pair of trajectories. The density is a maximum at the critical point for directions perpendicular to this line, (see Figure 7a), and this behavior is true for all points along the line defined by this pair of trajectories. Thus, basins of neighboring nuclei are linked by a

line through space along which the electron density is a maximum with respect to any neighboring line. In the general case, such a line is referred to as an atomic interaction line.

The existence of a (3,-1) critical point thus indicates that electron density is accumulated between the nuclei that are linked by the associated atomic interaction line. Both theory and observation concur that the accumulation of electronic charge between a pair of nuclei is a necessary condition for two atoms to be bonded to one another. This accumulation of charge is also a sufficient condition when the forces on the nuclei vanish and the system possesses a minimum energy equilibrium geometry. Thus the presence of an atomic interaction line in such an equilibrium geometry satisfies both the necessary and sufficient conditions that the atoms so linked to be bonded to one another. The necessary accumulation of electron density is also sufficient to balance the nuclear forces of repulsion. In this case the line of maximum charge density linking the nuclei is called a bond path and the (3,-1) critical point is referred to as a bond critical point, or BCP. Thus the interatomic surfaces and bond paths are defined by the trajectories of $\nabla\rho$ associated with just the BCPs of a molecular charge distribution, as illustrated in Figure 9c.

For a given configuration of the nuclei, a molecular graph is the network of bond paths linking pairs of neighboring attractors. The molecular graph isolates the pair-wise interactions present in an assembly of atoms which dominate and characterize the properties of the system, be it at equilibrium or in a state of change. The network of bond paths is found to coincide with the network of lines obtained by linking those pairs of atoms, which are assumed to be bonded to one another on the basis of chemical considerations. This has been demonstrated for many systems with interactions ranging from ionic to polar to covalent, for hydrogen bonds and van der Waals complexes, in both molecules and solids, including metals and alloys. Figure 10 shows the molecular graphs for a variety of molecules, showing that even in systems termed "electron deficient" in the topology of ρ, such as boranes, the accepted chemical structures are recovered.

Figure 10: Molecular Graphs of Selected Molecules

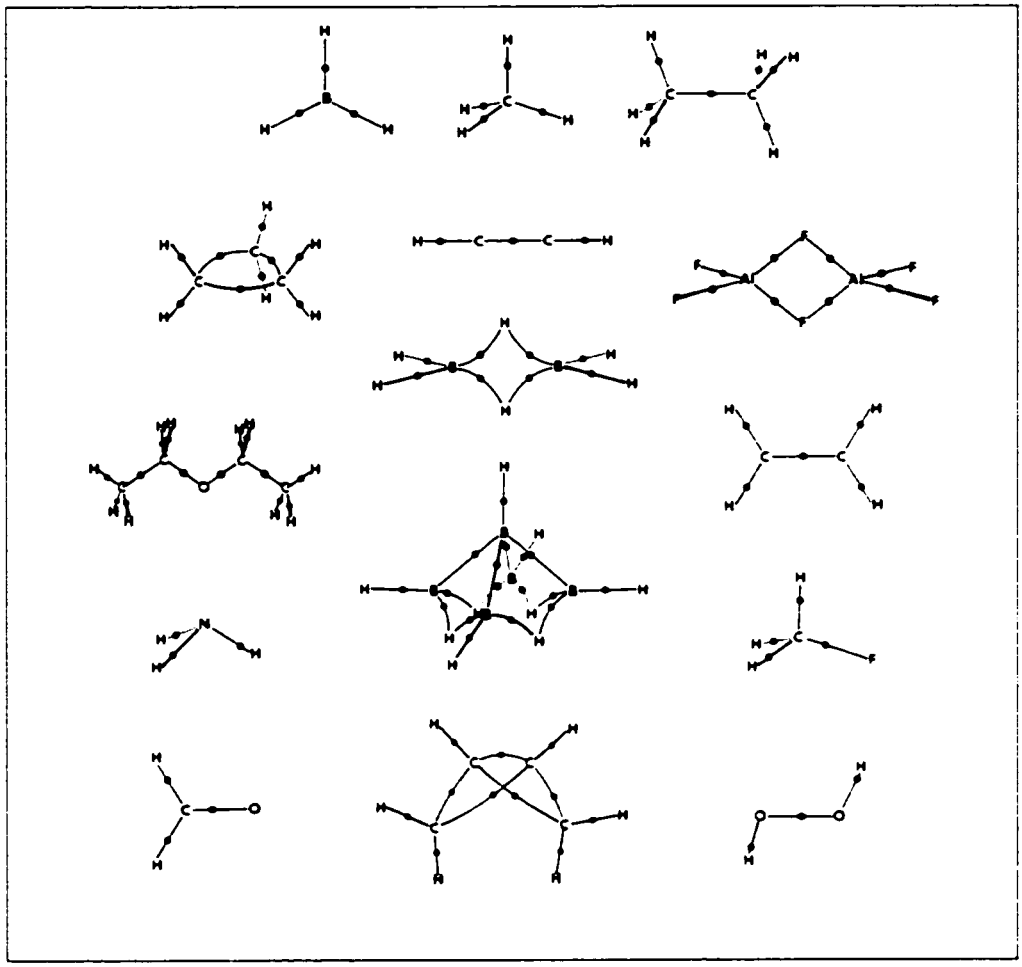

The recovery of a chemical structure in terms of a property of the charge distribution is a most remarkable and important result, not the least because the definition of structure so obtained is universal and applicable to all types of interactions. The representation of a structure by an assumed network of bonds has evolved through a synthesis of observations on elemental combination and models of how atoms combine. A great deal of chemical knowledge goes into the formulation of a chemical structure and, correspondingly, the same information is succinctly summarized by such structures. The demonstration that a molecular structure can be faithfully mapped onto a molecular graph imparts new information to them - that nuclei joined by a line in the structure are linked by a line through space along which the electron density, the glue of chemistry, is maximally accumulated. It has recently been shown that each bond path is

mirrored by a virial path, a corresponding line linking the same nuclei along which the potential energy density is maximally negative, an indication of how the topology of the electron density summarizes the physics of atomic interactions.

2.3.3 Rings and Cages

The remaining two stable critical points, rings and cages, occur as consequences of particular geometrical arrangements of bond paths and they define the remaining elements of molecular structure. If the bond paths are arranged to form a bonded ring of atoms, as they do in diborane with the bridging hydrogens, then a (3,+1) critical point is found in the interior of the ring, Figure 7b. The axes of the two positive curvatures of such a critical point define a surface spanned by a set of trajectories which originate at the critical point and define the ring surface. All of these trajectories terminate at the ring nuclei, except for the single trajectories that terminate at each of the bond critical points whose bond paths form the perimeter of the ring. Figure 11 shows the gradient vector field contour map of diborane, in the plane of the ring. The map on the right includes the trajectories that terminate at the bond critical points, (the BCPs are depicted as black circles), which are excluded from the otherwise identical map on the left. The top and bottom attractors, (where the gradient vectors converge to form dark circles) in Figure 11 represent the bridging hydrogens, while the larger attractors on the left and right, (shown as pale circles containing crosses), are the boron atoms. The unique axis associated with the negative curvature of this critical point defines the ring axis, perpendicular to the ring surface at $\mathbf{r}_c$. This axis is a line of intersection of the interatomic surfaces of the atoms forming the ring. A ring, as an element of structure, is defined as a part of a molecular graph that bounds a ring surface; the critical point found within is called a ring critical point (RCP).

Figure 11: Gradient Vector Field Map of Diborane, in Plane of Bridging Hydrogens

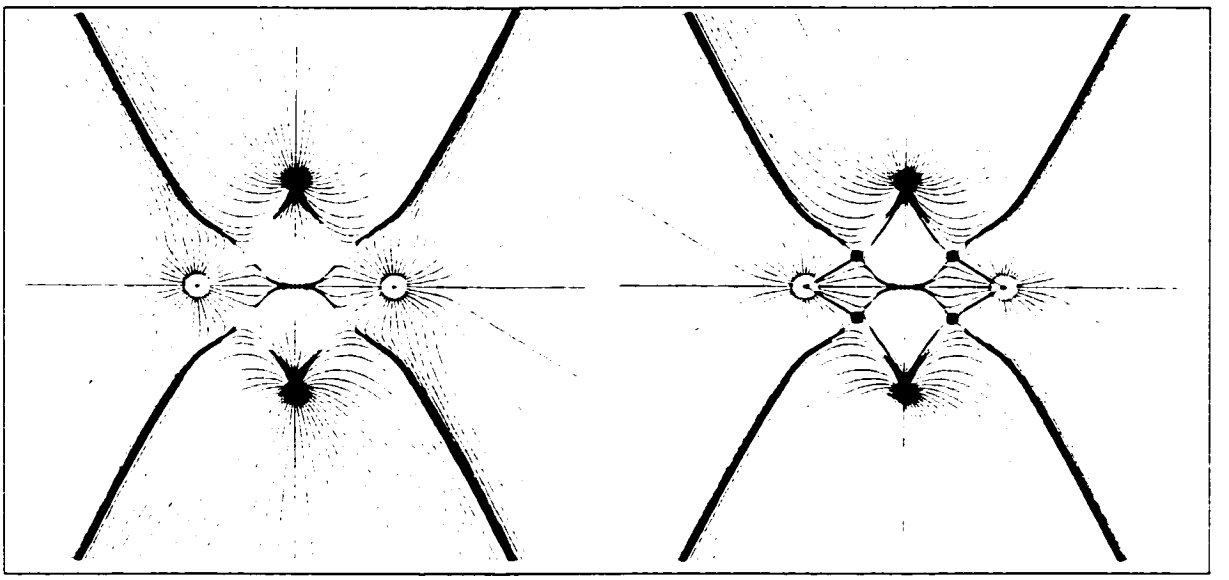

If the bond paths are so arranged as to enclose the interior of a molecule with ring surfaces, then a (3,+3) or cage critical point, (CCP), is found in the interior of the cage, Figure 12. A cage, as the final element of structure, is a part of a molecular graph which contains at least two rings, such that the union of the ring surfaces bounds a region of R^3 which contains a (3,+3) critical point.

Figure 12: Gradient Vector Field and Rho Contour Maps of Tetrahedrane

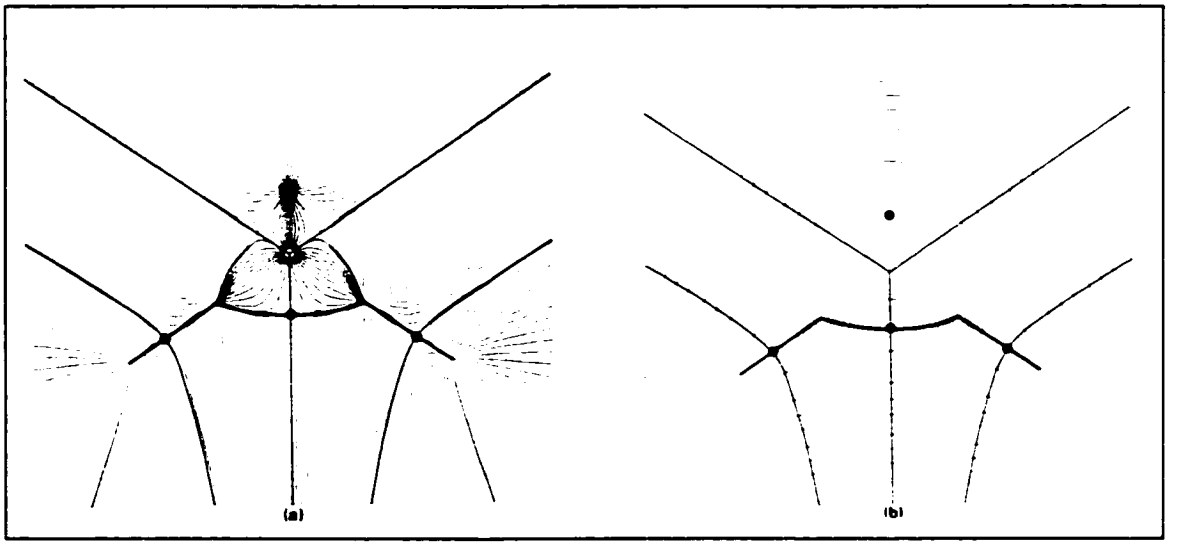

Figure 12 shows the cage critical point at the center of the tetrahedrane molecule. The point at the top of Figure 12b is the bond critical point linking the two out of plane carbons; here it behaves as a (2,-2) critical

point, and in the gradient vector field, all trajectories terminate at this point. The (3,-1) critical point linking the in plane carbon atoms behaves as a (2,0) critical point. The central point is the cage critical point, which behaves as a (2,+2) critical point in this plane, and has all trajectories originating there.

The number and type of critical points that can coexist in a system with a finite number of nuclei is governed by the Poincaré-Hopf relationship. With the above association of each type of critical point with an element of structure, this relationship states that

$$n - b + r - c = 1 \qquad (21)$$

where n is the number of nuclei, b the number of bond paths, r the number of rings and c the number of cages. For a system of infinite extent, this same set of numbers equals zero.

2.4 Characterization of Atomic Interactions

The properties of the electron density at a (3,-1) or bond cp, characterize the interaction defined by its associated trajectories. Applications of the concepts introduced here to a variety of systems have been previously detailed[105].

2.4.1 Bond Order and Bond Ellipticity

For bonds between a given pair of atoms the value of the electron density at the bond critical point, denoted by ρ_b, may be used to define a bond order. The extent of charge accumulation in the interatomic surface and along the bond path increases with the assumed number of electron pair bonds and this increase is faithfully monitored by the value of ρ_b. The ρ_b values for hydrocarbons for example, can be fitted to an expression to obtain C-C bond orders of 1.0, 1.6, 2.0 and 3.0 in ethane, benzene, ethene and ethyne, respectively. The value of ρ_b for the hydrogen bond in a series of similar complexes parallels the strength of the bond. (A non-empirical definition of bond order based on the electron pair density is given in Section 2.7).

The electron density in an interatomic surface attains its maximum value at the bond critical point, Figure 3, and the two associated curvatures of $\rho(\mathbf{r}_b)$, denoted by λ_1 and λ_2, are negative. In a bond with cylindrical symmetry, these two curvatures are of equal magnitude. However, if density is preferentially accumulated in a given plane along the bond path, (as it is for a bond with π-character for example), then

the rate of fall-off in ρ is less along the axis lying in this plane than in the one perpendicular to it, and the magnitude of the corresponding curvature of ρ is smaller. If λ_2 is the curvature of smallest magnitude, then the quantity $\varepsilon = [\lambda_1/\lambda_2 - 1]$, the ellipticity of the bond, provides a measure of the extent to which the density is preferentially accumulated in a given plane. The ellipticity of the bond density in ethene is 0.45 compared to the lesser value of 0.23 in benzene. The axis associated with the "soft" curvature λ_2, determines the plane within the molecule in which the density is preferentially accumulated. The chemistry of a three-membered ring is very much a consequence of the proximity of the bond and ring critical points which impart to the ring bonds a relatively high ellipticity. In cyclopropane for example, the ellipticity of a ring bond is greater than that in ethylene. The soft curvature necessarily lies in the plane of the ring and this structure accounts for both the unsaturated behavior exhibited by these systems and also their conjugational behavior with neighboring centers of unsaturation.

2.4.2 Energetics of Atomic Interactions

The properties of the laplacian of the electron density, the quantity $\nabla^2\rho$, are described in a later section, but we make use here of its basic mathematical property: that of determining where $\rho(\mathbf{r})$ is locally concentrated, where $\nabla^2\rho(\mathbf{r}) < 0$, and locally depleted, where $\nabla^2\rho(\mathbf{r}) > 0$, relative to points neighboring the point $\mathbf{r}$ in question. The electron density is a maximum in an interatomic surface at the bond critical point, and since the two associated curvatures of ρ_b are negative, electronic charge is also concentrated in the surface at this point. The electron density is a minimum at this same point along the bond path, the associated curvature of ρ_b being positive and electron density is locally depleted at the critical point with respect to neighboring points along the interaction line. Thus, the formation of an interatomic surface and an atomic interaction line is a result of a competition between the perpendicular contractions of ρ which lead to a concentration of electronic charge along the bond path, and the parallel expansion of ρ which leads to its depletion in the surface and to its separate concentration in the basins of the neighboring atoms. The sign of $\nabla^2\rho$ determines which of these two competing effects is dominant.

We can also anticipate a result from the demonstration that the laplacian of ρ appears in the local expression of the virial theorem:

$$\left(\hbar^2/4m\right)\nabla^2\rho = 2G(\mathbf{r}) + V(\mathbf{r}) \tag{22}$$

The quantity $G(\mathbf{r})$ appearing in this expression is a form of the kinetic energy density of the electrons that is positive everywhere and $V(\mathbf{r})$ is the potential energy density which is negative everywhere. This equation thus demonstrates that the lowering of the potential energy dominates the total energy in those regions of space where electronic charge is concentrated, where $\nabla^2\rho < 0$, while the kinetic energy is dominant in regions where $\nabla^2\rho > 0$.

In a shared interaction, electron density is both accumulated and concentrated along the bond path between the nuclei, as indicated by $\nabla^2\rho_b < 0$. The laplacian and its perpendicular curvatures are large in magnitude and the resulting concentration of charge density along the bond path yields a large value for ρ_b. Such interactions achieve their stability through the lowering of the potential energy resulting from the accumulation of electronic charge between the nuclei, an accumulation that is shared by both atoms.

The opposite extreme to a shared interaction occurs when two closed-shell systems interact, as found in ionic, hydrogen bonded, van der Waals and repulsive interactions. In such closed-shell interactions, the requirement of the Pauli exclusion principle leads to the removal of electron density from the region of contact, the interatomic surface. All of the curvatures of ρ_b are relatively small in magnitude but the positive curvature of ρ_b along the bond path is dominant and $\nabla^2\rho_b > 0$. Since the electron density contracts away from the surface, the interaction is characterized by a relatively low value of ρ_b and the electron density is concentrated separately in each of the atomic basins. Such interactions can be either attractive or repulsive depending on the disposition, relative to the nuclei, of the density that is separately concentrated in the neighboring basins.

In a strongly polar shared interactions, as found in CO for example, there is substantial charge transfer but the atomic densities do not approach those of polarized closed-shell ions. In these cases, all the curvatures of ρ_b are large in magnitude and there is a substantial accumulation of density along the bond path and ρ_b values typical of shared interactions. However, the polar nature of the interaction causes the positive curvature to dominate and $\nabla^2\rho > 0$. Another quantity used to determine the nature of the interaction is the energy density $H(\mathbf{r}) = G(\mathbf{r}) + V(\mathbf{r})$. Its value at the bond critical point is denoted by H_b[106].

Unlike the laplacian, whose sign is determined by the local virial expression Equation 22, the sign of H_b is determined by the energy density itself and is found to be negative for all interactions which result from the accumulation of electron density at the bond critical point.

2.5 Chemical and Quantum Constraints on the Definition of an Atom

The molecular structure hypothesis is the cornerstone of chemistry. It states that a molecule consists of a set of atoms with characteristic properties, linked by a network of bonds to give a resultant structure. We have seen that the topology of the electron density defines atoms, bonds and structure, together with a description of a system's structural stability. Now we can turn to the question of the properties of the atoms defined within the same theory. The observations of chemistry are classified empirically in terms of the properties exhibited by functional groups, a linked set of atoms. In chemistry we recognize the presence of a group in a given system and predict its effect upon the static and dynamic properties of the system in terms of the characteristic set of properties assigned to that group.

In the past there have been many failed attempts to define an atom in a molecule and its contributions, or those of a functional group, to the properties of the molecule. There was, and for some there remains, a prevailing belief that a unique definition of an atom in a molecule is not possible. Consider for example the following statement that appeared in the Journal of the American Chemical Society in 1994: "The atom (or functional group) in a molecule is not easily defined. There are always subjective factors for any definition, or strict partition of the molecule. What model one chooses is subject to one's particular needs."[107] These comments are made without reference to the existing literature. They represent the personal biases of the authors and they are easily disposed of using the published physics they chose to ignore. Their remark that how one defines an atom is a matter of expediency is at variance with the practice of science wherein one's attempts at definition and understanding are necessarily guided by observation and by theory. Any definition that does not recover the essential observations that are associated with the concept of an atom in a molecule serves no useful purpose. Any definition that does not ultimately allow for the quantum definition of the atom's properties cannot be a physically admissible one.

2.5.1 Chemical Constraints

There are three essential requirements imposed upon the definition of an atom in a molecule by the observations of chemistry:

- The first stems from the necessity that two identical pieces of matter exhibit identical properties. Since the form of matter is determined by the distribution of charge throughout real space, two objects are identical only if they possess identical charge distributions. This parallelism of properties with form exists not only at the macroscopic level, but as originally postulated by Dalton, is assumed to exist at the atomic level as well. It demands that an atom be a function of its form in real space, requiring that it be defined in terms of the charge distribution. It follows that if an atom exhibits the same form in the real space of two systems, or at two different sites within a crystal, it must contribute identical amounts to the total value of every property in each case.
- This requirement of property following form, as described above, demands in turn that summing the atomic contributions must yield the total value for the system. That is, the atomic contributions to some individual property must sum to yield the value of the property for the molecule. Only atoms meeting these two requirements can account for the observation of so-called additivity schemes wherein the atomic properties appear to be transferable as well as additive.
- Finally, the boundary defining an atom or functional group must be such as to maximally preserve its form and thereby maximize the transfer of chemical information from one system to another.

The topological atom meets all of these requirements, its form reflecting its properties and, as demonstrated below, recovering the properties of functional groups in those instances of essential transferability where they are susceptible to experimental measurement.

2.5.2 Quantum Constraints

The only subjectivity one can exercise in "a strict partition of a molecule" is to decide whether or not to adhere to the constraints imposed by physics or to ignore them and thereby abandon physics "subject to one's personal needs." The constraints imposed by quantum mechanics on the definition of an atom are best stated in the form of two questions: a) Does the state function, the function that contains all of the information that can be known about a system, predict a unique partitioning of the molecule into atoms?

and b) Does quantum mechanics provide a complete description of the atoms so defined? Affirmative answers to these two questions in effect require that quantum mechanics be extended to a uniquely defined set of open systems, termed *proper open systems*.

To understand the overall concept of a proper open system, one can take as an example the calculation of a property within an arbitrarily chosen open system. One can create expressions for the expectation values of observables, such as the kinetic energy, for any open system made through the definition of an arbitrary boundary. It has been shown that the Hamiltonian kinetic energy function K(r) is related to the Lagrangian kinetic energy function G(r) by the laplacian function L(r). For a one-electron system described by a wavefunction Ψ, one has:

$$\begin{aligned}
\nabla^2(\Psi^*\Psi) &= \nabla\cdot\left(\Psi^*\nabla\Psi + (\nabla\Psi^*)\Psi\right) \\
&= \Psi^*\nabla^2\Psi + (\nabla^2\Psi^*)\Psi + \nabla\Psi^*\cdot\nabla\Psi + \nabla\Psi\cdot\nabla\Psi^* \\
\textit{let: } K(\mathbf{r}) &= {}^{-\hbar^2}\!/_{4m}\left(\Psi^*\nabla^2\Psi + (\nabla^2\Psi^*)\ \Psi\right) \\
G(\mathbf{r}) &= {}^{\hbar^2}\!/_{2m}\left(\nabla\Psi^*\cdot\nabla\Psi\right)\ \ L(\mathbf{r}) = {}^{-\hbar^2}\!/_{4m}\nabla^2\rho(\mathbf{r}) \\
\therefore K(\mathbf{r}) &= G(\mathbf{r}) + L(\mathbf{r})
\end{aligned} \tag{23}$$

When these functions are integrated over an arbitrarily defined open system Ω, the L(r) function can be expressed as a surface integral via Gauss' theorem:

$$K(\Omega) = G(\Omega) - \left(\hbar^2/4m\right)\oint dS(\Omega)\nabla\rho(\mathbf{r})\cdot\mathbf{n}(\mathbf{r}) \tag{24}$$

When this open system represents the entire space of the molecule, $\rho(r)$ and thus $\nabla\rho(r)$ becomes zero, and the L(r) function vanishes, leaving the two kinetic energies equivalent, a result originally pointed out by Schrödinger. For any other open system, there must be a clear definition of the surface over which this open system must be integrated in order to cause the L(r) function to vanish and make the integrated kinetic energy a well-defined quantity with physical significance. This definition is the zero-flux surface of Equation 20. It is important to note that there are two means of making the second term in Equation 24 vanish for an open system Ω. There is the net zero flux, where there is a net property flux through the surface that sums to zero, and the local zero flux, where there is no flux at any point on the surface. It is this

latter local zero-flux condition that is required for an open system Ω to be well defined in the quantum mechanical sense.

This extension of quantum mechanics is possible within the framework of the generalized action principle and, as stated previously, its use has resulted in the identification of the proper open systems of quantum mechanics with the topological atom. The derivation of the quantum mechanics of a proper open system is not given here, but one can present an outline of the essential concepts. It is based on the reformulation of physics provided by the work of Feynman and Schwinger, an approach that makes possible the asking and answering of questions not possible within the traditional Hamiltonian framework. This results in an alternative to the use of existing models and arbitrary definitions of chemical concepts, in favor of a theory of atoms in molecules that is rooted in physics[102,108,109].

2.6 Atomic Properties

With the definition of an atom in a molecule established by quantum mechanics, one can proceed to determine the contribution of any atom to a given molecular property. For a given observable property A, one will have associated with it an operator $\hat{A}(\mathbf{r})$. The average of said observable is given by

$$\left\langle \hat{A} \right\rangle = (N/2)\int d\tau \left\{ \Psi^{*}\hat{A}(\mathbf{r})\Psi \; + \; \left(\hat{A}(\mathbf{r})\Psi\right)^{*}\Psi \right\} \tag{25}$$

where $d\tau$ indicates that integration occurs over all spin and space co-ordinates, and the operator $\hat{A}(\mathbf{r})$ is defined as the operator for a single electron. This follows directly from the principle of stationary action, where each generator that describes any change to an open system is a function of the field co-ordinates for a single particle[110]. The application of operator $\hat{A}(\mathbf{r})$ on the state function can also be performed so as to obtain a property density ρ_A, by integrating over all spin co-ordinates and all space co-ordinates save one, as denoted by $d\tau'$.

$$\rho_A(\mathbf{r}) = (N/2)\int d\tau' \left\{ \Psi^{*}\hat{A}(\mathbf{r})\Psi \; + \; \left(\hat{A}(\mathbf{r})\Psi\right)^{*}\Psi \right\} \tag{26}$$

To determine the value of the property A over the entire molecule, one integrates the density ρ_A. To determine the contribution to A from some open system Ω, one integrates the property density ρ_A over that

open system, (Equation 27); it is assumed that this open system meets the required boundary condition of zero flux, which defines an atom within the total system.

$$A(\Omega) = \int_{\Omega} d\mathbf{r}\, \rho_A(\mathbf{r}) \tag{27}$$

From this result and Equation 25, one concludes that the average value of property A for the entire system simply becomes the sum of the contributions of all the subsets, or atoms:

$$\left\langle \hat{A} \right\rangle = \sum_{\Omega} A(\Omega) \tag{28}$$

One now has at hand a system for determining the contributions of the atoms in a molecule to any property of that molecule; one need only apply the appropriate operator associated with that property.

2.6.1 Atomic Population and Charge

Atomic population is the easiest property to determine; the associated operator is simply the unit operator, yielding a property density that is the electron density $\rho(\mathbf{r})$.

$$N(\Omega) = \int_{\Omega} d\tau\, \rho(\mathbf{r}) \tag{29}$$

The charge of an atom then becomes the charge on the nucleus within Ω, Z_Ω, minus the integrated population $N(\Omega)$.

2.6.2 Dipole Moment

The dipole moment for a molecule is defined as a unit charge times the difference in centroids of the positive (nuclei) and negative (electron density) charge distributions:

$$\mu = e\sum_{\Omega} Z_\Omega \cdot \mathbf{X}_\Omega \; - \; e\int \rho(\mathbf{r})\mathbf{r}\, d\tau \tag{30}$$

where $\mathbf{X}_\Omega$ is the co-ordinate of nucleus Ω. To partition the second term in Equation 30, one replaces the vector $\mathbf{r}$ with $(\mathbf{r}_\Omega + \mathbf{X}_\Omega)$, thus breaking up the integral term; $\mathbf{r}_\Omega$ is the electronic position vector with the origin at the nucleus of atom Ω with position vector $\mathbf{X}_\Omega$[111]. The origin dependence of $\mathbf{r}$ is thus relegated to terms involving the nuclear co-ordinates. Integration over each atomic basin yields:

$$\begin{aligned}
\boldsymbol{\mu} &= \sum_{\Omega} Z_{\Omega} \cdot \mathbf{X}_{\Omega} - \int \rho(\mathbf{r})\mathbf{r}\, d\tau \\
&= \sum_{\Omega} Z_{\Omega} \cdot \mathbf{X}_{\Omega} - \sum_{\Omega}\left(\int \rho(\mathbf{r})\mathbf{r}_{\Omega}\, d\tau + \mathbf{X}_{\Omega}\int \rho(\mathbf{r})\, d\tau\right) \\
&= \sum_{\Omega}\left(Z_{\Omega} \cdot \mathbf{X}_{\Omega} - N(\Omega)\cdot \mathbf{X}_{\Omega}\right) - \sum_{\Omega}\left(\int \rho(\mathbf{r})\mathbf{r}_{\Omega}\, d\tau\right) \\
&= \sum_{\Omega}\left(q(\Omega)\cdot \mathbf{X}_{\Omega}\right) - \sum_{\Omega}\left(\int \rho(\mathbf{r})\mathbf{r}_{\Omega}\, d\tau\right) \\
&= \sum_{\Omega}\left(q(\Omega)\cdot \mathbf{X}_{\Omega}\right) - \sum_{\Omega}\mathbf{M}(\Omega)
\end{aligned} \tag{31}$$

The final line of Equation 31 contains two terms: the interatomic charge transfer term, and the polarization of the density within each atom, also known as the first moment $\mathbf{M}(\Omega)$, (the unit charge has been left out for ease of reading). To obtain atomic contributions to the dipole moment that are completely origin independent, one must partition the interatomic charge transfer term; this is done by regrouping the terms into contributions proportional to the charge that is transferred to or from each group neighboring the atom Ω. This technique was developed by Dr. Bader, and has no derivation.

$$\boldsymbol{\mu}(\Omega) = \mathbf{M}(\Omega) + \sum_{\Omega' \neq \Omega} q(\Omega') * \left[\mathbf{X}^{c}(\Omega|\Omega') - \mathbf{X}(\Omega)\right] \tag{32}$$

where $X^c(\Omega|\Omega')$ is the coordinate of the critical point linking the group of atoms Ω' to atom Ω. This second term can be re-expressed as a surface integral $d\mathbf{S}(\Omega|\Omega')\cdot\varepsilon(\mathbf{r}_{\Omega})$, where ε is the dipole flux through the surface denoted by $d\mathbf{S}$. It is computationally easier, however, to use Equation 32.

2.6.3 Quadrupole Moment

The quadrupole moment is another important polarization property that indicates how the electron density is polarized, and in which direction. The nine components of the quadrupole moment are obtained from an atom with the following operator:

$$Q_{zz}(\Omega) = -e\int_{\Omega}\left(3z_{\Omega}^{2} - r_{\Omega}^{2}\right)\rho(\mathbf{r})\, d\tau \tag{33}$$

with corresponding definitions for the xx, yy, xy, xz, and yz components. The resulting matrix is real and symmetric, and can thus be diagonalized, yielding principle components that correspond to the principle axes of the atom in the molecule. Polarization of the electron density of Ω along one of these axes results in

a principle component value that is less than zero; the sum of the other two components will be greater than zero, as the quadrupole matrix is traceless, with the sum of all three principle components equalling zero.

2.6.4 Atomic Volume

The atomic volume can be determined by calculating the volume of the basin bounded by its surfaces of zero flux. Rather than calculate the entire basin, one limits the calculation to the region of space formed by the union of the zero-flux surfaces and a density isosurface, usually the 0.001 au isosurface, which accounts for over 99 percent of the electronic charge of an atom.

2.6.5 Atomic Energy

Partitioning the energy of a molecule into its atomic contributions is a more complex issue, requiring the mathematical development of the physics of a proper open system, which can be found in a number of sources[102,112,113]. The primary theorem of an open system is the Ehrenfest force theorem, the theorem that defines the force acting on each element of the electron density and hence on an atom in a molecule. The local expression of this force, the Ehrenfest force density $\mathbf{F}(\mathbf{r})$, has a simple expression in terms of the divergence of the quantum stress tensor $\sigma(\mathbf{r})$,

$$\mathbf{F}(\mathbf{r}) = -\nabla \cdot \sigma(\mathbf{r}) \tag{34}$$

As in classical physics, the stress tensor enables one to determine the force imposed on a body arising from the application of a stress at any point. The Ehrenfest force density is a most remarkable quantity: it reduces all of the complex interactions between the electron at $\mathbf{r}$ and the remaining electrons and nuclei in the system, as determined by the many-particle wavefunction, to a density in real space. This is an example of a 'dressed property density' - a density dressed by the average interaction, appropriate to the property at hand, of the electron at $\mathbf{r}$ with the remainder of the system[113]. All properties are so described, enabling one to obtain the corresponding atomic contributions by a simple integration of the appropriate density over a region of real space bounded by the appropriate zero-flux surface.

The definition of the force density makes possible the definition of a potential energy density, an essential step in the spatial partitioning of the energy[102]. It was the inability to obtain a partitioning of the potential energies of interaction from physics that caused the failure of previous attempts at partitioning the

energy. How does one determine how much of the nuclear-electron attraction, or the electron-electron repulsion or the nuclear-nuclear repulsion energy belongs to a given atom in a molecule? Physics answers this question through the atomic statements of the Ehrenfest force and virial theorems and their associated dressed density distributions.

Taking the virial of the Ehrenfest force yields a potential energy density, a dressed density that determines the average energy of interaction of the electron at position $\mathbf{r}$ with the remainder of the system. This is accomplished by taking the scalar product of $\mathbf{F}(\mathbf{r})$ with the position vector $\mathbf{r}$, a step formally analogous to letting a force act through a distance to obtain a corresponding energy. This step yields the virial of the Ehrenfest force $\mathbf{r} \cdot \mathbf{F}(\mathbf{r})$, which may be identified with $V(\mathbf{r})$, an electronic potential energy density. Its integral over all space yields the electronic potential energy:

$$\int d\mathbf{r} V(\mathbf{r}) = \left\langle \hat{V}_{en} \right\rangle + \left\langle \hat{V}_{ee} \right\rangle + \left\langle \hat{V}_{nn} \right\rangle - \sum_{\alpha} X_{\alpha} \cdot F_{\alpha} = \left\langle \hat{V} \right\rangle - \sum_{\alpha} X_{\alpha} \cdot F_{\alpha} \qquad (35)$$

The symbol $< >$ denotes the average value of any contained operator - the electron-nuclear, electron-electron and nuclear-nuclear potential energy operators, respectively. $< \hat{V} >$ is the average of the potential energy operator, the quantity appearing in the expression for the total energy $E = < \hat{T} > + < \hat{V} >$. The final term in Equation 35 is the virial of the Hellmann-Feynman forces on the nuclei. If the molecule is in an equilibrium geometry, this term vanishes and the integral of the virial of the Ehrenfest force yields the total potential energy $< \hat{V} >$. The density $V(\mathbf{r})$ differs from the virial density $\mathcal{V}(\mathbf{r})$, whose integral over an atom yields the atomic virial $\mathcal{V}(\Omega)$, by a divergence term, $\mathbf{r} \cdot (\nabla \cdot \sigma)$. The integration of the divergence term yields the surface virial of the Ehrenfest force when integrated over an atom, a term which vanishes for the total system with a surface at infinity.

It may come as a surprise that the virial of the forces exerted on the electrons should include the nuclear-nuclear repulsion energy $< \hat{V}_{nn} >$ as well as the virial of the forces on the nuclei, although how this occurs is easily explained. The major component of the Ehrenfest force is the one exerted on the electrons by the nuclei. Upon taking the virial of the operator describing this force and applying Euler's theorem,

one obtains in addition to the corresponding potential energy contribution $<\hat{V}_{en}>$, the virial of the Hellmann-Feynman forces exerted by the nuclei on the electrons, the final term in Equation 36.

$$\left\langle\!\!\left(\sum_i -\mathbf{r}_i \cdot \nabla_i \hat{V}_{en} \right)\!\!\right\rangle = \left\langle \hat{V}_{en} \right\rangle + \sum_\alpha \mathbf{X}_\alpha \cdot \mathbf{F}_{e\alpha} \tag{36}$$

The nuclear virial in turn may be expressed in terms of $<\hat{V}_{nn}>$ minus the virial of the Hellmann-Feynman forces on the nuclei, as shown in Equation 37.

$$\sum_\alpha \mathbf{X}_\alpha \cdot \mathbf{F}_{e\alpha} = \left\langle \hat{V}_{nn} \right\rangle - \sum_\alpha \mathbf{X}_\alpha \cdot \mathbf{F}_\alpha \tag{37}$$

Adding $<\hat{V}_{ee}>$, the virial of the electron-electron Ehrenfest force, to the virial of the electron-nuclear forces in Equation 36, yields the virial of the Ehrenfest force as given in Equation 35. The atomic virial theorem, as does the theorem for the total system, equals twice the electronic kinetic energy of an atom to the negative of its virial, $2T(\Omega) = -\mathcal{V}(\Omega)$, where the atomic virial consists of the virial of the Ehrenfest forces over the atomic basin and surface. The molecules under study here are in equilibrium geometries. Under these conditions $E(\Omega)$, the energy of the atom, equals $-T(\Omega)$ and the total energy E is given by the sum of the atomic energies, as expressed by Equation 38.

$$E = \sum_\Omega E(\Omega), \quad \textit{where} \quad E(\Omega) = -T(\Omega) \tag{38}$$

2.7 Electron Localization and Fermi Correlation

The oft-quoted result of antisymmetrizing the wave function with respect to the permutation of the space-spin coordinates of every pair of electrons is that no two electrons with the same spin can occupy the same point in space. In chemistry however, one is most interested in the spatial distribution of the electrons. To determine the manner in which the exclusion principle affects the electron distribution and its properties in real space, one must determine how many pairs of electrons on the average contribute to the electron density over the region of interest. This information is given by the electron pair density, alternatively called the pair probability function.

2.7.1 The Pair Density

The electron density multiplied by an infinitesimal volume element, $\rho(\mathbf{r})d\mathbf{r}$, gives the number of electrons in $d\mathbf{r}$ and integrates to N, the total number of electrons. Similarly the product of the pair density with a corresponding pair of volume elements, $\rho(\mathbf{r}_1,\mathbf{r}_2)d\mathbf{r}_1d\mathbf{r}_2$, gives the number of electron pairs formed between these two elements and its double integration yields the number of distinct electron pairs, N(N-1)/2. The density of α-spin electrons at $\mathbf{r}_1$ is $\rho^{\alpha}(\mathbf{r}_1)$. The uncorrelated pair density for simultaneously finding α-spin density at $\mathbf{r}_1$ and $\mathbf{r}_2$ is given by the product $\rho^{\alpha}(\mathbf{r}_1)\rho^{\alpha}(\mathbf{r}_2)$. The correct correlated pair density, (Equation 39), is less than this everywhere and the Fermi hole, (Equation 40), determines the difference, which is a negative quantity, between the correlated and uncorrelated pair densities for same-spin electrons in a Hartree-Fock wavefunction[114,115].

$$\rho^{\alpha\alpha}(\mathbf{r}_1,\mathbf{r}_2) = (\tfrac{1}{2})\rho^{\alpha}(\mathbf{r}_1)\left[\rho^{\alpha}(\mathbf{r}_2) + h^{\alpha\alpha}(\mathbf{r}_1,\mathbf{r}_2)\right] \tag{39}$$

$$h^{\alpha\alpha}(\mathbf{r}_1,\mathbf{r}_2) = -\sum_{i}^{\alpha}\sum_{j}^{\alpha}\left[\varphi_i^{*}(\mathbf{r}_1)\varphi_i(\mathbf{r}_2)\varphi_j^{*}(\mathbf{r}_2)\varphi_j(\mathbf{r}_1)\right]\Big/\rho^{\alpha}(\mathbf{r}_1) \tag{40}$$

This difference is a measure of the degree to which density is excluded at $\mathbf{r}_2$ because of the spreading out of the same-spin density originating from position $\mathbf{r}_1$. Thus the Fermi-hole density determines the manner in which density at $\mathbf{r}_1$, in an amount equivalent to one electronic charge, contributes to the pair density at other points in space. Pictorially, one can imagine that as an electron moves through space, it carries with it a Fermi hole of ever changing shape, the density of the electron being spread out in the manner described by its Fermi hole and excluding an equal amount of same-spin density.

Since the charge of the electron is spread out in a manner described by the density of its Fermi hole, it follows that the quantum mechanical requirement for the localization of an electron to some particular spatial region in a many-electron system is that the density of its Fermi hole be totally and maximally contained within this region[116]. In this limiting situation, all other same-spin electrons are excluded from the region and, since the same behavior is obtained for an electron of opposite spin in a closed-shell system, the result is a spatially localized electron pair. The properties of the Fermi-hole density determine the local

extent of exclusion of same spin density, as demanded by Pauli's exclusion principle. In other words, an electron can go wherever its Fermi hole is different from zero and if the hole is localized, so is the electron.

2.7.2 Atomic Measures of Electron Localization and Delocalization

While displays of the Fermi-hole density are useful in determining its basic localized or delocalized nature relative to $\rho^{\alpha}(\mathbf{r})$, each display is for a single fixed position of the reference electron. What is needed is a measure of the extent to which some number of electrons is localized to a given spatial region. Bader and Stephens were able to show that the vanishing of the fluctuation in an electron population over a region of space, implying the complete absence of their exchange with any other electrons in the same system, requires that the Fermi hole for each of its electrons be totally contained within its boundaries. This work leads directly to the demonstration that the spatial localization of some number of electrons is determined by the corresponding localization of their Fermi-hole density[116].

Establishing the relation between the localization of the electron and the density of its Fermi hole leads to a direct physical measure of the extent to which some number of electrons are localized within the basin of a given atom. One first determines the total possible Fermi correlation contained within an atom Ω, a quantity denoted by $F^{\alpha\alpha}(\Omega,\Omega)$, and one readily determined at the Hartree-Fock level in terms of the products of overlap integrals of all pairs of orbitals over the basin of atom Ω.

$$F^{\alpha\alpha}(\Omega,\Omega) = \int_{\Omega} d\mathbf{r}_1 \int_{\Omega} d\mathbf{r}_2 \, \rho^{\alpha}(\mathbf{r}_1) h^{\alpha\alpha}(\mathbf{r}_1,\mathbf{r}_2) \tag{41}$$

If $N^{\alpha}(\Omega)$ electrons are completely localized within Ω, then the Fermi correlation attains its limiting value of $-N^{\alpha}(\Omega)$, that is, a corresponding number of same-spin electrons are excluded from Ω. The ratio $|F^{\alpha\alpha}(\Omega,\Omega)/N^{\alpha}(\Omega)|$ for electrons of either spin is thus the fraction of the total possible Fermi correlation per particle contained within a region Ω and this ratio, when multiplied by 100, is the per cent localization of the α electrons in atom Ω. Determining $F(\Omega,\Omega)$, the localization index for all electrons in Ω, is easily calculated for a Hartree-Fock wavefunction by adding the α-spin and β-spin delocalization indices for Ω:

$$F(\Omega,\Omega) = F^{\alpha\alpha}(\Omega,\Omega) + F^{\beta\beta}(\Omega,\Omega)$$
$$= -\sum_{ij}^{\alpha} S_{ij}^2(\Omega) - \sum_{ij}^{\beta} S_{ij}^2(\Omega) \quad (42)$$

where $S_{ij}(\Omega)$ is the overlap of the spin orbitals φ_i and φ_j over the region Ω. Extensive investigation of the contained Fermi correlation has shown that aside from core regions, electrons are not in general spatially localized to yield individual pairs[102,116]. It is possible, however, for some number of pairs of electrons to be spatially localized within an atomic basin in ionic systems. In NaF and MgF for example, the populations of the fluorine atoms approach the limiting value of 10 for a filled shell system and the localizations are in excess of 95%. Correspondingly, the quantity $F(\Omega,\Omega')$, involving products of orbital overlaps for both atoms, determines the extent to which the Fermi holes of the electrons in one atomic basin Ω are delocalized over another basin Ω', that is to say, it determines the extent of exchange of electrons between two atoms, a quantity that clearly provides a physical measure of their bond order[117].

$$F(\Omega,\Omega) + \sum_{\Omega' \neq \Omega} F(\Omega,\Omega') = -N(\Omega) \quad (43)$$

As Equation 43 indicates, $F(\Omega,\Omega)$ plus all $F(\Omega,\Omega')$ also yields $-N(\Omega)$, as all the electrons of atom Ω are accounted for, both localized and delocalized. It has been proposed that the spatial distribution of the Fermi-hole density as measured by $F(\Omega,\Omega')$ be used to provide a common, quantitative basis for the concept of electron delocalization, as it is used throughout chemistry[118].

The general conclusion drawn from the spatial pairing exhibited by the pair density in many-electron systems is that aside from core regions, the density is not characterized by the presence of strongly localized pairs of electrons. This observation is not at variance with the possibility of obtaining an equivalent description of a system by a transformation to a set of localized molecular orbitals, the pair density and its properties, as discussed above, being invariant to the required unitary transformation. Maximizing the contained Fermi correlation for a region Ω requires that each of the orbitals be localized to a separate spatial region Ω so that the overlap of the orbitals between two different regions vanishes. Thus, to achieve localization of N electrons into N/2 distinct spatial pairs requires that each orbital be separately

and completely localized to one of N/2 spatially distinct regions. While orbitals can appear localized in their displays, they actually exhibit a considerable degree of absolute overlap and they fail to satisfy the requirement of separate localization. This must be the case for the properties determined by the pair density. The ability to define a set of doubly occupied localized molecular orbitals does not imply physical localization of the electrons into spatial pairs. In ionic systems, even the canonical set of orbitals is strongly localized to the separate atomic basins, yielding atomic sets of localized electrons. If the canonical set is not localized, a unitary transformation to a localized set will leave the properties of the pair density and its predicted lack of electron pairing unchanged.

While the spatial pairing of electrons is not as extreme as was once perhaps pictured, there is no doubt that the extent of pairing of electrons throughout space is an important property of a system. The laplacian of the electron density, the subject of the following section, provides this information.

2.7.3 The Lewis Model and the Laplacian of the Electron Density

The topology of the electron density, while providing a faithful mapping of the concepts of atoms, bonds and structure, does not give any indication of the bonded and non-bonded electron pairs anticipated on the basis of the Lewis model[102,119]. However, as is well documented, the topology of the laplacian of the electron density, the quantity $\nabla^2\rho(\mathbf{r})$, does provide a physical basis for the Lewis model. The laplacian of a scalar field such as $\rho(\mathbf{r})$ determines where the field is locally concentrated and depleted. If $\nabla^2\rho(\mathbf{r}) < 0$, the value of $\rho(\mathbf{r})$ is greater than the average of its values in the immediate neighborhood of the point $\mathbf{r}$, and $\rho(\mathbf{r})$ is locally concentrated at $\mathbf{r}$. If $\nabla^2\rho(\mathbf{r}) > 0$, the reverse is true and $\rho(\mathbf{r})$ is locally depleted at $\mathbf{r}$. The corresponding local minima and maxima provide features that are absent from the topology of $\rho(\mathbf{r})$ itself. Since electronic charge is concentrated in regions where $\nabla^2\rho(\mathbf{r}) < 0$, it is convenient to define the function $L(\mathbf{r}) = -(1/4)\nabla^2\rho(\mathbf{r})$. A maximum in $L(\mathbf{r})$ then denotes a position at which the electron density is maximally concentrated; the (1/4) is included to retain consistency with instances where the laplacian appears, such as in Equations 22 and 23. Empirically, one finds that the local maxima in $L(\mathbf{r})$ provide a remarkably faithful mapping of the localized electron domains that are assumed to be present in the valence shell of the central atom in the VSEPR model of molecular geometry[120]. Not only is there a one-to-one correspondence in their

number, but of equal importance, in their angular orientation within the valence shell of the central atom and in their relative sizes.

2.7.4 The Topology of L(r)

The typical pattern of electron localization revealed by the topology of L(r) is illustrated in Figure 13.

Figure 13: Relief Maps of Rho and Laplacian of Argon

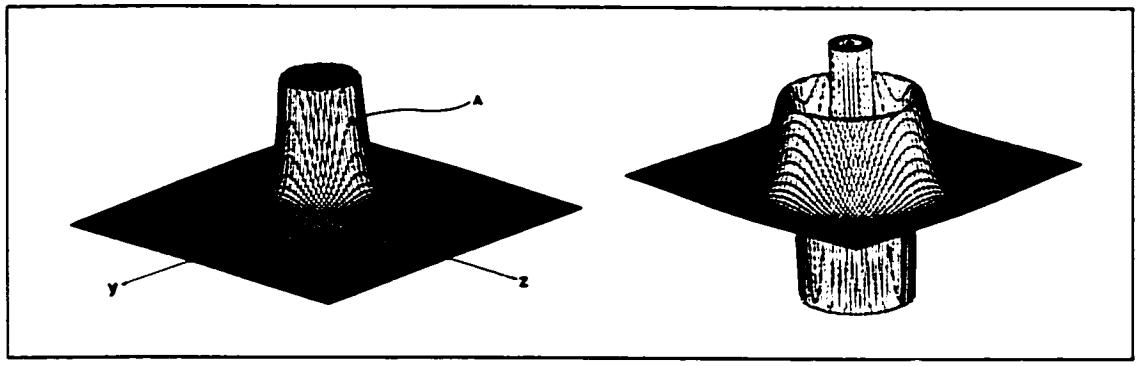

L(r) exhibits a shell structure wherein each shell is characterized by a shell of charge concentration, (which appears as a spike at the position of the nucleus for the inner shell), followed by one of charge depletion; such behavior is characteristic of elements with $Z < 40$. This property of L(r) enables one to identify the shell of interest.

The same topological analysis applied to ρ(r) can be applied to the critical points found in the outer shell of charge concentration of L(r), the valence shell charge concentration, (VSCC), of a main group element. The local maxima or (3,-3) critical points, whose presence denotes a bonded or non-bonded charge concentration, (CC), are linked one to another by the unique pair of trajectories that originate at an intervening (3,-1) critical point. This generates the atomic graph, the analogue of the molecular graph defined by the corresponding set of critical points in ρ(r). The atomic graph, in general, assumes the form of a polyhedron bounding the nucleus in question.

Figure 14: Sample Atomic Graphs: Methane and Formaldehyde

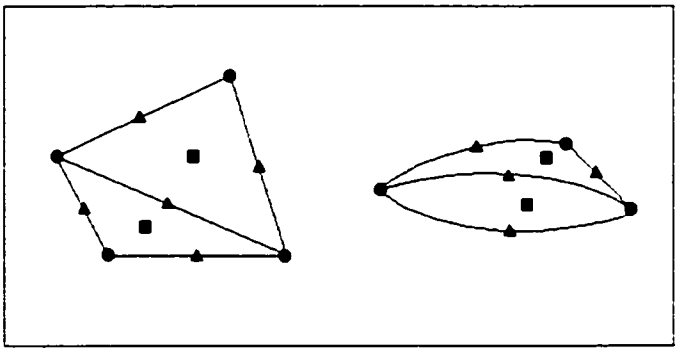

Figure 14 shows the shapes of atomic graphs typically found in the VSCCs of molecules; the circles denote maxima, the triangles, (3,-1) critical points, and the squares, (3,+1) critical points. The structure on the left is typical of a tetrahedral AX_4 molecule such as methane; there are four maxima surrounding the carbon, one lying in each C-H bond, six (3,-1) critical points forming the edges of the tetrahedron, and four (3,+1) critical points lying in the faces of the tetrahedron. Note: only the front of the tetrahedron is visible, for clarity. The structure on the right is typical of a planar AX_2Y molecule such as formaldehyde. The maximum on the left lies in the C=O bond, and the two maxima on the right lie in the C-H bonds. The C=O maximum is linked to each C-H maxima by two (3,-1) critical points, with a (3,+1) critical point in each 'face' thus formed. The C-H maxima are linked by one (3,-1) critical point. The three (3,-1) critical points above and below the maxima plane form the face of two more (3,+1) critical points. The Poincaré-Hopf relationship for the critical points defining an atomic graph is then readily transformed into the more familiar polyhedral formula of Euler.

$$V - E + F = 2 \tag{44}$$

The vertices are defined by the (3,-3) critical points or maxima in $L(\mathbf{r})$, the edges by the unique pairs of trajectories that originate at (3,-1) critical points and terminate at neighboring vertices, while the (3,+1) or ring critical points define the resulting faces of the polyhedron.

2.7.5 The VSEPR Model and L(r)

The $L(\mathbf{r})$ relief map for H_2O in the plane of the molecule and the included 'lone pairs' is illustrated in Figure 15. The relief maps of $\rho(\mathbf{r})$ of both planes, (on the left), show no details that can be associated with

bonded or non-bonded charge concentrations. One can see in the plots on the right, however, the bonded charge concentrations sitting in the O-H bond paths, and the non-bonded charge concentrations in the perpendicular plane in $L(\mathbf{r})$.

Figure 15: Rho and Laplacian Relief Maps of Water

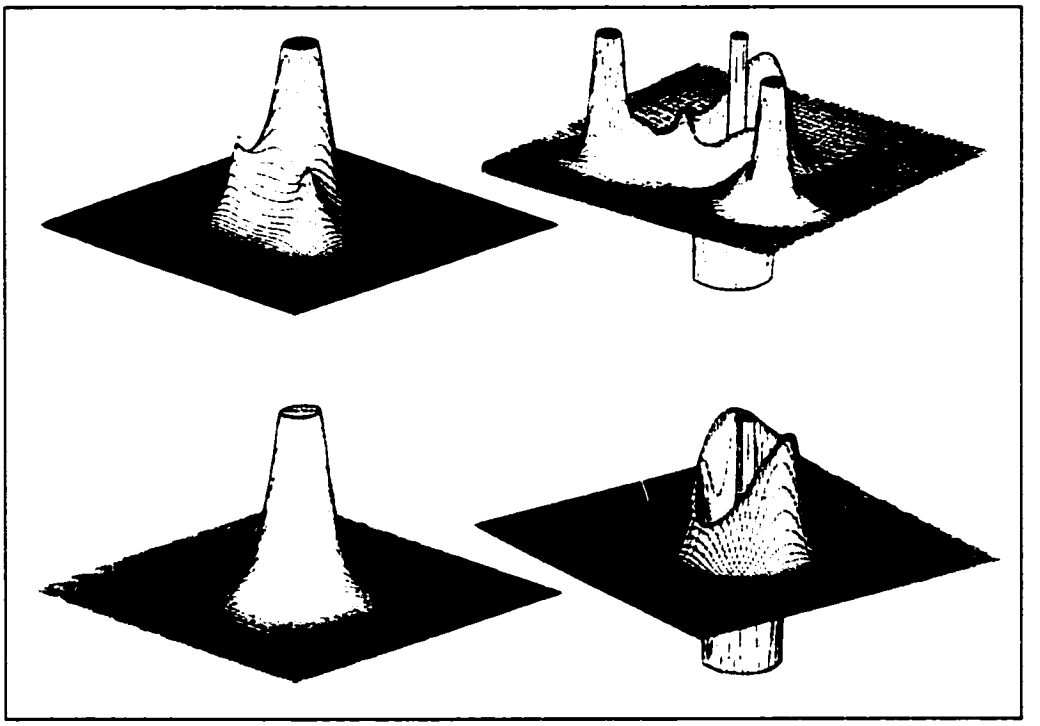

These non-bonded charge concentrations are much larger laterally than the bonded charge concentrations, and thus they spread out, pushing the bonded charge concentrations closer together. As a result, water has a bond angle of 103.8°, as opposed to the ideal tetrahedral angle of 109.5°.

This correspondence of the VSEPR model with the topology of L(r) is found for all molecules containing main group elements, the same systems whose geometries are correctly predicted by the VSEPR model. One may make the assumption that the pattern of local charge concentrations defined by the laplacian of the electron density denotes a corresponding pattern of partial condensation of the electron pair density to yield regions of space dominated by the presence of a single pair of electrons. While the condensation is less than complete, the laplacian provides a map of those regions where electron pairing is dominant throughout the electron density distribution. The physical basis of this correspondence is

strengthened by recent work which shows that the L(r) function is isomorphic with the laplacian of the conditional pair density, a density that shows where same-spin density accumulates when a reference electron is fixed at a given position[114].

2.7.6 L(r) and Atomic Reactivity

The properties of L(**r**) reproduce not only the geometrical aspects of the Lewis model, but also his definition of an acid-base reaction. A non-bonded CC is a Lewis base, serving as a nucleophilic center, while a ring critical point, since it defines the point where electronic charge is least concentrated in an atomic graph, is a Lewis acid site, serving as an electrophilic center. L(**r**) is usually negative at a ring critical point and this corresponds to the presence of a "hole" in the VSCC of the acid, that is, in a face of the polyhedron representing its atomic graph. A Lewis acid-base reaction corresponds to aligning a CC on the base with a "hole" on the acid, the alignment of the two critical points providing a guide to their relative angle of approach.

Figure 16: Contour and Relief Maps of L(r) of Methane and Fluoromethane

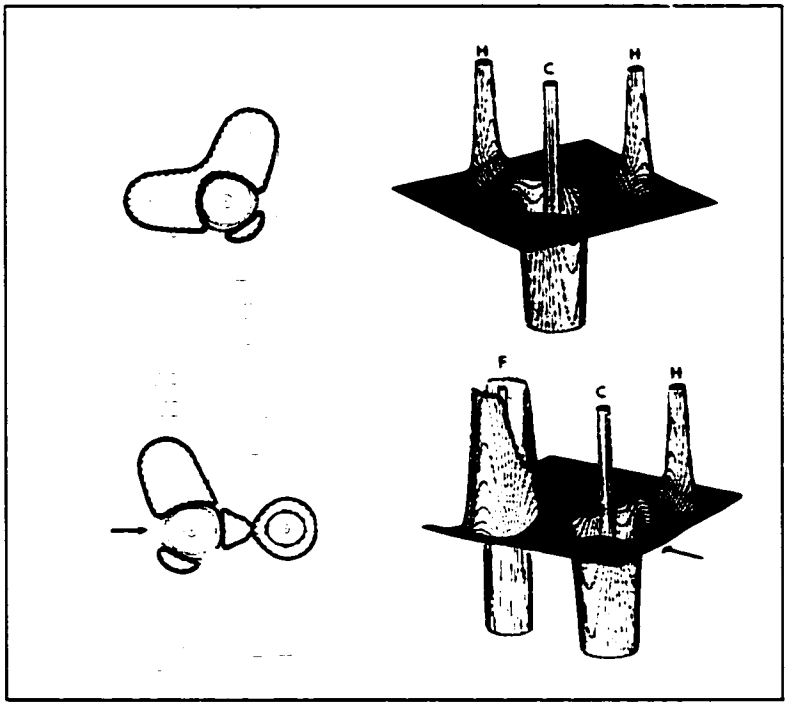

Figure 16 shows the L(r) relief maps of methane and fluoromethane; both molecules have maxima that lie on the C-H and C-F bond paths, and ring critical points that are in the faces opposite the maxima. The value

of L(r) at the ring critical point of methane is –0.03 au; in fluoromethane, this value is –0.08 au for the point opposite the fluorine, and –0.04 au for the other points. As the value of L(r) indicates greater local depletion of the electron density as the value becomes more negative, the fluoromethane preferred attack point is more attractive to a nucleophile than the (3,+1) points on methane; this, combined with the relative charges on carbon, (+0.18 au for methane, +0.77 au for fluoromethane), allows one to predict that fluoromethane will be more reactive to nucleophilic attack than methane. This same process can be applied to systems that undergo electrophilic attack, except that one looks for maxima in L(r).

2.8 Molecular Excitation

The concept of quantum mechanics evolved at the turn of the century, when Planck hypothesized that the absorption and radiation of energy by matter was not continuous, but occurred in finite amounts, or quanta. This idea was applied to molecular systems by Bohr, who used the principle of quantization to explain why the emission spectra of hydrogen consisted of distinct sharp frequencies. Bohr postulated that the angular momentum of electrons in atoms is quantized, and that the absorption and emission of light results in the electrons moving from one energy state to another. The idea of atoms or molecules absorbing or emitting light of specific energies in order to proceed from one state to another was next taken up by Einstein, who postulated that light also existed in quantized packets, or photons; this concept forms the entire basis of spectroscopic theory. Through quantum mechanics, one can calculate the energy states of the electrons in a molecule, and from that determine the electronic excitation energies of that molecule. However, not all of the possible excitations are actually observed: to predict which of these excitations are 'allowed', one must develop a selection rule for the transitions one wishes to study[121]. For electronic dipole transitions, the probability of finding a molecule entering a state k from a state n is proportional to the square of the transition dipole moment μ_{nk}:

$$\mu_{nk} = \int \Psi_k^* \mu \Psi_n d\tau = \int \Psi_k^* (-er) \Psi_n d\tau \qquad (45)$$

where μ is the dipole operator acting on Ψ_n and Ψ_k. This dipole has components in the x, y, and z directions. If the product of Ψ_n and Ψ_k has an irreducible symmetry representation that contains one of these components, then that transition is allowed.

2.8.1 Transition Intensity

The intensity of a transition can be determined from Beer's law, A = εbc, where b is the path length in cm, c is the molarity of the solution being studied, and ε is the molar absorptivity, (A is a unitless value). For a given absorption observed for a species, it is common practice to state the molar absorptivity at the wavelength in the absorption band where the intensity is greatest. This wavelength is usually the one given as λ_{max}. One can also express the intensity of an absorption by integrating the molar absorptivity over the entire excitation band:

$$I = \int \varepsilon(\upsilon) d\upsilon \tag{46}$$

where the I is in units of $L \cdot s^{-1} \cdot cm^{-1} \cdot mol^{-1}$ or $L \cdot cm^{-2} \cdot mol^{-1}$, depending on how the frequency is expressed. Assuming a Boltzmann distribution for the absorption band, one can relate the integrated intensity to the square of the transition dipole:

$$I = \frac{8\pi^3 N}{3000hc} \upsilon_{nk} |\mu_{nk}|^2 \tag{47}$$

where ν_{nk} is the frequency at the center of the absorption band. This integrated intensity is related to another term used to describe the transition intensity, the oscillator strength. While the integrated intensity is a measure of the intensity for a solution, the oscillator strength is the intensity of transition for a single atom or molecule. The expression thus developed takes the ratio of the observed integrated intensity versus the intensity of an electronic transition for a harmonically bound electron[122]:

$$f = \frac{\int \varepsilon(\upsilon) d\upsilon}{Ne^2/1000c^2m} = \frac{\int \varepsilon(\upsilon) d\upsilon}{2.31 \times 10^8} = 4.33 \times 10^{-9} \int \varepsilon(\upsilon)\ d\upsilon \tag{48}$$

where c is the speed of light, m is the mass of an electron, N is Avogadro's number, and e is the charge of an electron. The oscillator strength for this equation is unitless.

2.8.2 Transition Density and Transition Dipole

For a given transition from state *n* to state *k*, the probability for the transition taking place is the square of the amplitude connecting the corresponding state functions via a dipole operator:

$$P_{nk} = |\boldsymbol{\mu}_{nk}|^2 = N\left[\int d\tau \Psi_n^* (-er) \Psi_k\right]^2 \tag{49}$$

This transition probability can also be expressed in terms of a transition density[123]:

$$\begin{aligned} P_{nk}(r) &= \mu_{nk} \cdot \mu_{nk}(r) = \mu_{nk} \cdot (-e\ \ r)\rho_{nk}(r) \ \ \textit{where} \\ \rho_{nk}(r) &= N\int d\tau' \left(\Psi_n^{(0)*}\Psi_k^{(0)} + \Psi_k^{(0)*}\Psi_n^{(0)}\right)/2 \end{aligned} \tag{50}$$

This density describes how the mixing in of state *k* changes state *n*, and integrates to zero. Partitioning this density requires an understanding of perturbation theory for an open system.

2.8.3 Perturbation Theory for an Open System

The first-order correction to the energy of an open system in a state described by the wave function $\Psi_n^{(0)}$ resulting from the application of a perturbation $\hat{H}'$ to the total system, is the open system average of the perturbation over the zero-order wave function $\Psi_n^{(0)}$, as given in Equation 51:

$$E_n^{(1)}(\Omega) = \left\langle \Psi_n^{(0)} \middle| \hat{H}' \middle| \Psi_n^{(0)} \right\rangle_\Omega = N\int_\Omega dr \int d\tau' \left(\Psi_n^{(0)*} \hat{H}' \Psi_n^{(0)}\right) = \int_\Omega dr\, H_n^{(1)}(r) \tag{51}$$

The mode of integration indicated by $d\tau'$ yields a dressed property density for the first-order perturbation, as indicated by the quantity $H_n^{(1)}(r)$ in the final term of Equation 51. The corresponding contribution from the basin of the atom to the second-order correction to the energy is

$$\begin{aligned} E_n^{(2)}(\Omega) &= \left\langle \Psi_n^{(0)} \middle| \hat{H}' \middle| \Psi_n^{(1)} \right\rangle_\Omega \\ &= N\int_\Omega dr \int d\tau' \left(\Psi_n^{(0)*} |\hat{H}'| \Psi_n^{(1)} + \Psi_n^{(1)*} |\hat{H}'| \Psi_n^{(0)}\right)/2 = \int_\Omega dr\, H_n^{(2)}(r) \end{aligned} \tag{52}$$

where $\Psi_n^{(1)}$ is the first-order correction to the wave function for state *n* and $H_n^{(2)}(r)$ is the second-order perturbation density. In addition to the contribution given by the integration of $H_n^{(2)}(r)$ over the basin of the open system given by $E_n^{(2)}$ in Equation 52, a surface term denoted by $E_{nS}^{(2)}(\Omega)$ can arise, resulting from the change in the surface of the open system caused by an accompanying first-order change in the electron density[102]. The first-order change in the density, expressed in terms of the transition density ρ_{nk}, is given by Equation 53.

$$\rho_n^{(1)}(r) = \sum_{k \neq n} \left\langle \Psi_n^{(0)} \middle| \hat{H}' \middle| \Psi_k^{(0)} \right\rangle \left[E_n - E_k\right]^{-1} \rho_{nk}(r) \tag{53}$$

It is important to note that the matrix elements appearing in the coefficients for ρ_{nk} in Equation 53 are averaged over the total system, as required by the expansion of $\Psi_n^{(1)}$ in terms of the complete set of zero-order functions, while the atomic averaging of the perturbation densities $H_n^{(1)}(\mathbf{r})$ and $H_n^{(2)}(\mathbf{r})$ are resolved by reference to the zero-order interatomic surfaces.

2.8.4 Transition Probability

For the interaction of radiation with matter, the perturbation is given as $\hat{H}' = -N(e/mc)A(r)\bullet\hat{p}$, where A(r) is the vector potential, and $\hat{p}$ is the momentum operator for a single electron. If one makes the long wavelength assumption for the incoming radiation[124], the perturbation is proportional to $-\xi\bullet\mu_{nk}$, where μ_{nk} is the transition dipole derived through the integration of the transition density over the dipole operator, and ξ is a unit vector that points in the direction of A(r)[124]. The transition probability is usually expressed as the dot product of the transition dipole, as shown in Equation 50. When this probability is partitioned into atomic contributions, origin dependent terms develop; as with the electric dipole, these are dealt with by describing the transition dipole moment in terms of the first transition moment of each atom and the interatomic charge transfer terms. This results in the following equation:

$$\begin{aligned} P_{nk} &= \int dr P_{nk}(r) = \mu_{nk} \cdot \sum_{\Omega}\left[M_{nk}(\Omega) + q_{nk}(\Omega)X_{\Omega}\right] \quad \textit{where} \\ M_{nk}(\Omega) &= \int_{\Omega} dr(-e\,r_{\Omega})\rho_{nk}(r) \quad \textit{and} \quad q_{nk} = \int_{\Omega} dr\,\rho_{nk}(r) \end{aligned} \tag{54}$$

q_{nk} is the transition charge, (the negative value of the integrated transition density in Ω), and the vector $\mathbf{r}$ is replaced with $\mathbf{r}_{\Omega}+\mathbf{X}_{\Omega}$. As has been shown with the electric dipole moment, the interatomic charge transfer terms must themselves be rearranged, in order to remove the origin dependence, thus:

$$P_{nk}(\Omega) = \mu_{nk} \cdot \left[M_{nk}(\Omega) + \sum_{\Omega'}\left[X^{c}(\Omega|\Omega') - X_{\Omega}\right] q_{nk}(\Omega) \right] \tag{55}$$

It should be noted that the first term on the right side of Equation 55, (μ_{nk}), is the transition dipole for the entire system, whilst the bracketed term is for the region Ω. This second term represents the atomic contribution to the induced dipole discussed previously, and is a consequence of the application of

perturbation theory to an open system. While the transition probabilities are convenient, it is customary to express them in terms of the oscillator strength f_{nk}, (see Equation 48), expressed as

$$f_{nk}(\Omega) = \left(\frac{2}{3}\right)(E_k - E_n)P_{nk}(\Omega) \tag{56}$$

where the total oscillator strength is simply the sum of the atomic contributions.

3 Computational

During the course of this research, several computational programs and software packages were employed, and in some cases modified, to facilitate the study. The majority of these calculations were performed using Gaussian94™, an *ab initio* computation package[125]. This program provided not only the means to optimize molecular structures at either the Hartree-Fock level or beyond, but it also provided critical output in the form of an AIMPAC Wavefunction file. This file contained the data necessary to calculate the value of the electron density ρ at any point within the molecule under study. The calculation of ρ and other molecular properties were done using the AIMPAC software bundle, developed by the Bader group. It is this software that allows one to locate and obtain the properties of the critical points of ρ within a molecular wavefunction, and to integrate the property-weighted densities over the atomic basins within a molecule, such that their contributions to a molecular property can be calculated.

3.1 Electron Density Analysis

The general procedure for calculating the atomic contributions to the molecular properties of a wavefunction is as follows. Gaussian94 is first used to optimize the geometry of the subject molecule, using the desired basis set. The initial calculations in this research focused on an appropriate basis set for species containing silicon. It was found that a 6-311++G(2d,2p) basis set would be adequate for all the computations performed in these studies; higher level computations were found to provide minimal improvements to geometry and energy, given the additional computational costs. The polarization functions (2d,2p) were required to properly represent the strong polarizations in silane molecules, and the diffuse functions (++) were also required so as to enhance the diffuse valence density of silanes. The optimized geometries obtained at this basis set tend to have a computational error limit of 0.01 – 0.02 Å for bond lengths and 1.5° for bond angles, as is typical of calculations of this size[126]. The Gaussian94 calculation, once completed, generates a wavefunction file as part of its output. The next step is to analyze the topological features of the electron density field to locate the critical points within it. This is accomplished using the 'Extreme' program, developed by the Bader group, which locates and gives the properties of all

critical points within the wavefunction. The positions of these critical points are essential for the next step, integrating the atomic basins, using the Bader group program 'Proaimv'[127]. Once all the basins within the molecule are integrated, one then compares the sum of the contributions of each atomic basin to the number of electrons in the molecule, or the molecular energy. This ensures both that no significant integration errors have occurred, and also to gain a qualitative measure of the integration error.

3.2 Pair Density Analysis

A component of the integration is the atomic overlap matrix, which is used to calculate properties determined by the pair density for a given atom, (see Equations 41 and 42). The overlap matrices for all the atoms are processed via another program, 'Mmoments', (Bader group), which calculates an atomic Fermi correlation matrix. Elements of this matrix contain the number of alpha spin electrons localized within an atomic basin, as well as the number delocalized between pairs of atomic basins. This matrix also can be used to calculate the bond order between two atomic basins, which yields further information about the molecule's bonding properties.

3.3 Transition Density Analysis

Calculating the transition density for the excited state of a molecule requires a computational method beyond that of Hartree-Fock, which provides poor representations of excited state wavefunctions. There are many post-Hartree-Fock methods available for calculating excited states. For calculating the transition density, however, specific requirements had to be met, the most important being the ability to determine which orbitals were involved in the excitation. A single determinant excited state wavefunction, Ψ_k, would differ from the ground state wavefunction Ψ_n in that an occupied orbital ψ_a would be replaced with a virtual orbital ψ_r. The resulting wavefunction would thus provide a poor representation of the excited state molecule, even if the Hartree-Fock orbitals were reoptimized with respect to the new electron occupations, as such a wavefunction is more representative of an ionized state, rather than an excited state. The CI-Singles method corrects for this by considering all possible symmetry allowed determinants. Each determinant is given a weighting coefficient, and these coefficients are optimized to obtain the minimum energy of the excited state wavefunction[128]:

$$\Psi_k = \sum_i c_i \Psi_i^{ar} \tag{57}$$

where Ψ_i^{ar} is the ith Hartree-Fock wavefunction that has an occupied orbital ψ_a replaced with a virtual orbital ψ_r. This has the effect of 'softening' the excited state wavefunction, so that it properly represents an excited state. It is also advantageous for the purposes of this thesis, as one can then use the determinant coefficients and ground state Hartree-Fock orbitals to obtain the transition density.

$$\rho_{nk} = \sqrt{2} \sum_i c_i \psi_i^a \psi_i^r \tag{58}$$

The $\sqrt{2}$ factor is included to correct for the spin determinancy of ψ_a and ψ_r. When a CI-Singles calculation is performed, certain approximations can be made so as to minimize the computation time. One can specify, for example, a lower limit for the coefficients being optimized, which limits the calculation only to those determinants with a weighting greater than that minimum. Most software packages that perform CI-Singles calculations also limit the determinants used with respect to energy: any transitions from ψ_a to ψ_r that exceed a certain energy difference, (usually about 10-12 eV), will presumably have a negligible weighting in the final wavefunction, and are automatically discarded.

Calculating the transition density proved to be a challenge, for two reasons. Firstly, there was at that time no means of determining the transition density, requiring the software to be modified to yield this new property. Secondly, the data required for such a calculation could not be obtained from the standard computation packages such as Gaussian, requiring an alternative software package to be used for the research. This software was found in GAMESS, a freely distributed *ab initio* computation package available from the Gordon research group at Iowa State University[129]. This software proved invaluable for this segment of the research, as it provided the much needed data as part of its output, and, being a freely distributed program, could be modified as specifically required. For these calculations, GAMESS had to provide the following:

- the coefficients of each of the CI-Singles determinants, along with the specific orbitals involved,
- a wavefunction file that contained all the occupied and virtual Hartree-Fock orbitals that would be involved in the CI-Singles calculation.

GAMESS was modified to provide this particular data, as follows. Firstly, the PRCIVC subroutine within MTHLIB.SRC was modified to change the format of the data output for the CIS coefficients. This data was originally written to file in six decimal place floating-point format, which could result in computational errors due to loss of significant figures. The change in code resulted in the data being written to file in fourteen decimal place scientific format, which provided higher precision output. Secondly, modifications were made to the AIMPAC subroutine in PARLEY.SRC, because when a post-Hartree-Fock calculation such as CIS is performed with GAMESS, the wavefunction file output is that of the excited state, expressed as natural orbitals. This output was of no value in this research, as the calculation of the transition density requires the original, ground state Hartree-Fock orbitals, both occupied and virtual. To accomplish this, the file write commands within the AIMPAC subroutine were modified to give the ground state Hartree-Fock orbital data, as well as the ground state occupation numbers. With these changes, the required data for calculating the transition density became available. Finally, the subroutine SIGEND in STATPT.SRC was modified to ensure that the appropriate data was made available to PRCIVC, which is called from within SIGEND.

The changes to the AIMPAC software needed to calculate the transition density properties required an in-depth understanding of the program subroutines. This author then made the required modifications, which included adding variables for the CIS coefficient data and changing the output and property computation routines. The key subroutine needed by all of the programs was GETCIS, developed by the author and Dr. G. L. Heard. The GAMESS output alternates the spin determinants, so that all odd-numbered coefficients are ordered $\alpha\beta$-$\beta\alpha$, and all even-numbered coefficients are ordered $\beta\alpha$-$\alpha\beta$. The GETCIS routine was set up to test whether the coefficient was odd- or even-numbered, then switched the sign where appropriate to make all the coefficients $\alpha\beta$-$\beta\alpha$; the subroutine also determined which orbitals were involved in that determinant from the input, and listed the numbers with the coefficients.

Figure 17: Sourcecode From Program 'Tdproaim'

```
SUBROUTINE GETCIS
C
    IMPLICIT DOUBLE PRECISION (A-H,O-Z)
C
     PARAMETER(MCENT=50,MMO=500,MPRIMS=400,MPTS=1000)
    COMMON /CIS/ COEF(500),IOCC(500),IVIR(500),NOCSF
    COMMON /ORBTL/ EORB(MMO),PO(MMO),NMO
    DIMENSION JORB(MMO)
C
    READ (45,*) IO
    READ (45,*) IVO
    IO = IO - IVO
    DO 100 I=1,NOCSF
    READ (45,900) NCIS,COEF(I),(JORB(K), K=1,NMO)
    DO 90 J=1,NMO
    IF (JORB(J) .EQ. 1 .AND. IOCC(I) .EQ. 0) IOCC(I)=J+IVO
    IF (JORB(J) .EQ. 1 .AND. IOCC(I) .NE. J) IVIR(I)=J+IVO
90   CONTINUE
    NCIS=NCIS-1
    IPOS=NCIS-NCIS/IO*IO
    IF (IPOS.EQ.0) IPOS=IO
    IEVEN=IPOS-IPOS/2*2
    IF (IEVEN.EQ.0) COEF(I)=-COEF(I)
C
100  CONTINUE
    RETURN
900  FORMAT (I9,1PE22.14,2X,11011)
END
```

The remaining changes involved incorporating additional variables into the programs that would carry the transition density and transition dipole values. The transition density was calculated using a loop algorithm:

```
do 100  j = 1,noscf

        rhook(i) = rhook(i) + sqrt(2)*coef(j)*psi(i,iocc(j))*psi(i,ivir(j))

100   continue
```

where, for a position *i* within the array *rhook*, a loop is performed *nocsf* times, adding the *j*th weighted component, (via *coef(j)*), of the product of the values of the *j*th occupied, (*iocc(j)*), and virtual, (*ivir(j)*), orbitals at a given set of co-ordinates. In all cases, the overall algorithms of the programs were left as is, allowing the new variables to be carried along and computed.

With the software successfully modified and debugged, calculation of the transition dipole was achieved through the following protocol:

1. Starting with the optimized ground-state structure, perform a Gaussian94 CIS calculation, requesting data on the first *n* excited singlet states.

2. Given the transition dipole moment and oscillator strength data from step 1, study those excited states with non-zero oscillator strengths, and pick those states of interest, based on their symmetry and magnitude of oscillator strength. The values of these chosen states are retained as a check during the subsequent steps.

3. Perform a GAMESS CIS calculation on the same ground-state structure, choosing the desired excited state(s). The output of the calculation will provide the wavefunction file and the CIS coefficient data. An important time saving option is that of limiting the number of orbitals that are involved in the calculation. Excitation contributions involving core orbitals or high energy virtual orbitals are usually so small that they can be ignored, or frozen, without having any major effect on the final result.

4. Modify the GAMESS output file so that it contains only the CIS data of the desired excited state. Add to the beginning of the file two lines, the first being the number of occupied orbitals found in the wavefunction file, and the second the number of occupied orbitals that were set as frozen during step 3.

5. Calculate the critical points to be used for integration, using 'Extreme' and the wavefunction file produced in step 3. Note that as this wavefunction file is of the ground state, the resulting critical points, and zero-flux surfaces, will thus also be of the ground state.

6. Integrate over each atomic basin using the files generated in steps 3 and 4, and the critical points obtained in step 5. This will yield integrated transition densities and transition dipoles for all atomic basins in the molecule.

7. Calculate the atomic contribution to the molecular transition dipole moment using Equation 55, where $\mathbf{M}_\Omega$ is the calculated transition dipole of the basin being evaluated. The value $q(\Omega')$ is the transition charge, (the transition charge equals the negative of the integrated transition density), for all atomic basins other than the one being evaluated, that are linked to the evaluated basin by some critical point. $R^c(\Omega|\Omega')$ are the co-ordinates of those critical points linking basins Ω' to the evaluated basin, and R_Ω are the nuclear co-ordinates of the basin being evaluated.

When all atomic contributions are added together, one obtains the molecular transition dipole moment, which can then be cross-checked using Equation 54, where $\mathbf{M}_\Omega$ is the same as above, $q(\Omega)$ is the transition charge of the basin being evaluated, and R_Ω is the nuclear co-ordinates of the basin being evaluated. The oscillator strength of each atomic contribution to the transition dipole moment can be calculated using Equation 56, where ΔE is the excitation energy in au, μ_Ω is the transition dipole moment of the atomic basin Ω, and μ is the transition dipole moment of the entire molecule. These formulae make the transition dipoles and oscillator strengths for each atom additive, so that one can simply sum the atomic values to yield either the molecular oscillator strength or to find the contribution of a particular functional group.

4 Bond and Atomic Properties of Silicon and Carbon Compounds

The number, or electron, density provides a great deal of information about the molecule being studied. By studying the properties of the critical points of rho, one can determine the nature of the bonding between atoms. The integrated populations and energies of the atoms in the molecule give important information about the molecule's ability to attract nucleophiles or electrophiles. When this information is combined with data from L(r), both in terms of contour maps and critical points, one can obtain information about how the molecule reacts, and the relative reactivities of similar species.

4.1 Properties of MH_3-XH_n Series

The following series of simple molecular systems were calculated in order to ascertain the relative trends in chemical properties when a methyl or silyl group, MH_3, (M = C or Si), is bonded to an appropriately saturated functional group XH_n, where X is any second and third row element, as well as hydrogen. The properties of $MH3^+$, $MH3^\bullet$ and $MH3^-$ were also studied for further comparison. The series MH_2=XH_n was also calculated, where M = C or Si, and X = any second and third row element, in order to study the trend in bond properties of species containing double bonds. Given the ability of silicon to form hypercoordinate systems, the molecules $SiH5^-$, SiH_6^{2-}, SiF_4, SiF_5^- and SiF_6^{2-} were also studied for property trends.

4.1.1 Bond Properties of CH_3-XH_n

The general behavior that is studied for methyl compounds usually corresponds with the nature of the methyl group itself, and what form it takes: the methyl group can be cation-like, anion-like, or radical-like. The simplest way to study the nature of the methyl group is to look at its geometry, (see Table 3). By comparing the C-H bond lengths and H-C-X bond angles of different methyl compounds to isolated methyl species, one can gauge what type of methyl group is in the compound. (in Table 3 and subsequent tables, (HF) refers to results obtained from Hartree-Fock level calculations).

Table 3: Molecular Energies and Geometries of CH_3-XH_n Species (HF)

CH_3-X	E(HF) (au)	Bond Lengths (Å)			Bond Angles (°)			
		r(CX)	r(CH)	r(XH)	>(HCH)	>(HCX)	>(CXH)	>(HXH)
+	-39.2466		1.079		120.00			
rad.	-39.5764		1.071		120.00			
-	-39.5213		1.095		108.92			
H	-40.2123		1.082		109.47			
Li	-47.0349	1.984	1.091		106.25	112.53		
BeH	-54.8368	1.688	1.088	1.335	106.93	111.90	180.00	
BH_2	-65.4644	1.567	1.083	1.192	109.67	114.02	120.98	117.98
CH_3	-79.2573	1.524	1.084		107.68	111.21		
NH_2	-95.2517	1.453	1.082	0.997	107.40	109.35	111.08	107.80
OH	-115.0864	1.400	1.079	0.938	108.45	107.27	110.12	
F	-139.0891	1.363	1.080		110.12	108.81		
Na	-201.4244	2.338	1.088		107.70	111.19		
MgH	-239.7855	2.099	1.087	1.712	106.97	111.88	180.00	
AlH_2	-282.7014	1.961	1.085	1.582	108.32	112.40	120.67	118.66
SiH_3	-330.3172	1.878	1.084	1.477	108.08	110.83	110.54	108.38
PH_2	-381.5316	1.856	1.082	1.405	107.81	108.77	98.94	94.99
SH	-437.7478	1.820	1.079	1.325	109.02	106.29	98.10	
Cl	-499.1382	1.793	1.075		110.83	108.08		

The optimized geometries of the compounds listed in Table 3 agree with experiment, within the ±0.01 – 0.02 Å and ±1.5° computational error; Table 4 provides a direct comparison of experimental and calculated geometries, (references in parathenses).

Table 4: Comparison Between Experimental and Calculated Geometries of CH_3-X

	C-X Bond Length (Å)			C-X-H Bond Angle (°)		
	Exper.	Calc.	Diff.	Exper.	Calc.	Diff.
H	1.0919 (3)	1.082	0.010	109.5	109.47	0.03
CH_3	1.534 (5a)	1.524	0.010	110.0 (6)	111.21	-1.21
NH_2	1.474 (7)	1.453	0.021	112.3 (7)	111.08	1.22
OH	1.414 (8)	1.400	0.014	108.3 (8)	110.12	-1.82
F	1.383 (9)	1.363	0.020	--------	--------	--------
PH_2	1.863 (11)	1.856	0.007	97.3 (11)	98.94	-1.64
SH	1.819 (13)	1.820	-0.001	96.3 (13)	98.10	-1.80
Cl	1.781 (15)	1.793	-0.012	--------	--------	--------

The data in Table 4 shows that the molecular calculations do a good job of reproducing experimental results at the Hartree-Fock level. Typical experimental geometries, (derived from microwave spectroscopy)[130], have considerably lower error, usually ±0.001 Å and ±1°[131].

The geometries of the three 'standard' methyls shown in Table 3 change considerably as charge is added to the group. The C-H bond length of the methyl cation is 0.02 Å shorter than the methyl anion. This makes sense in the context of the carbon's reduced valence density: the hydrogens would be brought closer to the carbon, their density offsetting the reduced density of the carbon. It is the change in H-C-H bond angle, from 120° to 109°, that is the most striking difference. With the methyl carbon now experiencing excess charge on the carbon, and the hydrogens being effectively 'saturated' with electron density, (thus their longer bond length), the remaining excess valence density forms the classic lone pair predicted by VSEPR theory. By localizing the excess electron density of the carbon, the energy of the molecule is minimized. What is more surprising is the geometry of the methyl radical, which is more cation-like in bond length, (the C-H bond is actually shorter than in the cation), and bond angle. One would expect, given that there is a slight excess in valence density, that the radical would take on a more anion-like structure, though less pronounced than the methyl anion itself. This can be explained in terms of Fermi correlation: in the case of the anion, one has the equivalent of two electrons not involved in bonding with the hydrogens. These electrons will be of opposite spin, and would thus occupy the same region of space. As VSEPR theory predicts, a minimum energy structure results when this excess density is localized as a lone pair, minimizing the interaction of this density with the density involved in the C-H bonds. In the case of the radical, however, there is the equivalent of only one electron not involved in bonding. The Coulombic interaction between this one electron and the bonding density is reduced, and the energy gained by maximizing the distance between the C-H bonds dominates. The slightly shorter bond length in the methyl radical can be explained in terms of nuclear-nuclear interaction. In the methyl cation, there is less valence density than in the radical, and thus slightly more nuclear-nuclear repulsion that results in a slightly longer bond.

A comparison of the methyl compound geometries shows only anion-like or cation-like character in the methyl group. A clear trend is seen in the C-X bond length: as one proceeds along a periodic row, the bond length decreases. This can be explained in terms of the anionic or cationic character of the methyl group. With methyl lithium, one can treat the molecule as a methyl anion capped with a lithium cation, resulting in a relatively long bond. Methyl fluoride, which can be treated as a methyl cation capped with a

fluorine anion, will clearly be much shorter, as there is much less valence density between the carbon and the fluorine. In general, the bond length decreases quite rapidly at the electropositive end of a row, and shows a more gentle decrease as one approaches the electronegative end, indicating the relative insensitivity of the cation-like methyl group to increasingly electronegative groups. Another trend can be seen in the C-H bond lengths and H-C-X angles as the functional group element X changes. As one proceeds from lithium to fluorine, for example, the C-H bond also decreases from a length representative of a methyl anion to a length more representative of a methyl cation. The H-C-X angle also contracts, from 112° to 108°, indicating increased planar character in the methyl group.

The trends observed in the geometries should also be seen in the bond critical point data, and such is the case.

Table 5: Data of C-X Bond for CH_3-XH_n, in au (HF)

CH_3-X	r(CX)	r_b(C)	% r_b(C)	ρ_b	$L(r)_b$	ε
Li	3.754	2.443	65.15	0.045	-0.052	0.000
BeH	3.191	2.131	66.82	0.108	-0.063	0.000
BH_2	2.961	2.003	67.64	0.192	0.066	0.222
CH_3	2.881	1.440	50.00	0.250	0.153	0.000
NH_2	2.746	1.100	40.05	0.274	0.219	0.029
OH	2.646	0.858	32.43	0.266	0.086	0.005
F	2.576	0.819	31.78	0.241	-0.098	0.000
Na	4.418	2.550	57.71	0.036	-0.037	0.000
MgH	3.967	2.344	59.09	0.058	-0.065	0.000
AlH_2	3.705	2.243	60.54	0.089	-0.071	0.055
SiH_3	4.527	2.185	61.57	0.123	-0.039	0.000
PH_2	3.364	2.121	63.04	0.154	0.005	0.146
SH	3.440	1.633	47.47	0.177	0.064	0.097
Cl	3.387	1.428	42.15	0.178	0.062	0.000

The most obvious indication of the change from a cation-like to an anion-like structure is seen the carbon-BCP distance, shown in Table 5. The decrease in this distance as one proceeds along a row clearly indicates that the valence density between carbon and the element X is shifting from carbon to X, as X becomes more electronegative. The percentage of the bond length attributed to carbon shows clearly the shift from anionic to cationic character, when the value drops from greater than 50%, (anionic), to less than 50%, (cationic). It is interesting to note that the values only change by about 2-3% on each side of the trend: this may prove to be a clearer marker of methyl anionic and cationic character in the CH_3-XH_n series.

The values of ρ_b and L(r) at a BCP are strong indicators of the nature of the bond itself, and are summarized in Figure 18.

Figure 18: Rho and L(r) of C-X Bond in CH_3-XH_n, in au (HF)

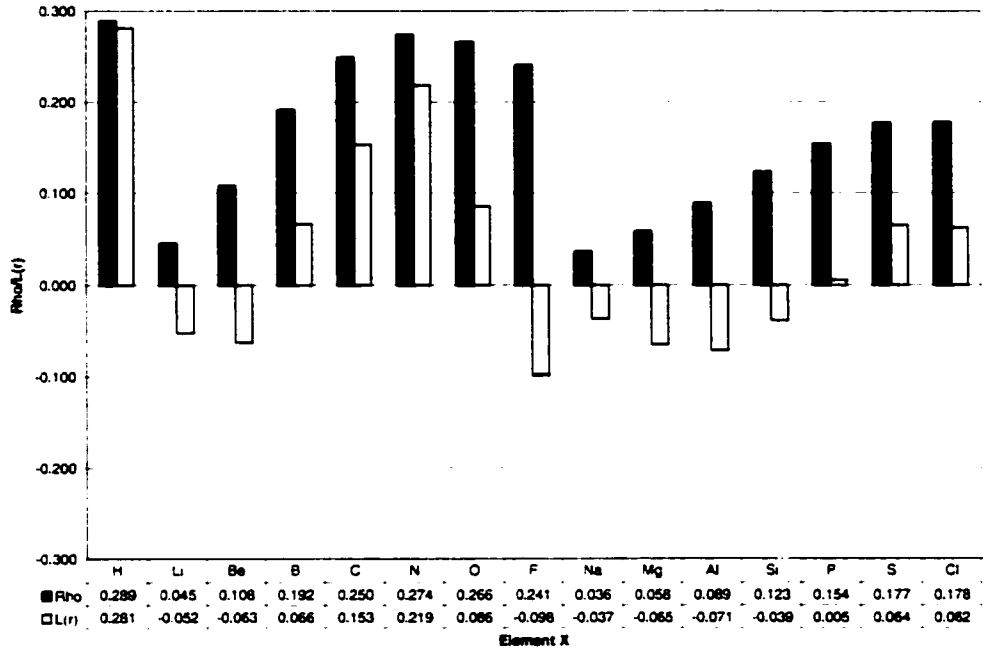

The value of ρ_b at a BCP provides a measure of the amount of electron density involved in a bond between two atoms, while L(r) indicates the type of bond. A positive L(r) is indicative of a covalent bond, when coupled with a value of ρ_b of 0.2 au or more. A negative L(r) indicates a more polarized bond, though the value of rho can still be relatively large. A value of ρ_b less than 0.2 au coupled with a negative and relatively small L(r) usually means that the bond has a great deal of ionic character. From these criteria, one can conclude that with the 2nd-row elements, the C-Li and C-Be bonds have the most ionic character, more so than the C-F bond. The remaining 2nd-row elements clearly form more covalent bonds, with the C-N bond appearing to have the most covalent character, in terms of electron density being localized in the bond, as opposed to the C-C bond. This, and the unexpectedly high amount of density in the C-B bond, can be explained by looking at the ellipticity of the BCPs: a value other than zero is usually indicative of some double bond character. This indicates that both the C-B and C-N bonds are being strengthened through a hyperconjugation mechanism, with density being donated by a C-H bond for the boron case, and the amine

lone pair in the nitrogen case. The trend in the 3rd-row elements is expectedly much different than the 2nd row. The switch from a bond with high ionic character to one that is more covalent comes much later in the row, consistent with the lower electronegativities of 3rd-row elements. The values of rho are also as a whole much lower, as is also expected from elements that will form much longer and more diffuse bonds.

The trends observed with the C-X bonds are also observed in the C-H BCP data shown on Table 6. While the differences in the C-BCP distances are much smaller, there are still notable trends that can be observed. In the case of the three 'methyls', the percentage of the length belonging to carbon decreases as one proceeds from a cation to a radical to an anion. While the C-H bond lengths only change by about 0.02 Å, clearly the BCP position changes radically; as more valence density is made available to the carbon, less density is taken from the hydrogens to compensate.

Table 6: Data of C-H Bond for CH_3-XH_n, in au (HF)

CH_3-X	r(CH)	r_b(C)	% r_b(C)	ρ_b	$L(r)_b$	ε
+	2.040	1.413	69.25	0.314	0.357	0.053
rad.	2.023	1.280	63.29	0.298	0.295	0.040
-	2.069	1.248	60.30	0.268	0.241	0.077
H	2.044	1.273	62.28	0.289	0.281	0.000
Li	2.062	1.254	60.79	0.272	0.246	0.065
BeH	2.056	1.269	61.75	0.277	0.255	0.046
BH_2	2.047	1.272	62.13	0.286	0.274	0.024
CH_3	2.040	1.271	62.30	0.291	0.283	0.008
NH_2	2.045	1.281	62.64	0.297	0.296	0.033
OH	2.040	1.291	63.32	0.303	0.309	0.046
F	2.041	1.300	63.69	0.306	0.313	0.059
Na	2.057	1.255	61.02	0.275	0.252	0.061
MgH	2.055	1.264	61.53	0.277	0.255	0.051
AlH_2	2.050	1.271	62.00	0.281	0.262	0.043
SiH_3	2.048	1.276	62.30	0.285	0.269	0.029
PH_2	2.091	1.281	61.27	0.286	0.263	0.008
SH	2.040	1.291	63.27	0.296	0.292	0.011
Cl	2.032	1.300	63.99	0.304	0.309	0.031

Also of note is the change in rho and L(r) between the three molecules. As more charge is put on the carbon, less is taken from the hydrogens. This results in a slight reduction in the density of the bond, consistent with its lengthening, as described previously. When these criteria are applied to the molecules bonded to 2nd- and 3rd-row elements, one sees the same trend observed in the geometries: the bond properties change from those of anion-like species to more cation-like species. It should be noted that none

of the BCPs of the C-H bonds have as much percent carbon length as the methyl cation, and at most have as much as the methyl radical. This is likely due to the fact that unlike the methyl cation, there is still a great deal of valence density remaining on the carbon even when an electronegative element is bonded to it. Unlike the geometries, there is a much smoother change in rho and the BCP position as one proceeds from cation to radical to anion, and this could prove a better measure of the methyl group's character than geometry.

The BCP data for the X-H bonds, shown on Table 7, are useful indicators of the role that the element X plays in the molecule, and whether it can be treated as an ionic species, or whether there is strong covalent bonding involved in the molecule.

Table 7: Data of X-H Bond for CH_3-XH_n, in au (HF)

CH_3-X	r(XH)	r_b(X)	% r_b(X)	ρ_b	$L(r)_b$	ε
BeH	2.522	1.086	43.05	0.096	-0.047	0.000
BH_2	2.252	0.956	42.43	0.184	0.061	0.265
NH	1.885	1.377	73.08	0.365	0.475	0.051
OH	1.773	1.447	81.60	0.402	0.784	0.025
MgH	3.235	1.649	50.97	0.054	-0.054	0.000
AlH_2	2.990	1.479	49.46	0.083	-0.062	0.037
PH_2	2.746	1.300	47.36	0.163	-0.025	0.148
SH	2.505	1.466	58.53	0.222	0.165	0.184

As can be seen in Table 7, electropositive elements such as Be and Mg form bonds with high ionic character with hydrogen as well as carbon, while nitrogen and oxygen form strong covalent bonds. This shows how the similarity in electronegativity of both carbon and hydrogen comes out quite clearly in the BCP data.

4.1.2 Atomic Properties of CH_3-XH_n

Equally as important as the bond properties are the integration properties, which describe the energies of each atom, as well as their populations. It has been observed in the BCP data shown earlier that carbon can take on significant charge density when the element X bonded to it is of lower electronegativity. As Table 8 shows, the methyl anion does retain significant charge on the carbon, holding more charge than the bonded hydrogens do. This demonstrates the relatively high capacity of carbon for holding valence density compared to hydrogen.

Table 8: Atomic Charges on CH_3-XH_n, in au (HF)

CH_3-X	q(C)	q(H[C])	q(CH_3)	q(X)	q(H[X])	q(XH_n)	q(tot)
+	0.217	0.261	1.000				1.000
rad.	-0.003	0.001	0.000				0.000
-	-0.406	-0.197	-0.998				-0.998
H	0.175	-0.044	0.044	-0.044		-0.044	0.000
Li	-0.559	-0.120	-0.919	0.916		0.916	-0.003
BeH	-0.711	-0.052	-0.868	1.728	-0.859	0.869	0.001
BH_2	-0.603	-0.043	-0.730	2.142	-0.712	0.717	-0.013
CH_3	0.184	-0.061	0.000	0.184	-0.061	0.000	0.000
NH_2	0.549	-0.045	0.414	-1.056	0.336	-0.384	0.030
OH	0.768	-0.022	0.703	-1.259	0.616	-0.643	0.061
F	0.773	-0.012	0.736	-0.736		-0.736	0.000
Na	-0.444	-0.119	-0.802	0.802		0.802	0.000
MgH	-0.583	-0.076	-0.810	1.621	-0.811	0.810	0.000
AlH_2	-0.650	-0.046	-0.787	2.376	-0.793	0.791	0.004
SiH_3	-0.628	-0.032	-0.723	2.924	-0.733	0.726	0.003
PH_2	-0.423	-0.024	-0.496	1.662	-0.582	0.497	0.001
SH	0.046	-0.003	0.036	0.151	-0.175	-0.024	0.012
Cl	0.254	0.018	0.307	-0.314		-0.314	-0.007

Compare this with the carbon populations of the methyl cation and methyl radical. In these cases, there is more of a balance in the sharing of valence density. The carbon of the methyl cation has slightly more density than the hydrogens, further illustrating carbon's ability to retain density in the molecule.

For the remainder of the methyl series, the charge on carbon varies quite substantially with the electronegativity of X, as shown on Figure 19. It is interesting to note how the charge on carbon is quite similar when that carbon is bonded to hydrogen or another carbon. With small negative charges on the hydrogens bonded to the carbon, (about –0.05 on average), it becomes clear why hydrocarbons are so unreactive: all the atoms are very similar in charge, leaving potential reagents nothing to attack. These large variations in the charge as X is varied, from –0.7 to +0.7, show the versatility of carbon in a variety of environments. Perhaps it is this ability to take on or lose valence density that illustrates why carbon became the principle element in organic molecules, being able to take on a number of biologically diverse roles.

Figure 19: Carbon Charges in CH_3-XH_n, in au (HF)

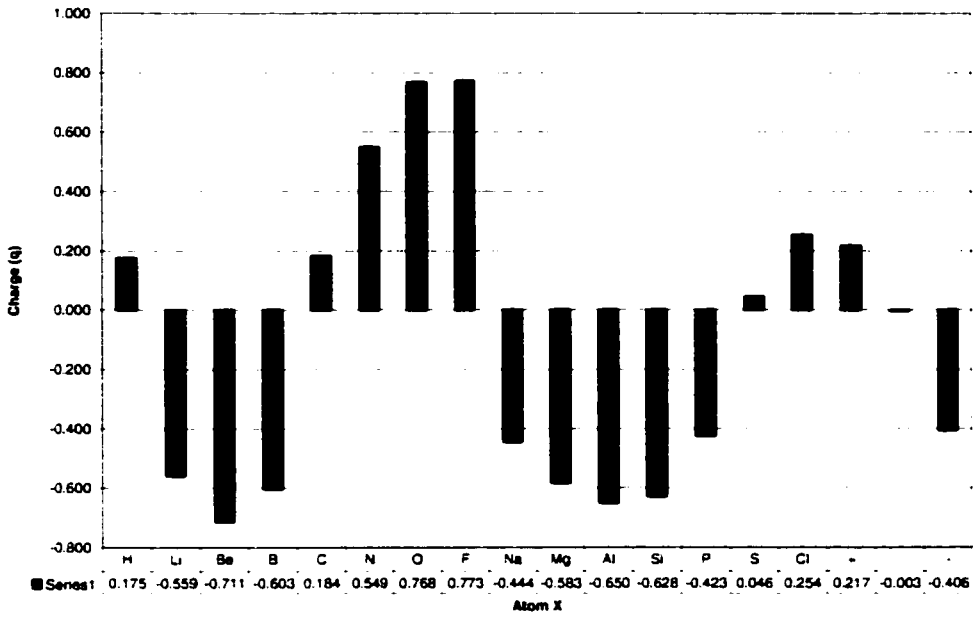

It is interesting to note how the charge of the hydrogens bonded to the carbon do vary only very little, even though the charge on carbon varies quite substantially. This further demonstrates the 'short-sighted' nature of atoms in molecules: the hydrogens only experience a small influence from X, even in the most extreme of cases.

The changes in atomic energy in the methyl series indicate the relative stabilizing or destabilizing effect of X on the carbon in the molecule. In the case of the three 'standard' methyls, it is interesting to note how the energy of carbon does not change significantly between the carbon cation and the carbon radical. What does change instead is the energy of the hydrogen: the addition of another electron to a methyl cation results in a net stabilization of the hydrogens. If another electron is added, the hydrogens are further stabilized, with a destabilization of the carbon.

Table 9: Atomic Energies on CH_3-XH_n, in au (HF)

CH_3-X	E(C)	L(C)	E(H[C])	L(H[C])	E(X)	L(X)	E(H[X])	L(H[X])
+	-37.7162	-0.00007	-0.5101	0.00002				
rad.	-37.7148	-0.00012	-0.6205	0.00005				
-	-37.5227	0.00068	-0.6663	0.00007				
H	-37.6593	-0.00013	-0.6383	0.00006				
Li	-37.7007	-0.00498	-0.6532	0.00006	-7.3739	0.00013		
BeH	-37.9309	-0.00018	-0.6318	0.00006	-14.2480	0.00041	-0.7625	-0.00004
BH_2	-38.0462	-0.00007	-0.6375	0.00008	-23.7692	-0.00049	-0.8766	0.00002
CH_3	-37.6721	-0.00005	-0.6522	0.00008	-37.6721	-0.00005	-0.6522	0.00008
NH_2	-37.4781	-0.00062	-0.6520	0.00008	-54.8012	-0.00034	-0.5025	0.00007
OH	-37.3216	0.00017	-0.6467	0.00008	-75.4499	0.00000	-0.3534	-0.00002
F	-37.3203	0.00034	-0.6439	0.00007	-99.8373	0.00007		
Na	-37.6513	-0.00009	-0.6538	0.00006	-161.8117	0.00009		
MgH	-37.7801	-0.00032	-0.6407	0.00007	-199.4335	0.00012	-0.6499	-0.00002
AlH_2	-37.8938	-0.00018	-0.6325	0.00007	-241.4384	0.00043	-0.7372	-0.00001
SiH_3	-37.9626	0.00010	-0.6305	0.00008	-288.0500	0.00244	-0.8046	0.00004
PH_2	-37.8935	-0.00138	-0.6329	0.00008	-340.1185	0.00086	-0.8091	0.00010
SH	-37.6902	-0.00087	-0.6294	0.00008	-397.4886	-0.00031	-0.6702	0.00012
Cl	-37.5955	-0.00662	-0.6270	0.00007	-459.6593	-0.00160		

The data provided in Table 9 describes both the energy of each atom in the molecule, but also the quality of each integration, as indicated by the $L(\Omega)$ values. As Equations 23 and 24 showed, $L(\Omega)$ should equal zero for an open system bounded by a zero-flux surface, and the values of $L(\Omega)$ thus provide a measure of how well the atomic basin was integrated. From Table 9, one can see that the overall trend in carbon stability is as follows: if carbon has a negative charge, it is stabilized. Loss of valence density from carbon has the effect of destabilizing it. In all cases, the energy of the methyl hydrogens do not change significantly, just as was seen in the atomic charges. Table 10 provides an overall measure of the quality of the integrations over and above the $L(\Omega)$ values, by comparing the total molecular energy with the sum of the integrated atomic energies. All errors in energy are within acceptable limits, having errors of about 0.03% in the worst cases. Those molecules with the highest error tend to be those that appeared to have some significant π-bond character in the C-X bond. The deformations in the C-X interatomic surface that result in the change in bonding may be the cause of the higher error.

Table 10: Error Between Summed Atomic Energies and Molecular Energies for CH_3-XH_n, in au (HF)

CH_3-X	E(tot.)	E(mol.)	diff(E)
+	-39.2466	-39.2466	0.0000
rad.	-39.5764	-39.5764	0.0000
-	-39.5216	-39.5213	-0.0003
H	-40.2124	-40.2123	-0.0001
Li	-47.0341	-47.0349	0.0007
BeH	-54.8369	-54.8368	-0.0001
BH_2	-65.4812	-65.4644	-0.0168
CH_3	-79.2574	-79.2573	-0.0001
NH_2	-95.2402	-95.2517	0.0115
OH	-115.0651	-115.0864	0.0214
F	-139.0893	-139.0891	-0.0002
Na	-201.4245	-201.4244	-0.0001
MgH	-239.7855	-239.7855	0.0000
AlH_2	-282.7041	-282.7014	-0.0026
SiH_3	-330.3180	-330.3172	-0.0008
PH_2	-381.5289	-381.5316	0.0027
SH	-437.7371	-437.7478	0.0107
Cl	-499.1357	-499.1382	0.0025

4.1.3 L(r) Properties of CH_3-XH_n

While BCP data provides clear information about the bonding within a molecule, the chemical reactions that molecule can undergo can be illustrated with contour plots of L(r)[132]. Four examples from the CH_3-XH_n series will be used: CH_4, CH_3-Li, CH_3-CH_3, and CH_3-Cl. The positive contour lines of L(r), (solid lines), indicate regions where the electron density is maximally concentrated, while the negative contour lines, (dashed lines), show regions of maximal depletion. An atomic graph can be generated from the critical points in the VSCC of the central atom, forming a polyhedral structure. A nucleophile, rich in electron density, would be attracted to a region containing an area of depletion in L(r), while an electrophile would be attracted to a region containing an area of concentration in L(r). The extent to which a nucleophile is attracted to depletions in different molecules depends on the size of the 'hole' in L(r), corresponding to a face of the polyhedron, and the value of L(r) at the (3,+1) critical point within the hole, as well as the respective charges of the atoms involved. Electrophilic attraction depends on the magnitude of the maximum in L(r), corresponding to a vertex in the polyhedron.

Methane is the simplest example of the carbon-based molecule, and as such is a good example for understanding the electronic structure of any of the methyl series.

Figure 20: L(r) Map of Methane (HF)

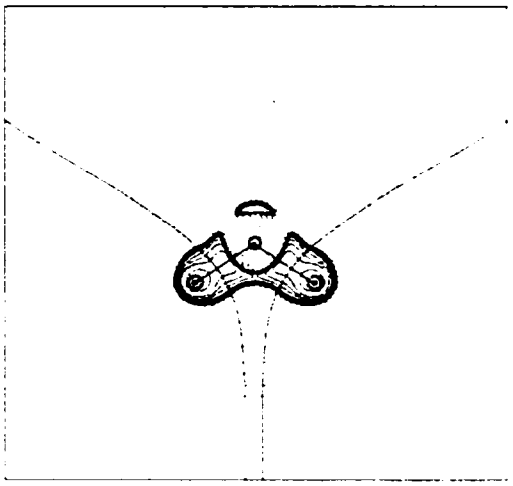

The plot of L(r) shows that the VSCC surrounding carbon contains a substantial amount of electron density, the critical points of which form a tetrahedral atomic graph that will be observed throughout this thesis. The areas of depletion in L(r) opposite the hydrogens are relatively small. At these 'holes' in L(r), one can find (3,+1) critical points in L(r): the value of L(r) at these points is –0.028 au. With a charge on carbon of 0.175 au, it is expected that only a very strong nucleophile would be attracted to these regions of charge depletion. In most cases, reagents such as strong bases are more likely to deprotonate the methyl group rather than perform a nucleophilic attack[133].

Methyl lithium is a good example of a species with an anionic methyl group, as it is known to be a powerful base and nucleophile. The L(r) plot of CH_3Li shows that there is no 'hole' at the face opposite the lithium, and is thus not attractive to a nucleophile. The value of L(r) at the (3,+1) critical point is +0.016 au, indicating some charge concentration at this point. With a charge on carbon of –0.559, nucleophiles will not attack at this point, or at any of the small charge depletions opposite the hydrogens. The value of the L(r) at these other points is -0.011, a smaller value than seen in the relatively neutral methane. An electrophile, however, would attack the charge concentration between the carbon and lithium: there is a maximum in L(r) here, with a value of +0.203 au.

Figure 21: L(r) Map of Methyllithium (HF)

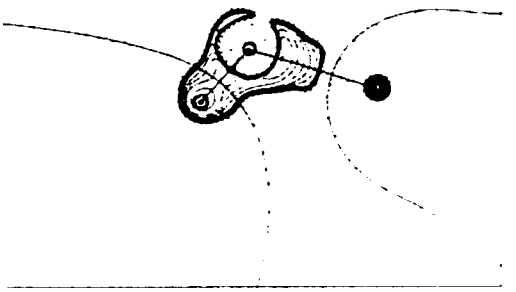

Ethane is another neutral molecule, like methane. Since the electronegativities of hydrogen and carbon are quite similar, as are the integrated charges on carbon for both species, one expects the regions of charge depletion to be similar in properties as well.

Figure 22: L(r) Map of Ethane (HF)

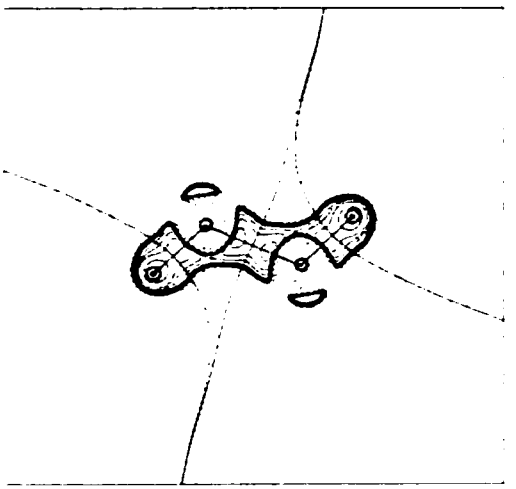

The L(r) plot shows that the areas of charge depletion are quite similar in size, despite having very different atoms in opposition to them. The (3,+1) critical point in the face opposite a carbon atom has an L(r) value of –0.035 au, while the point in the face opposite a hydrogen atom has an L(r) value of –0.029, a value nearly identical to that of methane. This indicates that the position opposite the methyl group is very

slightly more attractive for nucleophilic attack, but with the small charge on carbon in this species (0.184 au), attack at either position is still unlikely.

Methyl chloride is a good example of a species containing a cationic methyl group, as it is known to undergo facile nucleophilic attack.

Figure 23: L(r) Map of Methyl Chloride (HF)

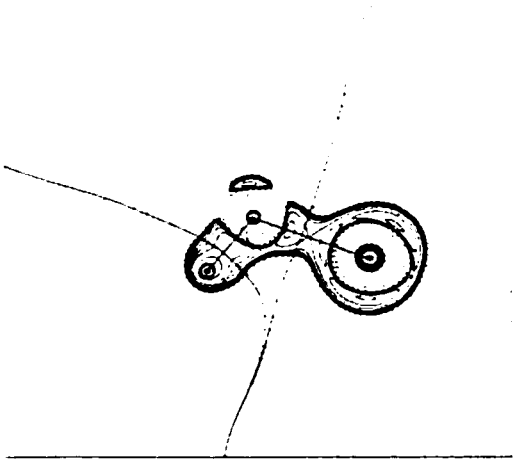

Unlike the examples of methane and ethane, the charge depletion opposite the chlorine is quite a bit larger. One can also see that the geometry of the methyl group is more planar than the other examples, implying more cationic character in the methyl group. Another feature of this molecule is the presence of shell structure in chlorine. A larger region of charge depletion surrounds the small inner core, which is in turn surrounded by chlorine's VSCC. The value of L(r) at the depletion in the face opposite chlorine is –0.054 au, a value nearly double that of the depletion critical points in methane. With a carbon population of +0.254 au, it is clear that methyl chloride will be preferentially attacked by nucleophiles opposite the chlorine, and that it will be far more reactive to nucleophiles than the other examples given.

Figure 24 shows the trend in the value of L(r) at the (3,+1) critical point in the face opposite the leaving group, where one can see the decrease in L(r) as a function of the electronegativity of X. As one would expect, those molecules with an L(r) value that is positive do not undergo nucleophilic attack at the face opposite X, while increasingly negative values correspond to molecules that are increasingly reactive with respect to nucleophiles.

Figure 24: Value of L(r) at (3,+1) Nucleophilic Attack Point in CH_3-X, in au

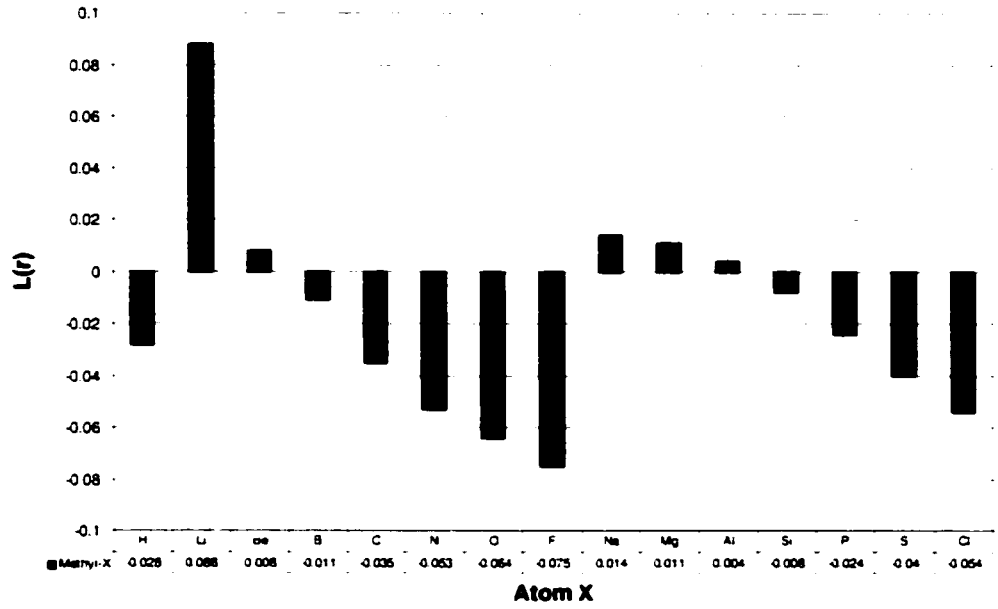

4.1.4 Bond Properties of SiH_3-XH_n

The geometrical data provided in Table 11 shows a considerably different pattern of behavior from the geometries as seen in the methyl series. The three standard 'silyl' species are more in keeping with the changes in geometry expected as one adds electron density to a silyl cation to form a radical, and yet more to form an anion. The bond lengths increase as one adds charge to the species, which is as expected: the increase in density placed on the silicon would result in less density being drawn in from the hydrogens. What is more interesting is the H-Si-H angle, which steadily decreases from cation to radical to anion, behavior that is more intuitive.

Table 11: Molecular Energies and Geometries of SiH_3-XH_n Species (HF)

SiH_3-X	E(HF) (au)	Bond Length (Å)			Bond Angle (°)			
		r(SiX)	r(SiH)	r(XH)	>(HSiH)	>(HSiX)	>(SiXH)	>(HXH)
+	-290.3589		1.455		120			
rad.	-290.6366		1.474		110.84			
-	-290.6423		1.532		96.89			
H	-291.2573		1.474		109.47			
Li	-298.1108	2.512	1.495		103.35	115.06		
BeH	-305.8787	2.219	1.482	1.333	107.00	111.85	180.00	
BH_2	-316.4990	2.039	1.478	1.189	108.07	107.47	121.28	117.40
CH_3	-330.3172	1.878	1.477	1.084	108.38	110.54	110.83	108.08
NH_2	-346.3436	1.715	1.480	0.993	107.52	114.91	120.19	110.56
OH	-366.1997	1.633	1.475	0.956	110.00	111.08	120.34	
F	-390.2167	1.583	1.467		110.76	108.15		
Na	-452.5106	2.821	1.496		103.23	115.16		
MgH	-490.8492	2.620	1.485	1.709	106.03	112.73	180.00	
AlH_2	-533.7495	2.491	1.480	1.581	107.32	110.13	120.73	118.54
SiH_3	-581.3635	2.373	1.477		108.67	110.27		
PH_2	-632.5958	2.278	1.474	1.406	109.16	112.88	96.23	95.62
SH	-688.8355	2.160	1.470	1.334	110.36	110.83	96.37	
Cl	-750.2454	2.072	1.465		110.93	107.98		

As with the methyl species, the optimized geometries of the silyl compounds of Table 11 deviate from experiment within the computational error limit of ±0.02 Å for the most part, as Table 12 shows (references in parathenses). The calculated bond angles show a larger deviation from experiment on average, which can be explained by the fact that the Hartree-Fock calculation tends to polarize the electron density, giving bond angles more in keeping with a molecule with slightly higher ionic character.

Table 12: Comparison Between Experimental and Calculated Geometries of SiH_3-X

	Si-X Bond Length (Å)			X-Si-H Bond Angle (°)		
	Exper.	Calc.	Diff.	Exper.	Calc.	Diff.
H	1.474 (4)	1.474	0.000	109.5	109.47	0.03
CH3	1.885 (6a)	1.878	0.007	114.6 (6)	110.54	4.06
NH2	1.706 (6a)	1.715	-0.009	115.4 (6)	114.91	0.49
OH	1.626 (4)	1.633	-0.007	109.6 (4)	111.08	-1.48
F	1.594 (10)	1.583	0.011	--------	--------	--------
PH2	2.249 (12)	2.278	-0.029	109.8 (12)	112.88	-3.08
SH	2.136 (14)	2.160	-0.024	108.7 (14)	110.83	-2.13
Cl	2.048 (10)	2.072	-0.024	--------	--------	--------

The overall changes in the bond angles are more pronounced than in the methyl species, which makes sense, considering the larger volume of the silicon atom: the hydrogens are more widely spaced, and thus have more freedom of movement.

The geometries of the SiH_3-X species do not show the same matches in patterns as do the methyl species, with geometries indicative of the three standard groups. The trend in the Si-X bond lengths are as expected, albeit with an overall greater change in bond lengths than the methyl series. This can be explained by the fact that the valence density of silicon is much more diffuse, due to silicon's greater size and lower electronegativity. As a result, any density in the Si-X bond will result in a longer bond. By contrast, the changes in the Si-H bond lengths are much smaller, ranging from slightly higher than the silyl radical for electropositive elements bonded to silicon, to slightly lower for electronegative elements. The H-Si-H bond angles also follow this same trend, increasing with increased electronegativity in X: the overall change is also not as pronounced as it is in the methyl series. The H-Si-X angles show no real trend at all: they fluctuate as one proceeds along the 2nd and 3rd rows, first decreasing as expected, then increasing at X = carbon, then decreasing again. It seems clear that for simple silyl species, geometrical data provide no strong clues for electronic structure. Perhaps this is a result of silicon's more diffuse valence density, which makes for a larger, loosely structured molecule that is less sensitive to geometric changes due to the groups attached.

Early in the thesis work, the question was raised about the importance of electron correlation in silicon computation[134]. Table 13 shows the geometrical data of selected silyl compounds optimized at the MP2 level, (the (MP2) refers to MP2 level computational results), to compare with the Hartree-Fock results.

Table 13: Molecular Energies and Geometries of SiH_3-XH_n Species (MP2)

SiH_3-X	E(MP2) (au)	Bond Lengths (Å)			Bond Angles (°)			
		r(SiX)	r(SiH)	r(XH)	>(HSiH)	>(HSiX)	>(SiXH)	>(HXH)
+	-290.5246		1.456		120.00			
rad.	-290.8057		1.471		111.15			
-	-290.8531		1.529		95.54			
H	-291.4410		1.471		109.47			
CH_3	-330.6628	1.872	1.475	1.086	108.45	110.48	110.93	107.98
NH_2	-346.7721	1.727	1.478	1.004	107.61	115.61	119.35	109.82
OH	-366.6709	1.657	1.473	0.956	108.10	111.43	117.39	
F	-390.6650	1.609	1.466		110.75	108.16		
SiH_3	-581.7095	2.356	1.474		108.92	110.02		

While the energies of the MP2 calculations are considerably lower than the H-F calculations, (as expected), the geometries show little change, averaging about 0.004 Å for bond lengths, and 1-2° for bond angles.

Such small differences are considered statistically insignificant: what effect correlation has on the electron density and its properties will be discussed later.

Table 14: Data of Si-X Bond for SiH_3-XH_n, in au (HF)

SiH_3-X	r(SiX)	r_b(Si)	% r_b(Si)	ρ_b	$L(r)_b$	ε
Li	4.748	3.294	69.38	0.029	-0.020	0.000
BeH	4.193	1.364	70.81	0.075	0.009	0.000
BH_2	3.855	1.459	37.84	0.111	0.018	0.015
CH_3	3.549	1.364	38.43	0.123	-0.039	0.000
NH_2	3.241	1.291	39.83	0.137	-0.142	0.125
OH	3.085	1.258	40.78	0.143	-0.225	0.058
F	2.992	1.246	41.65	0.141	-0.285	0.000
Na	5.331	3.313	62.15	0.024	-0.016	0.000
MgH	4.951	3.173	64.08	0.041	-0.020	0.000
AlH_2	4.707	3.078	65.39	0.064	-0.006	0.060
SiH_3	4.484	2.242	50.00	0.093	0.038	0.000
PH_2	4.304	1.504	34.95	0.096	0.017	0.019
SH	4.081	1.442	35.34	0.095	-0.019	0.076
Cl	3.915	1.410	36.00	0.093	-0.051	0.000

The BCP data of the silyl series provides more substantial information about the silyl group than geometries, as Table 14 shows. As was seen in the methyl series, there is a sharp change in the proportion of the Si-X bond belonging to silicon, as a direct function of electronegativity of X. This percentage drops from about 70% silicon for electropositive groups to an average of 37% for electronegative groups. Unlike the methyl series, where the percentages tended to fluctuate on each side of the elemental row, the values for the silyl percentages show much less variance. This could simply be the result of the longer Si-X bond, which would suppress variations somewhat. A summary of the values of rho and L(r) are summarized in Figure 25. Several important features of this data should be noted.

Firstly, the fact that all of the values of rho are much smaller than those of the BCPs of the C-X bonds, and no Si-X bond has a value above 0.2. It is interesting to note that for the more electronegative elements in a given row, the value of rho does not vary significantly. This may be because of the element's high electronegativity effectively stripping most of the valence density from silicon. Once this occurs, there would little further change in the bond properties, as silicon has little more to give up to the bonded element.

Secondly, almost all of the BCPs have L(r) values that are negative, indicative of bonds that are highly

polarized, and that have high ionic character. The exceptions are the Si-B, Si-Si and Si-P bonds: the percentage data in Table 14 shows that these bonds mark or lie near the shift in the percentage of the Si-X bond belonging to silicon, implying a somewhat higher degree of covalency in the bond.

Figure 25: Rho and L(r) at BCP of Si-X Bond in SiH_3-XH_n, in au (HF)

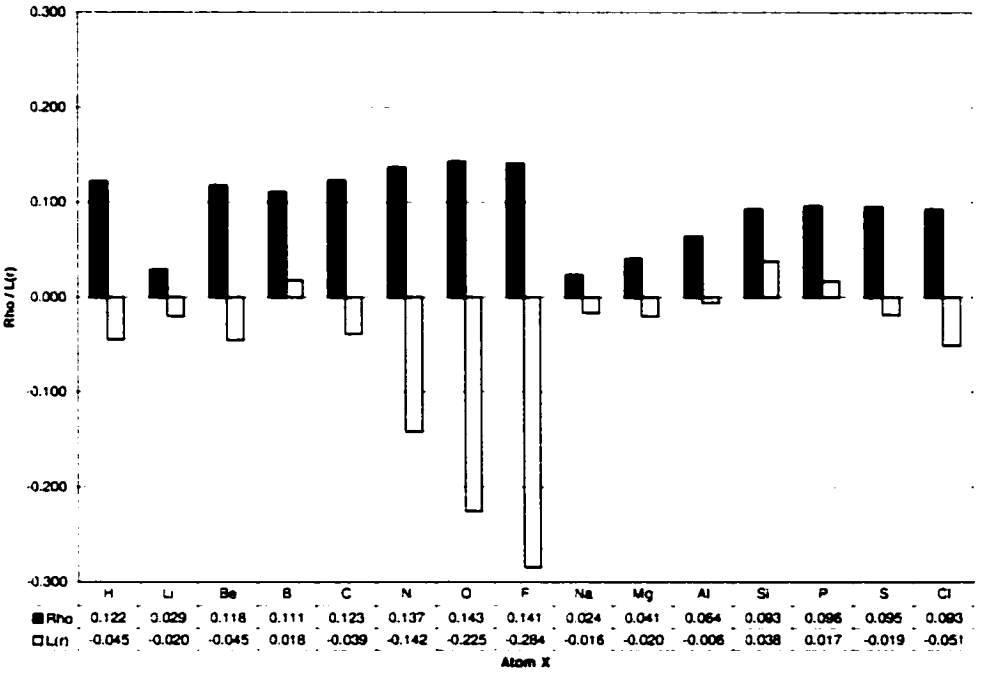

Bond ellipticity is, overall, unremarkable, except for the Si-N bond, which has an ellipticity of 0.125. One must be careful in making the wrong conclusions from this information: one could use such a value to cite p-d backbonding, despite the fact that the value of rho is much too low. Reviewing the geometric data provides a much simpler explanation. It is well-known that for silaamines, the amine group is nearly planar. This means that there is some double bond character in the Si-N bond, though most of the π-bond density is centered on the nitrogen.

Given the differences in environments with different bonded elements, BCP data is an excellent test of the effect of correlation on the electron density.

Table 15: Data of Si-X Bond for SiH_3-XH_n, in au (MP2)

SiH_3-X	r(SiX)	r_b(Si)	% r_b(Si)	ρ_b	L(r)$_b$	ε
CH_3	3.538	1.383	39.10	0.120	-0.030	0.000
NH_2	3.265	1.310	40.12	0.131	-0.122	0.122
OH	3.132	1.282	40.92	0.135	-0.187	0.061
F	3.041	1.270	41.77	0.133	-0.236	0.000
SiH_3	4.452	2.226	50.00	0.120	-0.036	0.000

The results shown on Table 15 prove quite promising, as rho differs by only about 0.002 au compared to Hartree-Fock calculations, and L(r) differs by less than 0.1 au, which is acceptable given the large fluctuations in the L(r) function of a molecular density function. These results indicate that whilst important for calculating the total energy of a molecule, correlation has no major effect on the electron density or its properties, and Hartree-Fock calculations should prove more than adequate for these studies.

The Si-H bond data provides the same information about the electronic structure of the silyl as the geometry does.

Table 16: Data of Si-H Bond for SiH_3-XH_n, in au (HF)

SiH_3-X	r(SiH)	r_b(Si)	% r_b(Si)	ρ_b	L(r)$_b$	ε
+	2.749	1.340	48.76	0.139	-0.031	0.027
rad.	2.786	1.359	48.80	0.122	-0.044	0.069
-	2.894	1.406	48.57	0.102	-0.035	0.094
H	2.785	1.356	48.69	0.122	-0.045	0.000
Li	2.826	1.375	48.66	0.113	-0.044	0.065
BeH	2.801	1.364	48.69	0.118	-0.045	0.040
BH_2	2.801	1.363	48.67	0.118	-0.045	0.029
CH_3	2.791	1.358	48.64	0.121	-0.044	0.003
NH_2	2.797	1.358	48.56	0.122	-0.041	0.027
OH	2.787	1.355	48.60	0.124	-0.041	0.034
F	2.773	1.349	48.65	0.127	-0.041	0.036
Na	2.827	1.376	48.67	0.113	-0.043	0.069
MgH	2.806	1.367	48.70	0.117	-0.045	0.054
AlH_2	2.801	1.364	48.70	0.118	-0.045	0.045
SiH_3	2.791	1.359	48.70	0.121	-0.045	0.029
PH_2	2.785	1.356	48.69	0.123	-0.044	0.016
SH	2.778	1.352	48.68	0.125	-0.043	0.009
Cl	2.769	1.348	48.69	0.128	-0.043	0.009

The percentage of the Si-H bond belonging to silicon remains more or less constant, with minor and patternless fluctuations with respect to the element X: even the three 'standard' silyl species change very little. The values of rho at the BCP are more helpful. Rho increases with increased electronegativity in X.

Similarly to the geometries, the change in rho is less pronounced, clustering around the rho value for the silyl radical, rather than ranging from the cation to anion values. As with the Si-X bond data, the Si-H bond data varies little when correlation is included in the calculation of the wavefunction.

Table 17: Data of Si-H Bond for SiH_3-XH_n, in au (MP2)

SiH_3-X	r(SiH)	r_b(Si)	% r_b(Si)	ρ_b	$L(r)_b$	ε
+	2.751	1.355	49.24	0.137	-0.021	0.023
rad.	2.781	1.372	49.34	0.122	-0.035	0.073
-	2.891	1.422	49.17	0.102	-0.028	0.088
H	2.78	1.368	49.21	0.122	-0.036	0.000
CH_3	2.787	1.370	49.17	0.121	-0.035	0.001
NH_2	2.794	1.371	49.09	0.122	-0.032	0.024
OH	2.784	1.367	49.12	0.124	-0.032	0.030
F	2.769	1.362	49.17	0.127	-0.032	0.034
SiH_3	2.785	1.372	49.26	0.120	-0.036	0.033

As with the methyl series, the BCP data for X-H bonds provides a picture of the structure of the X-H bond.

Table 18: Data of X-H Bond for SiH_3-XH_n, in au (HF)

SiH_3-X	r(XH)	r_b(X)	% r_b(X)	ρ_b	$L(r)_b$	ε
BeH	2.519	1.080	42.87	0.098	-0.047	0.000
BH_2	2.247	0.957	42.57	0.185	0.063	0.324
NH	1.877	1.382	73.61	0.359	0.482	0.045
OH	1.771	1.453	82.05	0.391	0.769	0.005
MgH	3.230	1.645	50.93	0.054	-0.055	0.000
AlH_2	2.987	1.477	49.46	0.083	-0.062	0.018
PH_2	2.657	1.305	49.11	0.163	0.021	0.124
SH	2.510	1.478	58.88	0.217	0.155	0.095

A noteworthy feature of the data in Table 18 is that the X-H bond data varies little in comparison with the X-H bond data for the methyl series in Table 7. This is significant in the context of Atoms in Molecules, as it demonstrates the shortsighted nature of a functional group. Its electronic structure is insensitive to its environment within different molecules, with its properties changing only slightly. This fact is further demonstrated in Table 19, where the effects of correlation cause little change in the BCPs and their properties.

Table 19: Data of X-H Bond for SiH_3-XH_n, in au (MP2)

SiH_3-X	r(XH)	r_b(X)	% r_b(X)	ρ_b	L(r)$_b$	ε
NH	1.898	1.390	73.23	0.341	0.421	0.039
OH	1.806	1.457	80.66	0.366	0.681	0.006

Also of note is the comparison between the BCP data of Table 18 with that of the Si-H BCP. It is important to place the Si-H bond in context with the data obtained on other elements bonded with hydrogen. Given the pattern that the Si-H bond data fits into, one can surmise that the Si-H bond is more ionic in nature than indicated by other theoretical work, a fact supported by experimental observation.

4.1.5 Atomic Properties of SiH_3-XH_n

In terms of the charge on silicon, there are two main points that show a significant difference from the carbon populations. The first is the greatly increased charge on silicon, as shown in Table 20.

Table 20: Atomic Charges on SiH_3-XH_n, in au (HF)

SiH_3-X	q(Si)	q(H[Si])	q(SiH_3)	q(X)	q(H[X])	q(XH_n)	q(tot)
+	2.897	-0.632	1.000				1.000
rad.	2.180	-0.726	0.002				0.002
-	1.378	-0.792	-0.997				-0.997
H	2.899	-0.724	0.728	-0.724		-0.724	0.005
Li	1.362	-0.750	-0.889	0.894		0.894	0.005
BeH	1.375	-0.727	-0.807	1.675	-0.866	0.810	0.002
BH_2	2.767	-0.718	0.612	0.805	-0.698	-0.591	0.021
CH_3	2.924	-0.733	0.726	-0.628	-0.032	-0.723	0.003
NH_2	3.018	-0.743	0.787	-1.565	0.377	-0.810	-0.023
OH	3.043	-0.735	0.838	-1.502	0.650	-0.852	-0.014
F	3.058	-0.722	0.891	-0.888		-0.888	0.003
Na	1.492	-0.754	-0.770	0.774		0.774	0.005
MgH	1.458	-0.735	-0.748	1.556	-0.806	0.750	0.002
AlH_2	1.485	-0.725	-0.690	2.270	-0.787	0.695	0.006
SiH_3	2.169	-0.722	0.004	2.169	-0.722	0.004	0.007
PH_2	2.791	-0.726	0.614	0.501	-0.559	-0.618	-0.004
SH	2.901	-0.723	0.733	-0.593	-0.144	-0.737	-0.004
Cl	2.941	-0.717	0.789	-0.801		-0.801	-0.012

Note that even in those cases where the silyl group has an overall negative charge, the silicon is still positive. The lower limit of the charge on silicon is about 1.4, going all the way to 3.0 for highly electronegative elements X. The next feature is the charge on the hydrogens bonded to silicon, averaging about –0.72: this is a huge density load on the hydrogen, resulting in properties more akin to a hydride. This reinforces the BCP data discussed earlier, which showed the Si-H bond to be highly polar. Even with

this extra charge, the influence of X on the population of H is minor.

Figure 26 illustrates the charges on silicon with variation in element X. Assuming from formal charges that a silicon atom should have four electrons worth of valence density, this means that for the more common elements bonded to silicon, only a little over one electron's worth of valence density is left to silicon.

Figure 26: Silicon Charges for SiH_3-XH_n, in au (HF)

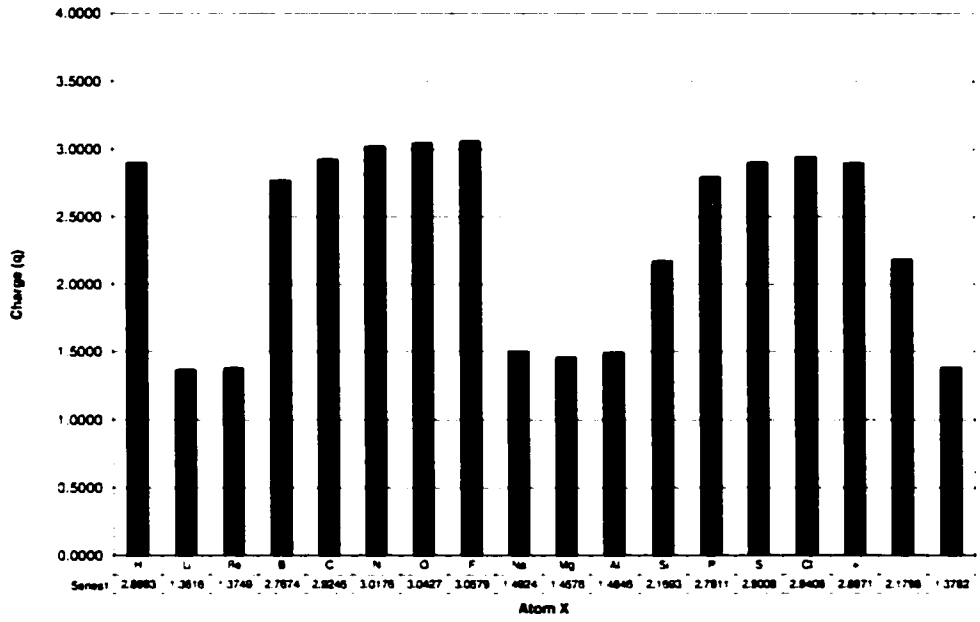

The significance of this observation cannot be overstated: not only does this go far to explain the chemistry of silanes, but lends much support to the idea of treating silicon species in terms of an ionic or nearly ionic model.

Table 21: Atomic Charges on SiH_3-XH_n, in au (MP2)

SiH_3-X	q(Si)	q(H[Si])	q(SiH_3)	q(X)	q(H[X])	q(XH_n)	q(tot)
+	2.767	-0.589	1.001				1.001
rad.	2.052	-0.684	0.001				0.001
-	1.241	-0.744	-0.992				-0.992
H	2.747	-0.686	0.689	-0.686		-0.686	0.004
CH_3	2.767	-0.695	0.683	-0.722	0.014	-0.681	0.002
NH_2	2.871	-0.708	0.747	-1.505	0.366	-0.773	-0.026
OH	2.899	-0.700	0.800	-1.417	0.604	-0.813	-0.013
F	2.920	-0.688	0.857	-0.855		-0.855	0.002
SiH_3	2.037	-0.679	0.002	2.037	-0.679	0.002	0.003

Table 21 provides populations of selected species calculated at the MP2 level. Overall, the charge on silicon decreases by about 0.1 – 0.2 au after correlation, a rather small change when one takes into consideration the change in molecular energy that occurs when correlation is included in the calculation.

Table 22: Atomic Energies on SiH_3-XH_n, in au (HF)

SiH_3-X	E(Si)	L(Si)	E(H[Si])	L(H[Si])	E(X)	L(X)	E(H[X])	L(H[X])
+	-288.0205	-0.00017	-0.7795	0.00001				
rad.	-288.2626	0.00178	-0.7915	0.00004				
-	-288.3513	0.00415	-0.7640	0.00005				
H	-288.0637	0.00393	-0.7987	0.00003				
Li	-288.3980	0.00355	-0.7841	0.00004	-7.3616	0.00006		
BeH	-288.4963	0.00176	-0.7897	0.00004	-14.2421	0.00001	-0.7717	-0.00004
BH_2	-288.1343	0.00143	-0.7892	-0.00001	-24.2450	0.00003	-0.8684	0.00002
CH_3	-288.0500	0.00244	-0.8046	0.00004	-37.9626	0.00010	-0.6305	0.00008
NH_2	-287.9698	0.00145	-0.8140	0.00004	-54.9845	-0.00022	-0.4768	0.00007
OH	-287.9602	-0.00247	-0.8151	0.00004	-75.4658	-0.00012	-0.3288	0.00004
F	-287.9737	0.00245	-0.8157	0.00003	-99.7966	-0.00019		
Na	-288.4136	0.00342	-0.7838	0.00004	-161.7467	0.00017		
MgH	-288.4598	0.00137	-0.7883	0.00004	-199.3731	0.00005	-0.6517	-0.00002
AlH_2	-288.4664	0.00150	-0.7887	0.00003	-241.4411	0.00030	-0.7355	-0.00001
SiH_3	-288.2986	0.00295	-0.7946	0.00004	-288.2986	0.00295	-0.7946	0.00004
PH_2	-288.0720	0.00148	-0.8020	0.00004	-340.5444	0.00121	-0.7889	0.00009
SH	-287.9980	0.00132	-0.8082	0.00004	-397.7674	-0.00037	-0.6485	0.00012
Cl	-287.9459	-0.00535	-0.8126	0.00004	-459.8724	0.00918		

As Table 22 shows, changes in silicon energy have less impact than in carbon, given the large overall contribution silicon makes to the molecular energy. From the three 'standard' silyl species, it can be seen that adding density to silicon has the opposite effect than that to carbon. Rather than cause a destabilization, added valence density serves to stabilize silicon within the molecule. This trend can be seen in the full silyl series, though the energies tend to fluctuate somewhat as the electronegativity of X increases. The stability of the hydrogens bonded to silicon also tends to increase slightly as X becomes more electronegative, even though the charge on hydrogen does not show any significant pattern of change. This is unlike the energies of the hydrogens bonded to carbon, which show no real pattern to changes in charge or energy as a function of X. The errors associated with the integration of the silyl species are shown in Table 23. It should be noted that on average, the integration errors are slightly higher than the methyl species, as the electron density of the molecule is much more diffuse, and thus harder to fully integrate.

Table 23: Error Between Summed Atomic Energies and Molecular Energies for SiH_3-XH_n, in au (HF)

SiH_3-X	E(tot.)	E(mol.)	diff(E)
+	-290.3589	-290.3589	0.0000
rad.	-290.6372	-290.6366	-0.0006
-	-290.6432	-290.6423	-0.0009
H	-291.2584	-291.2573	-0.0012
Li	-298.1119	-298.1108	-0.0011
BeH	-305.8792	-305.8787	-0.0004
BH_2	-316.4835	-316.4990	0.0155
CH_3	-330.3180	-330.3172	-0.0008
NH_2	-346.3497	-346.3436	-0.0061
OH	-366.1999	-366.1997	-0.0002
F	-390.2174	-390.2167	-0.0006
Na	-452.5116	-452.5106	-0.0010
MgH	-490.8495	-490.8492	-0.0004
AlH_2	-533.7448	-533.7495	0.0047
SiH_3	-581.3651	-581.3635	-0.0017
PH_2	-632.6001	-632.5958	-0.0044
SH	-688.8384	-688.8355	-0.0029
Cl	-750.2561	-750.2454	-0.0108

The effects of correlation on atomic energies would be expected to be considerable, and Table 24 shows this to be the case.

Table 24: Atomic Energies on SiH_3-XH_n, in au (MP2)

SiH_3-X	E(Si)	L(Si)	E(H[Si])	L(H[Si])	E(X)	L(X)	E(H[X])	L(H[X])
+	-288.1980	0.00113	-0.7745	0.00002				
rad.	-288.4379	0.00082	-0.7888	0.00004				
-	-288.5631	0.00383	-0.7626	0.00006				
H	-288.2572	0.00289	-0.7970	0.00004				
CH_3	-288.2475	0.00174	-0.8018	0.00004	-38.1661	-0.00040	-0.6144	0.00008
NH_2	-288.2069	0.00098	-0.8120	0.00004	-55.1736	-0.00005	-0.4816	0.00008
OH	-288.2032	-0.00024	-0.8133	0.00004	-75.6720	-0.00012	-0.3565	0.00005
F	-288.1745	0.00188	-0.8142	0.00005	-100.0507	-0.00012		
SiH_3	-288.4808	0.00129	-0.7903	0.00004	-288.4808	0.00129	-0.7903	0.00004

What must be noted here are not the differences between these values and their H-F counterparts, but the trend within the MP2 values themselves. The energy trend is the same as that observed in the H-F data: as X becomes more electronegative, and the charge on silicon increases, silicon becomes less stable. Table 25 shows the error of integration with respect to molecular energies of the MP2-level calculations. The integration errors of the MP2 wavefunctions are on par with the Hartree-Fock wavefunctions, as one would expect, given that the integration procedure is independent of the method used to generate the

wavefunction.

Table 25: Error Between Summed Atomic Energies and Molecular Energies for SiH_3XH_n, in au (MP2)

SiH_3-X	E(tot.)	E(mol.)	diff(E)
+	-290.5214	-290.5246	0.0032
rad.	-290.8043	-290.8057	0.0014
-	-290.8509	-290.8531	0.0022
H	-291.4451	-291.4410	-0.0041
CH_3	-330.6621	-330.6628	0.0007
NH_2	-346.7795	-346.7721	-0.0074
OH	-366.6716	-366.6709	-0.0007
F	-390.6679	-390.6650	-0.0029
SiH_3	-581.7037	-581.7095	0.0058

4.1.6 L(r) Properties of SiH_3-XH_n

It is to be expected that the contour maps of silyl species will be much different than their methyl counterparts. The L(r) maps do in fact show the marked differences in electronic structure, and thus in chemistry. Four examples will be discussed in detail here: SiH_4, SiH_3-Li, SiH_3-SiH_3 and SiH_3-Cl.

The simplest silane, SiH_4 is the best example to demonstrate the novel electronic structure of silyl compounds.

Figure 27: L(r) Map of Silane (HF)

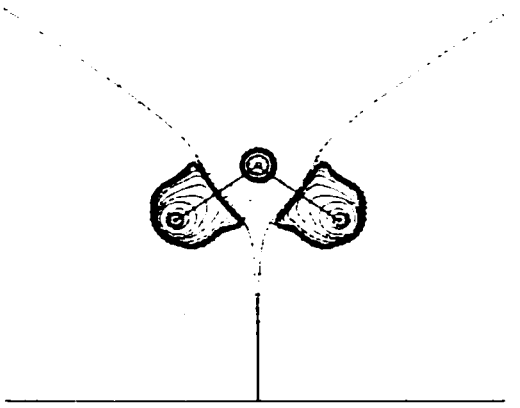

The plot of L(r) immediately shows the large and diffuse nature of this molecule, where most of the VSCC of silicon has been taken up by the hydrogens, leaving the core shells as the only region of charge concentration in silicon. This makes the curvatures of the critical points in L(r) very shallow: one can find

maxima on the hydrogens, and (3,-1) critical points linking them, but the (3,+1) critical points at the faces of the tetrahedron are too diffuse to locate. One can conclude from this that there is no significant VSCC in silane, since the maxima are on the ligands themselves. The closest approximation to a (3,+1) critical point one can make is to determine the value of L(r) at the midpoint of the (3,-1) critical points surrounding the massive hole at the faces of the tetrahedron formed by the maxima. The value for silane at such a point is −1.022 au. Such a large and negative value indicates that a nucleophile will be strongly attracted to any of the faces of silane: with a charge on silicon of +2.899 au, there is little doubt that silane is considerably more reactive than methane to nucleophiles.

Silyl lithium is a powerful nucleophile and base, and would thus be considered to still have much of its valence density, being in essence a silyl anion. Surprisingly, its L(r) map shows a large hole in the face opposite the lithium atom.

Figure 28: L(r) map of Silyllithium (HF)

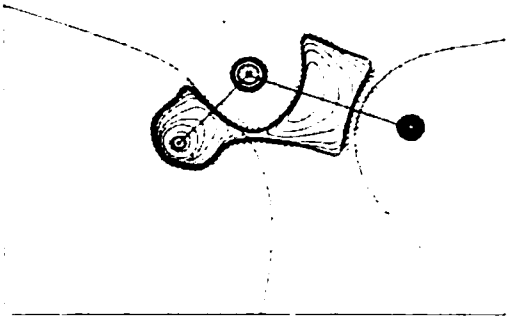

Even with a large maximum in the VSCC of silicon, there is still a large depletion opposite the lithium, with a definite (3,+1) critical point that has a value of –0.010 au. (it is likely that the additional valence density in silicon made the location of this critical point possible). It is interesting to note that despite having this maximum in the region of lithium, there are still large holes in the laplacian opposite the hydrogens. It is possible, under the right conditions, to deprotonate a silyl lithium, giving the silicon a formal charge of negative two: the (3,+1) critical point opposite the hydrogen has a L(r) value of –0.010 au

as well, and the charge of silicon is +1.362 au. Electrophiles would be strongly attracted to the maximum in the VSCC, as it is large and diffuse, and also easily accessible from a geometric standpoint. The value of the maximum at its (3,-3) critical point is +0.038 au; this is much smaller than that found at the maximum of methyl lithium, showing that the density at the maximum is indeed very diffuse compared to carbon.

Given what has been seen of silanes so far, one would expect silyl chlorides and other species with good leaving groups to undergo very facile nucleophilic attack, which they do. What is important to note is that the nucleophile need not attack the face opposing the chloride.

Figure 29: L(r) Map of Silyl Chloride (HF)

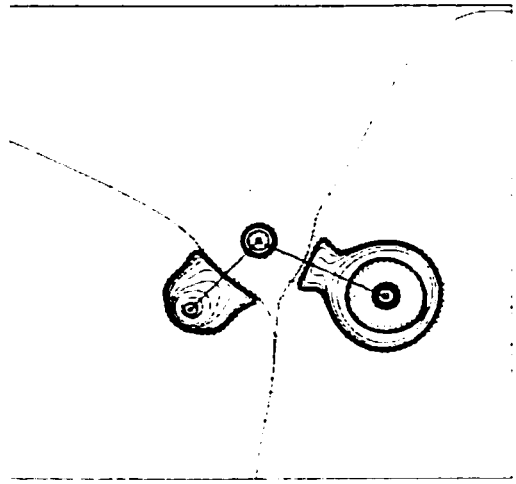

As was seen in the silane case, there is no discernible (3,+1) critical point at the face opposite the chlorine, meaning that this face would be highly vulnerable to nucleophilic attack. Using the same technique applied to silane results in an L(r) value of −1.832, about twice that of silane. This does not mean, however, that this is the only attack point available. As was described previously, a chiral silane can undergo nucleophilic substitution with retention or inversion of the chiral center. This can occur simply because the depletions in L(r) on each face of the silane are large enough to accommodate the nucleophile: the value of the (3,+1) critical point at these faces is –0.012 au. Combined with the positive charge on silicon, (+2.941 au), a nucleophile can attack any face of the molecule. The major factor governing the direction of the nucleophile attacks is whether a four-member ring structure forms during the reaction, (see Figure 2), which is controlled by the counterion involved with the nucleophile, the solvent, etc.

The last example is disilane, chosen not only for its interesting chemistry, but its unusual L(r) plot.

Figure 30: L(r) Map of Disilane (HF)

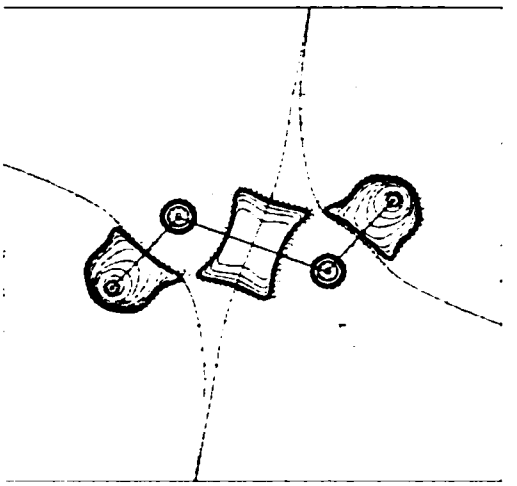

As with silane, the valence density in silicon is so depleted, that one cannot find (3,+1) critical points at any of the faces of the silicon VSCC tetrahedron; approximations at these points give L(r) values of -0.599 au at the face formed by the three hydrogen maxima, and -1.242 au at the other three. This is in spite of the fact that there are two small maxima in the charge concentration between the two silicons, with values of +0.047 au. This shows that there is very little density in the Si-Si bond, as the value of ρ_b for the Si-Si bond (0.093 au) indicates. It should also be noted that because it is large and diffuse, it should be very reactive: other AIM studies of Si-Si bonds show its diffuse nature quite clearly[135,136]. With this structure in mind, the chemistry of disilane makes sense: electrophiles can attack this concentration, the same way that they attack the π bond of ethylene, and nucleophiles can attack at any of the four faces in the atomic graph of L(r) surrounding each silicon. If this concentration is responsible for the π-bond like chemistry it can undergo, could it also influence the other properties of disliane and oligosilanes, namely their spectroscopic properties, which are often likened to conjugated π systems?

4.1.7 Bond Properties of CH_2=XH_n

Doubly bonded systems exhibit certain expected behavior, given the fact that there is increased density in the C=X bond. The bonds should be shorter than the single C-X bond, which Table 26 confirms.

Table 26: Molecular Energies and Geometries of CH_2=XH_n Species (HF)

CH_2=X	E(HF) (au)	Bond Lengths (Å)			Bond Angles (°)			
		r(CX)	r(CH)	r(XH)	>(HCH)	>(HCX)	>(CXH)	>(HXH)
CH_2	-78.0614	1.315	1.074		116.78	121.61		
NH	-94.0657	1.247	1.082	1.003	111.78	124.03	116.59	
O	-113.9083	1.178	1.092		116.31	121.84		
SiH_2	-329.0822	1.689	1.073	1.465	115.43	122.28	122.92	114.17
PH	-380.3311	1.646	1.072	1.410	115.91	124.66	99.03	
S	-436.5481	1.593	1.076		116.11	121.95		

As Table 27 shows, the calculated geometries for doubly-bonded species show little deviation from experiment, just as with the equivalent singly-bonded species. The bond angles average about 1-3% error in comparison with experimental values.

Table 27: Comparison Between Experimental and Calculated Geometries of CH_2=X

	C=X Bond Length (Å)			C=X-H Bond Angle (°)		
	Exper.[a]	Calc.	Diff.	Exper.	Calc.	Diff.
CH_2	1.330	1.315	0.015	122.5[b]	121.61	0.89
NH	1.273	1.247	0.026	117.9[c]	116.59	1.31
O	1.203	1.178	0.025	--------	--------	--------
SiH_2	1.702	1.689	0.013	122.7[c]	122.92	-0.22
PH	1.673	1.646	0.027	97.4[c]	99.03	-1.63
S	1.611	1.593	0.018	--------	--------	--------

What may prove less intuitive is that the C-H bonds grow slightly longer with increased electronegativity in X, the opposite of what is observed in the methyl series. Bond angles are unaffected by X, as shown by the H-C-H angles: the only differences are between 2nd and 3rd row elements, which is likely more a result of steric effects than electronic.

The BCP data of double bonds are useful not only for describing their electronic structure. They can also be used to determine the basic differences between the BCPs of single and double bonds that help to establish criteria that can be used to define the bond order of any bond, in particular those whose bond order is in dispute.

Table 28: Data of C=X Bond for CH_2=XH_n, in au (HF)

CH_2=X	r(CX)	r_b(C)	% r_b(C)	ρ_b	$L(r)_b$	ε
CH_2	2.485	1.242	50.00	0.371	0.336	0.352
NH	2.357	0.809	34.34	0.415	0.232	0.247
O	2.227	0.743	33.37	0.448	-0.035	0.104
SiH_2	3.193	1.909	59.80	0.157	-0.125	0.551
PH	3.111	1.891	60.80	0.198	-0.066	0.484
S	3.010	1.809	60.10	0.249	0.051	0.173

The most obvious difference between single and double bonds is the difference in rho at the BCP. Although the value of rho for most of the C=X bonds is from 30 to 65% larger than that of a single bond, it should not be assumed that bond order is a simple multiple of rho for a given bond. Another point is that how, unlike single bonds, double bonds seem to polarize more readily as a function of X, as illustrated in the L(r) values. This can be explained by the fact that the density of the π bond is more diffuse, not being localized between the nuclei. The most important measure of double bond character is the ellipticity, the ratio of the two hessian eigenvalues perpendicular to the bond axis. The 'strength' of a double bond, in terms of its attractiveness to electrophiles, can be gauged by the size of the ellipticity. The larger the value, the more oblong the double bond; this indicates a more diffuse π-bond density, which would be more reactive to electrophiles. This can be seen when one compares the ellipticities of C_2H_4 with CH_2=SiH_2: given that the valence density of silicon is so diffuse, it stands to reason that the Si=C bond could also be more diffuse.

The C-H BCP of a doubly bonded species tends to be very close in its value of rho to the singly bonded molecule. Unlike the methyl series, where X affected the C-H bond properties somewhat, the BCPs of methylene C-H bonds seem to be far less sensitive to the electronegativity of X, as shown in Table 29. The reason for this could be that the planar structure of a double-bonded species would be less affected by any steric effects on the C-H bond. There is the fact too that there is increased density in the C=X bond, which could shield the nearby C-H bonds from the effects of X.

Table 29: Data of C-H Bond for $CH_2=XH_n$, in au (HF)

$CH_2=X$	r(CH)	$r_b(C)$	% $r_b(C)$	ρ_b	$L(r)_b$	ε
CH_2	2.029	1.281	63.11	0.300	0.304	0.008
NH	2.046	1.296	63.37	0.300	0.305	0.008
O	2.063	1.322	64.09	0.300	0.307	0.010
SiH_2	2.029	1.285	63.33	0.293	0.287	0.003
PH	2.027	1.297	64.01	0.300	0.304	0.012
S	2.034	1.317	64.75	0.306	0.316	0.014

Surprisingly, The X-H BCP is very nearly the same in both C-X and C=X species. While this data is far from sufficient to draw a definite conclusion, the evidence suggests that the density properties of an X-H bond are rather insensitive to the type of bond formed between X and another element.

Table 30: Data of X-H Bond for $CH_2=XH_n$, in au (HF)

$CH_2=X$	r(XH)	$r_b(X)$	% $r_b(X)$	ρ_b	$L(r)_b$	ε
NH	1.895	1.391	73.40	0.363	0.483	0.023
PH	2.665	1.307	49.03	0.165	0.032	0.006

4.1.8 Atomic Properties of $CH_2=XH_n$

The population of the carbon atom in a double bond is considerably different from that of a single bond system, as Table 31 shows.

Table 31: Atomic Charges on $CH_2=XH_n$, in au (HF)

$CH_2=X$	q(C)	q(H[C])	$q(CH_2)$	q(X)	q(H[X])	q(XHn)	q(tot)
CH_2	0.034	-0.017	0.000	0.034	-0.017	0.000	0.000
NH	0.971	-0.023	0.924	-1.291	0.347	-0.943	-0.019
O	1.291	-0.010	1.271	-1.271		-1.271	0.000
SiH_2	-1.241	0.006	-1.229	2.690	-0.730	1.229	0.001
PH	-0.925	0.026	-0.872	1.469	-0.590	0.879	0.007
S	-0.447	0.042	-0.362	0.361		0.361	-0.001

The charge on carbon in ethylene is smaller than ethane, due to the increased density added by the π bond density. What is interesting is that, unlike the equivalent singly bonded systems discussed earlier, the charge on carbon increases more rapidly with increasing electronegativity of X, as does the charge on the methylene group. A simple explanation for this effect can be related to the bonds involved in the molecule. In singly bonded systems, X withdraws density from carbon through one bond, as opposed to two bonds in the doubly bonded systems. With more 'free' density available in the double bond, more density moves

onto element X. The charge on the methylene hydrogens also show a trend in these systems, losing charge as X becomes more electronegative.

The energy changes to carbon show the same trend observed in singly bonded systems, becoming less stable with increased electronegativity in X.

Table 32: Atomic Energies on $CH_2=XH_n$, in au (HF)

$CH_2=X$	E(C)	L(C)	E(H[C])	L(H[C])	E(X)	L(X)	E(H[X])	L(H[X])
CH_2	-37.7651	-0.00028	-0.6328	0.00007	-37.7651	-0.00028	-0.6328	0.00007
NH	-37.2339	-0.00001	-0.6393	0.00007	-55.0611	0.00008	-0.4975	0.00010
O	-37.0135	-0.00035	-0.6352	0.00005	-75.6244	0.00002		
SiH_2	-38.1010	0.00007	-0.6122	0.00009	-288.1647	0.00017	-0.7961	0.00004
PH	-38.1290	-0.00004	-0.6117	0.00010	-340.1683	0.00022	-0.8079	0.00012
S	-37.9766	-0.00119	-0.6121	0.00009	-397.3474	0.00003		

The energies of the methylene hydrogens do not change significantly with changes in X, as long as X corresponds to a 2nd or 3rd row element. This seems to be a trend that is insensitive to the electronic structure of the carbon it is bonded to. Table 33 shows the error in integrated energies versus total energy.

Table 33: Error Between Summed Atomic Energies and Molecular Energies on $CH_2=XH_n$, in au (HF)

$CH_2=X$	E(tot.)	E(mol.)	diff(E)
CH_2	-78.0613	-78.0614	0.0001
NH	-94.0711	-94.0657	-0.0054
O	-113.9082	-113.9083	0.0001
SiH_2	-329.0823	-329.0822	-0.0001
PH	-380.3286	-380.3311	0.0025
S	-436.5482	-436.5481	0.0000

4.1.9 L(r) Properties of $CH_2=XH_n$

Unlike the maps shown so far, which depict bonds that are more or less cylindrical in shape, maps of the L(r) of doubly-bonded species have two planes, the plane of the molecule, and the perpendicular plane that also lies on the bond axis. An atomic graph of a doubly-bonded species will of course have a different shape than a tetrahedron: the structure of this atomic graph is discussed in the theory section. Three examples will be discussed in detail: $CH_2=CH_2$, $CH_2=O$, and $CH_2=SiH_2$.

Ethylene is the simplest form of the carbon-carbon double bond, and as such is an excellent model to use to discuss π-bond chemistry.

Figure 31: L(r) Maps of Ethylene, Planar (left) and Cross-planar (right) (HF)

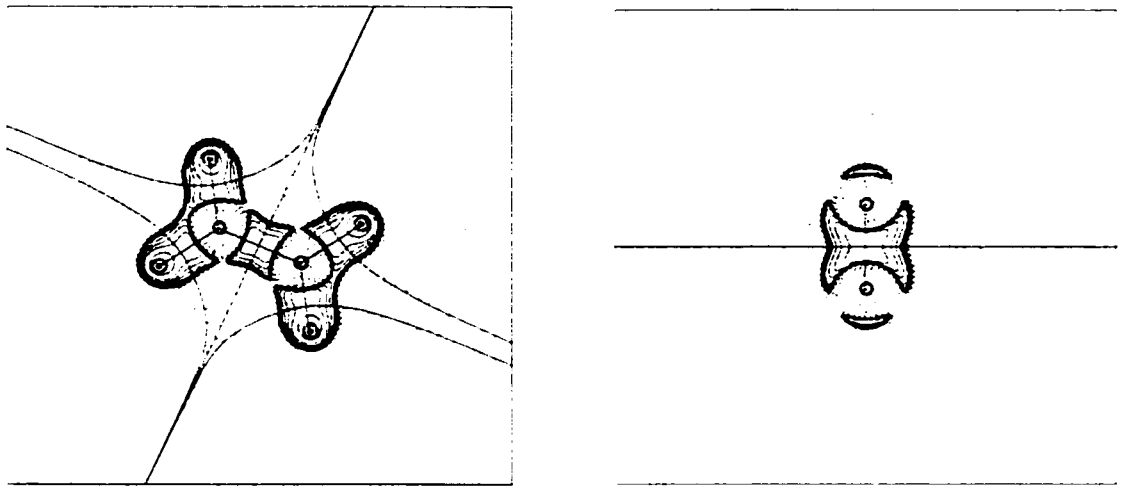

The plot of L(r) of ethylene in the molecular plane shows a strong buildup of density between the carbon atoms, as expected for a shorter, stronger bond. The cross-planar plot clearly shows the π-bond concentration, built up above and below the bond axis. Electrophilic attack would be quite facile here, as there is nothing to block the approach of the electrophile, and there is a great deal of electron density accumulated in this region, (the maxima within the π-bond have an L(r) value of +0.370 au). Nucleophilic attack would be less likely, as the depleted areas are quite small, having (3,+1) critical points with values of –0.013 au and a charge on carbon of +0.034 au. Usually a nucleophile is more reactive with an ethylene species when electron-withdrawing groups are attached to it, depleting the π-bond concentration. This would increase the size of the holes in L(r) above and below the carbon as well as increase the charge on carbon. Calculations of L(r) for acrylic acid showed that this is indeed the case: the (3,+1) critical point proved larger in the terminal methylene carbon, implying nucleophilic attack at this point, in essence providing a theoretical explanation of the Michael addition reaction[137]. An interesting alternative to the ellipticity of the BCP in rho is the ellipticity of L(r) at the same point[138]. It can provide a more realistic picture of the π-bond, as it shows the ellipticity of the charge concentration rather than the electron density. For the C=C bond, the ellipticity in L(r) is 0.607, as opposed to 0.352 for rho.

Formaldehyde is a well-studied molecule, and a good example of a double bond polarized by an electronegative element.

Figure 32: L(r) Maps of Formaldehyde, Planar (left) and Cross-planar (right) (HF)

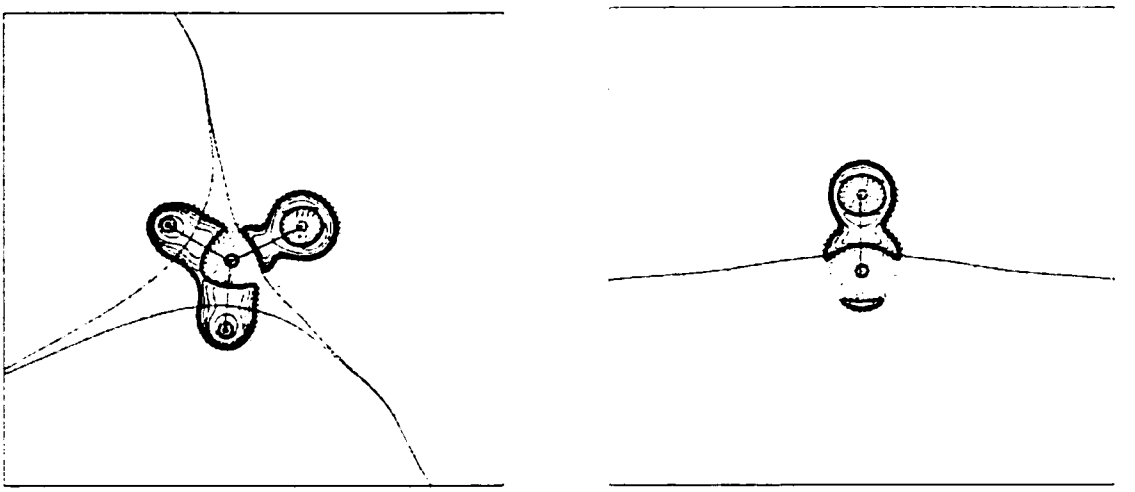

What becomes immediately obvious from the planar plot is how the C-O interatomic surface is shifted strongly towards the carbon. This places most of the bonding charge concentration on oxygen, in addition to its lone pair concentrations, which contain maxima with L(r) values of +1.469 au. The cross-planar plot also shows the π-bond concentration shifted mostly towards the oxygen, leaving a substantial depletion above and below the carbon: a (3,+1) critical point located here has a value of –0.032 au. An electrophile would readily attack the oxygen, either from above the molecular plane, or on the plane towards the lone pairs: it has a charge of –1.271 au. A nucleophile can also find facile reaction, attacking the carbon, (it has a charge of +1.291 au), from above the molecular plane. The position of the (3,+1) critical point with respect to the C=O bond axis provides a possible angle of attack for the nucleophile of 110°, which is the same angle of approach of a nucleophile to a carbonyl found in experiment[139]. The ellipticity of L(r) at the (3,-1) critical point found within the C=O bond is 0.482, compared with an ellipticity of 0.104 at the C=O BCP. The L(r) ellipticity is a better representation of the ellipticity, as it is within the charge concentration of the C=O bond, as opposed to the edge, where the C=O BCP is located.

The L(r) plot of silene will illustrate two effects on the electron density: that of an element less electronegative than carbon, and that of an element with larger, more diffuse valence density.

Figure 33: L(r) Maps of Silene, Planar (left) and Cross-planar (right) (HF)

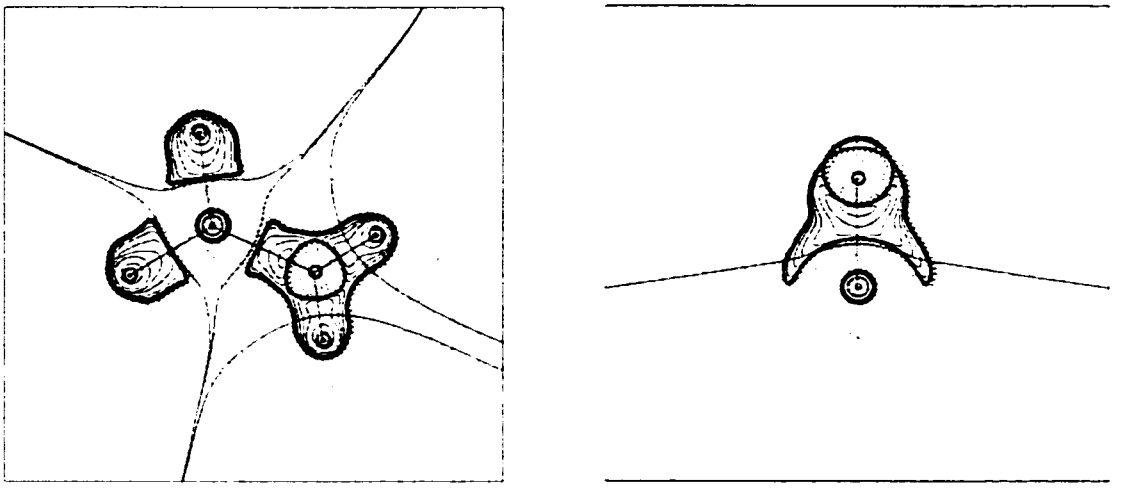

In this case, the planar plot shows how the interatomic surface of C=Si is shifted in the opposite direction to C=O, away from the carbon. Further, the charge concentration itself is almost entirely on carbon, with little valence density on silicon. The cross-planar plot shows just how diffuse the π-bond density is, much larger than ethylene or formaldehyde. Despite its diffusiveness, spreading nearly over the carbon, there is still a substantial hole in L(r) over the silicon. An approximation of the position of the (3,+1) point in L(r) results in a value of –0.245 au, with a charge on silicon of +2.690 au. An electrophile would be strongly attracted to the carbon, where the maximum observed in the contour plot has a L(r) value of +0.253 au, and the carbon atom has a charge of –1.241 au. The ellipticity at this maximum is 5.238, as opposed to the ellipticity of rho at the C=Si BCP, of 0.551: the L(r) ellipticity better reflects the diffuse nature of the C-Si π bond. In light of this plot, it becomes quite clear why silenes are so reactive, being isolable only when large, steric groups are attached.

4.1.10 Bond Properties of SiH_2=XH_n

The trends in geometry for the SiH_2=XH_n series are expectedly much different compared to the methylene series, as Table 34 shows.

Table 34: Molecular Energies and Geometries of $SiH_2=XH_n$ Species (HF)

$SiH_2=X$	E(HF) (au)	Bond Lengths (Å)			Bond Angles (°)			
		r(SiX)	r(SiH)	r(XH)	>(HSiH)	>(HSiX)	>(SiXH)	>(HXH)
CH_2	-329.0822	1.689	1.465	1.073	114.17	122.92	122.28	115.43
NH	-345.1085	1.568	1.473	0.994	111.92	128.27	125.54	
O	-364.9764	1.489	1.468		111.56	124.22		
SiH_2	-580.1325	2.127	1.464		115.14	122.43		
PH	-631.3919	2.058	1.468	1.409	111.68	126.05	92.29	
S	-687.6467	1.933	1.467		109.78	125.11		

The same trend in C=X bond lengths is seen with the $SiH_2=XH_n$ series, where the bond length shortens as X becomes more electronegative. The Si-H bond lengths also prove to be rather insensitive to X, just as in the $CH_2=XH_n$ series. It is the bond angles that show the biggest difference. Unlike the $CH_2=XH_n$ series, the H-Si-H angles vary considerably with X, growing smaller as X becomes more electronegative.

Table 35: Molecular Energies and Geometries of $SiH_2=XH_n$ Species (MP2)

$SiH_2=X$	E(HF) (au)	Bond Lengths (Å)			Bond Angles (°)			
		r(SiX)	r(SiH)	r(XH)	>(HSiH)	>(HSiX)	>(SiXH)	>(HXH)
CH_2	-329.4782	1.706	1.465	1.080	114.89	122.55	121.81	116.37
NH	-345.5924	1.607	1.475	1.011	112.50	129.66	120.30	
O	-365.5251	1.532	1.470		111.82	124.09		
SiH_2	-580.5103	2.143	1.464		116.06	121.97		

The deviation from experiment for these doubly-bonded species is similar in magnitude as to the singly-bonded species, as Table 36 illustrates.

Table 36: Comparison Between Experimental and Calculated Geometries for $SiH_2=X$

	Si=X Bond Length (Å)			X=Si-H Bond Angle (°)		
	Exper.[a]	Calc.	Diff.	Exper.	Calc.	Diff.
CH_2	1.702	1.706	-0.004	121.6[a]	122.55	-0.95
NH	1.585	1.607	-0.022	127.0[a]	129.66	-2.66
O	1.509	1.532	-0.023	122.5[a,b]	124.09	-1.59
SiH_2	2.157	2.143	0.014	119.7[a,b]	121.97	-2.27

Correlation has the effect of lengthening the Si-X double bond very slightly. This difference is within the limit of experimental error, and the remaining parameters show little difference from Hartree-Fock.

Table 37: Data of Si=X Bond for $SiH_2=XH_n$, in au (HF)

$SiH_2=X$	r(SiX)	r_b(Si)	% r_b(Si)	ρ_b	$L(r)_b$	ε
CH_2	3.193	1.283	40.20	0.157	-0.125	0.551
NH	2.963	1.220	41.18	0.183	-0.267	0.238
O	2.813	1.176	41.80	0.208	-0.421	0.072
SiH_2	4.019	2.010	50.00	0.109	0.046	1.111
PH	3.880	1.435	36.97	0.121	0.004	0.758
S	3.653	1.357	37.14	0.133	-0.054	0.244

The change in H-Si-H angles is clearly not a steric effect as the more electronegative groups have increasingly fewer hydrogens. The reason for this effect is clearly electronic, one that can possibly be explained later with the BCP data. The Si=X BCP data in Table 37 shows overall trends in rho similar to that of the C=X bond. It should be noted that, like the C=X BCPs, the rho values of Si=X are larger than the equivalent Si-X values, though not nearly double, as seen with the methylene series. The ellipticity values show quite interesting behavior in themselves. For example, the Si=O bond has a very low ellipticity compared to the other 2nd row elements, implying a bond with very little double bond character. The ellipticity of disilene is most intriguing, having the highest ellipticity of any of the doubly bonded molecules studied in this project. This is not surprising, considering how diffuse the valence density of silicon is: there is very little holding this π-bond density in place, and this molecule should be, and is, very reactive. While correlation has little effect of the Si-X double bond lengths, it does reduce the value of ρ_b somewhat. Surprisingly, the Si-Si double bond shows the least change with correlation, even though one would expect greater changes due to its diffuse electronic structure.

Table 38: Data of Si=X Bond for $SiH_2=XH_n$, in au (MP2)

$SiH_2=X$	r(SiX)	r_b(Si)	% r_b(Si)	ρ_b	$L(r)_b$	ε
CH_2	3.225	1.307	40.53	0.149	0.398	0.470
NH	3.040	1.251	41.15	0.166	0.832	0.208
O	2.895	1.210	41.79	0.184	1.313	0.061
SiH_2	4.050	2.025	50.00	0.103	-0.156	0.828

Despite the variations in the H-Si-H bond angles of this series, the Si-H BCP data varies little with changes in X.

Table 39: Data of Si-H Bond for $SiH_2=XH_n$, in au (HF)

$SiH_2=X$	r(SiH)	r_b(Si)	% r_b(Si)	ρ_b	$L(r)_b$	ε
CH_2	2.768	1.353	48.87	0.125	-0.044	0.082
NH	2.783	1.356	48.74	0.125	-0.039	0.064
O	2.773	1.353	48.79	0.128	-0.036	0.069
SiH_2	2.767	1.354	48.94	0.124	-0.046	0.076
PH	2.773	1.354	48.83	0.126	-0.042	0.046
S	2.773	1.352	48.75	0.128	-0.038	0.045

The only significant differences lie in the ellipticities, which are on a whole larger than the C-H ellipticities, and decrease with increasing electronegativity of X. This raises an interesting theory that relates this to the bond angle changes: perhaps the Si-H bonds in doubly bonded silanes are flattened somewhat with respect to the molecular plane. If electron density were removed from the hydrogens indirectly by the increased electronegativity of X, then this would reduce the size of the charge concentrations on the hydrogens. The hydrogens would experience less repulsion from each other, allowing them to be slightly closer together, without altering the bond length significantly. (it should be noted that the value of ellipticity is independent of its direction with respect to the molecular plane). The Si-H bond properties change very little with correlation: as Table 40 illustrates, most of the changes in the $SiH_2=XH_n$ series that result from correlation are in the Si-X double bond.

Table 40: Data of Si-H Bond for $SiH_2=XH_n$, in au (MP2)

$SiH_2=X$	r(SiH)	r_b(Si)	% r_b(Si)	ρ_b	$L(r)_b$	ε
CH_2	2.769	1.368	49.40	0.124	0.137	0.089
NH	2.788	1.374	49.27	0.123	0.113	0.066
O	2.777	1.369	49.30	0.126	0.104	0.069
SiH_2	2.767	1.370	49.50	0.123	0.145	0.084

Comparison of Table 41 with results in Table 18 and Table 19 illustrates once again the relative insensitivity of the X-H bond to the bond order of the Si=X bond, despite the fact that most of the Si=X bond density lies with the X, which should perturb the X-H bond more than the C=X bond would.

Table 41: Data of X-H Bond for $SiH_2=XH_n$, in au: HF and MP2

$SiH_2=X$	r(XH)	r_b(X)	% r_b(X)	ρ_b	$L(r)_b$	ε
NH (MP2)	1.878	1.391	74.09	0.355	0.487	0.028
PH (HF)	2.664	1.314	49.32	0.160	0.021	0.021

4.1.11 Atomic Properties of $SiH_2=XH_n$

As was seen in the singly bonded cases, the charge on silicon in the doubly bonded cases is much higher than the corresponding $CH_2=XH_n$ cases.

Table 42: Atomic Charges on $SiH_2=XH_n$, in au (HF)

$SiH_2=X$	q(Si)	q(H[Si])	$q(SiH_2)$	q(X)	q(H[X])	$q(XH_n)$	q(tot)
CH_2	2.690	-0.730	1.229	-1.241	0.006	-1.229	0.001
NH	2.899	-0.725	1.449	-1.853	0.395	-1.458	-0.009
O	2.999	-0.708	1.583	-1.584		-1.584	0.000
SiH_2	1.431	-0.728	-0.024	1.431	-0.728	-0.024	-0.049
PH	2.460	-0.720	1.021	-0.463	-0.554	-1.017	0.004
S	2.771	-0.712	1.347	-1.347		-1.347	0.000

As with the $CH_2=XH_n$ carbon populations, the silicon populations are slightly lower than the singly bonded species, though this effect is not as strong in the silicon case. The $SiH_2=XH_n$ hydrogen populations show no substantial change with X.

As with the singly bonded systems, the addition of correlation has the effect of softening the electron density, lowering the population of the silicon. However, the populations still increase with increased electronegativity of X.

Table 43: Atomic Charges on $SiH_2=XH_n$, in au (MP2)

$SiH_2=X$	q(Si)	q(H[Si])	$q(SiH_2)$	q(X)	q(H[X])	$q(XH_n)$	q(tot)
CH_2	2.449	-0.686	1.077	-1.160	0.042	-1.077	0.000
NH	2.633	-0.683	1.267	-1.641	0.368	-1.274	-0.007
O	2.750	-0.670	1.410	-1.410		-1.410	0.000
SiH_2	1.344	-0.672	0.000	1.344	-0.672	0.000	0.001

The silicon atom in a doubly bonded system shows the same trend as the singly bonded system, becoming less stable with increasing electronegativity of X.

Table 44: Atomic Energies on $SiH_2=XH_n$, in au (HF)

$SiH_2=X$	E(Si)	L(Si)	E(H[Si])	L(H[Si])	E(X)	L(X)	E(H[X])	L(H[X])
CH_2	-288.1647	0.00017	-0.7961	0.00004	-38.1010	0.00007	-0.6122	0.00009
NH	-288.0784	0.00038	-0.8003	0.00004	-54.9640	-0.00030	-0.4631	0.00010
O	-288.0594	0.00011	-0.8021	0.00004	-75.3128	-0.00036		
SiH_2	-288.4906	-0.00889	-0.7276	0.00004	-288.4906	-0.00889	-0.7276	0.00004
PH	-288.1970	0.00002	-0.8021	0.00004	-340.8297	-0.00060	-0.7753	0.00012
S	-288.0546	-0.00048	-0.8024	0.00005	-397.9747	-0.01256		

As with the singly bonded species, the $SiH_2=XH_n$ hydrogens that are bonded to silicon become more stable

with increasing electronegativity in X. Table 45 shows the integration errors in this series.

Table 45: Error Between Summed Atomic Energies and Molecular Energies on SiH_2=XH_n, in au (HF)

SiH_2=X	E(tot.)	E(mol.)	diff(E)
CH_2	-329.0823	-329.0822	-0.0001
NH	-345.1062	-345.1085	0.0023
O	-364.9763	-364.9764	0.0000
SiH_2	-579.8917	-580.1325	0.2408
PH	-631.4062	-631.3919	-0.0143
S	-687.6342	-687.6467	0.0126

The large error in energy in SiH_2=SiH_2 results from a non-nuclear attractor found in the Hartree-Fock wavefunction: this critical point disappears when the same molecule is calculated at the MP2 level. The energy of the non-nuclear attractor basin is 0.2146 au, giving an error of –0.0262 au, on par with the errors of the other 3rd-row elements.

The addition of correlation effects no significant changes in the trends observed in the energy of silicon. What does happen, however, is that as the electronegativity of X increases, the change in energy is smaller as compared to the Hartree-Fock calculations, (see Table 46). Correlation not only softens the electronic structure within the molecule, it also softens the trend within a similar series. As Table 47 shows, the error in integration increases with the inclusion of correlation: with the non-nuclear attractor found in the Hartree-Fock calculation of SiH2=SiH2, the error is significantly reduced.

Table 46: Atomic Energies on SiH_2=XH_n, in au (MP2)

SiH_2=X	E(Si)	L(Si)	E(H[Si])	L(H[Si])	E(X)	L(X)	E(H[X])	L(H[X])
CH_2	-288.4292	0.00024	-0.7903	0.00004	-38.2659	-0.00018	-0.5985	0.00009
NH	-288.3997	0.00027	-0.7934	0.00004	-55.1372	-0.00038	-0.4729	0.00010
O	-288.3823	0.00040	-0.7970	0.00004	-75.5463	-0.00028		
SiH_2	-288.7026	0.00011	-0.7784	0.00004	-288.7026	0.00011	-0.7784	0.00004

Table 47: Error Between Summed Atomic Energies and Molecular Energies on SiH_2=XH_n, in au (MP2)

SiH_2=X	E(tot.)	E(mol.)	diff(E)
CH_2	-329.4727	-329.4782	0.0055
NH	-345.5966	-345.5924	-0.0042
O	-365.5227	-365.5251	0.0024
SiH_2	-580.5188	-580.5103	-0.0085

4.1.12 L(r) Properties of SiH_2=XH_n

As silene has already been discussed, two other examples will be examined here, as these have been shown to have interesting bond properties. They are SiH_2=O and SiH_2=SiH_2.

Silanones are known to be highly reactive, forming silicone polymers almost immediately. The L(r) map shows why. This is contrast to silene, where there is some ellipticity to the Si=C bond visible in the plot, (0.157 at the BCP of rho, 5.238 at the maxima in L(r)). The oxygen charge concentration in the region of the Si=O bond appears to be nearly cylindrical, with an ellipticity of 0.072 at the BCP of rho, indicating that there is little to no π-bond density near the silicon. This is confirmed by the fact that there is little to no structure in the VSCCs of oxygen or silicon. Silicon is completely devoid of critical points in its valence region. An approximation of the position of a (3,+1) critical point has an L(r) value of -0.006 au, implying that this region of the molecule is close to the limit of having no electron density. The oxygen atom is similarly lacking in critical points, with a (3,-1) critical point in its VSCC that is opposite the silicon, with a value of 1.065 au. Without critical points in L(r) along the Si=O bond path, determining the ellipticity of L(r) in the vicinity of the oxygen requires choosing the point where the oxygen VSCC begins, approximately half way between the oxygen and silicon. The ellipticity at this point is 0.344, higher than the ellipticity of the Si=O BCP. Given that silicon has an integrated charge of +2.750 au, while oxygen has a charge of -1.410 au, this information, plus the contour plot itself, indicates that silanone tends to behave more like a zwitterion. The VSCC of oxygen shows little indication of the structure seen in the VSCC of oxygen in formaldehyde, which goes far to explain silanone's reactivity.

Figure 34: L(r) Maps of Silanone, Planar (left) and Cross-planar (right) (HF)

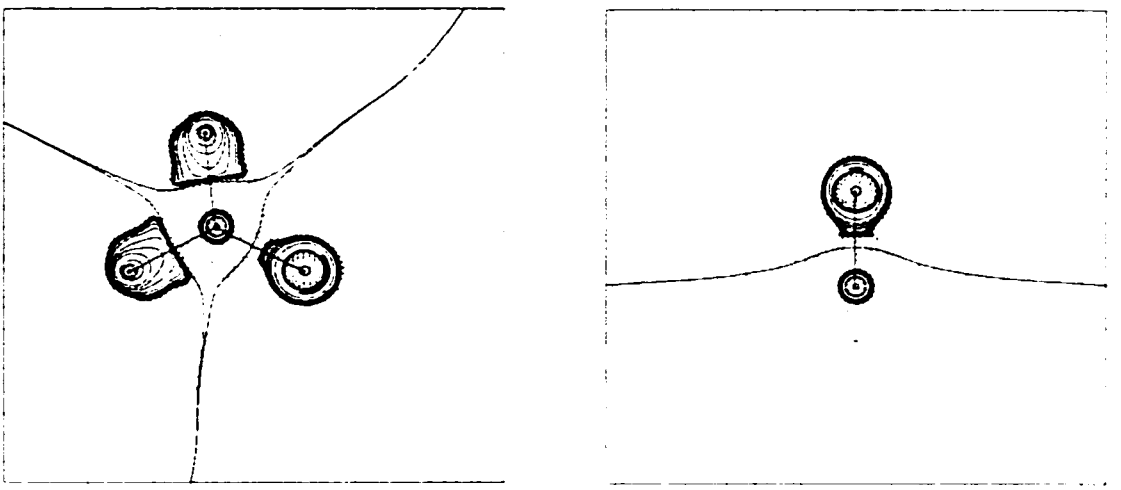

Disilene is also a highly reactive species, stabilized only by bulky substituents. The L(r) cross-planar plot shows why this is the case: the π-bond density is even more diffuse than silene, an easy target for even the weakest electrophile. So diffuse is this charge concentration, that only a central (3,-1) critical point and two (3,-1) maxima can be located along the Si-Si bond, in the central charge concentration. The maxima have a value of +0.047 au, and the ellipticity of L(r) at the (3,-1) critical point linking them is 1.425, indicating a very diffuse bond. This bond density can be easily polarized: even other disilenes can act as electrophiles, as the silicon has a charge of +1.344 au, and a (3,+1) critical point at the hole in L(r) has a value of –0.008 au. Unless large bulky ligands are used to prevent attack by electrophiles or nucleophiles, disilenes will spontaneously polymerize to form polysilanes.

Figure 35: L(r) Maps of Disilene, Planar (left) and Cross-planar (right) (HF)

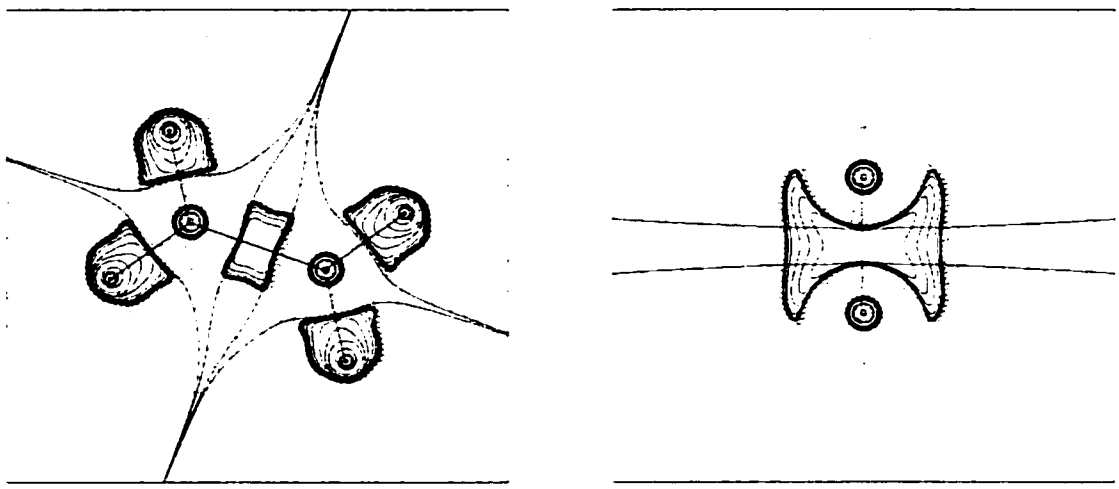

4.1.13 Bond Properties of Hypercoordinate Silicon Species

Given the focus on silicon in this thesis, it would be remiss to exclude an important aspect of silicon chemistry; that of hypercoordinate silanes. It is especially important to study these species in light of the conclusions that have been made about their electronic structure using MO theory, as many of the conclusions drawn make little sense in an experimental context. The simplest tetrahedral species were studied using Atoms in Molecules; the molecules SiH_4 and SiF_4, which were then compared with their hypercoordinate forms, SiH_5^- and SiF_5^-, and SiH_6^{2-} and SiF_6^{2-}, respectively.

What becomes clear from the geometric data in Table 48 is that even with ligands with different electronegativities, there is a distinct pattern when the co-ordination number of a silane is increased.

Table 48: Molecular Energies and Geometries of Hypercoordinate Silicon Species (HF)

	E(HF) (au)	Bond Lengths (Å)		Bond Angles (°)	
		$r(SiX_{axial})$	$r(SiX_{equatorial})$	$>(X_{eq}SiX_{eq})$	$>(X_{eq}SiX_{ax})$
SiF_4	-687.1194	1.541		109.47	
SiF_5^-	-786.6800	1.653	1.604	120.00	90.00
SiF_6^{2-}	-886.0483		1.695	90.00	
SiH_4	-291.2573		1.474	109.47	
SiH_5^-	-291.7665	1.627	1.515	120.00	90.00
SiH_6^{2-}	-292.1056		1.642	90.00	

The Si-X bonds all increase with increased coordination, with pentacoordinate silanes having longer axial bonds than equatorial bonds. This effect can easily be explained through steric hindrance: the more ligands that surround the silicon atom, the less room between ligands. The Si-X bonds increase accordingly to

offset the steric interaction as much as possible. This is especially true with the trigonal bipyramidal structure of pentacoordinate silane, as the axial ligands have less room than the equatorial ligands, and thus move farther away from the silicon.

With the bonds lengthening in this way, it stands to reason that the Si-X bonds will become weaker, with less electron density at the BCPs: Table 49 confirms this.

Table 49: Data of Si-X Bond for Hypercoordinate Silicon Species, in au (HF)

	r(SiX)	r_b(Si)	% r_b(Si)	ρ_b	L(r)$_b$	ε
SiF_4	2.912	1.217	41.79	0.163	-0.338	0.000
SiF_5^- eq	3.031	1.257	41.48	0.135	-0.256	0.008
SiF_5^- ax	3.123	1.289	41.28	0.118	-0.206	0.000
SiF_6^{2-}	3.204	1.318	41.13	0.103	-0.170	0.000
SiH_4	2.785	1.356	48.69	0.122	-0.045	0.000
SiH_5^- eq	2.863	1.386	48.40	0.108	-0.037	0.046
SiH_5^- ax	3.075	1.456	47.36	0.086	-0.021	0.000
SiH_6^{2-}	3.104	1.473	47.45	0.081	-0.018	0.000

One sees a drastic decrease in rho and L(r) as the Si-X bonds become longer. This indicates an increase in ionic character, up to the limit where rho and thus L(r) would become zero for completely separated ions. It is interesting to note that while the values of rho change significantly, the percentage of each bond length belonging to silicon remains fairly constant. This implies no real shift in valence density to or away from silicon, a conclusion that contradicts MO calculations, which predict an increase in the charge of silicon with increased co-ordination[79,140]. Only a population analysis of these species, described in the next section, would provide a concrete conclusion.

4.1.14 Atomic Properties of Hypercoordinate Silicon Species

Previous discussions within this thesis pointed to the possibility that there would be no major changes to the population of silicon with increased co-ordination. Table 50 shows this to be the case.

Table 50: Atomic Charges on Miscellaneous Silicon Species, in au (HF)

	q(Si)	q($X_{equatorial}$)	q(X_{axial})	q(tot)
SiF_4	3.432	-0.857		0.005
SiF_5^-	3.436	-0.884	-0.892	-1.000
SiF_6^{2-}	3.450	-0.907		-1.994
SiH_4	2.747	-0.686		0.003
SiH_5^-	2.888	-0.759	-0.806	-1.001
SiH_6^{2-}	2.850	-0.806		-1.984

In the case where the ligand is fluorine, the change in the population of silicon is smaller than the integration error, making any trends meaningless. What is more significant is the change in the populations of the fluorine atoms themselves. Rather than the additional charge being localized on one fluorine, or added to the silicon, it is distributed amongst all the fluorines, with more charge going to those ligands that are farther away. The reason why the silicon population does not increase significantly is an obvious one. The charge on silicon is already high in SiF_4, at 3.4: it would be energetically unfavorable to try to extract more valence density. It becomes clear why the ligands on a hypercoordinate silane become more labile with increased coordination. The silicon-ligand bonds are becoming increasingly ionic in nature, making it far easier for the ligands to come off during a chemical reaction.

The series using hydrogen as a ligand shows more significant changes in the population of silicon. Unlike the fluorine series, however, the charge on silicon actually decreases when co-ordination moves from five to six. Further, unlike the fluorine series, the charge on hydrogen shows a significant decrease of 0.1 au as the co-ordination moves from four to five. The charge on hydrogen decreases with increasing co-ordination as expected, but the changes in charge are much larger than in the fluorine series. This is probably due to the fact that that silicon does not have as large a positive charge as the fluorine series.

It has been stated previously that hypercoordinate silanes are only observed when the ligands involved are very electronegative. This can be explained by the fact that these systems become more ionic in their bonding, something that is only possible with electronegative ligands, which are more stable as negatively charged species.

Table 51: Atomic Energies on Miscellaneous Silicon Species, in au (HF)

	E(Si)	L(Si)	$E(X_{equatorial})$	$L(X_{equatorial})$	$E(X_{axial})$	$L(X_{axial})$
SiF_4	-287.6803	0.00574	-99.8598	-0.00023		
SiF_5^-	-287.4877	0.00041	-99.8452	-0.00011	-99.8284	-0.00008
SiF_6^{2-}	-287.3153	0.00559	-99.7888	-0.00002		
SiH_4	-288.0637	0.00393	-0.7987	0.00003		
SiH_5^-	-287.8554	-0.00095	-0.7950	0.00006	-0.7632	0.00008
SiH_6^{2-}	-287.6837	0.00898	-0.7371	0.00016		

As Table 51 shows, the silicon in the fluorine series becomes less stable with increased coordination, as do the fluorines. The destabilization of silicon, despite no significant change in population may be puzzling.

until one realizes that as more fluorines surround the silicon, the Si-F bonds grow longer, isolating the silicon somewhat. The fluorides become less stable for that same reason. The reason it is energetically favorable to increase the coordination of SiF_4 is due to the fact that SiF_4 is a non-polar gas, while SiF_5^- is a salt, gaining significant stabilization from lattice energy or solvent effects. The same trend is observed in the hydrogen series: the silicon destabilizes by about the same amount, though the hydrides do not destabilize to the same extent. While it is possible in theory to make a SiH_5^- salt, the ligands are simply too reactive, and such a compound would react explosively, even in air. Fluoride is quite stable, which is why SiF_5^- salts are also stable.

Table 52: Error Between Summed Atomic Energies and Molecular Energies of Miscellaneous Silicon Species, in au (HF)

	E(tot.)	E(mol.)	diff(E)
SiF_4	-687.1196	-687.1194	-0.0002
SiF_5^-	-786.6802	-786.6800	-0.0002
SiF_6^{2-}	-886.0478	-886.0483	0.0005
SiH_4	-291.2584	-291.2573	-0.0012
SiH_5^-	-291.7667	-291.7665	-0.0002
SiH_6^{2-}	-292.1065	-292.1056	-0.0009

4.1.15 L(r) Properties of Hypercoordinate Silicon Species

Given that silane shows little density in its VSCC, it would be expected that the VSCC of the equivalent hypercoordinate species would be even more depleted, with no (3,+1) critical points at the faces bounded by hydrogens. SiH_5^- does in fact show (3,+1) critical points in the vicinity of these faces, where the value is –0.011 au. The same holds true for SiH_6^{2-}: (3,+1) critical points can be found at the faces of the molecular octahedron, with values of -0.011 au. The fact that it becomes possible to locate the (3,+1) critical points may be due to the co-ordination itself. With the soft hydrogen ligands being pushed progressively closer together, the faces where the holes in L(r) are have slightly more density in them, giving L(r) in this region more substance. In the case of SiF_4, the only critical points in L(r) are centered about the atoms themselves: for silicon, in the region of the core shells, and fluorine, in the VSCC. Approximation of a (3,+1) critical point in L(r) at the center of a face bounded by three fluorines has a value of –1.667, higher that seen in silane (-1.022 au). This remains true for higher co-ordination systems containing fluorine. In SiF_5^-, the point at each face bounded by three fluorines has a L(r) value of –0.085,

and –0.026 for SiF_6^{2-}. The fact that the value becomes less negative with increased co-ordination follows the same logic proposed for the hydrogen ligands: the closer proximity of the ligands results in slightly more electron density at these points.

4.2 Comparisons Between Carbon and Silicon

From the molecular series studied so far, as well previous calculations[141], several conclusions can be drawn about the bond properties of silanes as compared to hydrocarbons:

- The interatomic surface of a Si-X bond is shifted relatively close to the silicon for most elements X, with respect to the percentage of the total bond length, as illustrated in Table 53.

Table 53: Properties of Select C-X and Si-X Bonds, in au

Atom X	% r_b(C)	ρ_b	$L(r)_b$	% r_b(Si)	ρ_b	$L(r)_b$
H	62.28	0.289	0.281	48.69	0.122	-0.045
C	50.00	0.250	0.153	38.43	0.123	-0.039
N	40.05	0.274	0.219	39.83	0.137	-0.142
O	32.43	0.266	0.086	40.78	0.143	-0.225
F	31.78	0.241	-0.098	41.65	0.141	-0.285
Si	61.57	0.123	-0.039	50.00	0.093	0.038
P	63.04	0.154	0.005	34.95	0.096	0.017
S	47.47	0.177	0.064	35.34	0.095	-0.019
Cl	42.15	0.178	0.062	36.00	0.093	-0.051

The data accumulated in this research show that as the atom X becomes more electronegative, the interatomic surface shifts closer to the carbon or silicon it is bonded to, (this is reference to the major changes in the $\%r_b$(M), rather than the half percent changes that are a consequence of the changes in total bond length). This implies, in the case of the Si-X bond, that a great deal of the density in the vicinity of the Si-X bond is within the atomic basin of X, leaving little valence density on silicon. While this is true for C-X bonds as well, X must be a very electronegative element, such as oxygen or fluorine. This shows that the differences in electronegativity between carbon and silicon have a marked effect on their densities; the valence density of silicon is much more easily polarized, even by elements with relatively low electronegativity.

- The value of ρ_b of the Si-X bond is much lower than the C-X bond[142]. It is important to remember that, within a density context, the concept of a standard 'single bond' is dependent on the elements involved in the bond itself. It is easy to assume that a bond is weak if its density is low; one will recall, however,

that the Si-O bond, while having a BCP density of only 0.143 au, has been measured experimentally as a bond with an extremely high energy of dissociation. One should treat bond density values as standards for a given element: a C-X bond will average at about 0.20 au when X is a 2nd-row element, and be less when X is a 3rd-row element. Most Si-X bonds average 0.10 au when X is a 2nd-row element, showing a similar, though smaller, decrease in density when X is a 3rd-row element.

- Si-X bonds tend to be much more polar than C-X bonds, as $L(r)_b$ is negative for most Si-X bonds[143]. L(r) values are always a good indication of the character of a bond, whether it is non-polar and covalent, highly polar, or more ionic. As Table 53 illustrates, only a few C-X bonds have L(r) values that are negative, such as the Si-C and C-F bonds, which are expected to be very polar. The opposite trend is seen in Si-X bonds: the majority of these bonds show a great deal of ionic character, with only a few having positive L(r) values. The polarity of the Si-X bond further strengthens the notion that the bonded element X is stripping the valence density away from silicon. This is illustrated well by the Si=O bond, which is so polarized, there is hardly any π-bond character to it at all.
- Silanes are highly susceptible to nucleophilic attack[144]. The plots of L(r) provide yet more evidence of the lack of valence density in silanes. Even elements such as hydrogen carry large concentrations of electron density in silanes, leaving silicon with very little valence density, (and thus large atomic charges), and large depletion gaps for nucleophiles to attack. Carbon-centered compounds, by contrast, show much smaller depletion gaps; only when electronegative elements are bonded to carbon do these depletion gaps become more substantial. When combined with the calculated atomic charges of carbon for each case, these compounds are considerably less reactive to nucleophiles than their silane counterparts.

The bond properties alone have gone far to explain the chemistry of silicon in terms that coincide well with experimental observation[145]. Atomic basin properties provide evidence that further strengthens these explanations, as well as shed light on matters that bond properties cannot explain alone.

The most significant difference between carbon and silicon in terms of their populations is the fact that unlike carbon, most elements can strip most of the valence density away from silicon's valence shell, leaving silicon with a positive charge in most cases, as shown in Table 54.

Table 54: Calculated Atomic Charge of Element X in MH_3-XH_n, in au

Atom X	M = C	M = Si
H	0.175	2.899
C	0.184	2.924
N	0.549	3.018
O	0.768	3.043
F	0.773	3.058
Si	-0.628	2.169
P	-0.423	2.791
S	0.046	2.901
Cl	0.254	2.941

Losing valence density destabilizes silicon somewhat, in that its atomic contribution to the molecular energy drops. Some energy, and density, is gained back if there is a double bond between silicon and another element, but that density polarizes even more strongly towards the bonding atom X as X becomes more electronegative, since the π bond density is much more diffuse. These differences provide numerical support for the L(r) contour maps seen earlier; silicon does in fact have little in the way of valence density of its own, which is why nucleophiles attack silanes so much more readily than the equivalent carbon species.

L(r) studies show that for carbon species containing ligands that are more electronegative than carbon, one can usually locate a (3,+1) critical point at which a nucleophile will attack. For cases where the ligand is less electronegative than carbon, one usually finds a maximum that will be attacked by an electrophile. As Figure 24 shows, the value of L(r) at the (3,+1) point drops with increased electronegativity of X, indicating decreasing density at this point, and therefore increased attractiveness to a nucleophile. These values agree with work done by Boyd et al[144]. In the case of silanes, the majority of species have little to no density in the valence region, effectively destroying any VSCC structure. In the few cases where they can be located, the value tends to be about –0.010 au. In other cases, one can approximate a (3,+1) critical point by analyzing L(r) at a midpoint between the (3,-1) critical points that can be found in the atomic graph.

which results in a large negative value. The relative reactivity of silanes with different leaving groups then becomes a matter of the stability of the leaving group itself, rather than accessibility of the nucleophile[38].

4.3 Comparisons Between AIM and MO

This work, in addition to providing a more comprehensive computational study of simple silanes and their carbon-based equivalents, helps to dispel two important misconceptions about silicon populations. Firstly, the charges on silicon are significantly higher than models based on molecular orbitals predict[75]. This is the fault of the population analyses based on atomic partitioning of MOs. Methods such as Mulliken population analysis simply divide the overlap population equally between two atoms, rather than analyzing the density and ascertaining what part of the density belongs to each atom. More advanced methods such as Natural Population Analysis (NPA) provide more realistic populations. As has been already discussed, however, this model does not accurately represent the valence density of molecules[77].

Table 55: Calculated Charge of Atom M in Selected MH_3X Species, in au

MH_3-X	Mulliken[75]	NPA[75]	AIM
CH_3-H	-0.660	-0.485	0.175
SiH_3-H	0.545	0.853	2.899
CH_3-Li	-0.781	-1.392	-0.559
SiH_3-Li	0.211	-0.089	1.362
CH_3-CH_3	-0.476	-0.636	0.184
SiH_3-CH_3	0.683	1.123	2.924
CH_3-OH	-0.167	-0.219	0.768
SiH_3-OH	0.897	1.437	3.043
CH_3-F	-0.063	-0.083	0.773
SiH_3-F	0.993	1.498	3.058
CH_3-Cl	-0.109	-0.598	0.254
SiH_3-Cl	0.727	1.107	2.941

As Table 55 shows, the Mulliken analysis technique provides integrated atomic populations that place a great deal of electron density on the central atom. For those species where the central atom is bonded to an electronegative element such as oxygen or fluorine, the calculated charge on the central atom is much lower than one would expect. In the cases of methanol and fluoromethane, the Mulliken technique calculates the charge on carbon to be negative, which is counterintuitive, given the electronegativity of the fluorine or oxygen atom. These low populations can be explained by the method used to partition the electron density, which does not take into account its polarization. Without a sound criterion upon which to assign electron

density to individual atoms in the molecule, one cannot obtain results that even make intuitive sense: one cannot resolve a negative charge on an atom within a species known to undergo facile nucleophilic attack. Mulliken analyses of silyl species provide silicon populations that at least have positive charges, as one would expect. Given the much greater nucleophilic reactivity of silyl species compared to the corresponding carbon species, however, these charges ought to be larger than one observes. One must also take into consideration the difference in electronegativity between carbon and silicon, which should result in a larger difference in atomic charges when the two atoms are placed in similar chemical environments. When compared to populations obtained through AIM, Mulliken populations are consistently too large, resulting in atomic charges that are more negative than those calculated by AIM.

Natural Population analysis provides no consistent comparison with Mulliken, in that most carbon charges are lower than Mulliken predicts, while silicon charges are higher. This is not even a consistent trend with the examples shown here: the charge on carbon in methane goes up when NPA is applied, while the charge on silicon in silyllithium goes down. The only consistency to be found is within the trend of atom X bonded to carbon or silicon: the charge on the central atom increases as X becomes more electronegative, for both Mulliken and NPA. The same intuitive arguments made for the Mulliken populations of carbon-centered species can be made for NPA, especially considering that NPA charges are even lower. Overall, one must retain consistency in results for examples of a population analysis technique. If some of the results obtained using a certain technique are questionable, then all results using this technique must be questioned.

The other misconception concerns hyperco-ordination. Many studies, using MO models, calculate that as the coordination around silicon increases, so does its charge. However, if a ligand such as fluoride is added to a silane, why would it try to gain more negative charge than it already has? If anything, the charge on silicon should decrease, taking the extra negative charge onto itself, or stay the same, allowing the negative charge to be distributed amongst the other ligands. AIM calculations show the latter to be the case, a result that is in agreement with other research[79,146]. This makes intuitive sense: the silicon would not gain the charge gained by the molecule, as the other electronegative ligands on silicon would strip it away. In

light of the fact that the silicon is already depleted, a saying comes to mind: 'you cannot get blood from a stone.'

4.4 Discussion: Chemistry of Silyl Species

The chemistry of silanes is centered mostly around the fact that a given Si-X bond is highly polarized, with most of the electron density centered on the more electronegative element X. This causes silicon to have a significant positive charge, while X has a negative charge. This highly polar bond has a very low density at the bond critical point, about half that of the equivalent C-X bond. Silicon, due to its large size, can handle co-ordination higher than four; the ligands surrounding silicon tend to become more negative as co-ordination increases, while the charge on silicon stays nearly the same, and the bonds become longer and more ionic. With this information in hand, the observed chemistry of silicon, as well as its geometric structure, is easily explained.

- Structure: Si-X bonds tend to be longer than C-X bonds, as is expected for a large element such as silicon, but smaller than predicted by sums of covalent radii. Certain geometric anomalies, such as the Si-O-Si bond angle, and the high degree of planarity of the amine group in the Si-N bond, can be explained by the fact that there is a great deal of ionic character in these bonds. As a result, the Si-O-Si angle is larger than expected, as predicted for a partly ionic system by VSEPR theory, and the amine can be treated more like an anion, which is planar in structure. The Si-O and Si-F bonds, shorter than covalent radii predict, are explained simply by not treating them as covalent bonds, but as having partial ionic character, which then predicts bond lengths more in keeping with observation.
- Coordination: Silicon shows the opposite trend to carbon in terms of coordination; low coordinate silanes are inherently unstable, while high coordination silanes are quite stable. The low stability of low coordinate species is explained by the diffuse nature of the valence density of silicon. A double bond between silicon and X will be polarized towards X, leaving the silicon with large depletions that can be attacked by even the weakest nucleophiles, including another Si=X molecule. High coordination systems behave like increasingly ionic systems as the coordination number increases. R_3SiH is unreactive towards electrophiles, but $F\text{-}R_3SiH$ acts a strong hydride donor. As another example, take the rate of formation of a pentacoordinate species. The rate of formation of the

hexacoordinate species will be faster, not because the charge on silicon has changed, but because the bonds between silicon and the existing ligands have become more ionic. It takes little energy to form an ionic bond in an already ionic system, as opposed to trying to form an ionic bond in a partly ionic system. Such systems only work when the ligand is electronegative, already having a strong negative charge.

- Reactivity: The Si-X bond is highly polar, with some positive charge on silicon, and negative charge on X. As a result, such a system is vulnerable to nucleophiles. The groups bonded to silicon are widely spaced because of silicon's size, allowing plenty of room for nucleophilic attack. Any reagent with a nucleophilic site can attack. Dipoles add across the Si-X bond, and even non-polar molecules such as halogens can have a dipole induced in them, promoting a reaction. Silanes are so open to attack that nucleophiles need not even attack the face opposite the leaving group. Under the right conditions, a nucleophile can attack the same side as the leaving group, leading to nucleophilic substitution with retention of any stereocenter, something never seen in carbon-based systems.

4.5 Disilane Revisited

This project started with the study of the simple silyl systems discussed above. The L(r) maps of these systems helped to provide a clear picture of the polarization of electron density that occurs when silicon is bonded to another element. The majority of results were expected, as even MO theory predicts a positive charge on silicon, albeit smaller than AIM predicts. The L(r) plot of disilane, however, proved surprising; the diffuse, isolated charge concentration between the silicon atoms was entirely unexpected, and provoked much speculation and discussion. Given the diffuse nature of the valence density around the silicon atom, would such a charge concentration be easily polarized by external influences? This naturally led to the matter of electronic excitation observed in polysilanes and 'sigma conjugation'. If one considered the conjugated π bond density of polyenes to be easily polarized, as it is not as tightly bound as the σ density is, could a string of charge concentrations forming along the backbone of a polysilane be the σ-bond equivalent of delocalization, an observable example of a sigma-conjugated system? It was decided at this point that the research take a new direction, and the properties of a series of simple oligosilanes be studied.

in hope of observing changes in properties that could be associated with a delocalized molecular system.

4.6 Properties of M_nH_{2n+2}

A series of molecules were calculated matching the formula M_nH_{2n+2}, where n ranged from 2 to 7, and M represents carbon or silicon[147]. All the chains possessed an all-trans conformation. In addition to a set of standard Hartree-Fock calculations, a second series were optimized using Self-Consistent Virial Scaling (SCVS)[102,109]. This technique scales the Hartree-Fock wavefunction, such that it satisfies the virial theorem exactly. This was done as part of a related subproject that studied the effects of SCVS on the additive properties of hydrocarbons, a project that was then expanded to include the equivalent oligosilanes. The additivity studies have been incorporated into this research in order to determine whether additivity can be used as a criterion for observing σ-conjugation in these systems.

4.6.1 Bond Properties of C_nH_{2n+2}

The bond properties of short-chain hydrocarbons have already been the subject of considerable study. This work is an expansion of these studies, with a series of molecules up to n = 7. For the sake of brevity, only the SCVS optimized series will be discussed in detail here; standard H-F data of these molecules will be discussed in detail later in the thesis.

Table 56: Comparison of Ethane, HF and HF + SCVS

Ethane Data	Hartree-Fock	Hartree-Fock + SCVS
C-C bond length (Å)	1.525	1.524
C-H bond length (Å)	1.084	1.084
C-C BCP, rho (au)	0.250	0.249
C-H BCP, rho (au)	0.291	0.291
Basin int. of C, rho (au)	5.816	5.816
Basin int. of H, rho (au)	1.061	1.061
Basin int. of C, energy (au)	-37.6721	-37.6721
Basin int. of H, energy (au)	-0.6522	-0.6522

The inclusion of SCVS has little effect on the properties of the hydrocarbon or oligosilane series, including geometry, bond properties and integrated basin properties, so there is little point in tabulating all the data for both sets of wavefunctions.

Table 57: Comparison of Disilane, HF and HF + SCVS

Disilane Data	Hartree-Fock	Hartree-Fock + SCVS
Si-Si bond length (Å)	2.373	2.373
Si-H bond length (Å)	1.477	1.477
Si-Si BCP, rho (au)	0.093	0.093
Si-H BCP, rho (au)	0.121	0.121
Basin int. of Si, rho (au)	11.831	11.834
Basin int. of H, rho (au)	1.722	1.722
Basin int. of Si, energy (au)	-288.2986	-288.2986
Basin int. of H, energy (au)	-0.7946	-0.7944

The most important point to gain from the geometry data of Table 58 is that the bond lengths achieve a constant value as the chain length increases. This is the first indication that the methylene groups within this series of molecules are transferable, as their properties do not change significantly with molecular chain length. If their properties do not change with chain length, then the groups are also additive, in that the properties of a hydrocarbon can obtained simply by summing up the properties of the appropriate standard groups.

Table 58: Bond Lengths and Angles of Hydrocarbon Series n = 2-7 (SCVS)

C_2H_6 D_{3d}		C_5H_{12} C_{2v}		C_7H_{16} C_{2v}	
r(C-C)	1.524	r(C1-C2)	1.525	r(C1-C2)	1.525
r(C-H)	1.084	r(C2-C3)	1.526	r(C2-C3)	1.526
>(H-C-C)	111.21	r(C1-H')	1.083	r(C3-C4)	1.526
>(H-C-H)	107.68	r(C1-H)	1.084	r(C1-H')	1.084
C_3H_8 C_{2v}		r(C2-H)	1.086	r(C1-H)	1.084
r(C1-C2)	1.525	r(C3-H)	1.087	r(C2-H)	1.086
r(C1-H')	1.084	>(C1-C2-C3)	113.21	r(C3-H)	1.087
r(C1-H)	1.085	>(C2-C3-C4)	113.53	r(C4-H)	1.087
r(C2-H)	1.085	>(H'-C1-C2)	111.28	>(C1-C2-C3)	113.20
>(C1-C2-C3)	112.96	>(H-C1-C2)	111.14	>(C2-C3-C4)	113.50
>(H'-C1-C2)	111.34	>(H'-C1-H)	107.74	>(C3-C4-C5)	113.48
>(H-C1-C2)	111.08	>(H-C1-H)	107.63	>(H'-C1-C2)	111.28
>(H'-C1-H)	107.77	>(H-C2-C1)	109.33	>(H-C1-C2)	111.14
>(H-C1-H)	107.62	>(H-C2-C3)	109.26	>(H'-C1-H)	107.73
>(H-C2-C1)	109.35	>(H-C2-H)	106.21	>(H-C1-H)	107.63
>(H-C2-H)	106.26	>(H-C3-C2)	109.23	>(H-C2-C1)	109.33
C_4H_{10} C_{2h}		>(H-C3-H)	106.14	>(H-C2-C3)	109.27
r(C1-C2)	1.525	C_6H_{12} C_{2h}		>(H-C2-H)	106.21
r(C2-C3)	1.526	r(C1-C2)	1.525	>(H-C3-C2)	109.18
r(C1-H')	1.083	r(C2-C3)	1.526	>(H-C3-C4)	109.29
r(C1-H)	1.084	r(C3-C4)	1.526	>(H-C3-H)	106.15
r(C2-H)	1.086	r(C1-H')	1.084	>(H-C4-C3)	109.23
>(C1-C2-C3)	113.23	r(C1-H)	1.084	>(H-C4-H)	106.17
>(H'-C1-C2)	111.29	r(C2-H)	1.086		
>(H-C1-C2)	111.13	r(C3-H)	1.087		
>(H'-C1-H)	107.74	>(C1-C2-C3)	113.20		
>(H-C1-H)	107.64	>(C2-C3-C4)	113.51		
>(H-C2-C1)	109.37	>(H'-C1-C2)	111.28		
>(H-C2-C3)	109.21	>(H-C1-C2)	111.14		
>(H-C2-H)	106.20	>(H'-C1-H)	107.74		
		>(H-C1-H)	107.63		
		>(H-C2-C1)	109.33		
		>(H-C2-C3)	109.27		
		>(H-C2-H)	106.21		
		>(H-C3-C2)	109.17		
		>(H-C3-C4)	109.28		
		>(H-C3-H)	106.16		

From this series, we see that the C-C bond standardizes to 1.526 Å, the methyl C-H bond to 1.084 Å, and the methylene C-H bond to 1.086 Å; all bond lengths in Table 58 are in angstroms. We have seen already that geometry provides a good indication of the electronic structure of the molecule being observed, so the fact that the geometries do not change with hydrocarbon chain length indicates that the other properties will not change appreciably either.

Table 59: BCP Data for Hydrocarbon Series n = 2-7, in au (SCVS)

	A-B	ρ_b	$L(r)_b$	$r_b(A)$	$r_b(B)$
C_2H_6	C1-C2	0.249	0.153	1.440	1.440
	C1-H3	0.291	0.283	1.271	0.776
C_3H_8	C1-C2	0.252	0.155	1.447	1.435
	C1-H4	0.291	0.283	1.271	0.777
	C1-H5	0.290	0.283	1.271	0.778
	C2-H7	0.292	0.285	1.270	0.781
C_4H_{10}	C1-C2	0.251	0.155	1.447	1.435
	C2-C3	0.253	0.157	1.442	1.442
	C1-H5	0.291	0.283	1.271	0.777
	C1-H6	0.290	0.281	1.271	0.778
	C2-H8	0.291	0.283	1.270	0.783
C_5H_{12}	C1-C2	0.251	0.155	1.447	1.435
	C2-C3	0.253	0.157	1.442	1.442
	C1-H6	0.291	0.283	1.271	0.777
	C1-H7	0.290	0.281	1.271	0.778
	C2-H9	0.291	0.283	1.269	0.783
	C3-H11	0.290	0.281	1.269	0.785
C_6H_{14}	C1-C2	0.251	0.155	1.447	1.435
	C2-C3	0.253	0.157	1.442	1.442
	C3-C4	0.253	0.157	1.442	1.442
	C1-H7	0.291	0.283	1.271	0.777
	C1-H8	0.290	0.281	1.271	0.778
	C2-H10	0.291	0.283	1.270	0.783
	C3-H12	0.290	0.281	1.269	0.785
C_7H_{16}	C1-C2	0.251	0.155	1.447	1.435
	C2-C3	0.253	0.157	1.442	1.442
	C3-C4	0.253	0.157	1.442	1.442
	C1-H8	0.291	0.283	1.271	0.777
	C1-H9	0.290	0.281	1.271	0.778
	C2-H11	0.291	0.283	1.269	0.783
	C3-H13	0.290	0.281	1.269	0.785
	C4-H15	0.290	0.281	1.269	0.785

Table 59 shows the changes in BCP data as a function of chain length of the hydrocarbons. From this data, one can see that the bond properties reach a standard value quite early in the series, at n = 4. This reflects the fact that, at this point and beyond, the methyl and methylene groups in each molecule experience no significant change in their environment. This is an illustration of the short-sighted nature of these groups. The influence of a group on atomic properties does not extend beyond the group adjacent to

the group in question. From this, one can conclude that for a linear long chain hydrocarbon, there are three types of functional groups. The methyl group, a methylene group that is bonded to a methyl group and a methylene group (also known as an α-methylene), and a methylene group bonded to two methylene groups (also known as an internal methylene). Such labels apply to all of the molecules in the series at n = 4 and beyond; the exceptions are ethane and propane, as the methyls and methylenes of these molecules do not exist in the same environments as the larger hydrocarbons.

One cannot appreciate the extent to which the hydrocarbon functional groups achieve standard properties without looking at contour maps of different members of this series. The following diagrams show the striking similarity of the methyl and α-methylene groups in hexane and heptane, both in terms of rho (Figure 36) and the Lagrangian kinetic energy function, or KEG (Figure 37).

Figure 36: Contour Map of Rho for C_6H_{14} (left) and C_7H_{16} (right) (SCVS)

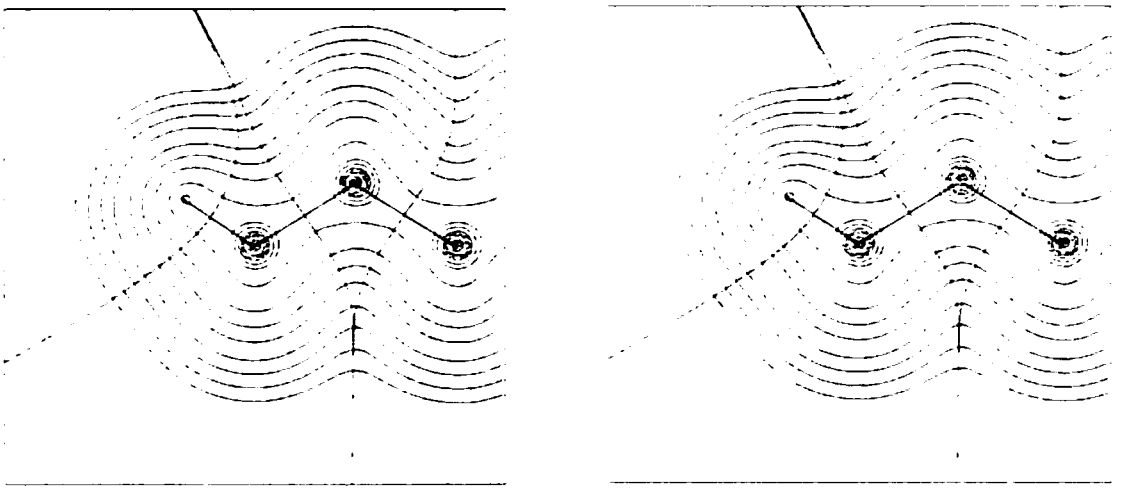

Figure 37: Contour Map of KEG for C_6H_{14} (left) and C_7H_{16} (right) (SCVS)

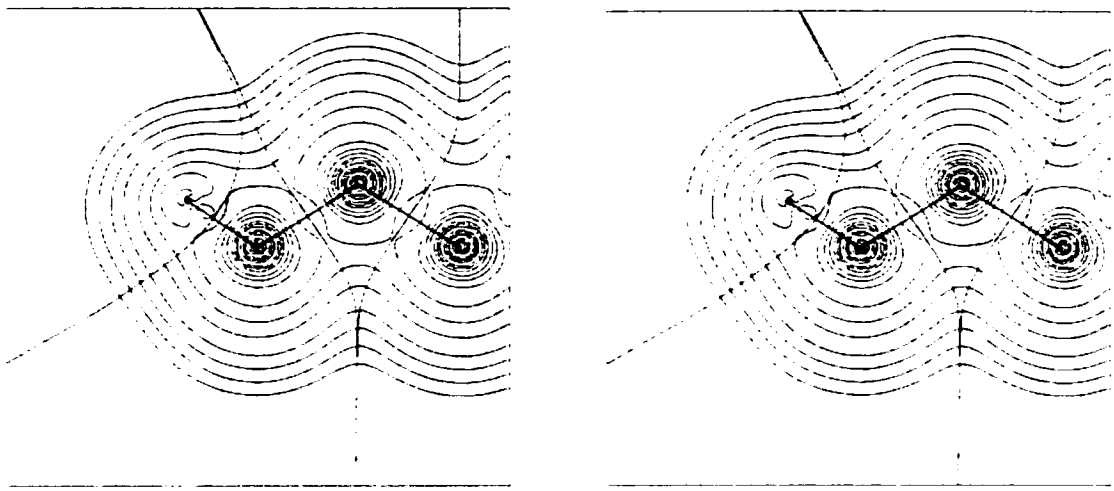

Anyone who might question whether these contour plots are identical need only copy them and observe the superimposed images. The fact that the contour plots are virtually indistinguishable clearly demonstrates their transferability, which will be a key issue when the subject of their additivity is addressed.

4.6.2 Atomic Properties of C_nH_{2n+2}

The definition of additivity is that a molecular property can be expressed as the sum of standard group contributions, and that any molecular property is simply the sum of the group properties. Table 60 shows the total energies and electron counts for the hydrocarbon series, along with integration errors, and the deviation of the molecular virial from two.

Table 60: Energies and Integration Errors of Hydrocarbons, in au (SCVS)

Molecule	E	(V/T) + 2	$\Sigma E(\Omega) - E_{mol}$	$\Sigma N(\Omega)-N_{mol}$
C_2H_6	-79.2574	8.00E-08	0.00007	0.0004
C_3H_8	-118.3038	-3.00E-08	0.00037	0.0013
C_4H_{10}	-157.3502	-2.00E-08	0.00050	0.0017
C_5H_{12}	-196.3965	-1.00E-08	0.00089	0.0031
C_6H_{14}	-235.4428	1.00E-08	0.00101	0.0035
C_7H_{16}	-274.4891	1.00E-08	0.00139	0.0049

Looking at the energies in Table 60, one cannot tell for certain if the energies observe a linear correlation with chain length: Figure 38 shows that the relationship is in fact linear. The molecular energies were subjected to a linear regression treatment; as can be seen, the molecular energies fit the regression line perfectly. This then allows us to express any property **A** in terms of a simple formula:

$$A_{C_nH_{2n+2}} = 2 * A_{CH_3} + \sum_{i=0}^{n-2} A_{CH_2} \qquad (59)$$

For the hydrocarbon series, E_{CH3} = -39.628735 and E_{CH2} = -39.04634, (for the basis set used in this thesis).

Figure 38: Regression Fit for Hydrocarbon Energies

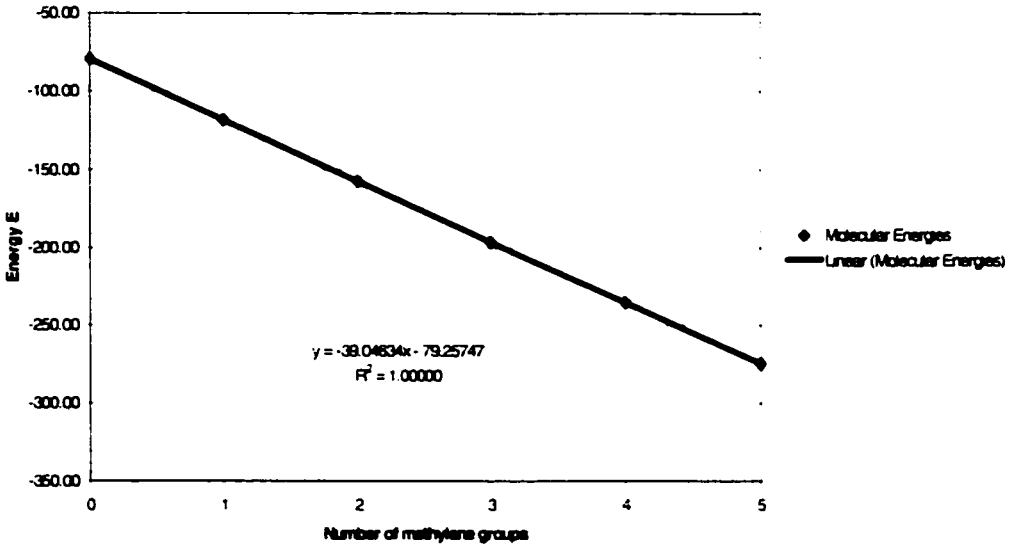

One finds that the group properties do not in fact fit the 'standard' group values that were calculated, even though the total molecular values do. This gives rise to an effect called 'compensatory transferability'[148].

Table 61: Atomic Properties of Hydrocarbons, in au

Atom Ω	N(Ω)	E (Ω)	L(Ω)	Atom Ω	N(Ω)	E (Ω)	L(Ω)
C_2H_6				C_6H_{14}			
$CH_3 - C$	5.816	-37.6721	-6.31E-05	$CH_3 - C$	5.826	-37.6856	1.25E-04
$CH_3 - H$	1.061	-0.6522	7.62E-05	$CH_3 - H'$	1.061	-0.6516	7.93E-05
C_3H_8				$CH_3 - H$	1.065	-0.6527	9.13E-05
$CH_3 - C$	5.826	-37.6874	6.77E-05	$^bCH_2 - C$	5.829	-37.7018	6.10E-04
$CH_3 - H'$	1.061	-0.6515	7.89E-05	$^bCH_2 - H$	1.077	-0.6648	1.10E-04
$CH_3 - H$	1.064	-0.6525	8.71E-05	$^cCH_2 - C$	5.840	-37.7176	6.91E-04
$CH_2 - C$	5.819	-37.6884	7.42E-04	$^cCH_2 - H$	1.080	-0.6652	1.24E-04
$CH_2 - H$	1.074	-0.6640	1.02E-04	C_7H_{16}			
C_4H_{10}				$CH_3 - C$	5.826	-37.6854	1.17E-04
$CH_3 - C$	5.827	-37.6863	-1.53E-04	$CH_3 - H'$	1.061	-0.6516	7.91E-05
$CH_3 - H'$	1.061	-0.6514	7.93E-05	$CH_3 - H$	1.065	-0.6527	8.71E-05
$CH_3 - H$	1.064	-0.6526	8.97E-05	$^bCH_2 - C$	5.829	-37.7018	7.42E-04
$CH_2 - C$	5.829	-37.7034	7.40E-04	$^bCH_2 - H$	1.077	-0.6648	1.09E-04
$CH_2 - H$	1.077	-0.6645	1.08E-04	$^cCH_2 - C$	5.839	-37.7171	8.54E-04
C_5H_{12}				$^cCH_2 - H$	1.080	-0.6653	1.22E-04
$CH_3 - C$	5.826	-37.6857	1.08E-04	$^aCH_2 - C$	5.840	-37.7168	8.75E-04
$CH_3 - H'$	1.061	-0.6515	7.91E-05	$^aCH_2 - H$	1.080	-0.6654	1.29E-04
$CH_3 - H$	1.064	-0.6527	8.94E-05				
$^bCH_2 - C$	5.830	-37.7024	7.41E-04				
$^bCH_2 - H$	1.077	-0.6647	1.10E-04				
$^cCH_2 - C$	5.839	-37.7185	8.71E-04				
$^cCH_2 - H$	1.080	-0.6651	1.27E-04				

The methyl group, with its extra hydrogen, is slightly more electron withdrawing than the methylene group. As a result, the methylene group loses some electron density to the methyl, giving it a slightly lower electron count than standard, and the methyl group gains some electron density, giving it a slightly higher electron count than standard. Table 62 shows the deviations of the group properties from their standard values. It clearly shows that the groups are in fact additive, but that the deviation in one group property is compensated exactly by the deviation in the adjacent group.

---

[a] Atomic properties of central methylene group of heptane.

[b] Atomic properties of α-methylene group.

[c] Atomic properties of internal methylene group.

Table 62: Net Charges and Energies of Methyl and Methylene Groups Relative to Standard Values[a]

Molecule	$q(CH_3)$	$q(CH_2)$	$q(CH_2)^b$	$\Delta E(CH_3)^c$	$\Delta E(CH_2)^c$	$\Delta E(CH_2)^{b,c}$
Ethane	0.000			0.0		
Propane	-0.016	0.033		-9.5	18.8	
Butane	-0.016	0.017		-8.9	8.7	
Pentane	-0.016	0.017	0.002	-8.7	9.1	-1.5
Hexane	-0.016	0.017	0.001	-8.6	9.4	-1.1
Heptane	-0.016	0.017	0.002 0.001[d]	-8.6	9.4	-0.9 -0.8[d]

What is truly remarkable about these results is the fact that this compensatory transferability is the same regardless of environment. For example, the deviation in energy of the methyl group is constant from butane on. To compensate for this, the deviation on the propane methylene is double that of the methyl, to compensate for the loss of energy of both of the methyls it is bonded to. In butane, the methylene deviation equals the methyl deviation in magnitude, as it is only bonded to one methyl group, and remains fairly constant for the rest of the series. The internal methylenes show small deviations in energy (about 1.0 au on average) from the standard values, so it can be said that the 'standard' methylene is one that is bonded to other methylenes. This confirms that there are three types of groups in hydrocarbons: methyls, α-methylenes, and internal methylenes, and that the integrated values of these three groups can be used as building blocks to form hydrocarbons of any length. One can calculate the properties of such hydrocarbons easily, simply by summing the properties of the appropriate groups involved.

4.6.3 L(r) Properties of C_nH_{2n+2}

Figure 39 shows the L(r) maps of propane and heptane. These maps illustrate how the valence density remains localized within the C-C and C-H bonds, even when the chain length changes considerably.

---

[a] $E(CH_3)$ = -39.62873 au., $E(CH_2)$ = -39.04634 au. using linear regression fit of the molecular energies of the series.
[b] This CH_2 is bonded only to other methylenes.
[c] Energies in kcal/mol.
[d] Central carbon in heptane.

Figure 39: L(r) Maps of Propane and Heptane (SCVS)

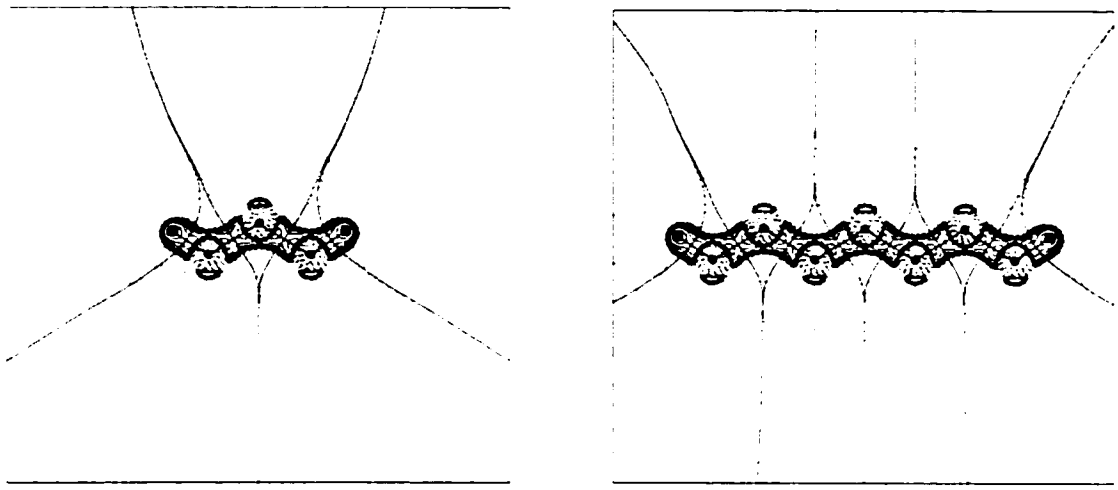

Given that all the ground state properties of hydrocarbons are additive and transferable, the critical points in L(r) should be similar to those observed in ethane, as should be its reactivity to nucleophiles. The critical points in L(r) of these molecules tend to follow a tetrahedral structure, as outlined in the theoretical section, with four maxima in the VSCC of each carbon, six (3,-1) critical points forming the edges, and four (3,+1) critical points forming the faces. Other (3,-1) critical points, located at the BCP positions for the C-C bonds, connect each tetrahedron with its neighbor. As with the bond data, these critical point values remain constant with chain length, reinforcing the idea that L(r) is also additive in this series. Figure 40 shows that the values of the critical points in L(r): spheres are maxima, triangles are (3,-1) critical points, and squares are (3,+1) critical points. The tetrahedra are positioned so that the (3,-1) critical points hanging off the bottom vertices link to other tetrahedra in C-C bonds, and the top vertices represent the maxima associated with C-H bonds. The values of these critical points are all positive, with the exception of the (3,+1) critical points at the tetrahedral faces, which reflects the fact that there is a great deal of density in the VSCC of carbon, all tightly bound within the C-C and C-H bonds.

Figure 40: Values of L(r) Critical Points for C_3H_8 (left) and C_7H_{16} (right), Central Carbon, in au.

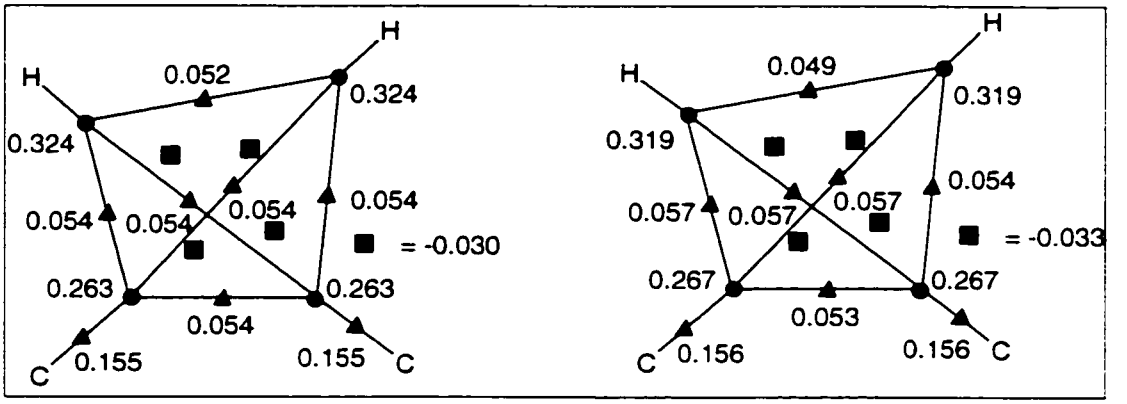

4.6.4 Bond Properties of Si_nH_{2n+2}

The concept of a standard bond, with BCP properties that are invariant to chain length could prove useful in addressing the issue of delocalization in the oligosilane series. Conjugated π-systems are known to have bonds that vary considerably from molecule to molecule; this is because of the differing levels of π-bond character that exist as a result of different extents of delocalization. In that sense, π-conjugated systems are not truly transferable as saturated systems are, as the π-bond density will distribute itself differently as a result of the molecules' size, and the amount of π-bond density available. Table 63 shows the geometric data for the series Si_nH_{2n+2}, where n ranges from two to seven. Like the data in Table 58, the bond lengths and angles also achieve a standard set of values. They are: 2.375 Å for the Si-Si bond between the silyl and α-silylene groups, 2.376 Å for the internal Si-Si bond, 1.477 Å for the silyl group Si-H bonds, and 1.480 Å for the silylene group Si-H bonds.

Table 63: Bond Lengths and Angles of Oligosilanes (SCVS)

Si_2H_6 D_{3d}		Si_5H_{12} C_{2v}		Si_7H_{16} C_{2v}	
r(Si-Si)	2.373	r(Si1-Si2)	2.375	r(Si1-Si2)	2.375
r(Si-H)	1.477	r(SI2-SI3)	2.376	r(Si2-Si3)	2.376
>(H-Si-Si)	110.27	r(Si1-H')	1.477	r(Si3-Si4)	2.376
>(H-Si-H)	108.66	r(Si1-H)	1.477	r(Si1-H')	1.477
Si_3H_8 C_{2v}		r(Si2-H)	1.480	r(Si1-H)	1.477
r(Si1-Si2)	2.375	r(Si3-H)	1.480	r(Si2-H)	1.480
r(Si1-H')	1.476	>(Si1-Si2-Si3)	112.21	r(Si3-H)	1.480
r(Si1-H)	1.477	>(Si2-Si3-Si4)	112.41	r(Si4-H)	1.480
r(Si2-H)	1.480	>(H'-Si1-Si2)	110.67	>(Si1-Si2-Si3)	112.22
>(Si1-Si2-Si3)	112.07	>(H-Si1-Si2)	110.04	>(Si2-Si3-Si4)	112.41
>(H'-Si1-Si2)	110.60	>(H'-Si1-H)	108.70	>(Si3-Si4-Si5)	112.38
>(H-Si1-Si2)	110.12	>(H-Si1-H)	108.63	>(H'-Si1-Si2)	110.68
>(H'-Si1-H)	108.69	>(H-Si2-Si1)	109.31	>(H-Si1-Si2)	110.04
>(H-Si1-H)	108.56	>(H-Si2-Si3)	109.02	>(H'-Si1-H)	108.70
>(H-Si2-Si1)	109.18	>(H-Si2-H)	107.88	>(H-Si1-H)	108.63
>(H-Si2-H)	107.96	>(H-Si3-Si2)	109.16	>(H-Si2-Si1)	109.30
Si_4H_{10} C_{2h}		>(H-Si3-H)	107.67	>(H-Si2-Si3)	109.02
r(Si1-Si2)	2.374	Si_6H_{12} C_{2h}		>(H-Si2-H)	107.88
r(Si2-Si3)	2.376	r(Si1-Si2)	2.375	>(H-Si3-Si2)	109.18
r(Si1-H')	1.477	r(Si2-Si3)	2.376	>(H-Si3-Si4)	109.09
r(Si1-H)	1.477	r(Si3-Si4)	2.376	>(H-Si3-H)	107.76
r(Si2-H)	1.480	r(Si1-H')	1.477	>(H-Si4-Si3)	109.02
>(Si1-Si2-Si3)	112.19	r(Si1-H)	1.477	>(H-Si4-H)	107.78
>(H'-Si1-Si2)	110.66	r(Si2-H)	1.480		
>(H-Si1-Si2)	110.04	r(Si3-H)	1.480		
>(H'-Si1-H)	108.71	>(Si1-Si2-Si3)	112.22		
>(H-Si1-H)	108.64	>(Si2-Si3-Si4)	112.42		
>(H-Si2-Si1)	109.29	>(H'-Si1-Si2)	110.68		
>(H-Si2-Si3)	109.08	>(H-Si1-Si2)	110.04		
>(H-Si2-H)	107.81	>(H'-Si1-H)	108.70		
		>(H-Si1-H)	108.63		
		>(H-Si2-Si1)	109.30		
		>(H-Si2-Si3)	109.02		
		>(H-Si2-H)	107.88		
		>(H-Si3-Si2)	109.19		
		>(H-Si3-Si4)	109.10		
		>(H-Si3-H)	107.74		

The fact that these are standard values puts into doubt the idea that BCP data will be able to demonstrate delocalization in the oligosilane series, which Table 64 confirms. Just as the geometric data indicated, one ends up with a standard set of bond properties for oligosilanes as well as hydrocarbons. Clearly delocalization of the electron density is not something that manifests in BCP data: it may become more

apparent in contour plots instead, where the density of the entire molecule can be observed, rather than specific points.

Table 64: BCP Data for Oligosilane Series n = 2-7, in au (SCVS)

	A-B	ρ	$L(r)_b$	$r_b(A)$	$r_b(B)$
Si_2H_6	Si1-Si2	0.093	0.038	2.242	2.242
	Si1-H3	0.121	-0.045	1.359	1.432
Si_3H_8	Si1-Si2	0.092	0.038	2.245	2.242
	Si1-H4	0.121	-0.045	1.359	1.431
	Si1-H5	0.121	-0.045	1.359	1.438
	Si2-H7	0.119	-0.045	1.362	1.434
Si_4H_{10}	Si1-Si2	0.092	0.038	2.237	2.250
	Si2-Si3	0.091	0.036	2.245	2.245
	Si1-H5	0.121	-0.045	1.359	1.431
	Si1-H6	0.121	-0.045	1.359	1.432
	Si2-H8	0.119	-0.045	1.362	1.435
Si_5H_{12}	Si1-Si2	0.092	0.038	2.238	2.249
	Si2-Si3	0.091	0.036	2.237	2.253
	Si1-H6	0.121	-0.045	1.359	1.431
	Si1-H7	0.121	-0.045	1.359	1.432
	Si2-H9	0.119	-0.045	1.362	1.434
	Si3-H11	0.119	-0.045	1.362	1.434
Si_6H_{14}	Si1-Si2	0.092	0.038	2.239	2.249
	Si2-Si3	0.091	0.036	2.239	2.252
	Si3-Si4	0.091	0.036	2.245	2.245
	Si1-H7	0.121	-0.045	1.359	1.431
	Si1-H8	0.121	-0.045	1.359	1.432
	Si2-H10	0.119	-0.045	1.362	1.434
	Si3-H12	0.119	-0.045	1.362	1.435
Si_7H_{16}	Si1-Si2	0.092	0.038	2.239	2.248
	Si2-Si3	0.091	0.036	2.239	2.251
	Si3-Si4	0.091	0.036	2.247	2.243
	Si1-H8	0.121	-0.045	1.359	1.431
	Si1-H9	0.121	-0.045	1.359	1.432
	Si2-H11	0.119	-0.045	1.362	1.434
	Si3-H13	0.119	-0.045	1.362	1.437
	Si4-H15	0.119	-0.045	1.362	1.437

Figure 41 shows that just as the BCPs of the oligosilane series achieve standard values irrespective of chain length, so do the density contours. Though integration data may show more subtle effects that the

contour maps cannot, it becomes increasingly clear that the electron density shows no properties that can be interpreted as σ-conjugation.

Figure 41: Contour Map of Rho for Si_6H_{14} (left) and Si_7H_{16} (right) (SCVS)

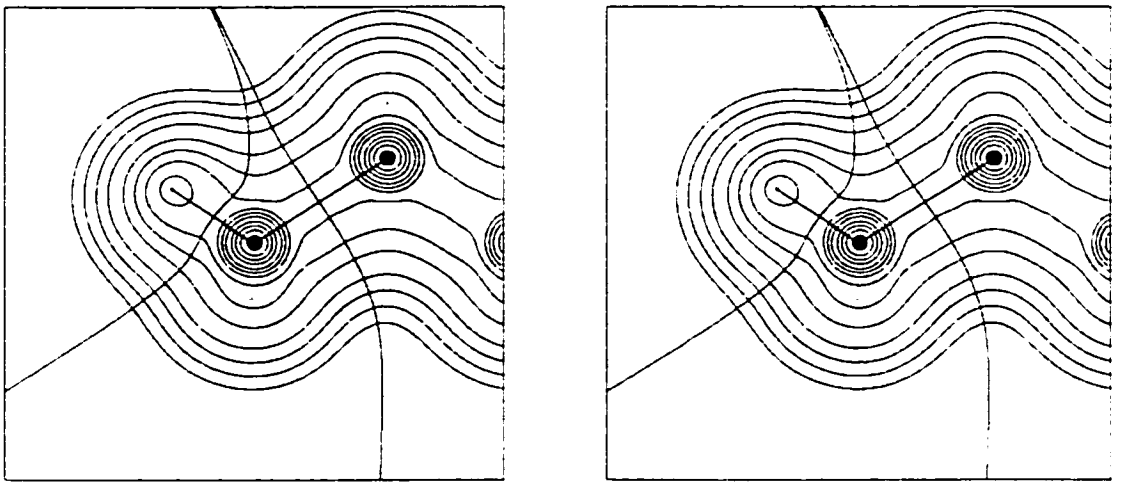

Figure 42: Contour Map of KEG for Si_6H_{14} (left) and Si_7H_{16} (right) (SCVS)

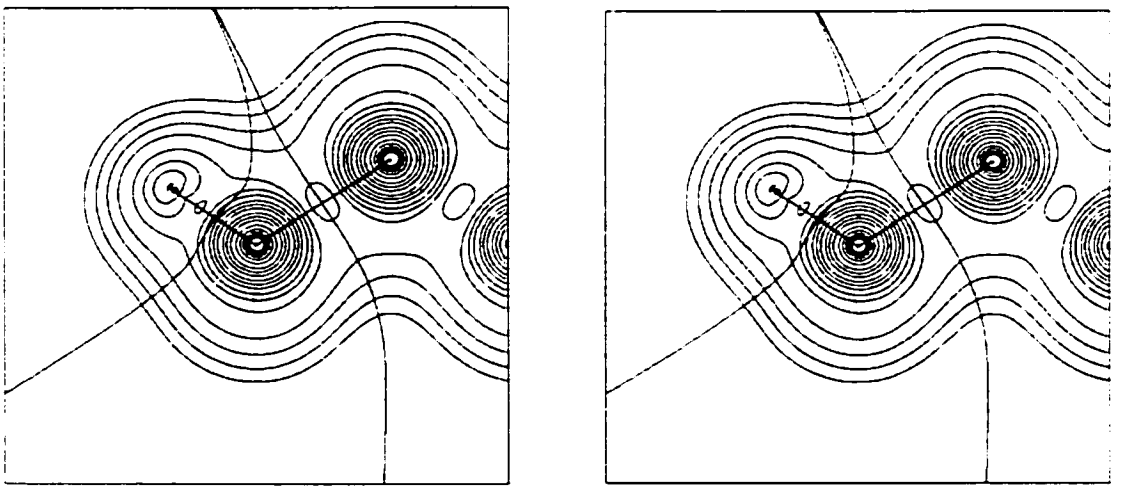

4.6.5 Atomic Properties of Si_nH_{2n+2}

From the BCP data of this series, one gets the impression that the atomic property data will be as similarly transferable as the hydrocarbons. Table 65 shows the energy data used to find the standard energies, while Figure 43 shows the regression fit of the silane energies.

Table 65: Energies and Integration Errors of Oligosilanes, in au (SCVS)

Molecule	E	(V/T) + 2	$\Sigma E(\Omega) - E_{mol}$	$\Sigma N(\Omega)-N_{mol}$
Si_2H_6	-581.3636	< 1.00E-08	0.00021	0.0006
Si_3H_8	-871.4711	1.00E-08	0.00024	0.0010
Si_4H_{10}	-1161.5789	< 1.00E-08	0.00076	0.0039
Si_5H_{12}	-1451.6866	1.40E-07	0.00097	0.0041
Si_6H_{14}	-1741.7944	-1.00E-08	0.00049	-0.0002
Si_7H_{16}	-2031.9022	< 1.00E-08	0.00116	0.0048

Figure 43: Regression Fit for Oligosilane Energies

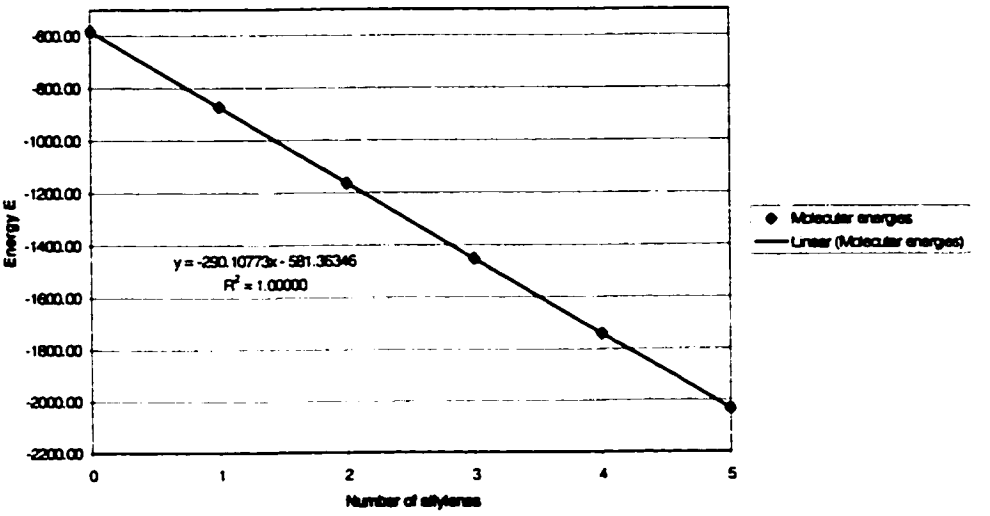

As Table 66 shows, the integrated group energies and electron counts do not match the standard values either; there is compensatory transferability in the oligosilanes as well. For oligosilanes, the standard group energies are $E(SiH_3)$ = -290.68173 au.and $E(SiH_2)$ = -290.10773 au, (for the basis set used in this thesis).

Table 66: Atomic Properties of Oligosilanes

Atom Ω	N(Ω)	E(Ω)	L(Ω)	Atom Ω	N(Ω)	E(Ω)	L(Ω)
Si_2H_6				Si_6H_{14}			
SiH_3 – Si	11.834	-288.2986	1.23E-04	SiH_3 – Si	11.821	-288.2940	-8.70E-05
SiH_3 – H	1.722	-0.7944	4.03E-05	SiH_3 – H´	1.721	-0.7943	3.93E-05
Si_3H_8				SiH_3 – H	1.722	-0.7950	4.19E-06
SiH_3 – Si	11.826	-288.2944	3.35E-04	[b]SiH_2 – Si	12.565	-288.5290	-9.34E-05
SiH_3 – H´	1.721	-0.7944	3.91E-05	[b]SiH_2 – H	1.721	-0.7910	2.75E-06
SiH_3 – H	1.723	-0.7950	1.28E-05	[c]SiH_2 – Si	12.562	-288.5253	3.07E-04
SiH_2 – Si	12.574	-288.5332	-7.96E-05	[c]SiH_2 – H	1.722	-0.7915	-2.42E-05
SiH_2 – H	1.720	-0.7904	4.16E-05	Si_7H_{16}			
Si_4H_{10}				SiH_3 – Si	11.820	-288.2943	9.79E-04
SiH_3 – Si	11.818	-288.2929	9.18E-04	SiH_3 – H´	1.721	-0.7943	3.79E-05
SiH_3 – H´	1.721	-0.7944	3.98E-05	SiH_3 – H	1.722	-0.7950	4.04E-06
SiH_3 – H	1.722	-0.7950	1.24E-05	[b]SiH_2 – Si	12.565	-288.5293	3.89E-04
SiH_2 – Si	12.572	-288.5306	4.89E-04	[b]SiH_2 – H	1.721	-0.7910	4.31E-07
SiH_2 – H	1.721	-0.7909	2.61E-06	[c]SiH_2 – Si	12.563	-288.5258	3.21E-04
Si_5H_{12}				[c]SiH_2 – H	1.722	-0.7915	-2.42E-05
SiH_3 – Si	11.819	-288.2938	9.74E-04	[a]SiH_2 – Si	12.553	-288.5230	3.03E-04
SiH_3 – H´	1.721	-0.7944	3.90E-05	[a]SiH_2 – H	1.722	-0.7915	-2.70E-05
SiH_3 – H	1.722	-0.7950	4.21E-06				
[b]SiH_2 – Si	12.563	-288.5285	3.68E-04				
[b]SiH_2 – H	1.721	-0.7910	5.92E-06				
[c]SiH_2 – Si	12.570	-288.5276	4.36E-04				
[c]SiH_2 – H	1.722	-0.7914	-2.36E-05				

While compensatory transferability does take place, the results are considerably different than those of the hydrocarbon case. The silyl group gains energy, rather than losing energy as the methyl does.

Table 67: Net Charges and Energies of Silyl and Silylene Groups Relative to Standard Values[d]

Molecule	q(SiH_3)	q(SiH_2)	q(SiH_2)[e]	ΔE(SiH_3)[f]	ΔE(SiH_2)[f]	ΔE(SiH_2)[e,f]
Disilane	0.000			0.0		
Trisilane	0.008	-0.015		1.9	-3.9	
Tetrasilane	0.017	-0.015		2.8	-3.0	
Pentasilane	0.015	-0.005	-0.015	2.3	-1.7	-1.7
Hexasilane	0.013	-0.007	-0.005	2.2	-2.0	-0.3
Heptasilane	0.014	-0.007	-0.007 0.004[g]	2.0	-2.2	-0.7 1.0[g]

[a] Atomic properties of central silylene group of heptasilane.
[b] Atomic properties of α-silylene group.
[c] Atomic properties of internal silylene group.
[d] E(SiH_3) = -290.68173 au, E(SiH_2) = -290.10773 au using linear regression fit of the molecular energies of the series.
[e] This SiH_2 is bonded only to other silylenes.
[f] Energies in kcal/mol.
[g] Central silicon in heptasilane.

Another unexpected result is that rather than staying constant, the deviation in the silyl group energy increases when another silylene group is added to form tetrasilane, then decreases and stays approximately constant from pentasilane on, rather than remaining constant from trisilane on. More intriguing is pentasilane: the α-silylene group deviation drops, and remains constant through the series by about half, causing the internal silylene group deviation to increase to compensate. The internal silylene group does not begin to approach the standard value until silaheptane, which seems to indicate that the compensatory effect has a longer reach than in hydrocarbons, requiring an α- and β-silylene group to compensate the deviation of the silyl group. This explains the odd trends observed in Table 67. Imagine a disilyl group that not only has a silyl group with a charge deviation of +0.15 and a silylene group with a charge deviation of –0.08, but a third 'phantom' silylene group, also with a charge deviation of -0.08. In trisilane, these groups would overlap, and their deviations would be accumulative. The silyl deviation would be reduced by the 'phantom' silylene group deviation, and the central silylene group of trisilane would have a deviation twice the size of a silylene group. In tetrasilane, the silyl deviation would be unaffected, but both silylene groups would have deviations twice as large as expected: in pentasilane, the silyl and α-silylene groups would be unaffected, and the central silylene group would have a deviation twice as large as expected. Only from hexasilane on are the deviations as expected, with the central silylene group in heptasilane approaching standard; at longer chain lengths, the central silylene groups should have values that closely approach standard. This fundamental difference in compensatory behavior may well be an effect of σ-conjugation: a silyl groups effect on another functional group is farther reaching than in hydrocarbons.

4.6.6 L(r) Properties of Si_nH_{2n+2}

The L(r) maps of trisilane and heptasilane provide a completely different impression, both with respect to the BCP data and the hydrocarbon L(r) plots.

Figure 44: L(r) Maps of Trisilane and Heptasilane (SCVS)

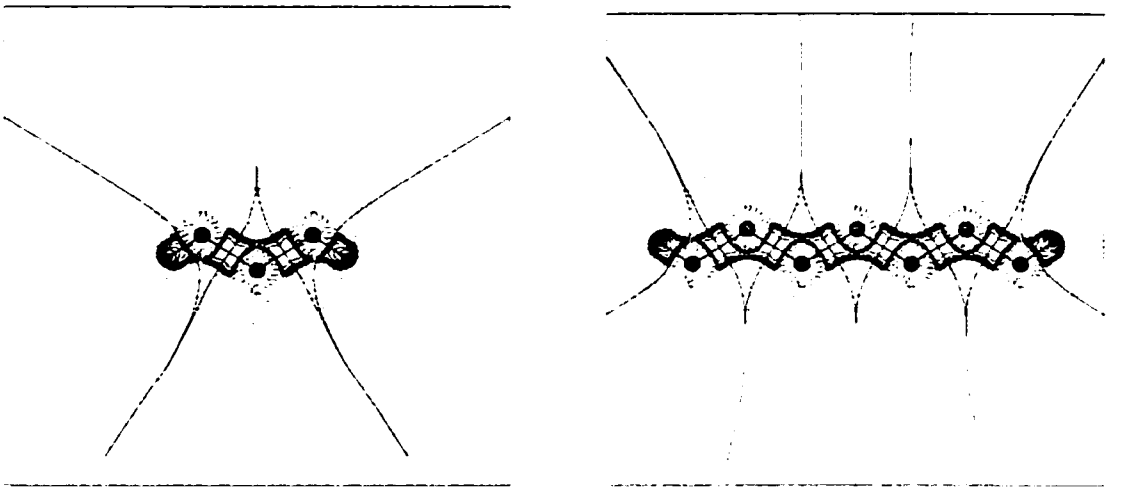

Unlike the plot of disilane, which shows all the charge concentrations, bond or hydrogen ligand, isolated from each other, the trisilane and heptasilane plots clearly show that these charge concentrations are linked together, much like the L(r) structure seen in the backbone of the hydrocarbons. The difference with the oligosilanes is that these charge concentrations still remain isolated from the hydrogen ligand concentrations, resulting in a string of linked charge concentrations that would have minimum interaction with the ligands. Critical points in the L(r) also follow a tetrahedral pattern, like the hydrocarbons: for these molecules, however, the Si-H bonded maxima lie on the hydrogens, with two maxima on each Si-Si bond, joined by a (3,-1) critical point. From this structure, one can conclude that there is no real VSCC for silicon. The (3,+1) critical points must be approximated with midpoints bounded by the (3,-1) critical points, where the values of L(r) range from –0.766 au to –1.439 in the central silicon of heptasilane; these values change very little with chain length, or position of the silicon in the chain.

Figure 45: Values of L(r) Critical Points for Si_3H_8 (left) and Si_7H_{16} (right), Central Silicon

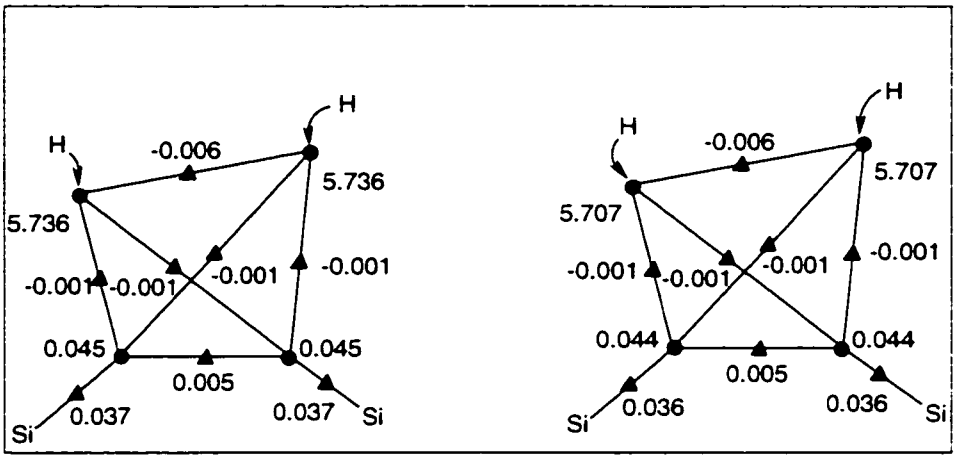

What is most notable is the magnitude of the top L(r) maxima, which coincide with the hydrogen atom positions. The other values are much smaller, and are on the whole almost all negative, indicating positions of depletion in L(r). This confirms that the hydrogen maxima are not linked to the backbone maxima, as is seen in the hydrocarbons. Only the (3,-1) critical points in the backbone of the molecule are positive, indicating some concentration of density at those points.

4.7 Transferability and Comparisons

The concept of transferability is an important one in chemistry, as it has been demonstrated that a given functional group's properties can be observed in a variety of chemical environments, and those properties show very little change, even when the environment changes[149]. It is remarkable how well both hydrocarbons and oligosilanes conform to the regimen of transferability[150]. Transferability is a necessary requirement of molecular additivity, as without it, a molecular property cannot be expressed in terms of a set of standard group properties, something that has been proved experimentally to a high degree of precision. The research described in this thesis shows clearly that hydrocarbons and oligosilanes can be broken down into functional groups whose properties show little or no change from molecule to molecule, either through bond properties, atomic integrations or property density plots. The functional group properties so derived provide the easiest route to proving that additivity can be theoretically demonstrated, be it for compounds like hydrocarbons, or more complex species[151].

4.8 Additivity and Comparisons

What becomes clear from the integration data is that both hydrocarbons and oligosilanes are additive to a high degree of accuracy, as shown from the regression fits to the molecular energies of each series. This provides theoretical confirmation to experimental work performed in this field, from molar volumes and polarization[152] to magnetic susceptability[153,154] to heats of formation[155] and other thermochemical properties. This data allows one to compute a 'standard' set of energies and electron counts for the different groups within the molecule[156]. However, these standard values do not correlate with the actual integrated energies and electron counts of the groups within the molecule, even though these values do become constant as each series progresses. This leads to the concept of 'compensatory transferability', where a pair of bonded groups loses and takes on electron density in such a way as to achieve maximum stability, while at the same time maintaining the overall additivity of the molecule. For the methyl group, a small amount of density is gained from the bonded methylene relative to the expected standard electron count, while the methylene bonded to the methyl loses an equal amount of density. Internal methylenes, not bonded to a methyl group, approach the standard methylene value. It can be said than that for straight-chain hydrocarbons, there is an 'end-group effect', which extends only to the group bonded to that end group. In propane, the methylene is subjected to the accumulative effect of two end-group effects, which is why its electron count deviation is twice as large as either methyl group. Oligosilanes experience the same reverse effect, and the details change significantly. The silyl group loses some charge from a bonded silylene group, while the silylene group gains some charge. Unlike the hydrocarbons, however, the 'end-group' effect of a silyl group has a farther reach, affecting not only the adjacent α-silylene group, but the β-silylene group as well. This accounts for the strange pattern of deviations observed for the oligosilane series. In trisilane, the positive deviation of one silyl group is tempered by the end-group effect of the other silyl group, while both affect the silylene group equally. In tetrasilane, each silyl group is outside the influence of the other silyl's end-group effect, leaving both silylene groups to be affected by the end-group effects of both silyl groups. In pentasilane, only the central silylene group is affected by both silyl groups, and from hexasilane on, all silylene groups are affected by only one silyl group, or none, as in the case of the central silylene group in heptasilane. The fact that the silyl group influences two adjacent groups, while

the methyl group effects only the methylene group adjacent to it, may be a reflection of the ability of the valence density of oligosilanes to be delocalized within the backbone of the molecule. The valence density would be more easily influenced by a change in chemical environment, and that influence would be transmitted farther in a system where the density is not bound tightly to a given bond.

The concept of additivity is not something that is limited to simple systems such as hydrocarbons, which are expected to possess such properties. More complex systems, such as polypeptides[157], or even aromatic species[147], can be described in terms of group contributions. In the latter case, the energy of pyridine (C_5H_5N) can be expressed as the average of the energies of benzene (C_6H_6) and pyrazine ($C_4H_4N_2$), to within 0.1 kcal/mol. This shows that species where additivity would not be expected, such as aromatic systems, do in fact exhibit additive properties.

5 Pair Density Properties of Silicon and Carbon Compounds

As has been shown in section 2.7.1 and 2.7.2 of this thesis, the pair density is a function that describes the exchange of electron density between two regions of space in a molecule. Such a function can be integrated over the atomic basins defined by the zero-flux surface condition to provide an index of localization: how many electrons in a given basin are localized within that basin (Equation 42), and how many are shared with other basins in the molecule (Equation 43). This index can be expressed either as the value, or as a percentage of a basins' electron population. The exchange of electrons between two atomic basins can also be used to generate a bond order, which describes the amount of electron density shared between two bonded atoms; by 'shared', it is meant that the electrons are delocalized between two atomic basins.

5.1 Delocalization Properties of MH_3-XH_n Series

The SiH_3XH_n and CH_3XH_n series studied previously will be studied again, this time with respect to the pair density. These results will describe how the silyl and methyl groups share density with other elements, and the differences in bond orders between carbon-atom bonds and silicon-atom bonds.

5.1.1 Localization Indices of CH_3-XH_n Series

To better illustrate the localization indices for this series of molecules, it was decided to express them as percentages, as it is easier to graph. The percentages shown represent the valence density only, where possible. To include the core density, which is completely localized on one atom, would skew the results, and dilute any fine details in the trends. To ensure that the core electrons are in fact completely localized within the silicon atom, one can analyze the atomic overlap matrix that is generated during the integration of an atomic basin, this matrix contains the S_{ij} terms described in Equation 42. In the case of SiH_4, the elements of the matrix that correspond to the core electrons sum to -9.976 au, showing clearly that the core electrons in silicon experience no exchange with other atoms.

Figure 46: Percentage Localization and Delocalization on Carbon in CH_3-XH_n, X = H, Li – F (HF)

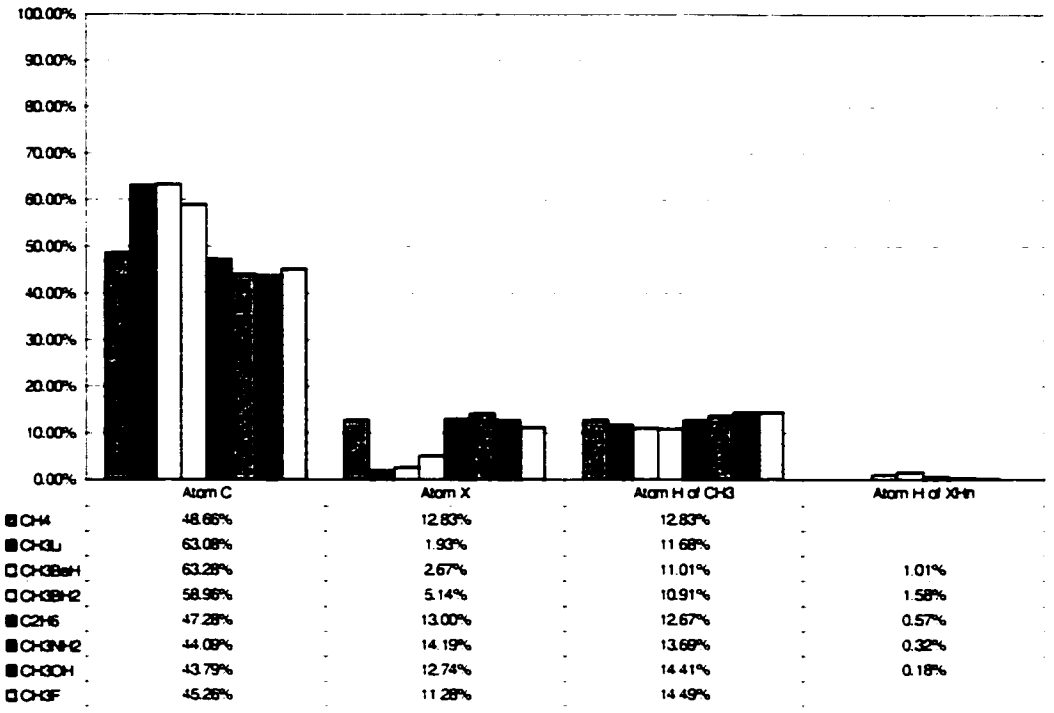

	Atom C	Atom X	Atom H of CH3	Atom H of XHn
CH4	48.66%	12.83%	12.83%	
CH3Li	63.08%	1.93%	11.68%	
CH3BeH	63.28%	2.67%	11.01%	1.01%
CH3BH2	58.96%	5.14%	10.91%	1.58%
C2H6	47.28%	13.00%	12.67%	0.57%
CH3NH2	44.09%	14.19%	13.69%	0.32%
CH3OH	43.79%	12.74%	14.41%	0.18%
CH3F	45.26%	11.28%	14.49%	

Figure 46 shows the localization percentages for carbon in the methyl series, where X is a second row element. The percentage of the electron density localized on carbon varies from 63% to 43%. It is interesting to note how the percentage changes very little after X = carbon, indicating that more electronegative elements have little influence on delocalizing the density of carbon. As the C-X bond becomes more polar, more density is lost to X, thus lowering the amount localized on carbon. When carbon is bonded to an electropositive element, there is more density on carbon, raising the percentage. The section of Figure 46 that graphs the delocalization of carbon density onto element X maps this very trend, only in reverse: electronegative elements pull some density away from carbon, increasing their percentage, while electropositive elements lose density. The delocalization percentages for hydrogens bonded to carbon and X show little variation in X, a trend seen in previous data. Very little if any of the density of carbon delocalizes onto the hydrogen bonded to X, showing very clearly the shortsighted nature of these systems.

Figure 47: Percentage Localization and Delocalization on Carbon in CH_3-XH_n, X = H, Na – Cl (HF)

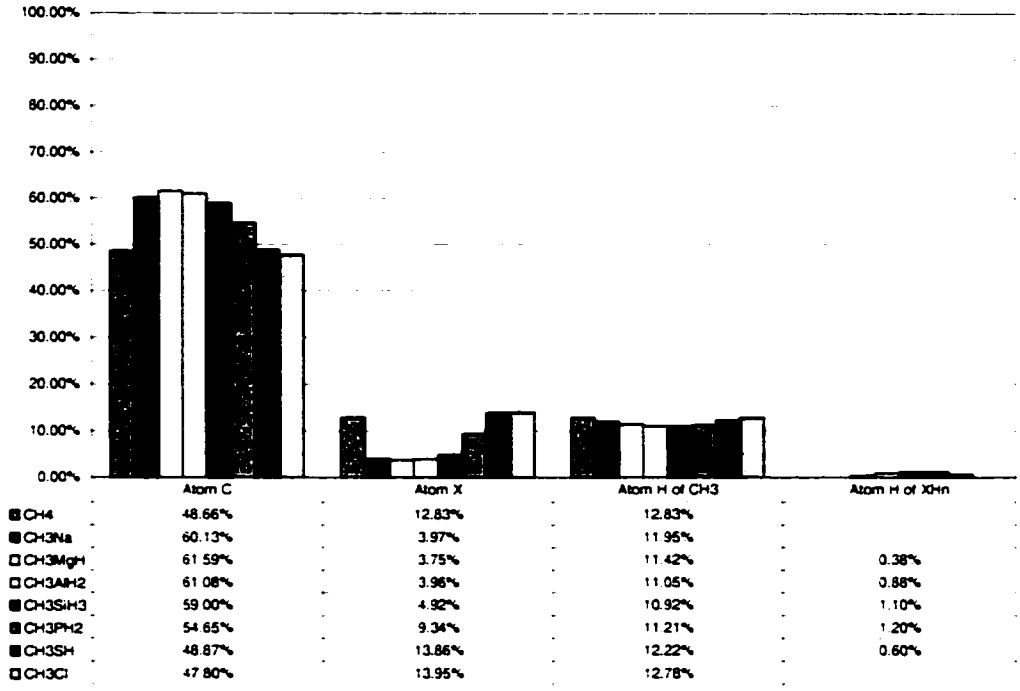

Figure 47 completes the data series for carbon, with localization percentages for elements X from the 3rd row. Most of the localization percentages on carbon are above 50%, showing how most of the elements in the 3rd row are less electronegative than carbon, and thus lose density to it. This is also reflected in the delocalization of carbon density onto X. Like in the 2nd-row elements, the percentage increases from about 5% to 10% as X becomes more electronegative than carbon. This shows that for the 3rd row of elements, it is sulfur that is approximately equal to carbon in electronegativity. The percentage delocalization on hydrogen does not change appreciably from 2nd-row elements to 3rd-row elements, again indicating the shortsighted nature of atoms.

Figure 48: Percentage Localization and Delocalization on Atom X in CH_3-XH_n, X = H, Li – F (HF)

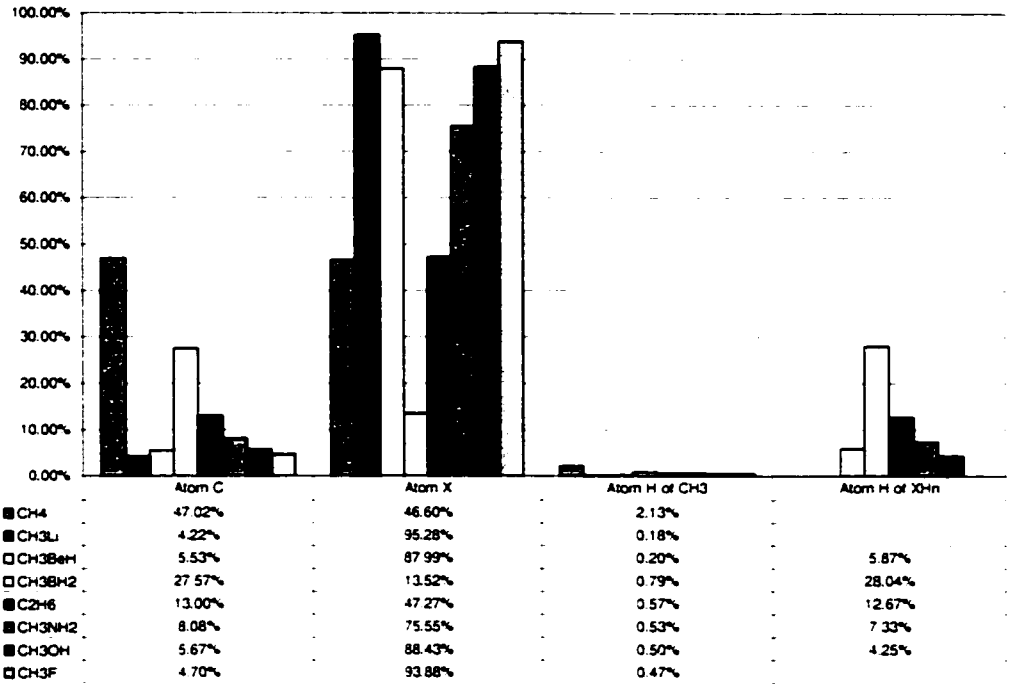

	Atom C	Atom X	Atom H of CH3	Atom H of XHn
CH4	47.02%	46.60%	2.13%	
CH3Li	4.22%	95.28%	0.18%	
CH3BeH	5.53%	87.99%	0.20%	5.87%
CH3BH2	27.57%	13.52%	0.79%	28.04%
C2H6	13.00%	47.27%	0.57%	12.67%
CH3NH2	8.08%	75.55%	0.53%	7.33%
CH3OH	5.67%	88.43%	0.50%	4.25%
CH3F	4.70%	93.88%	0.47%	

The next pair of figures show the localization percentages for the element X in this series of molecules. As one would expect, the localization on X increases, as X becomes more electronegative, holding onto its valence density more tightly. The values for X = lithium and beryllium show that these elements are very nearly ionic in nature. Most of the density included in the percentage is in fact the core density, which is understood to be highly localized within its atomic basin. The fact that the percentages are less than 100% indicates that a small amount of valence density is localized on these elements. Beryllium is slightly more electronegative than lithium, so its percentage is smaller. As one proceeds further along the 2nd row, the percentage of density localized on element X drops at boron. Boron is sufficiently electronegative that it retains a significant amount of valence density relative to its core density, which can be excluded from the calculation. The percentage increases again along the row, as the element X becomes more electronegative and hold its valence density more tightly. The amount of density shared with the various hydrogens varies considerably with X. For the hydrogens bonded to carbon, the percentage is nearly zero, a trend seen with the previous charts. For the hydrogens bonded to X, the percentage drops as X becomes more

electronegative, and holds onto its valence density more tightly. Interestingly, this percentage delocalization is almost identical with the percentage delocalized onto the carbon: this makes sense, given that carbon and hydrogen have very similar electronegativities.

Figure 49: Percentage Localization and Delocalization on Atom X in CH_3-XH_n, X = H, Na – Cl (HF)

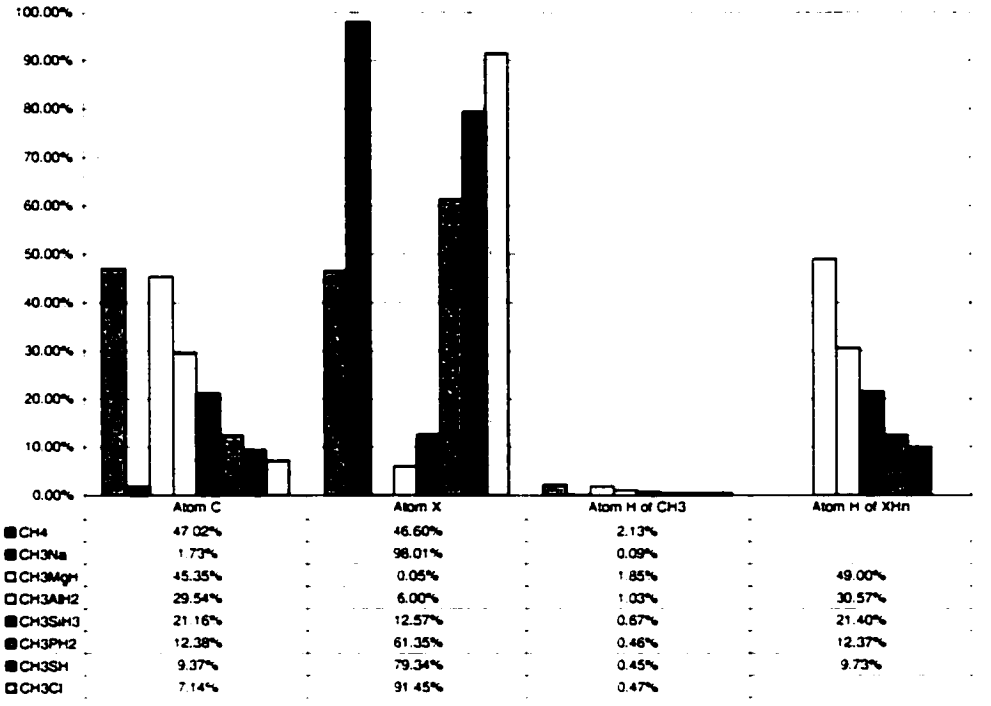

The same trend seen in Figure 48 is continued in Figure 49: sodium shows the large percentage due to total loss of valence density, as seen in the lithium and beryllium examples. Magnesium has just enough valence density that one can ignore the core electrons, obtaining a percentage that is nearly zero. The amount of density shared by the carbon and the hydrogen bonded to X still follows the same trend, only the percentage starts out higher for magnesium, and decreases more quickly along the 3rd row.

While these charts make it clear how the density of an element in CH_3XH_n is delocalized amongst the other atoms, a calculation of group delocalization is also useful. The values shown on Table 68 and Table 69 are the localization and delocalization indices of groups within the CH_3XH_n series, which show the tug-of-war that is taking place between methyl and its bonded group containing the element X.

Table 68: Group Localization Indices for CH_3-XH_n, X = Li – F (HF)

CH_3Li		CH_3	Li
	CH_3	9.8222	
	Li	0.0994	1.9858
CH_3BeH		CH_3	BeH
	CH_3	9.675	
	BeH	0.1924	3.9386
CH_3BH_2		CH_3	BH_2
	CH_3	9.2826	
	BH_2	0.4340	5.8488
CH_3CH_3		CH_3	CH_3
	CH_3	8.3438	
	CH_3	0.6556	8.3436
CH_3NH_2		CH_3	NH_2
	CH_3	7.9886	
	NH_2	0.6288	8.7550
CH_3OH		CH_3	OH
	CH_3	7.8156	
	OH	0.5414	9.1010
CH_3F		CH_3	F
	CH_3	7.7892	
	F	0.4734	9.2622

The trend in shared density between methyl and the X group is an interesting one. The group localization index value for methyl steadily decreases as X becomes more electronegative, as expected. The shared density, indicating the amount of carbon density delocalized onto the X group, increases as more density is retained by an increasingly electronegative X, until it reaches a maximum in ethane, where a true covalent bond is expected. The shared density then starts to decrease, as X becomes more electronegative than carbon: X holds onto its valence density very tightly, and there is less sharing in the C-X bond. These shared density values prove useful in indicating the nature of interaction between two bonded groups: whether the density that forms their bond is shared covalently, or is centered more on one or another group, forming a system with more ionic character. It is noted that taking the sum of the group delocalization values for a given molecule gives one the total number of electrons in the molecule.

Table 69: Group Localization Indices for CH_3-XH_n, X = Na – Cl (HF)

CH_3Na		CH_3	Na
	CH_3	9.5926	
	Na	0.2026	9.9948
CH_3MgH		CH_3	MgH
	CH_3	9.5946	
	MgH	0.2126	11.9770
CH_3AlH_2		CH_3	AlH_2
	CH_3	9.4904	
	AlH_2	0.3002	13.9082
CH_3SiH_3		CH_3	SiH_3
	CH_3	9.2930	
	SiH_3	0.4296	15.8418
CH_3PH2		CH_3	PH_2
	CH_3	8.9052	
	PH_2	0.5930	15.9084
CH_3SH		CH_3	SH
	CH_3	8.3050	
	SH	0.6710	16.3528
CH_3Cl		CH_3	Cl
	CH_3	8.0728	
	Cl	0.6262	16.6882

The same trend is observed in Table 69, except that the shared density peaks for X = sulfur, indicating that for C-X bonds where X is a 3rd-row element, the C-S bond has the most covalent character.

The $F(\Omega,\Omega')$ values between bonded atoms can be used to calculate something akin to a bond order. As Equation 42 shows, the localization indices contain the orbital overlap integrals within an atom. For a delocalization index between two bonded atoms, these overlap integrals represent the amount of electron density shared between those atoms.

Table 70: Bond Orders for CH_3-XH_n (HF)

CH_3Li		CH_3OH		CH_3SiH_3	
C-Li	0.1760	C-O	0.8236	C-Si	0.4552
C-H	1.0648	C-H	0.9336	C-H	1.0112
CH_3BeH		O-H	0.6172	Si-H	0.4604
C-Be	0.2512	CH_3F		CH_3PH_2	
C-H	1.0376	C-F	0.7276	C-P	0.8264
Be-H	0.2668	C-H	0.9348	C-H	0.9920
CH_3BH_2		CH_3Na		P-H	0.8260
C-B	0.4732	C-Na	0.3524	CH_3SH	
C-H	1.0044	C-H	1.0620	C-S	1.0960
B-H	0.4812	CH_3MgH		C-H	0.9668
CH_3CH_3		C-Mg	0.3436	S-H	1.1388
C-C	0.9920	C-H	1.0464	CH_3Cl	
C-H	0.9672	Mg-H	0.3712	C-Cl	1.0448
CH_3NH_2		CH_3AlH_2		C-H	0.9572
C-N	0.9792	C-Al	0.3684	CH_4	
C-H	0.9448	C-H	1.0280	C-H	0.9816
N-H	0.8880	Al-H	0.3812		

These values, shown on Table 70, indicate bond order in single-bond systems quite well. The C-C and C-H bonds are very near one, as expected for these covalent bonds. With other C-X bonds, the trend is similar to the group shared densities: the bond order is low for C-Li, an ionic bond, and increases to approach one in the C-C bond. The bond order starts to drop again as X becomes more electronegative, indicating an increase in ionic character in the C-X bond once again. Just as was seen in the group shared densities, it is the C-S bond that has the highest bond order of the 3rd-row elements. The fact that the C-Na bond order is higher than the C-Li bond order can be explained by the fact that lithium is a harder cation. As a result, the density of sodium can be polarized somewhat, adding a little more density to the bond.

5.1.2 Localization Indices of SiH_3-XH_n Series

With the carbon system, one expected the percentage localizations on carbon to not vary too strongly. The valence density on carbon is held quite tightly, and even fluorine can only draw so much of that density away. It has been show so far that most of the valence density of silicon is lost when it is bonded to most other elements, so the percentage localization on silicon should be quite low in most cases.

Figure 50: Percentage Localization and Delocalization on Silicon in SiH_3-XH_n, X = H, Li - F (HF)

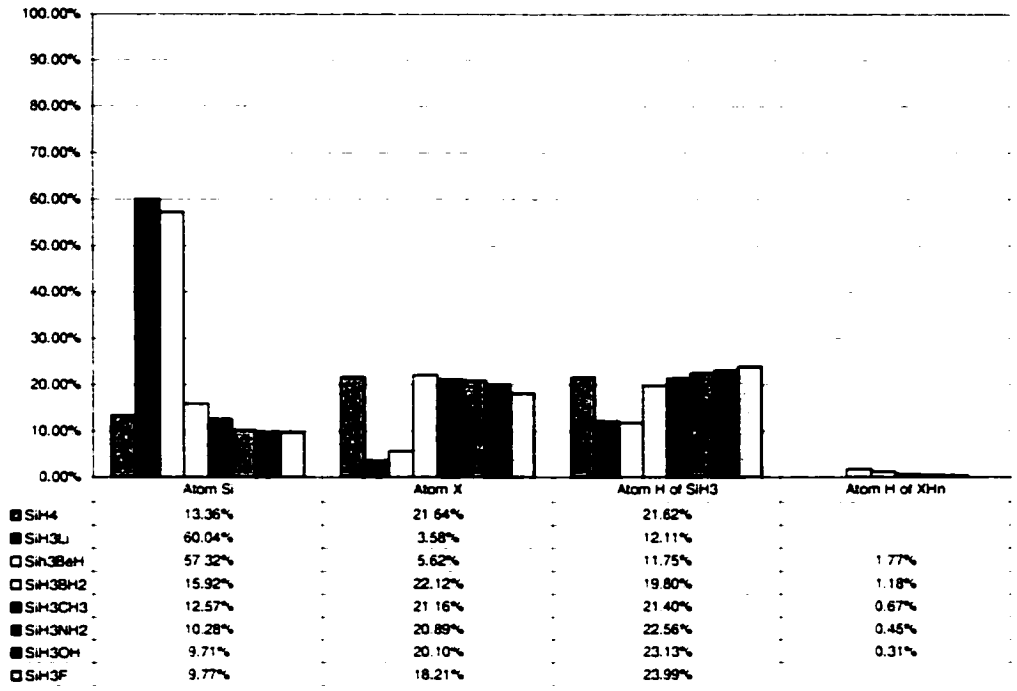

	Atom Si	Atom X	Atom H of SiH3	Atom H of XHn
SiH4	13.36%	21.64%	21.62%	
SiH3Li	60.04%	3.58%	12.11%	
SiH3BeH	57.32%	5.62%	11.75%	1.77%
SiH3BH2	15.92%	22.12%	19.80%	1.18%
SiH3CH3	12.57%	21.16%	21.40%	0.67%
SiH3NH2	10.28%	20.89%	22.56%	0.45%
SiH3OH	9.71%	20.10%	23.13%	0.31%
SiH3F	9.77%	18.21%	23.99%	

Figure 50 shows this to be the case. The percentages on silicon are consistently low with the exception of lithium and beryllium, two elements in this series that are less electronegative, allowing silicon to retain some of its density. Despite the very low values, a trend is still observed, as the percentage decreases with increasing electronegativity of X. The delocalization onto X, except for lithium and beryllium, remains fairly constant, decreasing only slightly with different elements X. What is more interesting is that, unlike carbon, the hydrogens bonded to silicon are influenced by the different X groups. The delocalization onto silyl hydrogen is quite low for lithium and beryllium, and becomes more constant for the rest. These low values show that when silicon gains valence density from an electropositive X, it pulls some density away from the hydrogens as well. One would expect the opposite to occur, with hydrogen gaining a higher percentage as more silicon valence density became available to take. The increase in hydrogen percentage as X becomes more electronegative is observed in the methyl series as well: the trend is very small, however, and it is risky to associate behavior to it. One must be careful in interpreting this behavior, however. The delocalization of silicon density onto hydrogen does in fact decrease as X takes more density

away from silicon. Since the percentages are calculated using the number of electrons on silicon, the net loss on the hydrogens is smaller than the loss on silicon, giving the impression that the percentages are in fact increasing with electronegativity of X.

Figure 51: Percentage Localization and Delocalization on Silicon in SiH_3-XH_n, X = H, Na – Cl (HF)

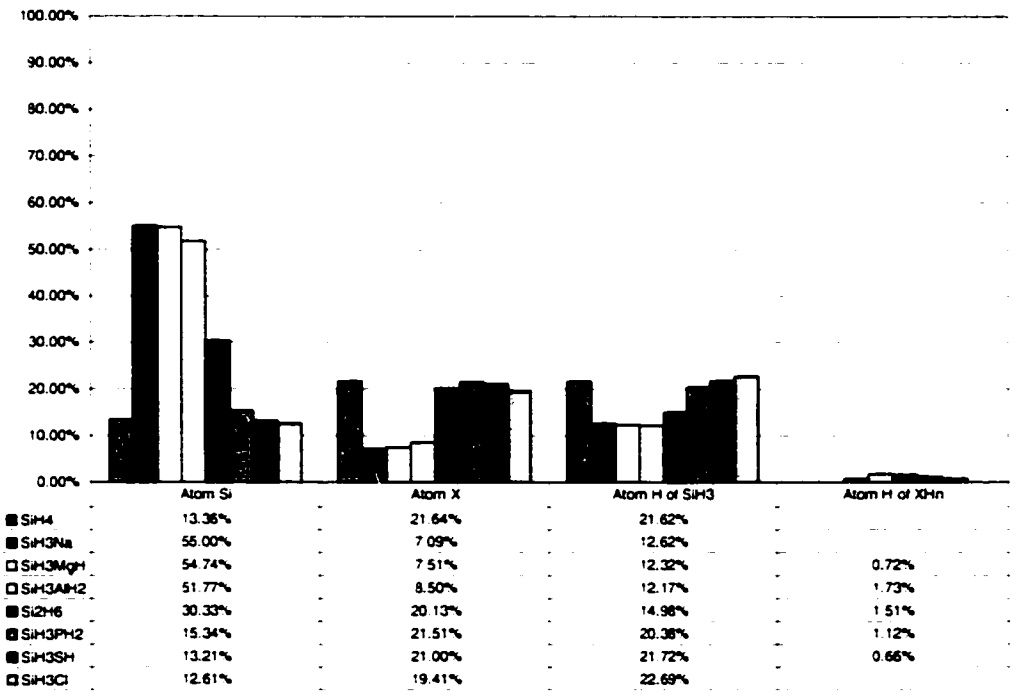

Figure 51 shows a similar trend with 3rd-row elements. As these elements are not as electronegative, the localization on silicon is higher, dropping when X = silicon, when the two groups are equally sharing. The delocalization of silicon density onto X increases accordingly, but this increase is real, unlike that seen in the delocalization of X onto the silyl hydrogens. In both the 2nd- and 3rd-row elements, the delocalization of silicon density onto hydrogens bonded to X is almost non-existent, showing that the silicon density does not delocalize much farther than the element it is bonded to.

As would be expected with silicon delocalizing most of its density to bonded elements, the localization of density on the various elements X should be appropriately large. Figure 52 shows this to be the case.

Figure 52: Percentage Localization and Delocalization on Atom X in SiH_3-XH_n, X = H, Li – F (HF)

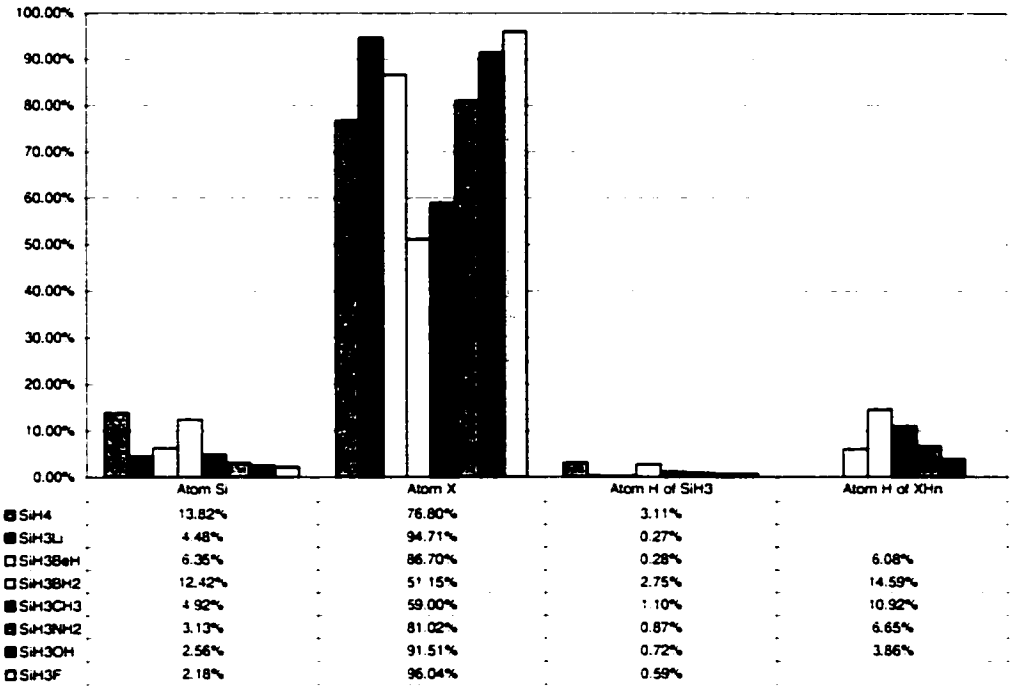

A similar trend to that seen in the methyl series is seen here, only it is far more pronounced. Even though silicon is far less electronegative than carbon, it is still able to strip lithium and beryllium of nearly all of their valence densities. From boron on, the localization on X increases, just as in the carbon series, except that the percentage starts at a higher value. The trend continues in Figure 53, which shows the percentages of 3rd-row elements. Once again, sodium is all but stripped of its valence density, and the localization increases from magnesium on, only this time, magnesium starts with a higher value. The delocalization of X onto both carbon and silicon follow the same trend, except that the percentages are much smaller for the silicon case, reflecting the fact that silicon is not as effective at withdrawing electron density. Surprisingly, the delocalization of X density onto carbon and silicon is almost identical for most of X when X is a 3rd-row element. Perhaps it is the fact that, like silicon, the valence densities of 3rd-row elements are more diffuse, and thus cannot retain their valence densities as well as 2nd-row elements. These elements share their density more freely, even when the element bonded to X is a good electron-withdrawing element, like carbon.

Figure 53: Percentage Localization and Delocalization on Atom X in SiH_3-XH_n, X = H, Na – Cl (HF)

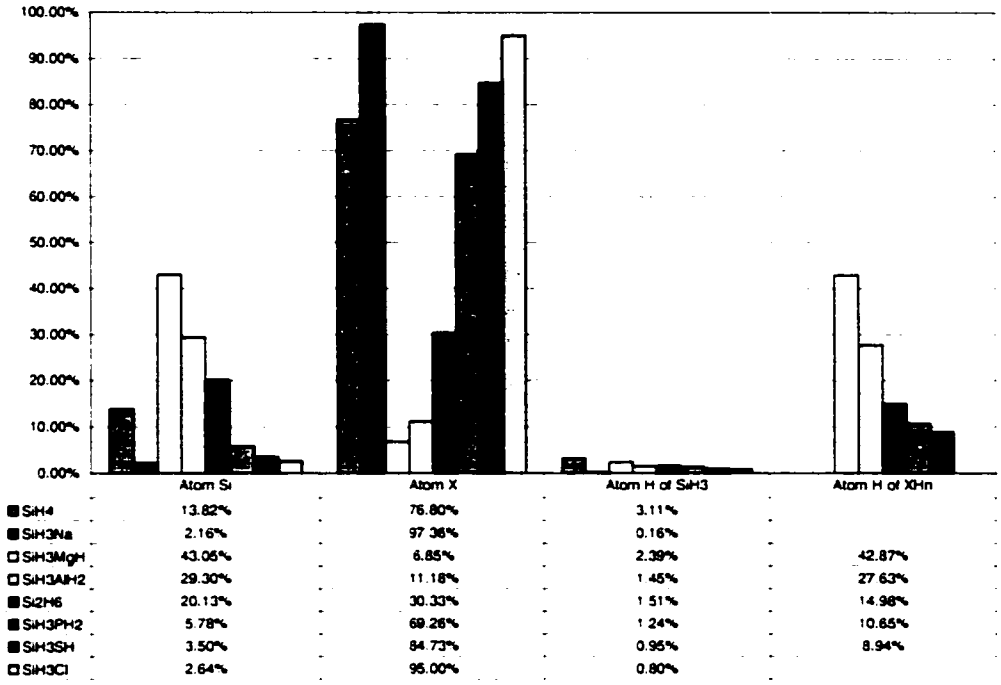

The group delocalizations were very helpful in describing the interaction between carbon and the X group it was bonded to, and Table 71 is no exception. The group delocalization value drops sharply at boron, before levelling to a near constant value. This reflects the fact that the more electronegative elements in the 2nd row have all but stripped silicon of its valence density: silicon cannot delocalize its valence density any more, because it has very little left. As previous data suggests, the highest shared density is found with X = boron, and declines steadily from there. Also expected is the fact that these shared densities on the whole are not as large as those seen in the methyl series. This is logical enough, as the bond between silicon and X is weaker, and more strongly polarized.

Table 71: Group Localization Indices for SiH_3-XH_n, X = Li – F (HF)

SiH_3Li		SiH_3	Li
	SiH_3	17.7724	
	Li	0.1112	1.9948
SiH_3BeH		SiH_3	BeH
	SiH_3	17.5828	
	BeH	0.2204	3.9698
SiH_3BH_2		SiH_3	BH_2
	SiH_3	15.9178	
	BH_2	0.4858	7.1046
SiH_3CH_3		SiH_3	CH_3
	SiH_3	15.8418	
	CH_3	0.4296	9.2930
SiH_3NH_2		SiH_3	NH_2
	SiH_3	15.7936	
	NH_2	0.4008	9.4170
SiH_3OH		SiH_3	OH
	SiH_3	15.7954	
	OH	0.3558	9.4974
SiH_3F		SiH_3	F
	SiH_3	15.7950	
	F	0.3114	9.5762

Table 72 shows the remainder of the group delocalizations in this series. The decrease in pair density on the silyl group drops sharply with this series as well, before leveling out at phosphorus and on. Once again the shared density rises as X becomes more electronegative, maximizing at X = silicon, before dropping again. The sharp increase in shared density in this series is a contrast to the electron density shared between silyl and 2nd-row groups, and the methyl series. This is likely because of the fact that the valence density of 3rd-row elements is considerably more diffuse. The valence density of systems such as silicon-aluminum and silicon-phosphorus are not as strongly polarized as in the other series, and as such tend to be shared more evenly. The shared density values between 3rd-row groups and silicon are still much smaller overall than the shared density values between 3rd-row groups and carbon, indicating carbon's greater ability to draw valence density from other elements.

Table 72: Group Localization Indices for SiH_3-XH_n, X = Na – Cl (HF)

SiH_3Na		SiH_3	Na
	SiH_3	17.5472	
	Na	0.2168	10.0086
SiH_3MgH		SiH_3	MgH
	SiH_3	17.4978	
	MgH	0.2460	12.0034
SiH_3AlH_2		SiH_3	AlH_2
	SiH_3	17.3404	
	AlH_2	0.3488	13.9544
SiH_3SiH_3		SiH_3	SiH_3
	SiH_3	16.4274	
	SiH_3	0.5642	16.4274
SiH_3PH_2		SiH_3	PH_2
	SiH_3	15.8982	
	PH_2	0.4776	17.1384
SiH_3SH		SiH_3	SH
	SiH_3	15.8240	
	SH	0.4338	17.3028
SiH3Cl		SiH3	Cl
	SiH3	15.8262	
	Cl	0.3922	17.411

As would be expected from the group delocalization data, the bond orders for Si-X bonds should be much smaller that of C-X bonds. Table 73 shows these values. The typical bond order on the Si-H bond only about 0.48: this is similar to the relative BCP rho values of the C-H and Si-H bonds (0.3 and 0.12 au, respectively). This provides yet another measure of relative bond polarities, which can in turn be related to chemical reactivity. As with the group delocalizations, the bond orders of the Si-X bonds find maximum values on the Si-B and Si-Si bonds. What is interesting is how the Si-H bond orders change significantly with X; as X becomes more electronegative, the bond order drops from about 0.62 to about 0.45. This is in sharp contrast to the C-H bond orders, which stay nearly constant at around 1.0. This implies a more covalent Si-H bond being formed when silicon has a surplus of valence density, something that would be expected, as the silyl hydrogens have more silicon valence density to share. This is, however, in sharp contrast to the BCP data for Si-H bonds, which increase as X grows more electronegative, rather than less.

This is likely a result of the Si-H bond lengths decreasing with increased eelctronegativity of X (see Table 16), and should not be interpreted as an argument against using these values to gauge relative bond character.

Table 73: Bond Orders for SiH_3-XH_n (HF)

SiH_3Li		SiH_3OH		SiH_3SiH_3	
Si-Li	0.1888	Si-O	0.3848	Si-Si	0.7372
Si-H	0.6392	Si-H	0.4428	Si-H	0.5484
SiH_3BeH		O-H	0.5788	SiH_3PH_2	
Si-Be	0.2952	SiH_3F		Si-P	0.5200
Si-H	0.6168	Si-F	0.3432	Si-H	0.4928
Be-H	0.2828	Si-H	0.4520	P-H	0.9588
SiH_3BH_2		SiH_3Na		SiH_3SH	
Si-B	0.5452	Si-Na	0.3556	Si-S	0.4616
Si-H	0.4880	Si-H	0.6328	Si-H	0.4776
B-H	0.6404	SiH_3MgH		S-H	1.1792
SiH_3CH_3		Si-Mg	0.3820	SiH_3Cl	
Si-C	0.4552	Si-H	0.6264	Si-Cl	0.4112
Si-H	0.4604	Mg-H	0.3804	Si-H	0.4808
C-H	1.0112	SiH_3AlH_2		SiH_4	
SiH_3NH_2		Si-Al	0.4276	Si-H	0.4764
Si-N	0.4104	Si-H	0.6124		
Si-H	0.4432	Al-H	0.4032		
N-H	0.8736				

5.1.3 Localization Indices of CH_2=XH_n Series

From the data seen so far, atoms that are bonded to each other have been shown through the pair density to share valence electron density. The extent of that sharing is measured by the delocalization index for that atom. So far, the systems studied have been simple single-bond systems. There should then be increased delocalization in a double-bond system: the π-bond density of each atom is being shared as well as the σ-bond density. In a π-conjugated molecule, that delocalization should extend beyond the atoms adjacent to the atom being studied, with all the π-conjugated atoms holding some percentage of that atoms' pair density. Previous work in this area has shown this to be the case for simple π-conjugated species containing carbon, and this work will demonstrate the extent to which this occurs in double-bond species containing silicon as well.

A comparison between Figure 54 and Figure 46 shows that there is a significant difference in delocalization values when single bonds are compared to double bonds.

Figure 54: Percentage Localization and Delocalization on Carbon in $CH_2=XH_n$ (HF)

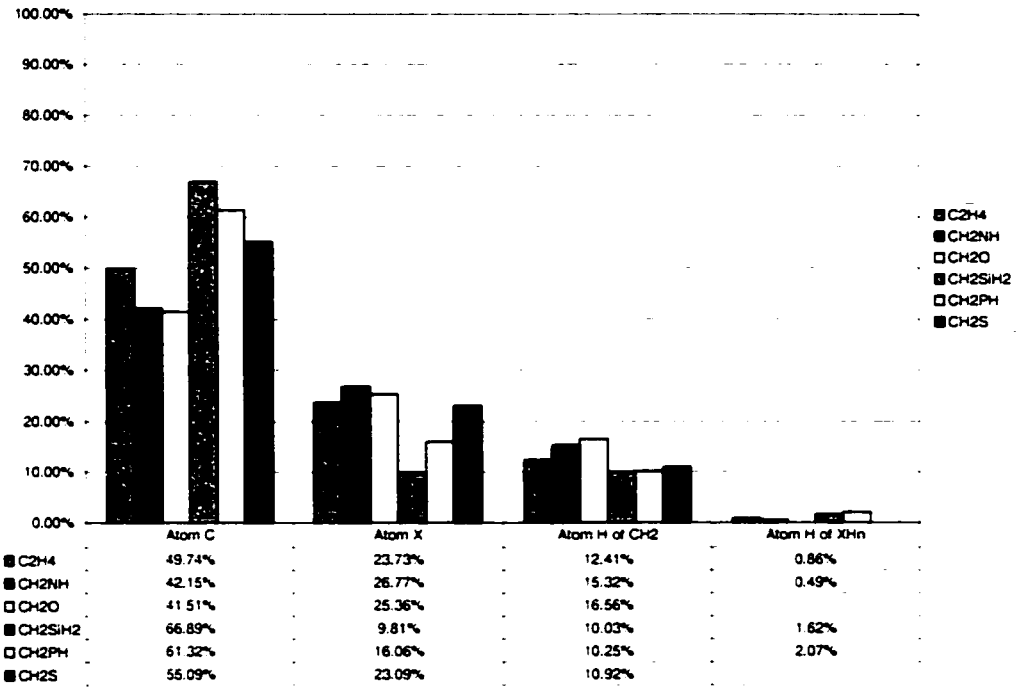

	Atom C	Atom X	Atom H of CH2	Atom H of XHn
C2H4	49.74%	23.73%	12.41%	0.86%
CH2NH	42.15%	26.77%	15.32%	0.49%
CH2O	41.51%	25.36%	16.56%	
CH2SiH2	66.89%	9.81%	10.03%	1.62%
CH2PH	61.32%	16.06%	10.25%	2.07%
CH2S	55.09%	23.09%	10.92%	

For single bond systems, the extent of delocalization onto X is small, only about 13% on average for the carbon-nitrogen-oxygen trio. As Figure 54 shows, this percentage doubles for these three, indicating the amount of additional density incorporated into the C=X bond. Interestingly, the localization on carbon is not much lower than in the single bond systems, and the delocalization onto the methylene hydrogen is slightly higher in the double bond systems. This can be explained by the fact that there are only three atoms bonded to carbon in this case, as opposed to four. If about 60% of the density on carbon is delocalized onto the adjacent atoms, this means that all of the delocalization percentages will be higher. When carbon forms a double bond with 3rd-row elements, the trend changes. The localization on carbon increases, reflecting the decreased ability of X to draw density from carbon, and the delocalization onto X drops accordingly. The delocalization onto the methylene hydrogen stays fairly constant with 3rd-row elements X. This has been observed before, where the BCPs of the C-H bonds in methylene showed little change when X was a 3rd-row element.

The localization of the electron density of X is shown in Figure 55. What is surprising is that, despite the radically different electronic structures of carbon, nitrogen and oxygen in single and double bonds, the percentage localization in both single and double bond cases is nearly the same.

Figure 55: Percentage Localization and Delocalization on Atom X in $CH_2=XH_n$ (HF)

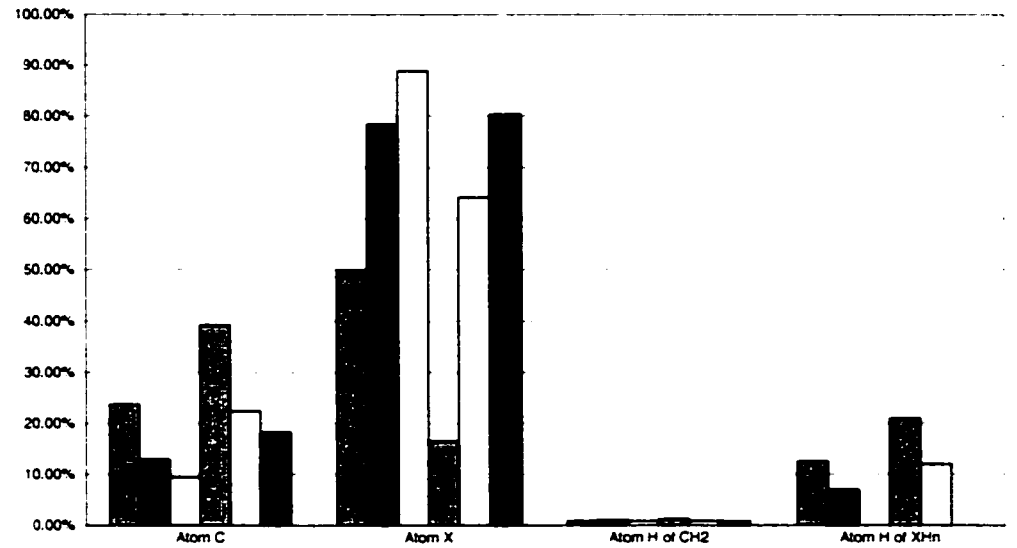

	Atom C	Atom X	Atom H of CH2	Atom H of XHn
C2H4	23.73%	49.74%	0.86%	12.41%
CH2NH	12.89%	78.38%	0.92%	6.96%
CH2O	9.45%	88.85%	0.85%	
CH2SiH2	39.23%	16.47%	1.21%	20.91%
CH2PH	22.40%	64.18%	0.79%	11.96%
CH2S	18.21%	80.33%	0.73%	

The delocalization onto carbon is again nearly double, and the delocalization onto the hydrogen bonded to X stays nearly the same for both single and double bond cases. The localization percentages of 3rd-row elements does not change appreciably either, despite the fact that this density is more diffuse, and should be drawn away by carbon much more easily. In all cases, the delocalization onto the methylene hydrogen is constant at around 1%, so one would expect delocalization in π-bonded species to be mostly involved in those atoms with π bonds.

The group delocalization values, shown on Table 74, show the same overall trends as seen in the single bond series.

Table 74: Group Localization Indices for CH_2=XH_n (HF)

CH_2CH_2		CH_2	CH_2
	CH_2	6.9022	
	CH_2	1.0982	6.9022
CH_2NH		CH_2	NH
	CH_2	6.1096	
	NH	0.9468	7.9964
CH_2O		CH_2	O
	CH_2	5.918	
	O	0.8104	8.4608
CH_2SiH_2		CH_2	SiH_2
	CH_2	8.4956	
	SiH_2	0.7320	14.0374
CH_2PH		CH_2	PH
	CH_2	7.9192	
	PH	0.8422	14.1620
CH_2S		CH_2	S
	CH_2	7.2536	
	S	1.1092	14.5300

The localization on methylene decreases with increasing electronegativity of the X group, and the shared density values maximize for X = carbon and sulphur, just as was seen in the methyl series. The main difference lies in the shared density values themselves, which are all nearly double that of the methyl series equivalents. This is a strong indicator that there is in fact a double bond between these two groups.

One would expect the bond orders for these 'doubly-bonded' molecules to also be double the bond order of the single bond counterparts, but it is in fact not the case. Ethylene, for example, has a bond order of 1.88 rather than exactly 2. This is because there is some delocalization of the carbon electron density onto the hydrogens as well as onto the other carbon, lowering the amount of density shared between the two carbons. Such an effect should also be seen in systems where the atoms involved in the double bond are more electronegative, drawing their electron density more tightly onto themselves.

Table 75: Bond Orders for $CH_2=XH_n$ (HF)

CH_2CH_2		CH_2SiH_2	
C-C	1.8820	C-Si	1.0280
C-H	0.9840	C-H	1.0512
CH_2NH		Si-H	0.5480
C-N	1.6216	CH_2PH	
C-H	0.9280	C-P	1.5816
N-H	0.8780	C-H	1.0092
CH_2O		P-H	0.8444
C-O	1.3736	CH_2S	
C-H	0.8972	C-S	2.0536
		C-H	0.9708

For example, the fact that the bond order decreases with increased electronegativity of X should be expected, given that the bond order of the single bonds also decreased. The fact that the bond order decreases more rapidly in the double bond case shows that the π-bond density is more easily polarized than the σ-bond density. This is reflected in the fact that the C=Si bond order is about one, reflecting the fact that most of the π-bond density is on the carbon.

5.1.4 Localization Indices of $SiH_2=XH_n$ Series

From the previous sets of data, one can see that an element like silicon will tend to delocalize substantially onto adjacent atoms. For a Si=X bond, this delocalization should be even higher, as the easily-polarized π-bond density should be drawn onto the more electronegative X element. Figure 56 shows that the localization percentage on silicon actually increases by a few percent compared to the single bond silyl species. This would reflect the increased amount of valence density made available through the π-bond density; even though a lot of the density would be lost to X, there is still more on the silicon than in the single-bond cases. The delocalization onto X is once again nearly double that of the single bond series, again showing the ability of X to draw density from silicon. The delocalization onto the silylene group hydrogen is still nearly the same as that of the silyl series. The 3rd-row element values are slightly lower, complementing the higher values of localization on silicon when doubly bonded to a 3rd-row element. This is once again an artifact of the calculation: the hydrogen values do decrease, but the population of silicon decreases more quickly.

Figure 56: Percentage Localization and Delocalization on Silicon in $SiH_2=XH_n$ (HF)

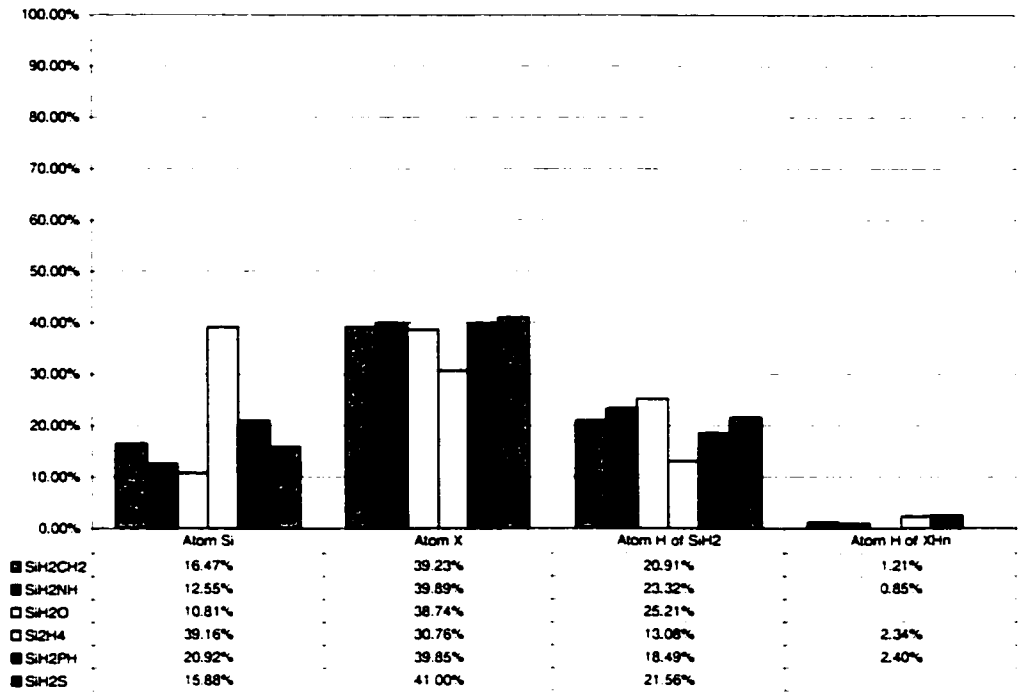

The localization on X is expectedly quite large, as Figure 57 shows, larger than the equivalent single bond cases. The percentages start at a much higher value than the single bond series, but approach similar values when X is oxygen. This may be another case of silicon losing almost all of its valence density, in essence forming a zwitterionic single bond system, as bond and integration data had previously shown. The only value that is reasonably high compared to the other is, of course, X = silicon: even the other 3rd-row elements hold onto their valence density more tightly.

Figure 57: Percentage Localization and Delocalization on Atom X in $SiH_2=XH_n$ (HF)

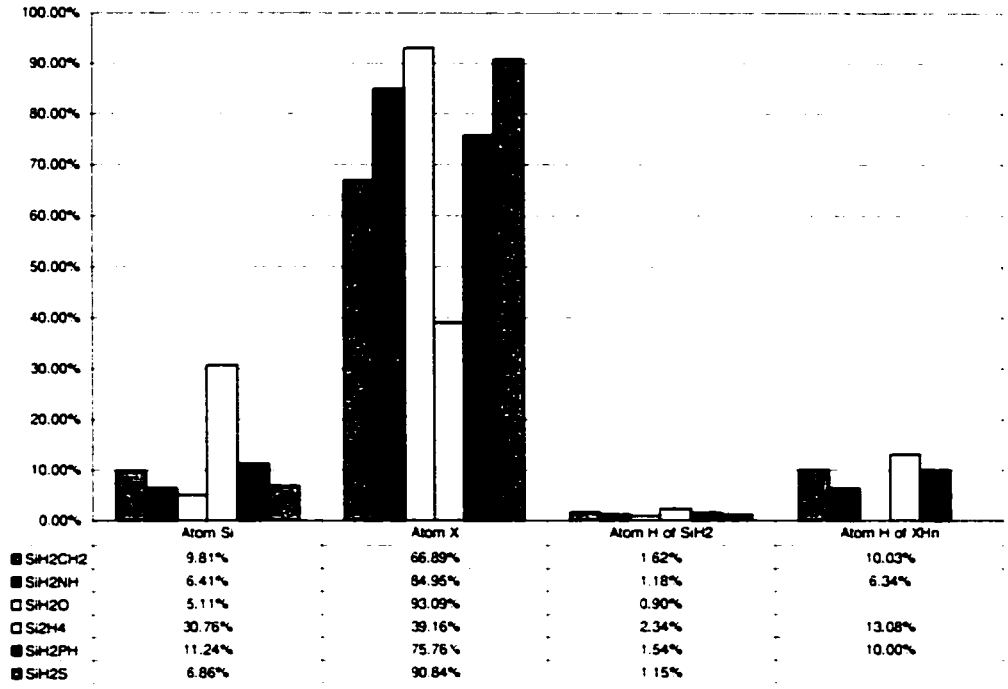

One expects the group delocalizations, shown in Table 76, to be considerably smaller than the C=X counterparts, yet larger than the Si-X shared densities. This is in fact the case, though the Si=X shared density values are smaller than expected. Rather than being slightly less than double the Si-X shared density values, they are in fact much closer to the single bond shared densities.

Table 76: Group Localization Indices for $SiH_2=XH_n$ (HF)

SiH_2CH_2		SiH_2	CH_2
	SiH_2	14.0374	
	CH_2	0.7320	8.4956
SiH_2NH		SiH_2	NH
	SiH_2	13.9292	
	NH	0.6114	8.8464
SiH_2O		SiH_2	O
	SiH_2	14.0278	
	O	0.5238	9.0596
SiH_2SiH_2		SiH_2	SiH_2
	SiH_2	14.9902	
	SiH_2	1.0576	14.9902
SiH_2PH		SiH_2	PH
	SiH_2	14.151	
	PH	0.8320	16.185
SiH_2S		SiH_2	S
	SiH_2	13.9800	
	S	0.6728	16.6742

This indicates what the electron density calculations on this series also show: that there is less double-bond character in these molecules than in the C=X series. The bond order data, in Table 77, however, tells a different story.

Table 77: Bond Orders for $SiH_2=XH_n$ (HF)

SiH_2CH_2		SiH_2SiH_2	
Si-C	1.0280	Si-Si	1.5808
Si-H	0.5480	Si-H	0.6720
C-H	1.0512	SiH_2PH	
SiH_2NH		Si-P	1.2276
Si-N	0.8788	Si-H	0.5696
Si-H	0.5136	P-H	1.0928
N-H	0.8688	SiH_2S	
SiH_2O		Si-S	1.0080
Si-O	0.7756	Si-H	0.5300
Si-H	0.5048		

When compared to the equivalent Si-X bond order, the bond orders above are very nearly doubled, unlike the C=X bond orders, which on a whole were less than two times the C-X bond order. Perhaps this reflects the fact that the bonding density in these systems is much more diffuse, and thus not as polarized as one

would expect. Despite the strong polarizations implied in Si=X bond data, the sharing of π-bond density is greater than previous data indicates.

5.1.5 Localization Indices of Miscellaneous Silicon Species

The bond and integration data of hypercoordinate silicon species showed clearly that the Si-X bonds became more ionic as the coordination around silicon increased, even though the population of silicon remained fairly constant. Figure 58 shows that there is very little sharing of density going on in these systems.

Figure 58: Percentage Localization and Delocalization on Si in Miscellaneous Silicon Species (HF)

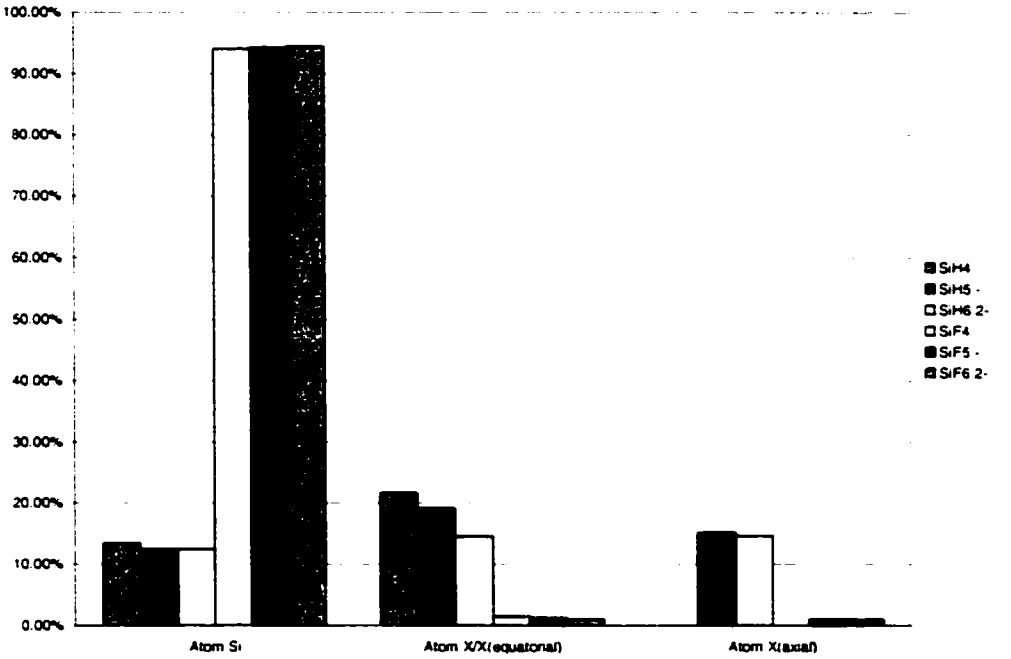

The localization percentages for X = hydrogen remain fairly constant, and are quite low. For X = fluorine, nearly all of the valence density of silicon is stripped away, leaving high percentages that represent the core density. What is more interesting are the values of delocalization onto the X ligands. For hydrogen, the percentages decrease as co-ordination increases. This corresponds nicely to the bond and integration data of this series: increased ionic character in the bonds means less sharing between the atoms. For the fluorine series, this lack of sharing of density is even more apparent, approaching zero, as would be expected for ionic bonds.

Figure 59 shows the localization on the ligands themselves. It becomes quite clear that most of the density on X, whether it be hydrogen or fluorine, stays on X, and very little of the density is shared with silicon.

Figure 59: Percentage Localization and Delocalization on Atom X in Miscellaneous Silicon Species (HF)

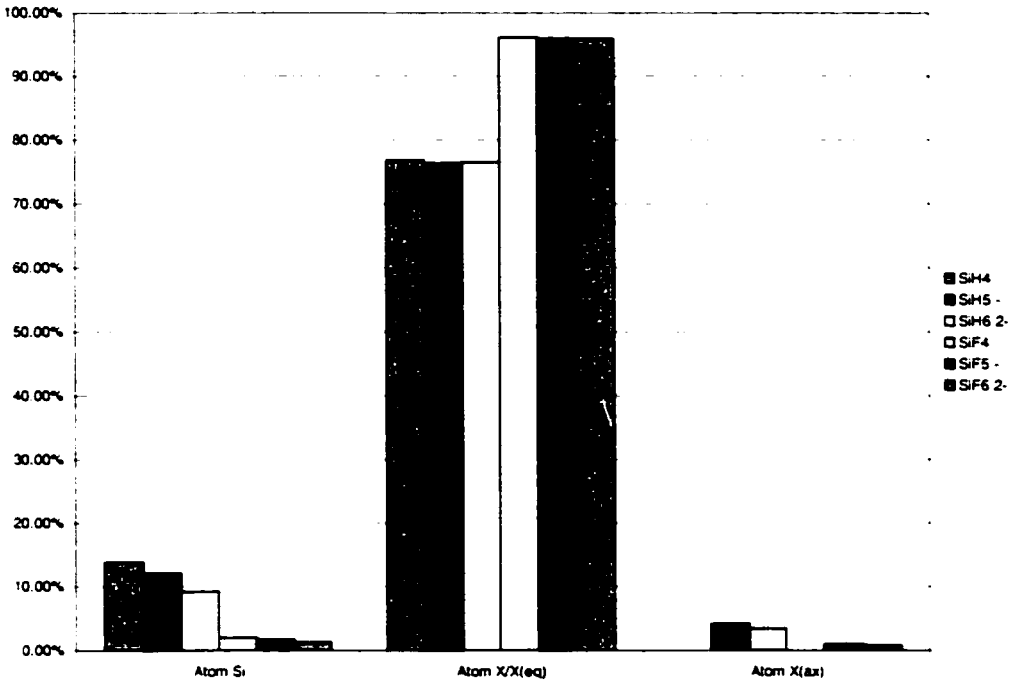

The differences between the localization percentages of hydrogen and fluorine reflect the ability of these ligands to hold a negative charge. Fluorine is a very hard anion, holding its valence density very closely. The amount of sharing of density between fluorine and most elements, silicon in particular, is going to be minimal. Hydrogen forms a much softer, more diffuse anion, so there is more sharing between it and silicon. What is interesting to note is, as in the previous chart, the delocalization onto silicon from X decreases as the co-ordination around silicon increases, reflecting the increased ionic character of the Si-X bonds.

Table 78 and Table 79 give the actual pair density values for the various species. As with the populations, the integrated pair density does not change substantially with increased coordination. What does change is the delocalization onto the ligand, which decreases with increased coordination.

Table 78: Localization Indices for SiH_n Species (HF)

SiH_4	Si 1	H 2	H 3	H 4	H 5		
Si 1	10.1470						
H 2	0.2382	1.3238					
H 3	0.2380	0.0536	1.3238				
H 4	0.2380	0.0536	0.0536	1.3238			
H 5	0.2380	0.0536	0.0536	0.0536	1.3238		
SiH_5^-	Si 1	H 2	H 3	H 4	H 5	H 6	
Si 1	10.1376						
H 2	0.2128	1.3418					
H 3	0.2126	0.0294	1.3418				
H 4	0.2126	0.0294	0.0294	1.3418			
H 5	0.1680	0.0730	0.0732	0.0730	1.4058		
H 6	0.1680	0.0730	0.0732	0.0730	0.0126	1.4058	
SiH_6^{2-}	Si 1	H 2	H 3	H 4	H 5	H 6	H 7
Si 1	10.1426						
H 2	0.1672	1.3816					
H 3	0.1670	0.0608	1.3816				
H 4	0.1670	0.0608	0.0110	1.3816			
H 5	0.1672	0.0110	0.0608	0.0608	1.3816		
H 6	0.1682	0.0608	0.0608	0.0608	0.0608	1.3816	
H 7	0.1682	0.0608	0.0608	0.0606	0.0606	0.0110	1.3816

What is interesting about these delocalization values is the fact that the values decrease with bond length. The axial hydrogens in Table 78 have significantly lower pair densities than the equatorial hydrogens. This extends even to the hexacoordinate system, though the differences there are much smaller. This shows that the pair density can reveal fine details in electronic structure that one does not see in the electron density. The BCPs of the hexacoordinate system are identical, and there is no geometrical way to distinguish between axial and equatorial in that system.

The fluoride series shows the same general trends as in the hydrogen series. There is the same difference in axial and equatorial pair densities in the pentacoordinate case, but the differences in the hexacoordinate case are very small. This may be another feature difference between the ligand types: soft ligands may show some distortion from a perfect octahedron, while hard ligands do not.

Table 79: Localization Indices for SiF_n Species (HF)

SiF_4	Si 1	F 2	F 3	F 4	F 5		
Si 1	9.9446						
F 2	0.1566	9.5556					
F 3	0.1554	0.0480	9.5558				
F 4	0.1554	0.0480	0.0480	9.5558			
F 5	0.1554	0.0480	0.0480	0.0480	9.5558		
SiF_5^-	Si 1	F 2	F 3	F 4	F 5	F 6	
Si 1	9.9554						
F 2	0.1302	9.5640					
F 3	0.1300	0.0204	9.5640				
F 4	0.1300	0.0204	0.0204	9.5640			
F 5	0.1092	0.0744	0.0744	0.0744	9.5580		
F 6	0.1092	0.0744	0.0744	0.0744	0.0008	9.5580	
SiF_6^{2-}	Si 1	F 2	F 3	F 4	F 5	F 6	F 7
Si 1	9.9640						
F 2	0.0976	9.5802					
F 3	0.0976	0.0568	9.5802				
F 4	0.0976	0.0568	0.0008	9.5802			
F 5	0.0976	0.0008	0.0568	0.0568	9.5802		
F 6	0.0980	0.0568	0.0568	0.0568	0.0568	9.5802	
F 7	0.0980	0.0568	0.0568	0.0568	0.0568	0.0008	9.5802

Bond orders for these species should be very small, as they are simply twice the shared density between two atoms. In both cases, bond order is a function of bond length: as the bonds become longer with increased co-ordination, so they also become more ionic.

Table 80: Bond Orders for Miscellaneous Silicon Species (HF)

SiH_4		SiF_4	
Si-H	0.4764	Si-F	0.3108
SiH_5^-		SiF_5^-	
Si-H ax	0.3360	Si-F ax	0.2184
Si-H eq	0.4256	Si-F eq	0.2600
SiH_6^{2-}		SiF_6^{2-}	
Si-H	0.3344	Si-F	0.1952

Despite being very different ligands, both sets of molecules have their bond orders decrease by about the same relative amount; the hexacoordinate bond order is about 68% of the tetracoordinate bond order. This implies that the hydride and the fluoride are about the same volume. If one were larger, than the decrease in bond order would be greater, as the ligands would have to be farther from the silicon in order to fit around it.

5.2 Discussion: Delocalization Differences

In general, carbon retains its valence density to a much greater extent than silicon. As a result, there is much more sharing between carbon and its bonded atoms, compared to silicon. On average, the localization percentage on carbon is about 54%, as opposed to about 28% on silicon; Figure 60 illustrates the trend observed in the localization on carbon and silicon as a function of atom X. When X is bonded to carbon, there is a more gradual change in localization with changing X. This is not seen in silicon, which shows regions of relatively small change in localization spaced between points where the localization changes drastically. This can be considered indicative of a system containing an atom whose valence density is loosely held. Either the localization is high, the result of X being less electronegative than silicon, which allows silicon to retain its valence density somewhat, or very low, the result of X being more electronegative, which strips the valence density of silicon away.

Figure 60: Percent Localization on Atom M in MH_3XH_n (HF)

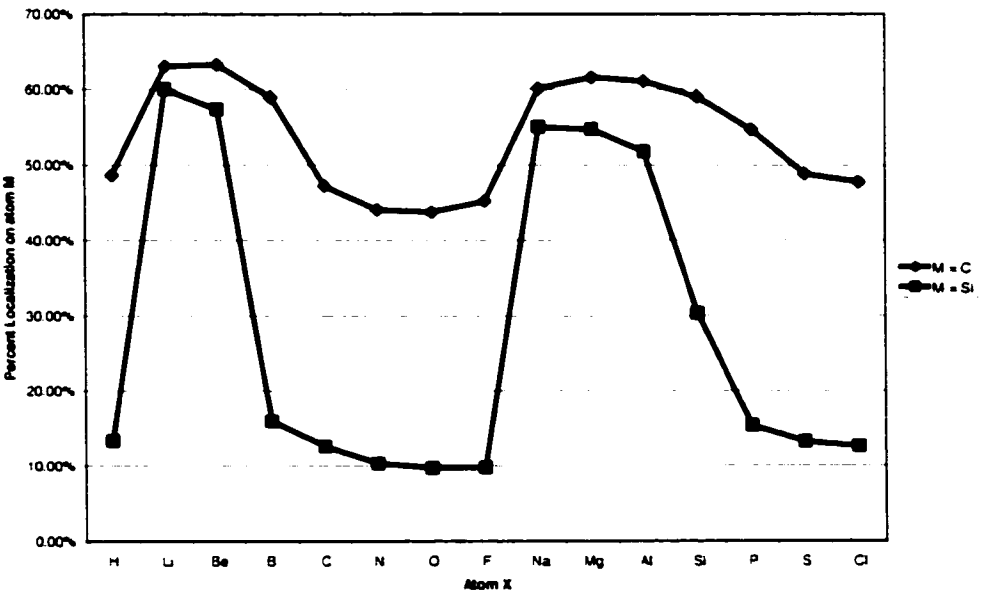

As the graph also shows, the change in localization in silicon is far greater than that of carbon, demonstrating the greater ability of carbon to retain its valence density. The remaining 46% of carbon's valence density is delocalized amongst those atoms it is bonded to, and very little density is delocalized to atoms beyond those bonded to carbon. How much density is delocalized onto each atom depends on the

atoms bonded to carbon, but overall, the distribution is surprisingly even, provided that the atoms have a relatively high electronegativity, which is true for silicon also. For carbon, the delocalization percentage averages around 9%, while values for silicon average around 16%, as shown in Figure 61. Much like Figure 60, the changes in delocalization of silicon valence density onto X show small changes with X, as well as points of drastic change. While the same pattern is observed for carbon, the changes in percentage are much smaller.

Figure 61: Percent Delocalization of Atom M onto Atom X in MH_3XH_n (HF)

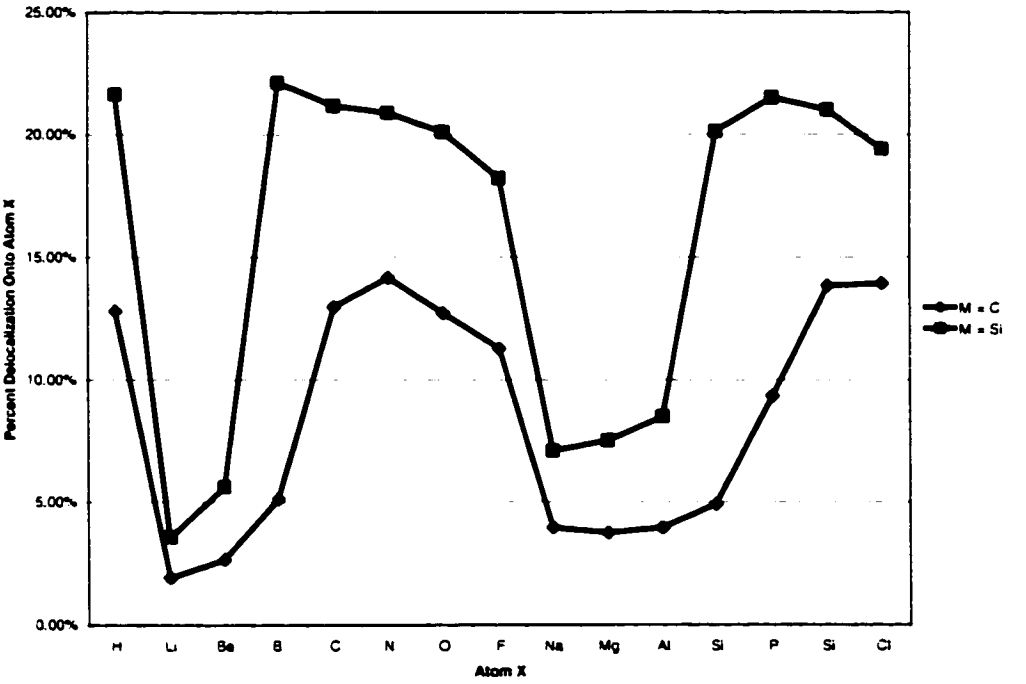

It appears that for a system MH_3XH_n, the nature of X has little bearing on how the valence density of M delocalizes through the molecule. Obviously, the values vary a great deal more for some element X bonded to carbon or silicon, given that the electronegativity of X is changing through the series. The general trend is that localization increases with electronegativity. A silicon atom bonded to X will push the percentages up 1-2%, but will not change the trend significantly. The delocalization of X onto carbon or silicon also follows a similar trend, except that the percentages on carbon are about double that of silicon.

Species of the type $MH_2{=}XH_n$ also follow similar trends with change in X. The localization on both carbon and silicon decrease as the electronegativity of X increases. This trend is more pronounced in doubly-bonded species, as opposed to singly bonded, where there is little change in the values. On average the percentage localization on silicon is about a third that of carbon, while the delocalization percentages are approximately doubled. Localization on X varies some when X is bonded to carbon or silicon, even though the same trend is observed. The localization on X is higher when X is bonded to silicon, reflecting the amount of density X draws from silicon. The delocalization of X onto silicon or carbon is similar in trend, with the silicon values being lower, corresponding to the localization values.

Hypercoordination of silicon results in increased ionic character in the Si-X bond, and the localization percentages reflect this for both hydrogen and fluorine. The localization on all atoms in these series remain constant with increased coordination, while delocalization decreases, reflecting the increased ionicity of the silicon-atom bonds.

5.3 Pair Density Properties of M_nH_{2n+2}

One of the goals of this research was to find evidence of delocalization in polysilanes, through a means other than MO models. A thorough study of the electron density properties as described in the last section showed that oligosilanes exhibit additivity and transferability, regardless of chain length, just as hydrocarbons do, thus showing no evidence of σ-conjugation and delocalization. The only interesting difference was that the 'end-group effect' had a longer range of influence in the silyl group. While the methyl group in hydrocarbons only affected the α-methylene, the silyl group in oligosilanes affected both the α- and β-silylene groups. This was still insufficient evidence to explain the delocalization behavior observed in polysilanes, so the pair density of these compounds were then studied, to hopefully observe the delocalization directly.

5.3.1 Localization Indices of C_nH_{2n+2}

The hydrocarbon and oligosilane series showed interesting properties of transferability and additivity, with respect to geometry, bond properties, and basin properties. Table 81 shows that hydrocarbons also possess additive pair densities as well. The localization on methyl remains constant throughout the series:

the integrated α-methylene pair density, from butane on, also becomes constant, as do the internal methylenes. In fact the delocalization of internal methylene density onto adjacent methylenes also stays fairly constant, once the methylene is sufficiently far from the methyl group that it does not have any real influence. The delocalization values for all adjacent groups average closely around 0.6, implying that even the presence of the methyl group nearby minimally influences the extent of delocalization. Another interesting feature is the sum below each column of values. As was stated earlier, the total number of an atom's electrons delocalized over the entire molecule equals the total population of that atom. This is not only a feature that makes physical sense, it serves as a test to ensure that the group delocalization values have been calculated correctly.

Table 81: Group Localization Indices of C_nH_{2n-2} (SCVS)

C_2H_6	$C1H_3$			C_3H_8	$C1H_3$	$C2H_2$		
$C1H_3$	8.344			$C1H_3$	8.342	0.615		
$C2H_3$	0.656			$C2H_2$	0.615	6.736		
				$C3H_3$	0.058	0.615		
Sum	8.999							
				Sum	9.016	7.966		
C_4H_{10}	$C1H_3$	$C2H_2$		C_5H_{12}	$C1H_3$	$C2H_2$	$C3H_2$	
$C1H_3$	8.341	0.614		$C1H_3$	8.341	0.614	0.051	
$C2H_2$	0.614	6.735		$C2H_2$	0.614	6.735	0.581	
$C3H_2$	0.051	0.582		$C3H_2$	0.051	0.581	6.734	
$C4H_3$	0.009	0.051		$C4H_2$	0.008	0.044	0.581	
				$C5H_3$	0.001	0.008	0.051	
Sum	9.015	7.982						
				Sum	9.014	7.982	7.997	
C_6H_{14}	$C1H_3$	$C2H_2$	$C3H_2$	C_7H_{16}	$C1H_3$	$C2H_2$	$C3H_2$	$C4H_2$
$C1H_3$	8.341	0.614	0.051	$C1H_3$	8.341	0.613	0.050	0.008
$C2H_2$	0.614	6.735	0.580	$C2H_2$	0.613	6.735	0.601	0.039
$C3H_2$	0.051	0.580	6.734	$C3H_2$	0.050	0.601	6.734	0.600
$C4H_2$	0.007	0.045	0.580	$C4H_2$	0.008	0.039	0.600	6.733
$C5H_2$	0.001	0.006	0.044	$C5H_2$	0.001	0.007	0.045	0.600
$C6H_3$	0.000	0.001	0.007	$C6H_2$	0.000	0.001	0.006	0.045
				$C7H_3$	0.000	0.000	0.001	0.006
Sum	9.014	7.981	7.997					
				Sum	9.013	7.996	8.0377	8.0312

The bond orders of the hydrocarbons, shown in Table 82, also show the additivity of this series.

Table 82: Bond Orders of C_nH_{2n+2} (SCVS)

	C1-C2	C2-C3	C3-C4		C1-H	C2-H	C3-H	C4-H
C_2H_6	0.9920				0.9672			
C_3H_8	0.9784				0.9668	0.9524		
C_4H_{10}	0.9784	0.9656			0.9668	0.9480		
C_5H_{12}	0.9784	0.9656			0.9668	0.9480	0.9436	
C_6H_{14}	0.9784	0.9656	0.9656		0.9668	0.9480	0.9436	
C_7H_{16}	0.9784	0.9656	0.9656		0.9668	0.9480	0.9436	0.9436

All of the bond orders in this series reach a constant value almost immediately: the standard bond order for a methyl-methylene C-C bond is 0.9784, while a standard internal C-C bond is 0.9656. Given the apparent sensitivity of the pair density to changes in bonding properties, as was seen with the hypercoordinate silanes, this serves to illustrate the strong role that additivity plays in this series.

5.3.2 Localization Indices of Si_nH_{2n+2}

Given the observed behavior of polysilanes associated with delocalization, and the additivity of the localization indices of hydrocarbons, there should be some differences seen in the pair density of oligosilanes. The pair density seems to be far more sensitive to changes in functional groups, far more so than the electron density. If there is any delocalization in oligosilanes, the pair density should reveal it.

Table 83 shows the pair densities for various groups in the oligosilane series. What becomes immediately clear is that just as oligosilanes are additive with respect to the electron density and its properties, so too is it additive with respect to the pair density. While it takes somewhat longer for the silyl group to achieve a constant value compared to methyl, it does so, as do the silylene groups. The delocalization values also reach a constant value within the series, indicating no differences in group properties with respect to chain length. A more surprising feature appears when one compares the percentage localizations of carbon to silicon. Even correcting for the core density, the silyl and silylene groups are actually more localized than the methyl and methylene groups. The localization percentage is 90% on methyl and 78% on methylene, with 9% delocalization between them. The silyl group, however, has 92% localization: the percentage localization on the silylene group is 82%, with 8% delocalization between them. As surprising as these numbers seem, they do make sense when one considers the respective electronic structures of the two molecules. Hydrogen and carbon have similar electronegativities, so the

sharing of density between two groups is reasonably good, and there is considerable valence density on carbon. In the case of the silyl group, most of the valence density is on the hydrogens. This density does not get shared with other groups, so there is far less density in the valence shell of silicon to share with the adjacent group. While the differences are relatively small, it is the exact opposite result one would hope to obtain to describe delocalization.

Table 83: Group Localization Indices of Si_nH_{2n+2} (SCVS)

Si_2H_6	$Si1H_3$			**Si_3H_8**	$Si1H_3$	$Si2H_2$		
$Si1H_3$	16.431			$Si1H_3$	16.414	0.544		
$Si2H_3$	0.563			$Si2H_2$	0.544	14.924		
				$Si3H_3$	0.031	0.543		
Sum	16.994							
				Sum	16.989	16.011		
Si_4H_{10}	$Si1H_3$	$Si2H_2$		**Si_5H_{12}**	$Si1H_3$	$Si2H_2$	$Si3H_2$	
$Si1H_3$	16.402	0.541		Si1H3	16.404	0.541	0.027	
$Si2H_2$	0.541	14.915		Si2H2	0.541	14.905	0.524	
$Si3H_2$	0.027	0.527		Si3H2	0.027	0.524	14.906	
$Si4H_3$	0.005	0.028		Si4H2	0.004	0.024	0.524	
				Si5H3	0.000	0.005	0.026	
Sum	16.976	16.010						
				Sum	16.976	15.998	16.008	
Si_6H_{14}	$Si1H_3$	$Si2H_2$	$Si3H_2$	**Si_7H_{16}**	$Si1H_3$	$Si2H_2$	$Si3H_2$	$Si4H_2$
$Si1H_3$	16.407	0.542	0.027	$Si1H_3$	16.404	0.541	0.026	0.003
$Si2H_2$	0.542	14.907	0.524	$Si2H_2$	0.541	14.906	0.524	0.024
$Si3H_2$	0.027	0.524	14.897	$Si3H_2$	0.026	0.524	14.898	0.522
$Si4H_2$	0.004	0.024	0.523	$Si4H_2$	0.004	0.026	0.522	14.887
$Si5H_2$	0.001	0.004	0.024	$Si5H_2$	0.001	0.004	0.026	0.522
$Si6H_3$	0.000	0.001	0.004	$Si6H_2$	0.000	0.000	0.004	0.027
				$Si7H_3$	0.000	0.000	0.000	0.004
Sum	16.981	16.002	15.999					
				Sum	16.9767	16.001	16.000	15.9890

The bond order data on Table 84 further illustrates the additivity of oligosilanes with respect to the pair density. The values reach a constant quite quickly, and it is interesting how the bond order of an internal Si-Si bond is higher than that of a silyl-silylene Si-Si bond. This can be explained by the fact that the silylene group only has two hydrogens to draw density from it as opposed to three on silyl. Thus there is more valence density within the silylene silicon to be shared with adjacent groups, even though the BCP value of rho for an internal Si-Si bond is slightly lower than that of a silyl-silylene bond.

Table 84: Bond Orders of Si_nH_{2n+2} (SCVS)

	Si1-Si2	Si2-Si3	Si3-Si4		Si1-H	Si2-H	Si3-H	Si4-H
Si_2H_6	0.7376				0.5496			
Si_3H_8	0.7624				0.5484	0.6240		
Si_4H_{10}	0.7600	0.7888			0.5472	0.6208		
Si_5H_{12}	0.7596	0.7860			0.5472	0.6200	0.6188	
Si_6H_{14}	0.7600	0.7860	0.7836		0.5476	0.6204	0.6180	
Si_7H_{16}	0.7592	0.7856	0.7832		0.5476	0.6200	0.6180	0.6176

5.4 Comparisons Between Carbon and Silicon

Both the hydrocarbons and oligosilanes possess additive behavior, not only with respect to the electron density, but also the pair density[147]. The value of the integrated pair density for methyl remains constant throughout the series of hydrocarbons at 8.34, as do the localization values for the methylene groups, both alpha to the methyl and internal, with a value of 6.37. The largest delocalization values are those adjacent to the group under study, which remain constant at 0.58, and then increase to 0.60 in heptane, a minor increase with respect to the localization value. The delocalization value for an α-methylene onto methyl is slightly higher at 0.61. The silyl group takes longer to reach a constant value of 16.40, reaching it at silabutane: a constant silylene group pair density value is not reached until pentasilane. The delocalization values for oligosilanes are smaller than for hydrocarbons. It is 0.54 for delocalizations onto and off of the silyl group, and 0.52 for internal silylene groups. The most striking difference between these two sets of molecules is the fact that despite being a molecule that exhibits behavior associated with conjugation, the pair density is slightly more localized, by about 3% compared to hydrocarbons.

5.5 Discussion: Meaning of Delocalization in Pair Density Context

The realization that the pair density is more localized on an oligosilane, and by inference a polysilane, than on a hydrocarbon, is certainly cause for reflection. The electron density properties did not yield results that suggested an obvious answer: bond properties and integrations remained constant, proving that polysilanes are just as additive as hydrocarbons. The pair density was thus pursued further. Despite no strong evidence of conjugation in the electron density calculations, experimental observation proves that it exists, indicating that the problem had to be addressed from a different perspective, and a different property

density. It was at this point that the same situation arose: the pair density gave indications of increased localization, which meant that this was not the correct density to study either.

The main criterion for polysilanes being delocalized stemmed from the fact that they show bathochromic behavior, or a decrease in excitation energy as a function of chain length, something observed in π-conjugated systems. Thus, the conjugative behavior observed in polysilanes is not a ground state property, and thus cannot be calculated through ground state densities. This led to the studies of the transition density, as it is a density used frequently in excited state calculations. The transition density is essential for calculating the transition dipole for a given excitation, which in turn allows one to calculate the probability of that excitation, a value related directly to the intensity of a UV absorption band. The transition density, like any other density, can be partitioned into atomic contributions, enabling one to obtain the atomic contributions to the transition dipole and the probability of excitation.

6 Transition Density Properties of Silicon and Carbon Compounds

The results of studying the number and pair densities of oligosilanes showed that there is no evidence of delocalization or conjugation within these systems. The next property to test was that associated with electronic excitation, one that should clearly illustrate whether the electronic excitations associated with these molecules are in fact delocalized over the entire molecule. The transition density determines the degree of delocalization upon electronic excitation. From this density one can calculate the transition dipole moment of an excitation, which in turn provides the oscillator strength, which further holds a direct relation to the extinction coefficients observed in UV spectra, as described in Section 2.8.

6.1 Development Studies

In the course of developing the theory and software that would calculate the properties of the transition density, small molecules with well-understood excitation properties were used for the initial application[158]. The two systems chosen were formaldehyde and ammonia: both are molecules whose excited states have been studied extensively[159,160], and are relatively easy to perform calculations with. Both molecules exhibit Rydberg excitations, where a non-bonded electron is excited to higher energy atomic orbitals, eventually converging to the ground state ionized system. An important point must be made, that the transition density, which is a mixture of the ground and excited state of study, has no relation to the change in electron density as a result of the electronic excitation. It should also be noted that all of the excitations studied in this thesis are vertical excitations. Partitioning the excitation energy was not done in this thesis, as all the excited states studied here are vertical excitations. A proper partitioning of the excitation energy would require the determination of the energy of an excited molecule in a relaxed geometry, which was not considered important for this study.

6.1.1 Formaldehyde

The carbonyl chromophore is well known in chemistry, as it has a characteristic excitation that is used to identify the functional group.

Table 85: Properties of Ground State Formaldehyde

CH_2O			
E	-113.9082945	C = O bond	
-V/T	2.00061644	ρ_b	0.4475
Error in E	0.0001	$L(r)_b$	-0.0348
C – H	1.0918	C – H bond	
C – O	1.1785	ρ_b	0.3003
H – C – H angle	116.3131	$L(r)_b$	0.3068
H – C – O angle	121.8435		

The ground state configuration of formaldehyde is $...5a_1^2\ 1b_1^2\ 2b_2^2$: the lowest energy excitations result from promotion of an electron from the $2b_2$ orbital on oxygen, which is assigned the label 'n', indicating non-bonded electrons in the plane of the molecule[160]. The first three allowed excitations were studied for this portion of the research, corresponding to $n \rightarrow 6a_1$ (3s), giving the 1^1B_2 state, $n \rightarrow 7a_1$ ($3p_z$), giving the 2^1B_2 state, and $n \rightarrow 3b_2$ ($3p_y$), giving the 2^1A_1 state. The excitations studied are summarized in Table 86.

Table 86: Excited States of Formaldehyde, as Calculated by Gaussian94

	Energy (eV)		Transition Dipole			Osc. Strength
	Calc.	Exp.	x	y	z	
1^1B_2	8.5326	7.099	0.0000	-0.4019	0.0000	0.0338
2^1B_2	9.4291	7.970	0.0000	0.4573	0.0000	0.0483
2^1A_1	9.6282	8.160	0.0000	0.0000	-0.6439	0.0978

It is important to study not only the transition density properties, but also the changes in the electron density properties as a result of each excitation. For this research, the main properties that were studied are the populations, the quadrupole moments, and the volumes[161] of each atom.

Table 87: Ground and Excited State Bond Data for Formaldehyde

	r	$r_b(C)$	$\% r_b(C)$	ρ_b	$L(r)_b$	ε
X^1A_1						
C=O	2.2272	0.7432	33.37	0.4475	-0.0348	0.1043
C-H	2.0632	1.3223	64.09	0.3003	0.3068	0.0101
$n \rightarrow 3s$						
C=O	2.2271	0.7394	33.20	0.4467	-0.0814	0.0456
C-H	2.0634	1.4281	69.21	0.2797	0.3001	0.0284
$n \rightarrow 3p_z$						
C=O	2.2270	0.7387	33.17	0.4465	-0.0860	0.0356
C-H	2.0631	1.4134	68.51	0.2798	0.2965	0.0284
$n \rightarrow 3p_y$						
C=O	2.2271	0.7385	33.16	0.4454	-0.0996	0.0859
C-H	2.0632	1.4259	69.11	0.2834	0.3066	0.0242

Table 87 shows how the bond critical points change as a result of each excitation. The change in rho at the BCPs is quite small, as there is no change in the molecular geometry. The change in L(r) at the C-H BCP is also quite small, as would be expected, considering the electron being excited comes from the non-bonded region of oxygen. This is reflected in the large charges in the C=O BCP L(r). Table 88 shows the changes in integrated values for each excited state: quadrupole moments for hydrogen are small compared to carbon and oxygen, and provide no additional information about the change in density upon excitation. The main axis of formaldehyde in this molecule is the z-axis, with the hydrogens pointing along the y-axis.

Table 88: Atomic Properties and their Change Upon Excitation for Formaldehyde

$X\ ^1A_1$	$N(\Omega)$	$Q_{xx}(\Omega)$	$Q_{yy}(\Omega)$	$Q_{zz}(\Omega)$	$v(\Omega)$
O	9.271	-0.076	-0.386	0.462	139.81
C	4.709	-1.003	-0.104	1.108	56.09
H	1.010				49.70
$n \rightarrow 3s$	$\Delta N(\Omega)$	$\Delta Q_{xx}(\Omega)$	$\Delta Q_{yy}(\Omega)$	$\Delta Q_{zz}(\Omega)$	$\Delta v(\Omega)$
O	-0.173	-2.918	0.950	1.968	13.51
C	0.266	-1.484	0.639	0.844	24.41
H	-0.046				33.85
$n \rightarrow 3p_z$	$\Delta N(\Omega)$	$\Delta Q_{xx}(\Omega)$	$\Delta Q_{yy}(\Omega)$	$\Delta Q_{zz}(\Omega)$	$\Delta v(\Omega)$
O	0.035	-2.948	0.653	2.295	40.13
C	0.360	3.903	5.108	-9.013	62.88
H	-0.197				14.86
$n \rightarrow 3p_y$	$\Delta N(\Omega)$	$\Delta Q_{xx}(\Omega)$	$\Delta Q_{yy}(\Omega)$	$\Delta Q_{zz}(\Omega)$	$\Delta v(\Omega)$
O	-0.289	0.158	-0.791	0.633	9.77
C	0.182	1.295	-1.235	-0.061	11.99
H	0.056				79.99

The excitation of the non-bonded electron to these diffuse Rydberg states results in a significant increase in the molecular volume. Different atoms in formaldehyde show the majority of the volume increase, depending on which orbital is being excited to, which is also true of the population changes. The quadrupole moments of carbon and oxygen show how the polarization of their electron densities changes with excitation, which explains how the density rearranges in each atom. The contour maps of rho for the excited states of formaldehyde (Figure 62) reinforce the data of Table 88. All three excited states show the addition of diffuse density to the outer regions of the molecule. Any doubts as to the symmetry of the virtual orbital are dispelled by the contour maps; the $n \rightarrow 3p_z$ and $n \rightarrow 3p_y$ excitations are especially telling, showing clearly the direction of the diffuse density.

Figure 62: Contour Plots of Electron Density of States of Formaldehyde

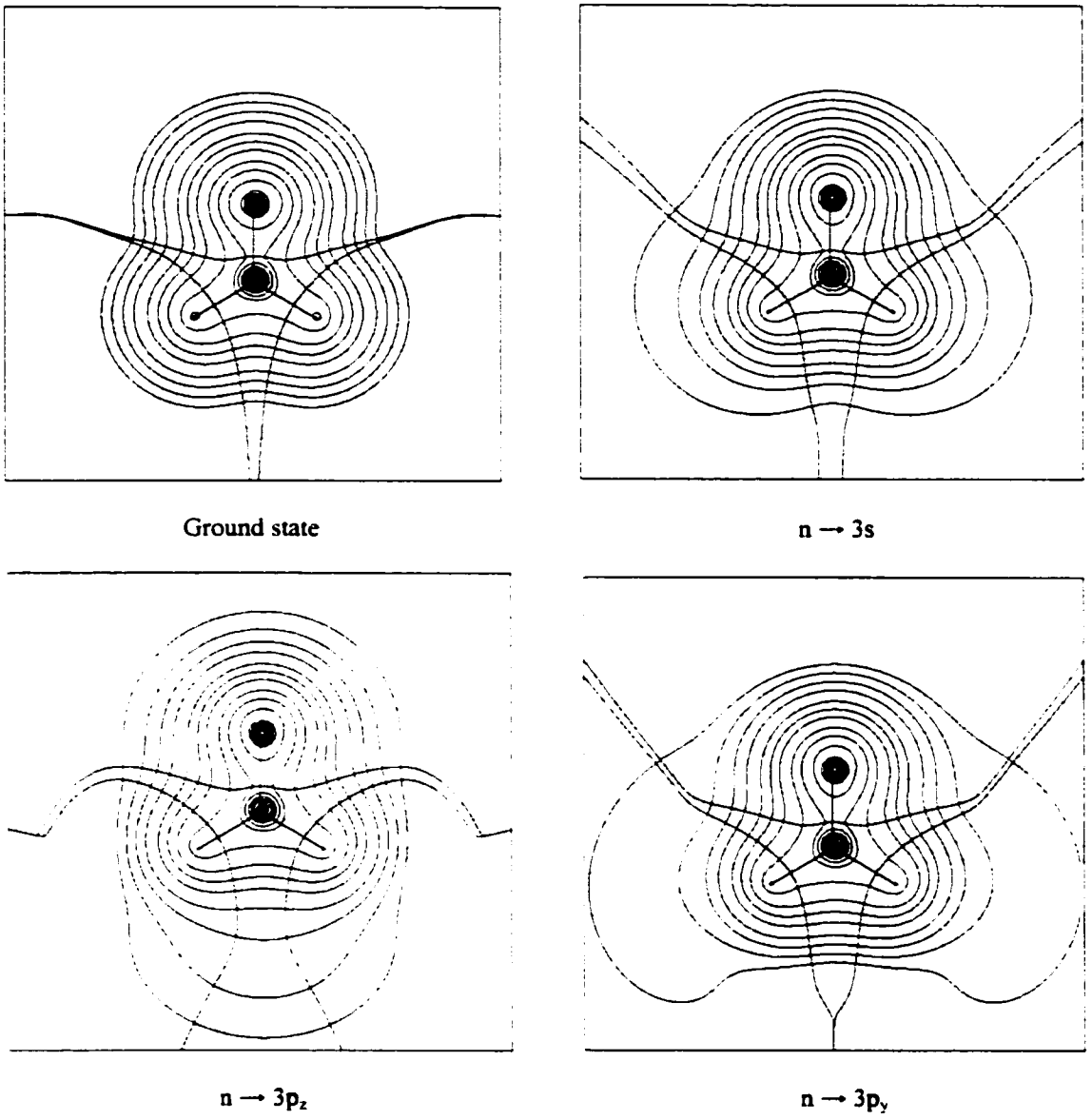

The contour maps of L(r) of the states of formaldehyde were omitted, as the only difference in the ground and excited states was the loss of the charge concentrations around oxygen corresponding to the lone pairs. The changes in density shown in Figure 62 did not appear in the L(r) maps, indicating that these density changes are very diffuse.

6.1.1.1 Formaldehyde 1^1B_2 Transition

The n → 3s (1^1B_2) transition was calculated by GAUSSIAN94 to have a transition dipole moment with a magnitude of 0.4019 au, an oscillator strength of 0.0338 au, and an excitation energy of 8.533 eV. This energy is higher than the experimental energy, (7.099 eV): the CI-singles method tends to overestimate the excitation energy. Forseman *et al* studied the same states of formaldehyde, and obtained results similar to these[128].

In terms of the BCP properties, the most telling change is in L(r) and the ellipticities, as shown in Table 87. The ellipticity of the C=O bond drops by about half, and L(r) becomes more negative, indicating a more polar bond. This can be explained by the addition of the diffuse 3s density, which obscures the ellipticity of the π bond. The loss of density from the non-bonded region of oxygen results in some rearrangement from the π-bond density of oxygen, further polarizing the bond. There is a net transfer of 0.25 electronic charges to carbon from the rest of the molecule upon excitation, as well as shift in the polarization in both oxygen and carbon, as shown in the quadrupole data of Table 88. The ground state has its main polarization along the x-axis of oxygen, which is the direction of the π bond. A minor polarization along the y-axis comes from the non-bonded density. Upon excitation, this minor polarization is lost, and the main polarization increases. Because the electron being promoted comes from this non-bonding region, this is expected. The same shifts in polarization are also seen in carbon, but are smaller in magnitude. The contour plot of rho for this excited state confirms the integration data. The outer density becomes more diffuse overall, except in the area of the non-bonded density of oxygen, indicating no net increase in density in that region. Table 89 provides information on the partitioning of the transition dipole of this state: μ_{nk} is defined by Equation 45, q_{nk} by Equation 54, and f_{nk} by Equation 56.

Table 89: Atomic Contributions to n → 3s Transition Probability in Formaldehyde (au)

n → 3s	$q_{nk}(\Omega)$	$\mu_{nk}(\Omega)$ x	$\mu_{nk}(\Omega)$ y	$\mu_{nk}(\Omega)$ z	$\lvert\mu_{nk}\rvert(\Omega)$	$f_{nk}(\Omega)$
C	0.0000	0.0000	-0.1936	0.0000	0.1936	0.0162
O	0.0000	0.0000	0.2008	0.0000	0.2008	-0.0168
H	0.1024	0.0000	-0.2036	-0.1143	0.2335	0.0170
H	-0.1024	0.0000	-0.2036	0.1143	0.2335	0.0170
Tot	0.0000	0.0000	-0.4000	0.0000		0.0335

Of particular note are the opposing transition dipoles of oxygen and the carbon and hydrogens. This results in the oscillator strengths of carbon and oxygen nearly cancelling, leaving the majority of the oscillator strength of the molecule centered on the hydrogens. The overall result is that, for this excitation, the carbonyl group makes nearly no contribution to the excitation. A more complex carbonyl compound excited to the 1^1B_2 state should exhibit contributions almost exclusively from the groups bonded to the carbonyl carbon. Figure 63 shows a contour map of the n → 3s transition density in the plane of the molecule. This plot indicates how the electron density oscillates when the molecule interacts with the radiation field of the photon. The induced polarizations are counter to one another, between different quantum shells of a given atom, and between neighboring atoms, a phenomenon generally observed in polarizations induced by a static external field[149].

Figure 63: Contour Map of n → 3s Transition Density of Formaldehyde

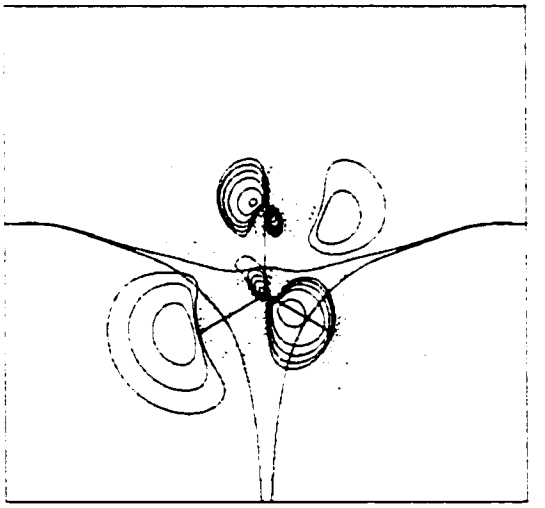

6.1.1.2 Formaldehyde 2^1B_2 Transition

The n → $3p_z$ (2^1B_2) transition has the same symmetry as the n → 3s transition, but with a slightly larger dipole moment (0.4573 au) and oscillator strength (0.0483 au), as well as a higher excitation energy (9.429 eV). As with the n → 3s transition, the C=O bond loses ellipticity and becomes more polar; in this case, it is the addition of $3p_z$ density to the region of the C=O bond, which points in the same direction. The amount of electron density transferred between atoms does not change appreciably compared to the n → 3s transition. The big change, however, is in the quadrupole moments of oxygen, which shifts from the y-axis

to the x-axis. Looking at the plot of rho of the n → $3p_z$ excited state shows why this is the case, as one can clearly see the $3p_z$ density, which extends past the non-bonded regions of the hydrogens. Table 90 shows the atomic contributions to the transition dipole. As with the n → 3s transition, the atomic contributions sum to form a dipole pointing along the y axis, a dipole in the plane of the molecule but perpendicular to the main symmetry axis.

Table 90: Atomic Contributions to n → $3p_z$ Transition Probability in Formaldehyde (au)

n → $3p_z$	$q_{nk}(\Omega)$	$\mu_{nk}(\Omega)$ x	$\mu_{nk}(\Omega)$ y	$\mu_{nk}(\Omega)$ z	$\lvert\mu_{nk}\rvert(\Omega)$	$f_{nk}(\Omega)$
C	0.0000	0.0000	-0.0847	0.0000	0.0847	0.0089
O	0.0000	0.0000	-0.2536	0.0000	0.2536	0.0267
H	-0.1410	0.0000	-0.0591	-0.1640	0.1743	0.0062
H	0.1410	-0.0000	-0.0591	0.1640	0.1743	0.0062
Tot		0.0000	-0.4564	0.000000		0.0481

However, unlike the n → 3s transition, all the dipoles point in the same direction, resulting in atomic oscillator strengths that are all positive. For this state, the carbonyl group makes a sizeable contribution to the excitation intensity, namely 74%. The oxygen alone contributes 55% of the oscillator strength, and Figure 64 shows why this is the case.

Figure 64: Contour Map of n → $3p_z$ Transition Density of Formaldehyde

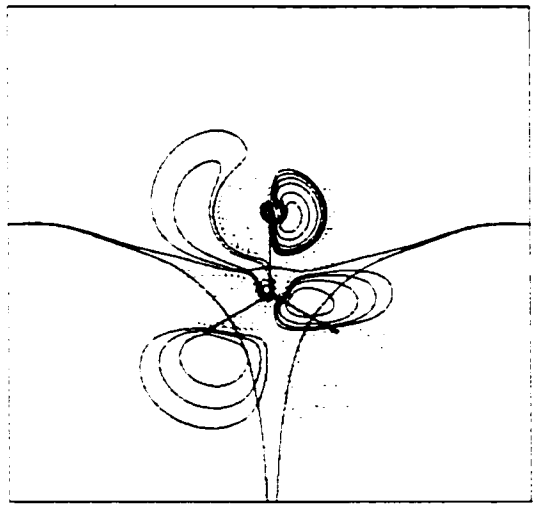

Unlike the n → 3s transition, where there is little to no interaction between the transition densities of carbon and oxygen (see Figure 63), the carbon transition density donates strongly into the oxygen, resulting in a strong oscillation by the entire carbonyl group rather than by individual atoms.

6.1.1.3 Formaldehyde 2^1A_1 Transition

The n → $3p_y$ transition is the strongest of the three transitions (0.6439 au dipole and 0.0973 au oscillator strength) as well as the only A_1 transition, meaning that the induced dipole runs along the main symmetry axis of the molecule. In terms of the excited state density, this results in an accumulation of density along the y-axis, in the region of the hydrogens. The ellipticity of the C=O bond does not decrease significantly in this excited state. The net transfer of density to the carbon is also smaller, with hydrogen gaining a small amount of density in this state. The quadrupole moments of oxygen and carbon show a strong shift in polarization from the x axis to the y-axis. The large increase in the volume of hydrogen confirms that most of the diffuse $3p_y$ density is within the hydrogen basins. The contour plot of the n → $3p_y$ state shows this volume increase quite clearly. Table 91 describes how the transition dipole partitions.

Table 91: Atomic Contributions to n → $3p_y$ Transition Probability in Formaldehyde (au)

n → $3p_y$	$q_{nk}(\Omega)$	$\mu_{nk}(\Omega)$ x	$\mu_{nk}(\Omega)$ y	$\mu_{nk}(\Omega)$ z	$\lvert\mu_{nk}\rvert(\Omega)$	$f_{nk}(\Omega)$
C	-0.1105	0.0000	0.0000	-0.1652	0.1652	0.0250
O	-0.0255	0.0000	0.0000	-0.2867	0.2867	0.0434
H	0.0678	0.0000	-0.1834	-0.0952	0.2067	0.0144
H	0.0678	0.0000	0.1834	-0.0952	0.2067	0.0144
Tot	-0.0004	0.0000	0.0000	-0.6423		0.0973

Again, the atomic contributions to the transition dipole all point in the same direction, resulting in all positive contributions to the oscillator strength. This is expected, given that the dipole lies in the same direction as the carbonyl bond in this case. The carbonyl group contributes 70% to the oscillator strength, but in this case the contribution from the carbon is slightly higher, 25% for this state as opposed to only 18% for the n → $3p_z$ transition. Figure 65 shows that though the interaction between the carbon and oxygen is not as strong as the n → $3p_z$ transition (though considerably better than the n → 3s transition), the symmetry of the excitation 'forces' the atomic dipoles to point in the same direction. The relative size of the overall transition dipole can be explained by the symmetry as well. With the previous two transitions, the 'n' electron was excited to Rydberg-like orbitals, the 3s orbital having the lowest energy. The two 3p orbitals have different energies because of their symmetry relative to the molecule. The $3p_z$ orbital lies along the carbonyl bond, placing the oxygen in its vicinity. This lowers the orbital's energy, as the electron

is more inclined to enter an orbital containing a strong electron 'attractor'. The $3p_y$ orbital only has the hydrogens to act as attractors; while slightly negatively charged, they are not as effective as oxygen in attracting the excited electron, and the orbital is thus higher in energy. Figure 65 shows the diffuse nature of the $3p_y$ orbitals, which place diffuse density on the hydrogens.

Figure 65: Contour Map of $n \rightarrow 3p_y$ Transition Density of Formaldehyde

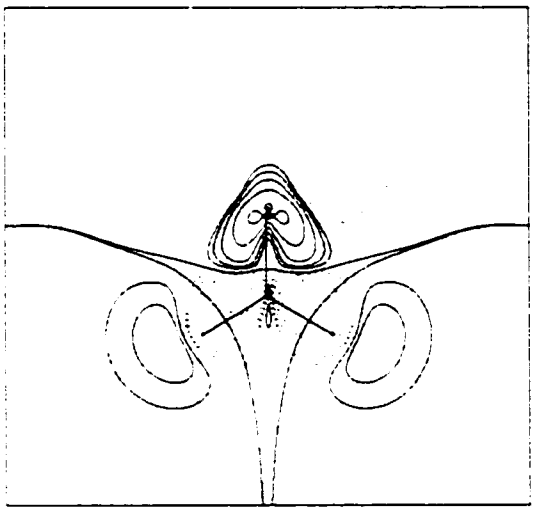

6.1.2 Ammonia

Ammonia is another molecule whose excited states have been thoroughly studied, and which provided a nice contrast to formaldehyde.

Table 92: Properties of Ground State Ammonia

NH3	
E	-56.2185707401
V/T	2.02005218
Error in E	0.0000
N – H	0.9995
H – N – H angle	108.0432
Dihedral	116.6620
N-H	
ρ_b	0.3595
$L(r)_b$	-1.8781

The electronic configuration of ammonia is $1a_1^2\ 2a_1^2\ 1e^4\ 3a_1^2$; the lowest energy excitations of ammonia also result from promotion of a non-bonded electron, this time from the $3a_1$ orbital on nitrogen[162]. The first

three excitations studied correspond to $n \rightarrow 4a_1$ (3s), giving the A^1A_1 state, $n \rightarrow 2e$ ($3p_x/3p_y$), giving the A^1E state, and $n \rightarrow 5a_1$ ($3p_z$), giving the B^1A_1 state. The excitations studied are summarized in Table 93.

Table 93: Excited States of Ammonia, as Calculated by Gaussian94

	Energy (eV)		Transition Dipole			Osc. Strength
	Calc.	Exp.	x	y	z	
A^1A_1	7.3782	6.392	0.0000	0.0000	0.6864	0.0852
A^1E	8.8828	7.915	0.0000	0.1412	0.0000	0.0043
A^1E	8.8828	7.915	0.1412	0.0000	0.0000	0.0043
B^1A_1	10.7771	8.269	0.0000	0.0000	0.0404	0.0004

The excited state bond properties of ammonia demonstrate the nature of the excitations taking place, as Table 94 shows.

Table 94: Ground and Excited State Bond Data for Ammonia

	r	$r_b(N)$	% $r_b(N)$	ρ_b	$L(r)_b$
X^1A_1					
N-H	1.8889	1.3836	73.25	0.3595	0.4695
$n \rightarrow 3s$					
N-H	1.8889	1.4916	78.96	0.3586	0.6392
$n \rightarrow 3p_x$					
N-H(x)	1.8889	1.5203	80.48	0.3560	0.6724
N-H(y)	1.8889	1.4810	78.40	0.3616	0.6371
$n \rightarrow 3p_z$					
N-H	1.8889	1.4676	77.69	0.3595	0.6135

As ammonia is not a double-bonded system, bond ellipticities are not as useful as they were for formaldehyde, as there are no double bonds present. L(r) of the N-H bond of ammonia is large and positive, indicating a high degree of covalent character; which increases upon excitation.

Table 95: Atomic Properties and their Change Upon Excitation for Ammonia

X^1A_1	$N(\Omega)$	$Q_{xx}(\Omega)$	$Q_{yy}(\Omega)$	$Q_{zz}(\Omega)$	$v(\Omega)$
N	8.048	1.400	1.400	-2.800	137.67
H	0.651				32.11
$n \rightarrow 3s$	$\Delta N(\Omega)$	$\Delta Q_{xx}(\Omega)$	$\Delta Q_{yy}(\Omega)$	$\Delta Q_{zz}(\Omega)$	$\Delta v(\Omega)$
N	0.091	-0.570	-0.570	1.136	52.66
H	-0.031				25.33
$n \rightarrow 3p_x$	$\Delta N(\Omega)$	$\Delta Q_{xx}(\Omega)$	$\Delta Q_{yy}(\Omega)$	$\Delta Q_{zz}(\Omega)$	$\Delta v(\Omega)$
N	-0.118	-5.692	1.719	3.973	11.90
H (y)	-0.071				8.18
H (x)	0.264				125.07
$n \rightarrow 3p_z$	$\Delta N(\Omega)$	$\Delta Q_{xx}(\Omega)$	$\Delta Q_{yy}(\Omega)$	$\Delta Q_{zz}(\Omega)$	$\Delta v(\Omega)$
N	0.485	7.464	7.464	-14.928	237.51
H	-0.164				-2.89

The excited state integration data, shown in Table 95, shows considerable changes in populations for each excited state, unlike formaldehyde, where population changes remained similar despite the different orbitals that electrons were excited to. The main axis of ammonia is along the z-axis, with one hydrogen in the xz plane. Figure 66 shows graphically the changes in density resulting from these excitations. Like formaldehyde, the diffuse density of the excited states is clearly visible.

Figure 66: Contour Plots of Electron Density of States of Ammonia

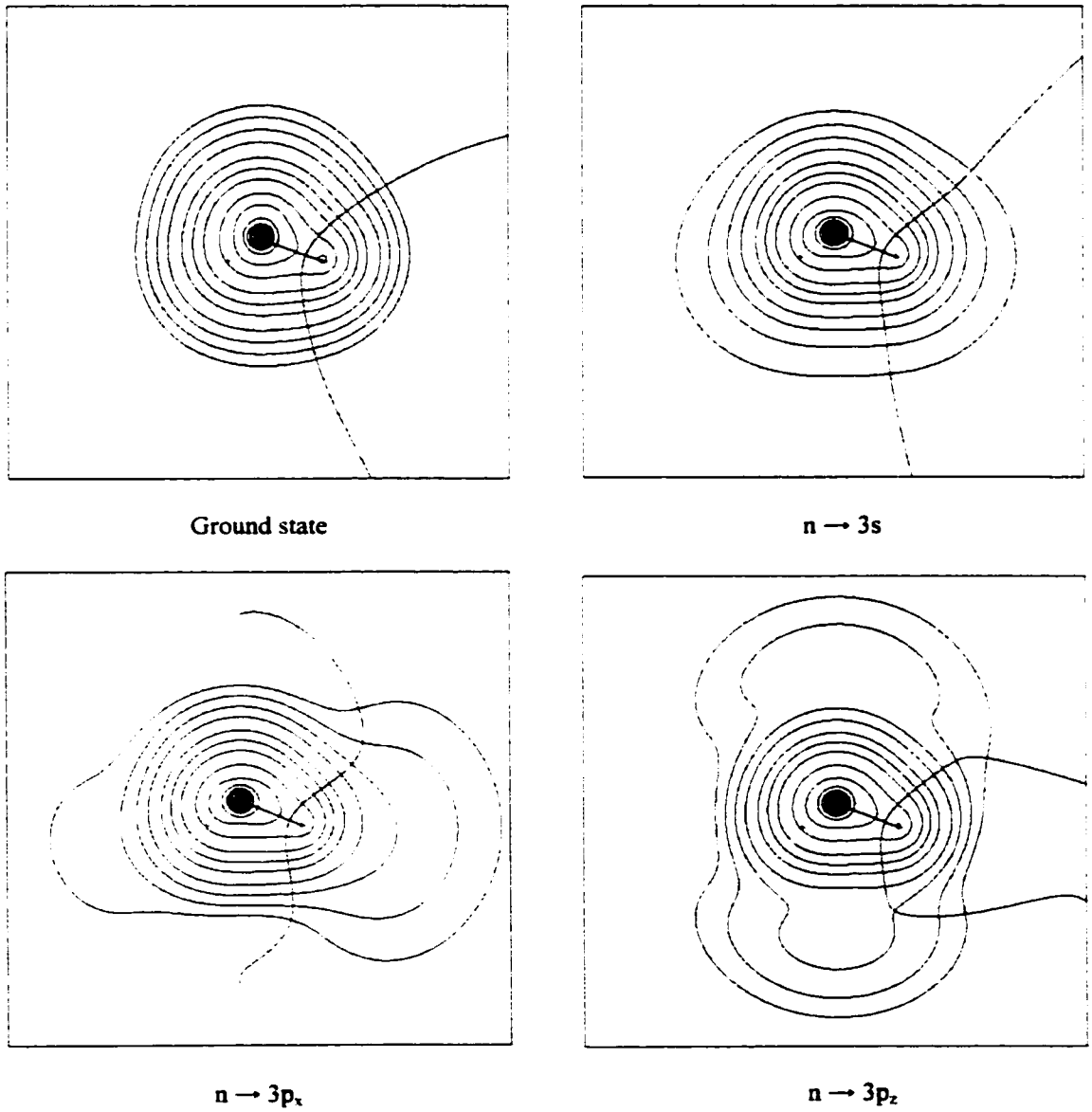

Unlike the L(r) plots of formaldehyde, the diffuse density of the excitation is visible in L(r) of the excited states of ammonia. Figure 67 shows clearly the diffuse density of the excited states as small concentrations at the outer regions of the molecule, as well as the loss of charge concentration in the region of the lone pair on nitrogen.

Figure 67: Contour Plots of L(r) of States of Ammonia

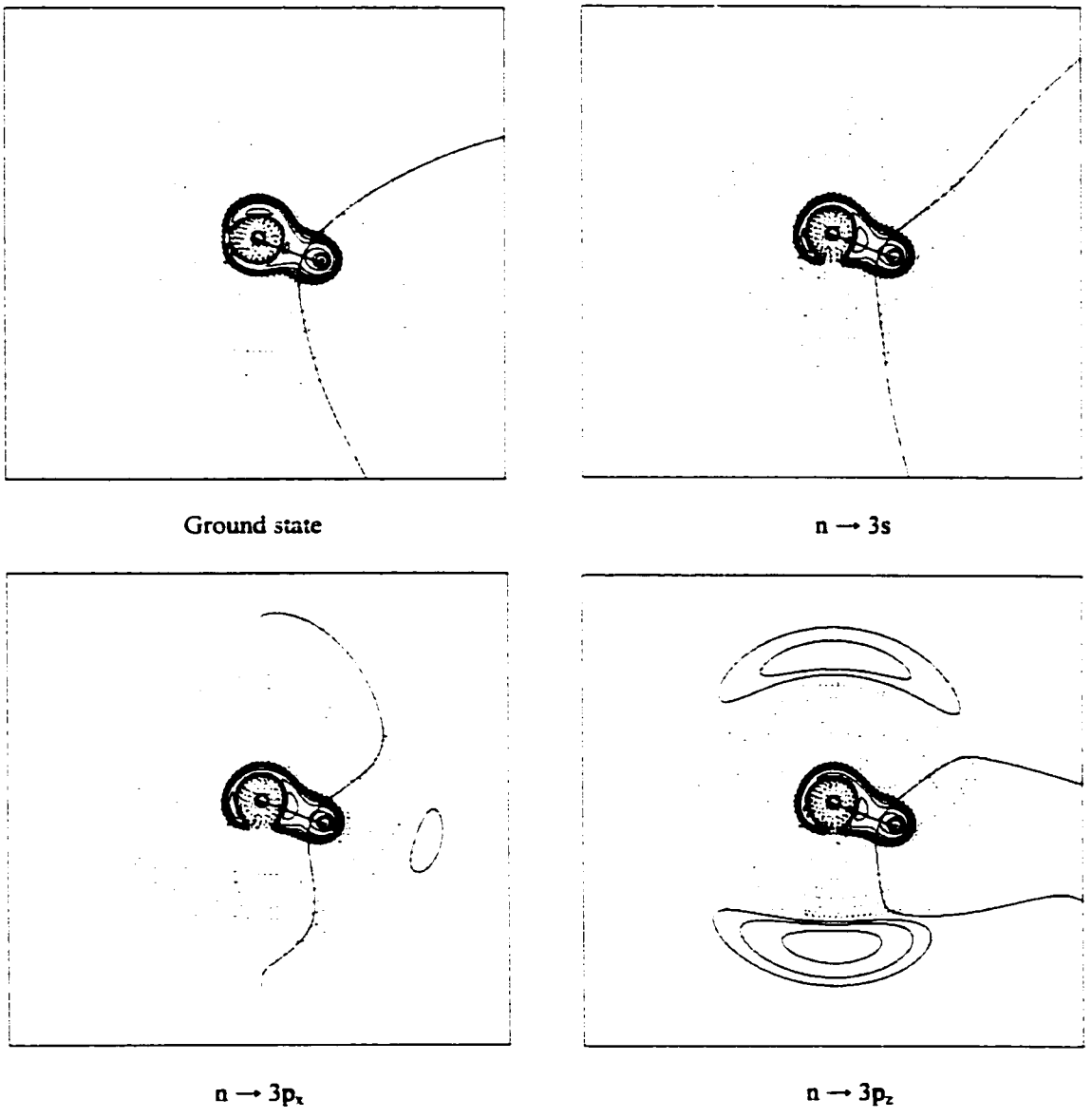

6.1.2.1 Ammonia A^1A_1

The strongest excitation is the first, n → 3s, with a transition dipole of 0.6864 au and oscillator strength of 0.0852 au. With all the excited states, one observes a shift in the N-H BCP towards the hydrogen, and an increase in the value of L(r), indicating increased covalency in the bond. This can be interpreted as a net transfer of density from the lone pair to the N-H bonding regions of the molecule: for n → 3s, the entire molecule would be thus affected. Table 95 shows that there is a small net transfer of 0.10 au from the hydrogens to the nitrogen, which explains the shift in the BCP position closer to the hydrogens. The quadrupole moment of nitrogen shows that the polarization of the density is still along the z-axis and thus the lone pair, but is not as pronounced. This indicates a 'smoothing out' of the electron density expected for an n → 3s transition. The n → 3s contour plots of Figure 66 and Figure 67 show this smoothing out of the density. The rho plot shows the density being flattened out towards the hydrogen basins, and the L(r) plot shows loss of density from the lone pair charge concentration maximum. The transfer of charge should thus be considered inconsequential, and the changes in electron density be that of movement of density towards the hydrogen regions. From Table 96, one can see that the majority of the excitation is centered on the nitrogen, which contributes 67% of the molecular oscillator strength. Also notable is the direction of the transition dipoles on hydrogen, which point along each N-H bond.

Table 96: Atomic Contributions to n → 3s Transition Probability in Ammonia (au)

n → 3s	$q_{nk}(\Omega)$	$\mu_{nk}(\Omega)$ x	$\mu_{nk}(\Omega)$ y	$\mu_{nk}(\Omega)$ z	$\lvert\mu_{nk}\rvert(\Omega)$	$f_{nk}(\Omega)$
N	0.1028	0.0000	0.0000	0.4560	0.4560	0.0564
H(x)	-0.0343	-0.0451	0.0000	0.0761	0.0885	0.0094
H	-0.0343	0.0225	-0.0390	0.0761	0.0885	0.0094
H	-0.0343	0.0225	0.0390	0.0761	0.0885	0.0094
Tot	-0.0001	0.0000	0.0000	0.6844		0.0847

The contour map of this transition (Figure 68) further illustrates how the majority of the transition is centered on the nitrogen atom.

Figure 68: Contour Map of n → 3s Transition Density of Ammonia

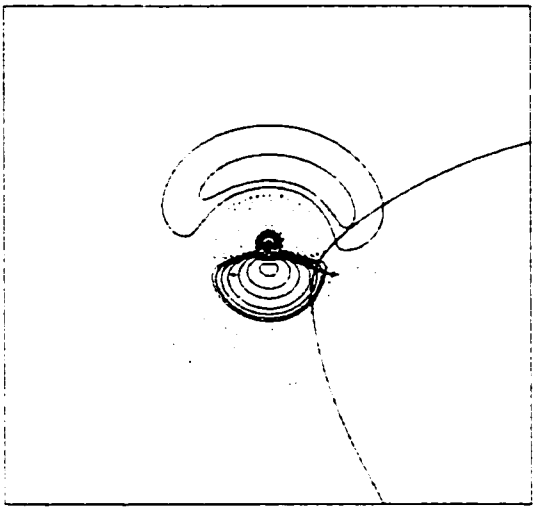

As has been observed in the formaldehyde states, there are three countering polarizations, in this case pointing along the main axis of the molecule. The core polarization is countered by a polarization in the valence region, which is in turn countered by another polarization in the third quantum shell, which is appropriately diffuse.

6.1.2.2 Ammonia A^1E_x

The next transition consists of two degenerate excitations, corresponding to transfer of density to the $3p_x$ and $3p_y$ orbitals. For this work, only the n → $3p_x$ transition will be studied in detail. The bond properties of this excited state are mostly in the N-H bond that lies along the x-axis, which would be the one that gains the most from the $3p_x$ density. It shows a higher increase in L(r) than the two other equivalent N-H bonds, indicating a marked increase in the amount of density in that region. The integration data of Table 95 confirms this, as there is a net transfer of 0.25 au of density to this hydrogen from the rest of the molecule. The quadrupole moment shows a shift from a polarization along the z-axis to along the x-axis, and the volume of this hydrogen increases by a factor of five. This volume change is clear in the n → $3p_x$ contour plot in Figure 66 and Figure 67. One can see a small charge concentration in the L(r) plot in the non-bonding region of this hydrogen.

Table 97: Atomic Contributions to n → $3p_x$ Transition Probability in Ammonia (au)

n → $3p_x$	$q_{nk}(\Omega)$	$\mu_{nk}(\Omega)$ x	$\mu_{nk}(\Omega)$ y	$\mu_{nk}(\Omega)$ z	$\lvert\mu_{nk}\rvert(\Omega)$	$f_{nk}(\Omega)$
N	0.0000	-0.0294	0.0000	0.0000	0.0294	0.0009
H(x)	-0.0388	-0.0624	0.0000	0.0902	0.1096	0.0019
H	0.0194	-0.0254	0.0214	-0.0451	0.0560	0.0008
H	0.0194	-0.0254	-0.0214	-0.0451	0.0560	0.0008
Tot	0.0000	-0.1425	0.0000	0.000000		0.0044

The largest contribution to the oscillator strength comes from the hydrogen on the x-axis, providing 43% of the oscillator strength. While all the atomic transition dipoles point in the same direction, the overall intensity of this transition is smaller than the n → 3s transition by a factor of 20. This can be explained by the fact that the spatial extent of the transition density for excitation into $3p_x$ is greatly reduced, resulting in small induced atomic dipoles. Figure 69 shows how the planar hydrogen makes a large contribution to the transition, while the nitrogen suffers partial internal neutralization of its dipole along the molecular axis. The majority of nitrogens' dipole comes in fact from the interaction between nitrogen and the planar hydrogen.

Figure 69: Contour Map of n → $3p_x$ Transition Density of Ammonia

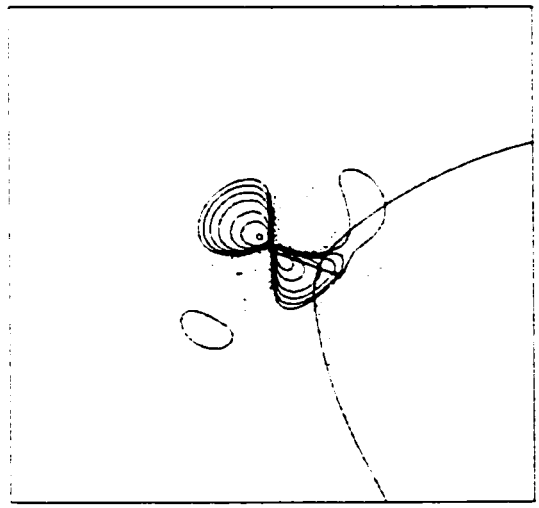

6.1.2.3 Ammonia B^1A_1

The third excitation is $^1A_1$ like the first excitation, only considerably weaker, by a factor of 200. The increase in L(r) of the N-H BCP is the smallest of all the excitations, as is the shift in the BCP position. Integration data shows a much larger net transfer of charge from the hydrogens to the nitrogen than the n →

3s transition. The quadrupole moment shows an increase in polarization along the z-axis by a factor of over five, and a near tripling of hydrogens' volume. The fact that this density resides in a $3p_z$ orbital becomes clear when looking at the rho and L(r) maps for this excitation: as with the $n \rightarrow 3p_x$ transition, one can see charge concentrations corresponding to the $3p_z$ density. Table 98 shows why this excitation is so weak.

Table 98: Atomic Contributions to $n \rightarrow 3p_z$ Transition Probability in Ammonia (au)

$n \rightarrow 3p_z$	$q_{nk}(\Omega)$	$\mu_{nk}(\Omega)$ x	$\mu_{nk}(\Omega)$ y	$\mu_{nk}(\Omega)$ z	$\lvert\mu_{nk}\rvert(\Omega)$	$f_{nk}(\Omega)$
N	0.0711	0.0000	0.0000	0.1347	0.1347	0.0014
H(x)	-0.0238	-0.0286	0.0000	-0.0318	0.0428	-0.0003
H	-0.0238	0.0143	-0.0247	-0.0318	0.0428	-0.0003
H	-0.0238	0.0143	0.0247	-0.0318	0.0428	-0.0003
Tot	-0.0003	0.0000	0.0000	0.0392		0.0004

For this excitation, the transition dipole of the nitrogen opposes that of the hydrogens. While the hydrogen oscillator strengths do not completely counteract the nitrogen, the overall effect dramatically reduces the transition probability for the molecule. Figure 70 shows that despite the presence of the hydrogens, the overall transition density has an overall symmetry plane perpendicular to the molecular axis. If not for the hydrogens, this excitation would have a oscillator strength of nearly zero.

Figure 70: Contour Map of $n \rightarrow 3p_z$ Transition Density of Ammonia

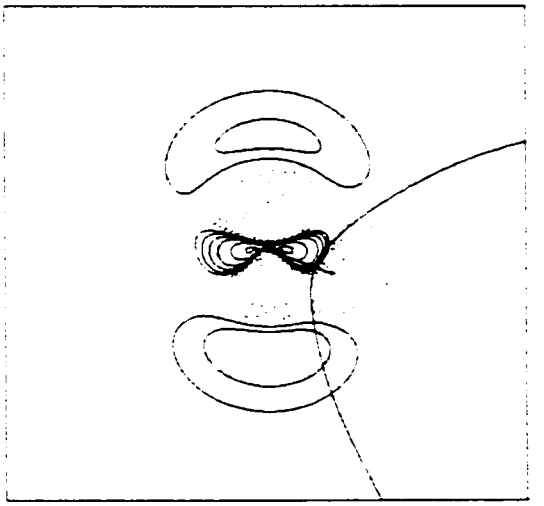

6.1.3 Discussion: Chromophoric Behavior

A great deal of information was obtained from these species that shed light on one type of electronic excitation. It has been known for a long time that functional groups exhibit particular properties nearly

independent of their chemical environment, which is the foundation on which analytical chemistry has developed. UV spectroscopy is a commonly used tool to analyze unknown species: the observation of telltale excitations allows one to confirm or discover the presence of said functional groups within the sample. This work has shown that these functional groups do indeed possess characteristic properties, not only for the commonly studied ground state, but also properties associated with electronic excitation. The carbonyl group is a good example of this. In most of the cases studied above, the majority of the excitation was localized to the carbonyl group, about 70% of the total excitation. The exception to this was the n → 3s transition, where the carbonyl group made almost no contribution at all. In all cases, the excitation intensity is directly dependent on the carbonyl group, which either contributes most or nearly none of the excitation intensity. The same argument holds true for ammonia, where it is the nitrogen that is the 'functional group' of the molecule. In ammonia, there are two types of excitations: strong transitions, where the nitrogen contributes most of the intensity, or weak transitions, where the nitrogen does not contribute the majority of the intensity. This work shows that the basic tenets of Atoms in Molecules apply to any property that one cares to study, including the transition dipole.

6.2 Oligosilane Studies

A question that has already been asked in this thesis is the following: why is it that oligosilanes and hydrocarbons have such very different excitation properties, even though they are both saturated molecules? Calculation of the excited states of hydrocarbons show that their excitations are very weak, and the energy of excitation changes very little with chain length. Oligosilanes, on the other hand, undergo much more intense transitions, and the energy of excitation decreases dramatically with chain length[163,164].

Table 99: Strongest Intensity Excitations of Selected Hydrocarbons and Oligosilanes

Molecule	Energy (eV)	Transition Dipole			Osc. Strength
		x	y	z	
C_2H_6	9.6938	0.0000	0.0000	-0.5361	0.0682
C_7H_{16}	9.3576	-0.1824	0.0000	0.0000	0.0076
Si_2H_6	8.5207	0.0000	0.0000	2.0258	0.8567
Si_7H_{16}	6.2621	-3.8024	0.0000	0.0000	2.2178

Table 99 shows examples of the most intense transitions for ethane and heptane, and their corresponding oligosilanes, as calculated by Gaussian94 using the CI-Singles method. There are some common features to

both sets of molecules. Both have their transition dipoles pointing in the same direction. The ethane/disilane transition dipole points along the main axis of the molecule, and the heptane/silaheptane transition dipole points along the backbone. All similarities end here. The difference in excitation energy between each pair is quite remarkable. The difference in excitation energy for the silicon species is six times greater than that of the hydrocarbons. Also, the silicon transition dipoles are much larger, and the oscillator strengths are at least a factor of twelve times larger, increasing to a factor of nearly 300 for heptane/silaheptane. It is interesting to note that the excitation intensity actually decreases with chain length for the hydrocarbons, the opposite of what is observed for the oligosilanes.

Figure 71: Excitation Energies of Selected Hydrocarbons and Oligosilanes

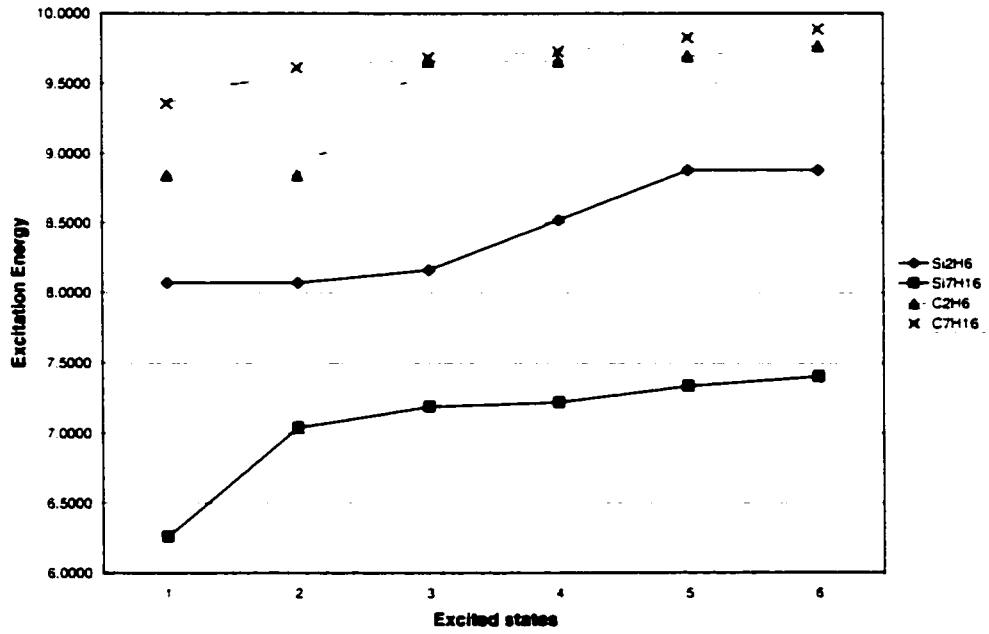

Figure 71 shows the first six excitation energies for these four molecules. What is important to note about the hydrocarbon excitations is that if one ignores the two lowest excitations of ethane, there is almost no difference in excitation energy as one proceeds from ethane to heptane. Clearly the bathochromic shift observed in polysilanes is a potent electronic phenomenon, easily reproduced by computation. Why this occurs has been the basis for a great deal of research, and has resulted in many empirical models. It is

hoped that by studying the transition density of oligosilanes, a clear picture of the mechanism of this process, based on quantum mechanics, will emerge.

Experimental studies of the electronic properties of polysilanes revealed an interesting phenomenon. It was found that, when large bulky ligands were placed on a polysilane of a given chain length, the excitation energy of that polysilane was lower than that of an equivalent polysilane bearing smaller ligands. This brought about the idea of conformational dependence in polysilane excitation. The accepted model for this is that each Si-Si bond twist disrupts the conjugation within the molecule; twisting the central Si-Si bond in a long-chain polysilane would result in an excitation energy equivalent to a molecule of half the length. Given the low torsion energy in the Si-Si bond, this results in experimental electronic excitations that are much higher than models such as Sandorfy predict. This led to the development of the Ladder model, which incorporates an additional resonance term whose value is dependent on the conformation of the backbone. However, rather than having to apply corrections to a model each time an instance occurs where the model does not work, one can use quantum mechanics to obtain the results directly.

The first set of calculations seek to study the connection between electronic excitation and chain length, and how the transition probability of each molecule partitions into its atomic contributions. If the transition probability is delocalized throughout the molecule, then the excitation is as well. The series Si_nH_{2n+2}, where n = 2 – 7, were geometrically optimized in the ground state, after which a CI-Singles single-point calculation was performed to obtain the excitation energies and transition dipoles of the first six excited states, as outlined in the computational and theoretical sections. Those states that best represent the UV absorption spectra of the molecule were kept, and used to obtain both the excited state density and the data required for the transition state density. Atoms in Molecules was then used to provide atomic integrations of the ground state, excited state and transition densities, yielding atomic contributions to the transition dipole, the oscillator strength, and the number of electrons in the excited state atoms. The second set of calculations study an important feature of polysilane excitation: the dependence of excitation energy on backbone conformation. To study this, a series of Si_6H_{14} molecules were optimized, with the central Si-Si dihedral angle fixed at different values. The angle was changed by 30° for each molecule, from 0° to 180°. A CI-Singles calculation was performed on each conformer, to obtain data on the first six excited

states. The appropriate excited state density, along with the corresponding transition density, was partitioned with respect to atomic contributions.

6.2.1 Chain Length Study

What becomes apparent in this series of calculations is that there is a substantial decrease in excitation energy as a function of chain length, along with a strong increase in oscillator strength. Figure 72 shows the excitation energies of the first six excited states for each oligosilane. Figure 73 indicates the energy of the most intense excitation of each molecule.

Figure 72: Excitation Energies of Si_nH_{2n+2}, n = 2 - 7

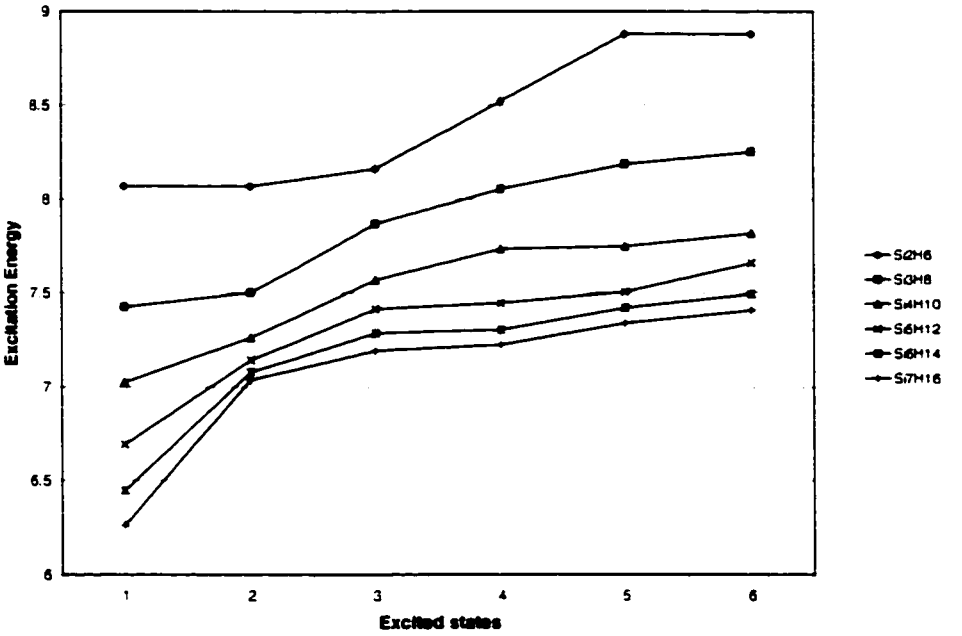

Figure 73: Excitation Energies of Most Intense Transitions of Si_nH_{2n+2}, n = 2-7

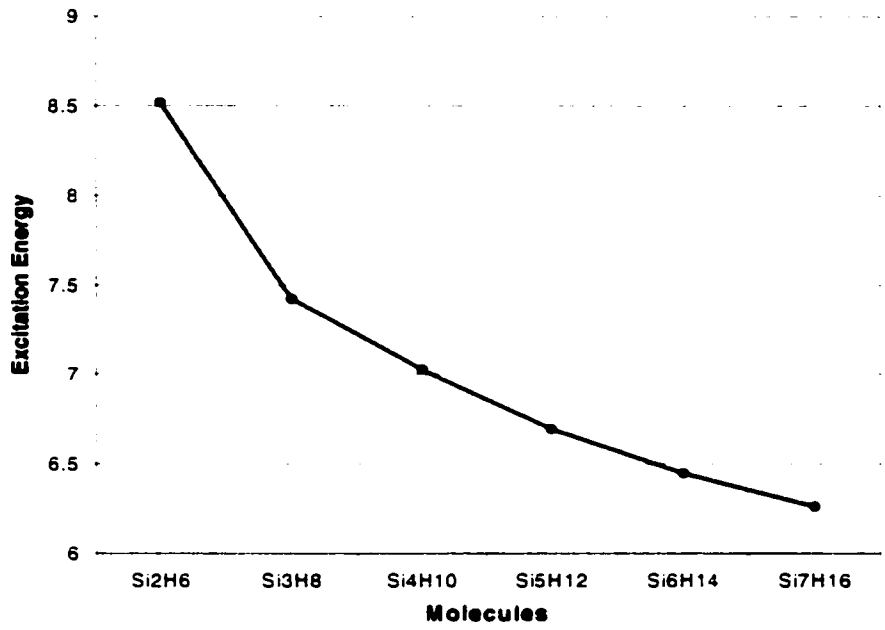

Of this series, only disilane and trisilane have any complexity to their excitation spectra. Disilane's lowest energy excitation is a doubly degenerate E state of low intensity, followed by an intense transition into an A_2 state (see Table 100); this is the state studied, having the highest oscillator strength, thus being the dominant excitation in a UV spectrum.

Table 100: Excitation Data for Si_2H_6

Excited State	Energy (eV)	Transition dipole			Osc. Strength
1: 1^1E_y	8.0702	0.0001	-0.4792	0.0000	0.0454
2: 1^1E_x	8.0702	0.4792	0.0001	0.0000	0.0454
3: 1^1A_1	8.1627	0.0000	0.0000	0.0000	0.0000
4: 1^1A_2	**8.5207**	**0.0000**	**0.0000**	**2.0258**	**0.8567**
5: 2^1E_x	8.8789	0.0000	0.0000	0.0000	0.0000
6: 2^1E_y	8.8789	0.0000	0.0000	0.0000	0.0000

Trisilane has two transitions of similar intensity. While the higher energy B_2 state is more intense, the first B_2 state was chosen for study, based on its transition density contour map; this will be discussed in more detail later in this section.

Table 101: Excitation Data for Si_3H_8

Excited State	Energy (eV)	Transition dipole			Osc. Strength
1: 1^1B_2	**7.4240**	**0.0000**	**-1.2452**	**0.0000**	**0.2820**
2: 1^1A_2	7.5028	0.0000	0.0000	0.0000	0.0000
3: 1^1B_2	7.8697	0.0000	0.6176	0.0000	0.0736
4: 1^1A_1	8.0547	0.0000	0.0000	0.7624	0.1147
5: 1^1B_2	8.1882	0.0000	-1.6690	0.0000	0.5588
6: 1^1B_1	8.2538	-0.4436	0.0000	0.0000	0.0398

The remaining oligosilanes, by contrast, have far simpler spectra; the first excited state has a very large intensity, at least 100 times stronger than any other transition for a given species. Molecules with an odd number of silicons are excited to a B_2 state, while those with even numbered silicons are excited to a B_u state.

Table 102: Excitation Data for Si_4H_{10} to Si_7H_{16}

State	Energy (eV)	Transition dipole			Osc. Strength
Si_4H_{10}: 1^1B_u	7.0248	2.2054	0.0000	0.0000	0.8371
Si_5H_{12}: 1^1B_2	6.6937	-2.8317	0.0000	0.0000	1.3149
Si_6H_{14}: 1^1B_u	6.4470	-3.3514	0.0000	0.0000	1.7739
Si_7H_{16}: 1^1B_2	6.262	-3.8024	0.0000	0.0000	2.2178

The intensity of the transition was not the only criterion for choosing which excited state to study, though most of the rejected excitations were so weak as to have oscillator strengths near zero. The other important criterion was the common direction of the dipole moment for each molecule; in each case, the dominant intensity excitation has a transition dipole moment that runs along the backbone of the molecule. The transition density, which will be discussed later, also revealed a common factor for each molecule. The transition density of each dominant excitation had a similar pattern to their contour plot, which is why the first B_2 state of trisilane was chosen over the higher energy B_2 state.

6.2.1.1 Transition Dipoles

One striking feature of this series of molecules is how the oscillator strength is related to the chain length, as shown in Figure 74.

Figure 74: Oscillator Strength vs Chain Length for Si_nH_{2n-2}

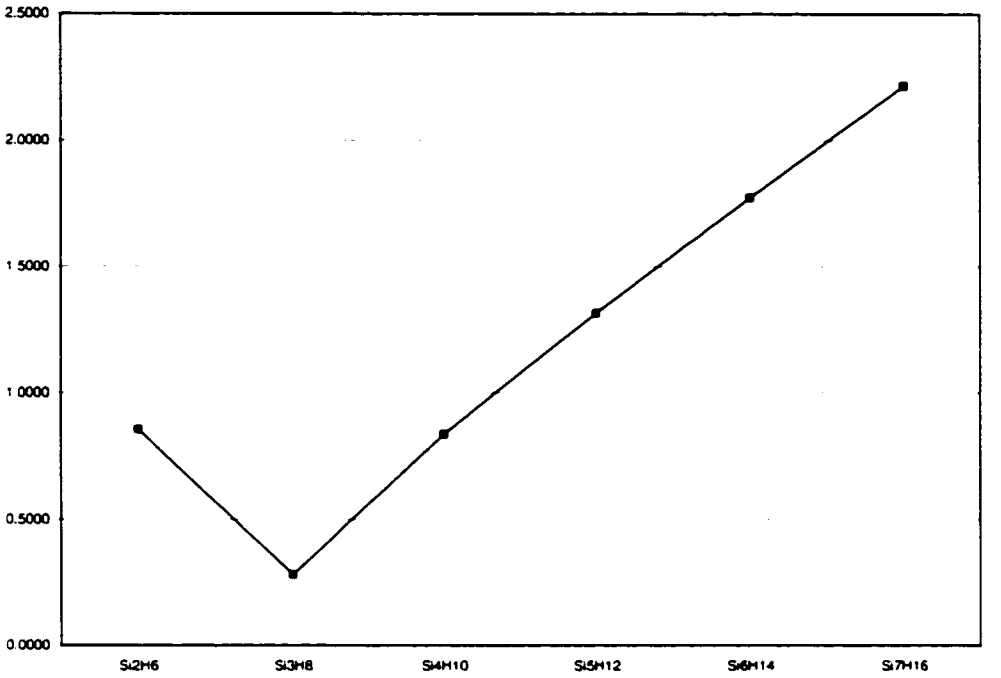

With the exception of disilane, which undergoes an excitation of a different symmetry to the others, there is a near perfect linear relationship between oscillator strength and oligosilane chain length. This would indicate, as seen with the work done in the electron density section of this thesis, that the oscillator strength of oligosilanes follows an additivity scheme, as does the number density and pair density properties. This in itself is an important discovery, as it provides a strong link to σ-conjugation within oligosilanes. As the oscillator strength increases linearly with chain length, one must conclude that each silylene unit in the oligosilane contributes an equal amount to the excitation intensity, something that could only occur if the excitation intensity were delocalized throughout the entire molecule.

Table 103: Group Contributions to Transition Probability in Si_nH_{2n+2} (au)

Molecule	$q_{nk}(\Omega)$	$\mu_{nk}(\Omega)$ x	$\mu_{nk}(\Omega)$ y	$\mu_{nk}(\Omega)$ z	$\lvert\mu_{nk}\rvert(\Omega)$	$f_{nk}(\Omega)$
Si_2H_6						
$Si1H_3$	0.0000	0.0000	0.0000	-1.0136	1.0136	0.4289
$Si2H_3$	0.0000	0.0000	0.0000	-1.0136	1.0136	0.4289
Total	0.0000	0.0000	0.0000	-2.0272	2.0272	0.8578
Si_3H_8						
$Si1H_3$	0.0905	0.0000	-0.4149	0.0099	0.4165	0.0939
$Si2H_2$	0.0106	0.0000	-0.4157	-0.0315	0.4168	0.0944
$Si3H_3$	0.0847	0.0000	-0.4149	0.0099	0.4165	0.0939
Total	0.0048	0.0000	-1.2455	-0.0116	1.2456	0.2823
Si_4H_{10}						
$Si1H_3$	-0.1447	0.5067	-0.0032	0.0000	0.5067	0.1925
$Si2H_2$	-0.0209	0.5973	0.0946	-0.0000	0.6048	0.2291
$Si3H_2$	0.0232	0.5973	0.0946	-0.0000	0.6048	0.2291
$Si4H_3$	0.1501	0.5067	-0.0032	0.0000	0.5067	0.1925
Total	0.0077	2.2080	0.1827	-0.0000	2.2156	0.8431
Si_5H_{12}						
$Si1H_3$	0.1523	0.3418	0.0000	-0.0240	0.3570	0.1584
$Si2H_2$	0.0170	0.6114	0.0000	-0.0040	0.6821	0.3133
$Si3H_2$	0.0404	0.7763	0.0000	-0.0807	0.7805	0.3602
$Si4H_2$	-0.0835	0.6114	0.0000	-0.0040	0.6821	0.3133
$Si5H_3$	-0.1416	0.3418	0.0000	-0.0240	0.3570	0.1584
Total	-0.0054	2.8165	0.0000	-0.1367	2.8198	1.3037
Si_6H_{14}						
$Si1H_3$	0.1143	0.3983	0.0440	0.0000	0.4007	0.2091
$Si2H_2$	0.0521	0.5611	-0.0898	0.0000	0.5682	0.2975
$Si3H_2$	0.0260	0.7096	-0.0140	0.0000	0.7098	0.3743
$Si4H_2$	-0.0272	0.7096	-0.0140	0.0000	0.7098	0.3743
$Si5H_2$	-0.0573	0.5611	-0.0898	0.0000	0.5682	0.2975
$Si6H_3$	-0.1158	0.3983	0.0440	0.0000	0.4007	0.2091
Total	-0.0080	3.3379	-0.1197	0.0000	3.3400	1.7618
Si_7H_{16}						
$Si1H_3$	-0.1227	0.3834	0.0000	-0.0167	0.3921	0.2214
$Si2H_2$	-0.0200	0.4879	0.0000	-0.0159	0.4895	0.2817
$Si3H_2$	-0.0561	0.6431	0.0000	0.0033	0.643`	0.3708
$Si4H_2$	0.0243	0.7480	0.0000	-0.0569	0.7502	0.4325
$Si5H_2$	0.0603	0.6431	0.0000	0.0033	0.643`	0.3708
$Si6H_2$	0.0153	0.4879	0.0000	-0.0159	0.4895	0.2817
$Si7H_3$	0.0984	0.3834	0.0000	-0.0166	0.3921	0.2214
Total	-0.0003	3.7766	0.0000	-0.1153	3.7784	2.1802

Partitioning these transition dipoles into their group contributions revealed some fascinating properties of these systems. Table 103 summarizes the data by silyl and silylene group. It should be noted that $q_{nk}(\Omega)$ is the integrated transition charge as calculated directly from the integration procedure. This value should integrate to zero, as it represents the mixing of two orthogonal orbitals, φ_a and φ_r, (see Section 3.3): non-

zero values are the result of integration error. $\mu_{nk}(\Omega)$ and $f_{nk}(\Omega)$, however, are averaged between equivalent silyl and silylene groups in a given molecule. This reflects the fact that the electric field produced by the incoming radiation oscillates along the backbone of the molecule, resulting in an overall symmetrizing of the transition dipole moment. Figure 75 shows how the atomic percentage contributions to the total oscillator strength of each molecule are not only symmetric, the result of the averaging, but also take on a bell-like distribution as the chain length increases. This shows that the transition density is delocalized throughout the entire molecule: if there were a localized chromophore in the system, its percentage contribution would remain constant, as would the contributions of non-chromophoric regions.

Figure 75: Average Percentage Contribution of Silyl and Silylene Groups to Oscillator Strength

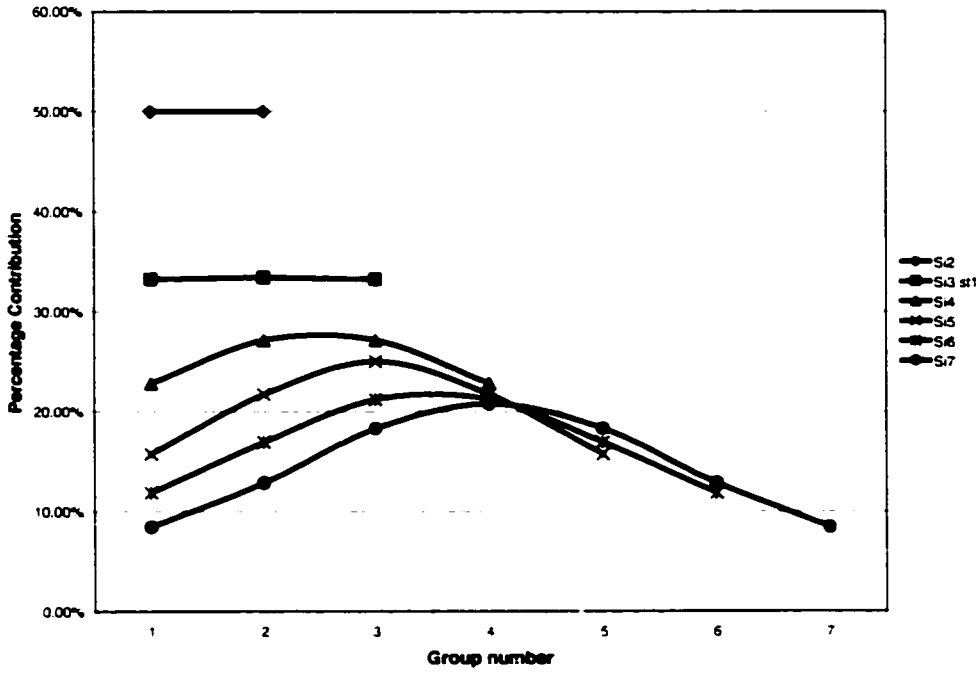

Figure 76 shows the unaveraged percentage contribution of each group to the oscillator strength. These values are more in keeping with a molecule whose electron density is perturbed by a static electric field, with oscillator strength losing intensity along the backbone as a function of distance from the electric field source.

Figure 76: Unaveraged Percentage Contributions of Silyl and Silylene Groups to Oscillator Strength of Heptasilane

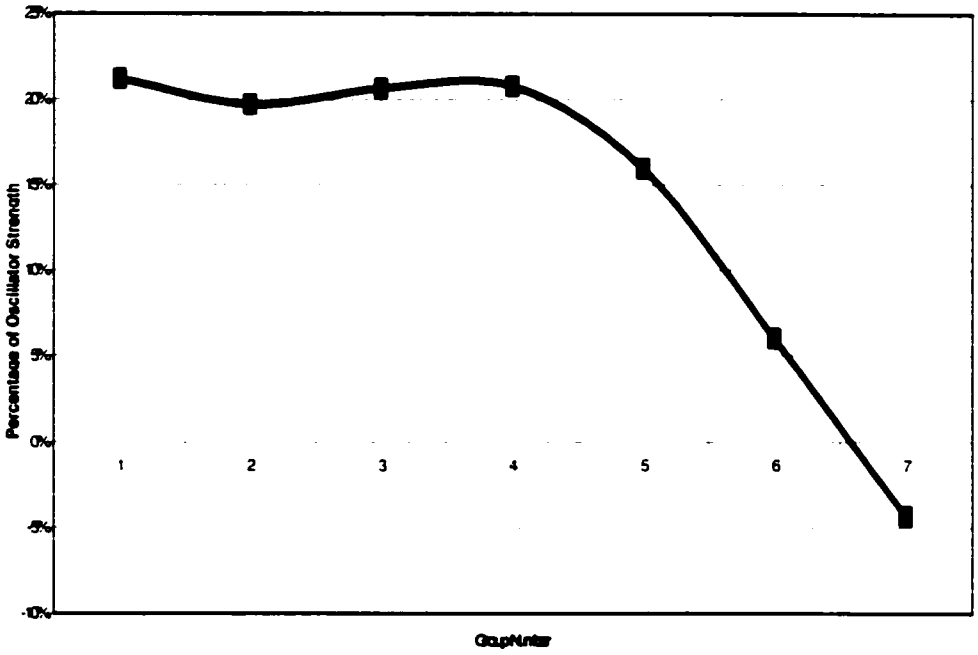

Another important feature of this data is the fact that both the transition dipoles and oscillator strengths do not change appreciably within a group type, despite changes in chain length: Figure 77 and Figure 78 illustrate this phenomenon.

Figure 77: Group Oscillator Strength Changes with Chain Length

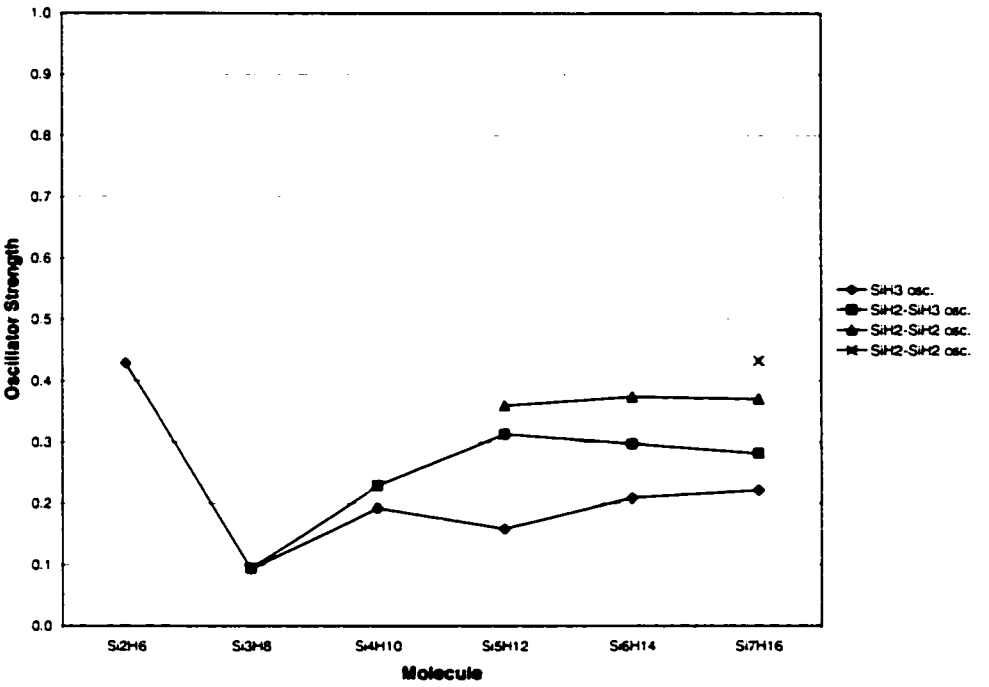

As Figure 77 shows, from trisilane on, the oscillator strength of each silyl and silylene group increases with chain length, then plateaus somewhat at about pentasilane, forming a type of additivity scheme for transition intensity. Such a pattern establishes two points. First, it provides a simple model for the bathochromic behavior observed in polysilanes: each group within the molecule adds a set amount to the overall transition intensity, such that the intensity increases as the molecular chain lengthens. The second and more intriguing result is that this model provides the means of easily predicting the transition intensity of any oligosilane. A silyl group adds approximately 0.2 au to the intensity, an α-silylene group about 0.3 au, and an internal silylene group, about 0.4 au. Note that this model is only valid for a molecule containing at least five groups, as the group values are considerably lower in short chains. This can be explained by the fact that, as seen in the additivity of other properties, a 'standard' group would not be observed until pentasilane, where each group type exists in a more or less constant environment.

Unlike oscillator strengths, transition dipole moments are more sensitive to changes in chain length, as Figure 78 shows.

Figure 78: Group Dipole Moment Magnitude Changes with Chain Length

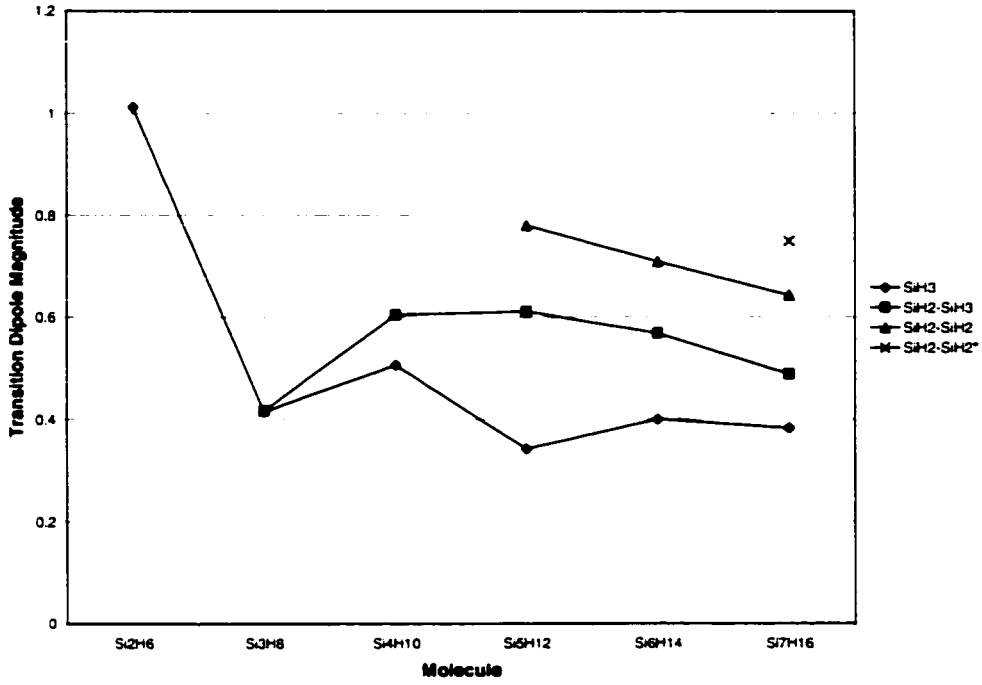

While the magnitude of the transition dipoles do not show as steady a pattern, they do reach something of a 'standard' value themselves. Since oscillator strengths are derived from these dipoles, this is to be expected. From Figure 78, one can see that the silyl transition dipole steadies at about 0.4 au, while the α-silylene group averages about 0.5 au, and internal silylene group averages at about 0.7 au. These transition dipoles are not only relatively constant in magnitude, but also direction. The silyl transition dipole is perpendicular to the plane formed by the silicon and out of plane hydrogens, and the silylene group transition dipole is perpendicular to the silylene group molecular plane. Such vectors all point in the same direction in an oligosilane, which is parallel to the molecular backbone, and the string of Si-Si charge concentrations that lie along it. When one has 'standard' values for both the oscillator strength and transition dipole moment, one can then estimate the excitation energy of a given species, by building the oscillator strength and transition dipole from standard group values, then using Equation 56 to solve for the excitation energy.

6.2.1.2 Transition Densities

The contours of the transition densities for this series show clearly why each group contributes to the overall intensity of the excitation.

Figure 79: Transition Density of Disilane

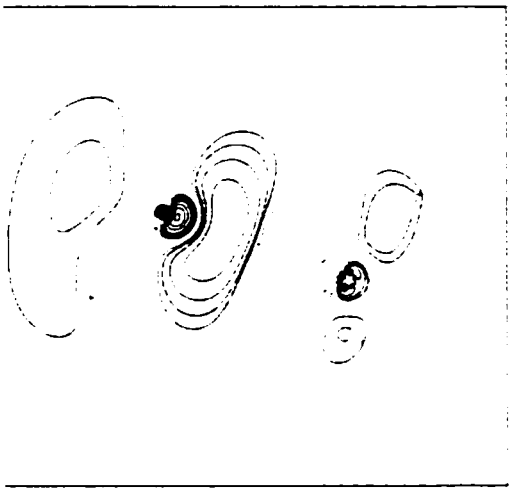

The transition density for disilane, shown in Figure 79, shows how the central charge concentration between the silicons polarizes in the direction of the Si-Si bond, inducing opposing polarizations in the hydrogens. The excited state of disilane is the exception of the series, as its symmetry is different than the other molecules in the series. The excited states of trisilane are somewhat more complex; there still remains the justification for choosing the 1^1B_2 state rather than the higher energy and more intense 3^1B_2 state. Figure 80 explains why this was done.

Figure 80: Transition Densities for Most Intense Excitations of Trisilane

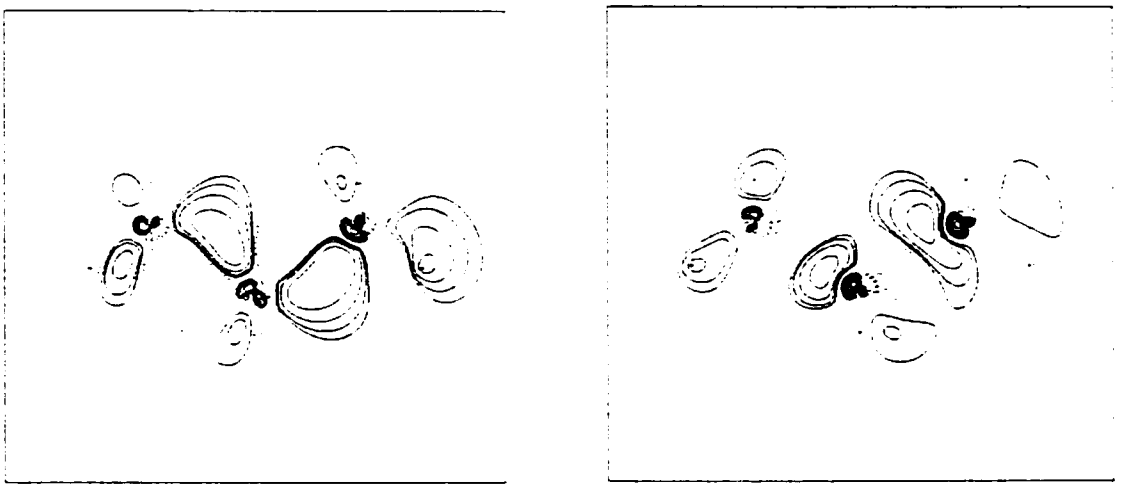

1^1B_2 3^1B_2

As one can see, these transition densities have very different structures, with the one on the left representing the excitation chosen for this series. As explained previously, the transition density contour plot was the main justification for choosing this excitation, as well as the fact that the energy of this excited state better fit the bathochromic shift trend observed in the calculations. The pattern of polarization between the silicons matched that of the transition densities of the other oligosilanes: Figure 81 shows tetrasilane as an example. In this, and all other cases, there is a distinct pattern common to each silylene group. The charge concentration area between each Si-Si bond is polarized to one side, resulting in each silylene group providing a small polarization that adds to the total molecular transition dipole.

Figure 81: Transition Density of Tetrasilane

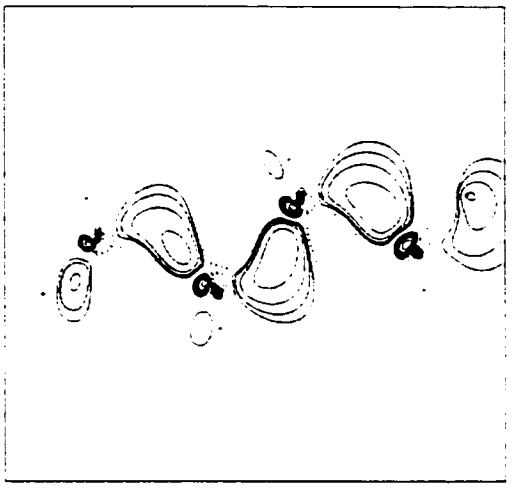

This pattern also justifies the averaging of the group contributions within a given molecule. If one considers the electric field of the approaching photon to be oscillating, then both silyl groups in tetrasilane would be equivalent, and should feel an average effect of that electric field. As the other transition densities are similar in structure, only the contour of heptasilane will be shown, in Figure 82. As one can see, the pattern of the transition density remains unchanged, even for heptasilane, and presumably even longer chain species.

Figure 82: Transition Density of Heptasilane

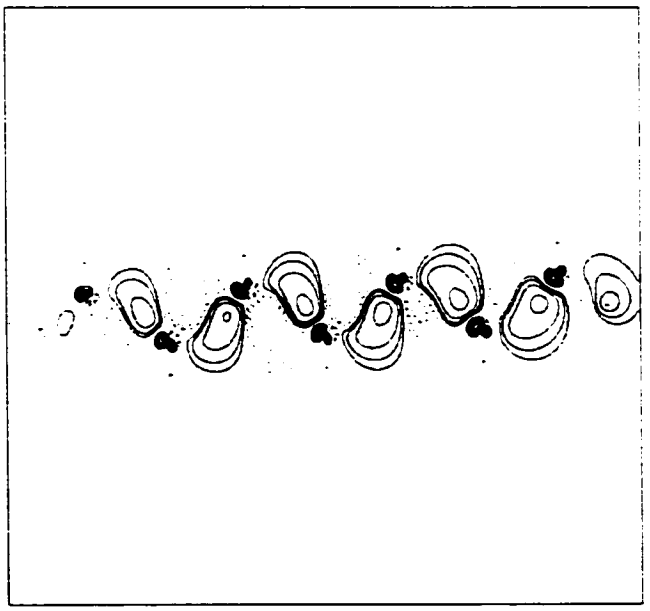

These contour plots confirm the results of the transition dipole calculations. The probability of a molecule entering an excited state results from contributions from every group in the molecule, not just one localized chromophore.

6.2.1.3 Excited State Properties

While the transition dipole results explain why polysilane excitations become more intense with chain length, they do not explain why the excitation energy decreases. To understand this, one must look to the molecular properties before and after excitation, to see how the density changes, and what those changes signify. The following tables have particular data that must be noted: first, the quadrupole moments are for the silicons only, for the same reasons given in the formaldehyde and ammonia treatments. Also, all the quadrupole moments have been aligned so as to follow a standard axis. The backbone of the molecule lies in the y-z plane, with the long axis of the molecule lying along the z-axis, and the short axis along the y-axis. From the data presented in Table 104, a clear pattern emerges. In disilane, there is a net transfer of electron density from the silicon to the hydrogens: silicon loses about 0.09 au of density. The volume of each increases as one would expect, as density shifts to the hydrogens. The quadrupole moment shows the polarization along the bond axis of the molecule: as expected, this value drops with excitation, indicative of a reduction in density in the Si-Si bond. Trisilane, with a different excitation symmetry, shows a much different change in its density upon excitation: there is a net transfer of about 0.066 au of charge to the central silylene group from the silyl groups. The quadrupole moment, showing polarization along the long z-axis of the molecule, shows a shift upon excitation to the short y-axis of the molecule, indicating a movement of density to a region between the silyl silicons. The group volume increases are smaller than that of disilane, indicating less transfer of density to the ligands. From tetrasilane on, the pattern in the integration properties is as follows. Upon excitation, there are very small net transfers of density from the internal silylene groups to the silyl groups; the amount of density gained by the silyl groups stays fairly constant at about 0.005 – 0.009 au. The quadrupole moment of each silicon shows a shift in polarization. The density of each silicon is polarized along the long axis of the molecule in the ground state (averaging about –2.2 au along the z-axis), and is polarized in plane along the short axis in the excited state (averaging about –2.8 au along the y-axis).

Table 104: Group Properties and their Change Upon Excitation for Oligosilanes

Si_2H_6					
$X\ ^1A_1$	N(Ω)	Q_{xx}(Ω)	Q_{yy}(Ω)	Q_{zz}(Ω)	ν(Ω)
$Si1H_3$	17.0000	1.2842	1.2842	-2.5685	358.14
$X^1A_1 \rightarrow 1^1A_2$	ΔN(Ω)	ΔQ_{xx}(Ω)	ΔQ_{yy}(Ω)	ΔQ_{zz}(Ω)	Δν(Ω)
$Si1H_3$	0.0000	-0.1741	-0.1741	0.3484	35.66
Si_3H_8					
$X\ ^1A_1$	N(Ω)	Q_{xx}(Ω)	Q_{yy}(Ω)	Q_{zz}(Ω)	ν(Ω)
$Si1H_3$	16.9913	1.2347	-0.0147	-1.2200	358.25
$Si2H_2$	16.0166	2.7553	-0.2811	-2.4742	294.77
$X^1A_1 \rightarrow 3^1B_2$	ΔN(Ω)	ΔQ_{xx}(Ω)	ΔQ_{yy}(Ω)	ΔQ_{zz}(Ω)	Δν(Ω)
$Si1H_3$	-0.0325	0.0057	-1.1338	1.1281	14.47
$Si2H_2$	0.0656	1.3887	-4.2394	2.8507	15.36
Si_4H_{10}					
$X\ ^1A_g$	N(Ω)	Q_{xx}(Ω)	Q_{yy}(Ω)	Q_{zz}(Ω)	ν(Ω)
$Si1H_3$	16.9828	1.2170	0.4696	-1.6866	357.46
$Si2H_2$	16.0142	2.7246	-0.3832	-2.3414	294.42
$X^1A_g \rightarrow 3^1B_u$	ΔN(Ω)	ΔQ_{xx}(Ω)	ΔQ_{yy}(Ω)	ΔQ_{zz}(Ω)	Δν(Ω)
$Si1H_3$	0.0166	-0.0948	-2.4759	2.5708	8.06
$Si2H_2$	-0.0134	0.4242	-1.8224	1.3982	6.56
Si_5H_{12}					
$X\ ^1A_1$	N(Ω)	Q_{xx}(Ω)	Q_{yy}(Ω)	Q_{zz}(Ω)	ν(Ω)
$Si1H_3$	16.9858	1.2325	-0.0515	-1.1810	357.63
$Si2H_2$	16.0069	2.7212	-0.4042	-2.3171	293.72
$Si3H_2$	16.0134	2.7233	-0.4681	-2.2552	293.85
$X^1A_1 \rightarrow 1^1B_2$	ΔN(Ω)	ΔQ_{xx}(Ω)	ΔQ_{yy}(Ω)	ΔQ_{zz}(Ω)	Δν(Ω)
$Si1H_3$	0.0044	-0.0665	-0.8287	0.8951	6.92
$Si2H_2$	0.0061	0.3589	-2.6066	2.2479	5.76
$Si3H_2$	-0.0195	0.3115	-3.1878	2.8763	6.21
Si_6H_{14}					
$X\ ^1A_g$	N(Ω)	Q_{xx}(Ω)	Q_{yy}(Ω)	Q_{zz}(Ω)	ν(Ω)
$Si1H_3$	16.9868	1.2288	0.1722	-1.4010	357.95
$Si2H_2$	16.0079	2.7132	-0.4105	-2.3117	294.06
$Si3H_2$	16.0045	2.6817	-0.4754	-2.2063	293.87
$X^1A_g \rightarrow 1^1B_u$	ΔN(Ω)	ΔQ_{xx}(Ω)	ΔQ_{yy}(Ω)	ΔQ_{zz}(Ω)	Δν(Ω)
$Si1H_3$	0.0067	-0.0428	-0.6272	0.6701	4.76
$Si2H_2$	-0.0004	0.2522	-2.1053	1.8621	3.85
$Si3H_2$	-0.0043	0.3095	-2.9218	2.6123	5.18
Si_7H_{16}					
$X\ ^1A_1$	N(Ω)	Q_{xx}(Ω)	Q_{yy}(Ω)	Q_{zz}(Ω)	ν(Ω)
$Si1H_3$	16.9863	1.2334	-0.0525	-1.1810	357.66
$Si2H_2$	16.0084	2.7268	-0.4094	-2.3174	293.82
$Si3H_2$	16.0063	2.7044	-0.5001	-2.2024	293.64
$Si4H_2$	15.9969	2.6775	-0.5233	-2.1542	294.28
$X^1A_1 \rightarrow 1^1B_2$	ΔN(Ω)	ΔQ_{xx}(Ω)	ΔQ_{yy}(Ω)	ΔQ_{zz}(Ω)	Δν(Ω)
$Si1H_3$	0.0088	-0.0367	-0.4398	0.4766	2.68
$Si2H_2$	-0.0005	0.1026	-1.5169	1.4143	2.41
$Si3H_2$	-0.0073	0.1450	-2.4010	2.2541	3.55
$Si4H_2$	0.0013	0.2086	-2.7646	2.5560	3.66

This polarization shift increases as one proceeds from the silyl to the central silylene group, and becomes smaller in all groups as the chain length increases. The volume increase upon excitation also grows smaller

with chain length, indicating that the ligands play a negligible role in the rearrangement of electron density upon excitation. Figure 83 shows the sum of the density changes for the atoms in each oligosilane, grouped by the sum changes in the backbone and the sum changes in the hydrogen ligands. One can see that the total shift in electron density from the ligands to the backbone of each oligosilane averages about 0.002 au; this is a remarkable result, in that the shift in density remains fairly constant regardless of chain length.

Figure 83: Total Change in Charge Upon Excitation, in Silicon Backbone and in Ligands, for Oligosilanes

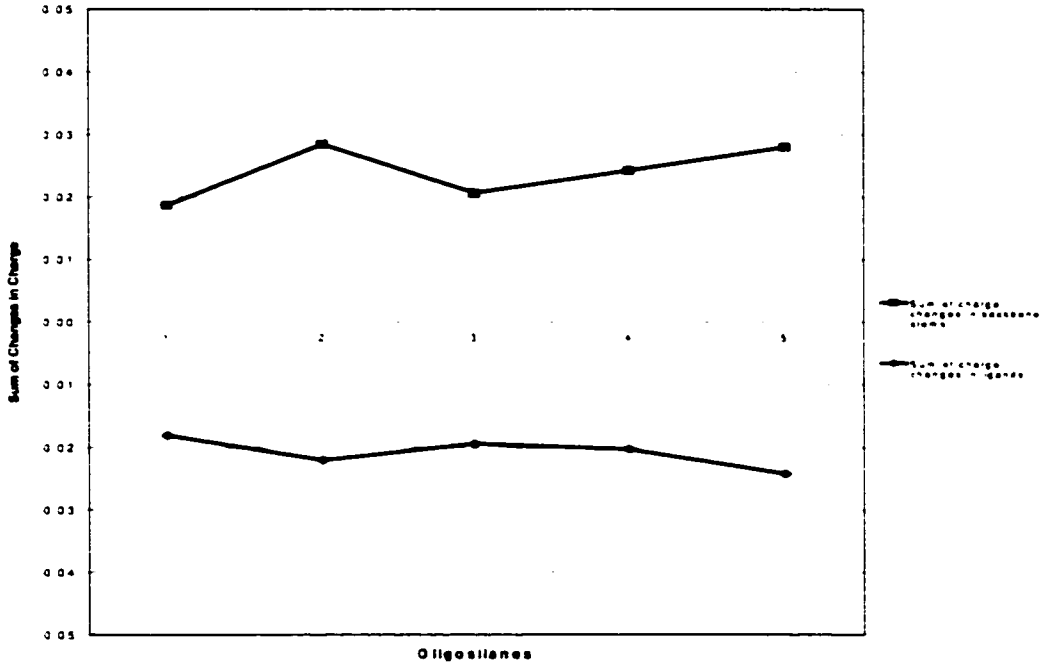

From this data, one can conclude the following: there is little net transfer of density between the ligands and the backbone, or between silyl and silylene groups. The density of each silicon in the backbone rearranges, resulting in a shift in its polarization, from along the axis that runs along the length of the backbone to the short axis of the plane of the backbone.

6.2.1.4 Excited State Densities

Contour maps of the ground and excited states of these oligosilanes help to explain the results shown by the integration data. Disilane experiences a transfer of density from the Si-Si bond to the hydrogens, as Figure 84 illustrates.

Figure 84: Contour Plots of Electron Density in Disilane.

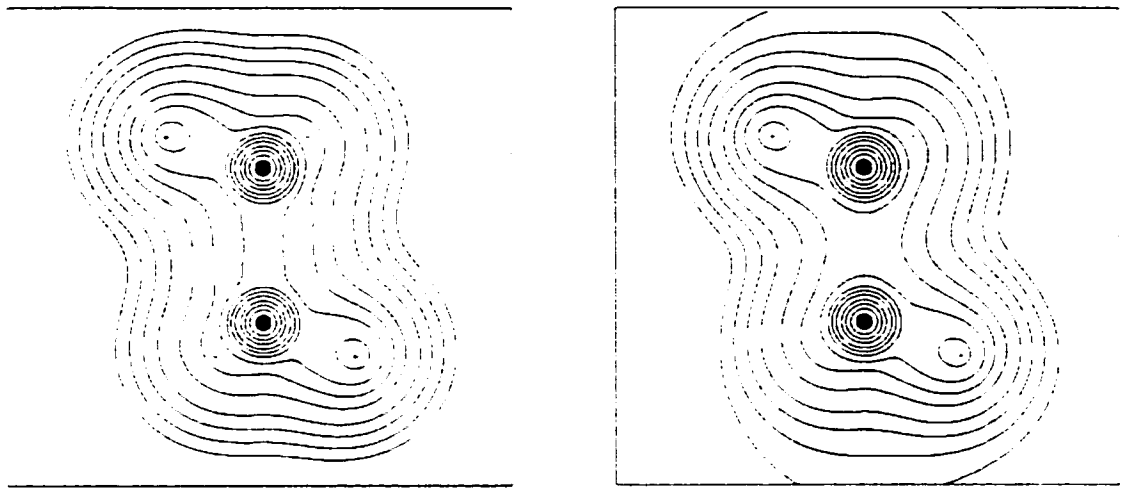

X^1A_1 $X^1A_1 \rightarrow 1^1A_2$

The plot on the left is that of the ground state, and the plot on the right is that of the dominant excited state. Note how the 0.2 au contour line is missing from the Si-Si bond region, indicating a loss of density within the Si-Si bond, and an accumulation of density in the hydrogen regions of the molecule. Figure 85 shows this even more clearly, through a plot of L(r) of the ground and excited states. This contour plot shows not only a weakening of the Si-Si bond, but a separation. The two maxima in the Si-Si charge concentration become more pronounced, indicative of a pulling of this density by the two silicons. Unlike the ground state, shown on the left, there is a definite accumulation of charge concentration between the Si-Si charge concentration and the hydrogens, which explains the increase in the hydrogen populations.

Figure 85: Contour Plots of L(r) in Disilane

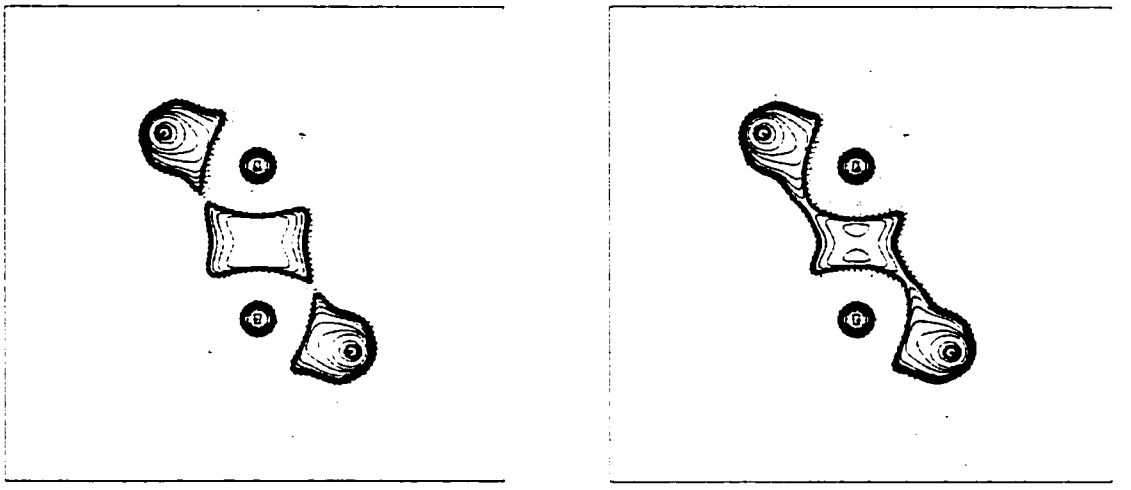

X^1A_1 $X^1A_1 \rightarrow 1^1A_2$

Trisilane also shows significant changes to its density upon excitation, as shown in Figure 86.

Figure 86: Contour Plots of Electron Density in Trisilane

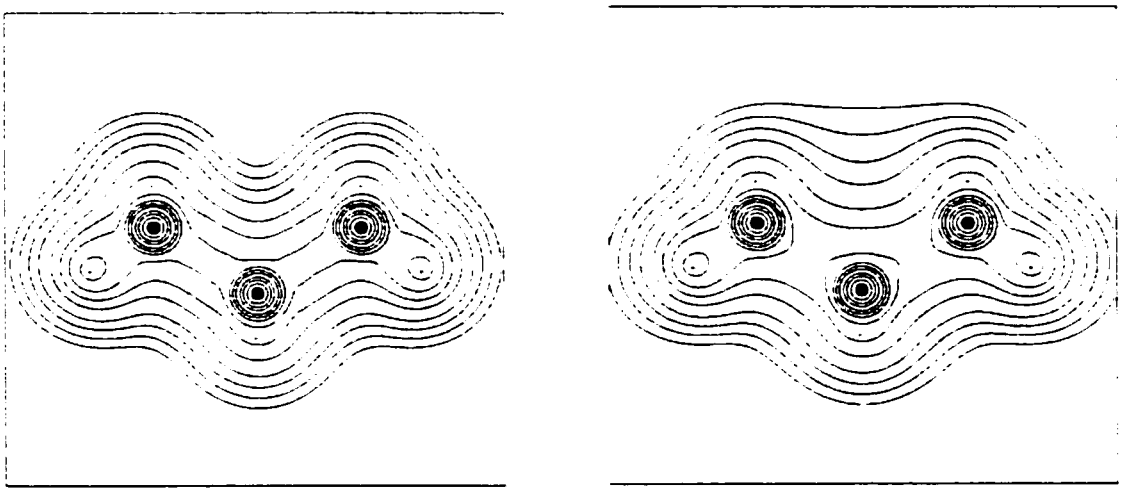

X^1A_1 $X^1A_1 \rightarrow 1^1B_2$

Again, there appears to be some loss of density between the Si-Si bonds. Figure 87 shows that more is happening than just a depletion of electron density in the Si-Si bonds.

Figure 87: Contour Plots of L(r) in Trisilane

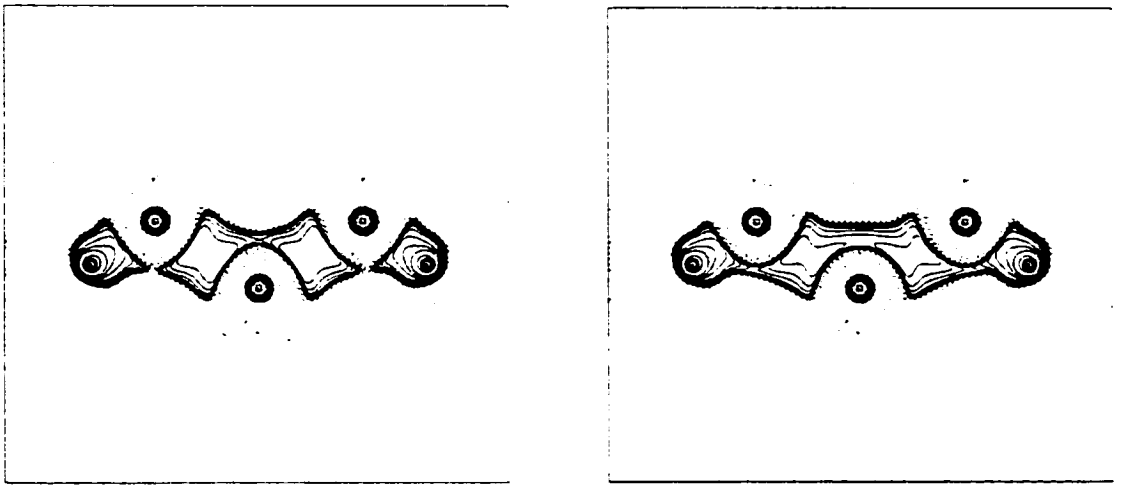

X^1A_1 $X^1A_1 \rightarrow 1^1B_2$

Most notable about these L(r) contours is the accumulation of density at the (3,-1) critical point linking the two backbone maxima of the silylene group. This explains the increase in density in the silylene group, as well as the change in the direction of the quadrupole polarization. This result brings to mind the photochemistry of trisilane, where the molecule rearranges, forming silylene and disilane: one can visualize this density pulling the silyl groups closer together, eventually forming a new Si-Si bond and extruding silylene.

Figure 88: Contour Plots of Electron Density of Pentasilane

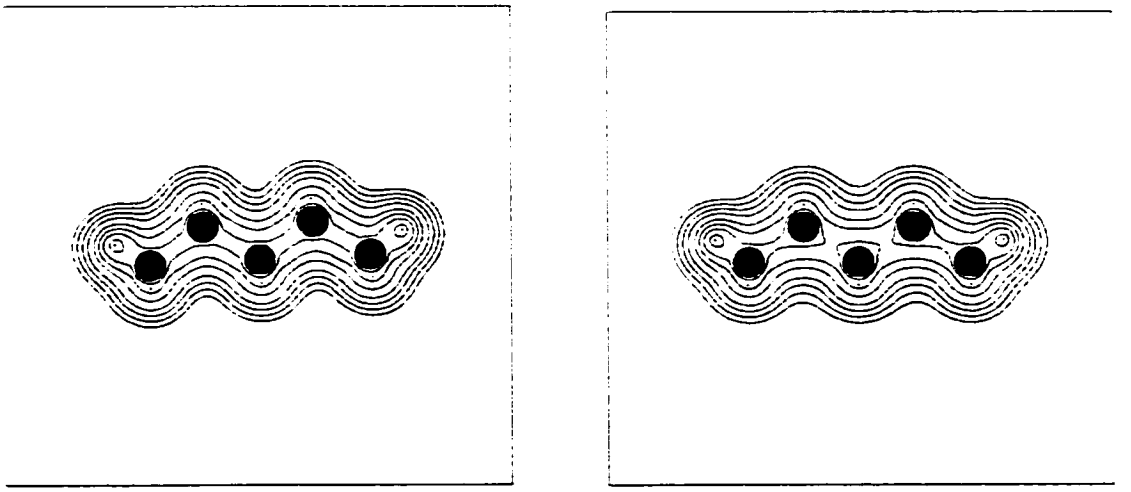

X^1A_1 $X^1A_1 \rightarrow 1^1B_2$

This rearrangement of the oligosilane backbone is seen throughout the rest of the series. Figure 88 shows the changes in rho in pentasilane, and L(r) in Figure 89.

Figure 89: Contour Plots of L(r) of Pentasilane

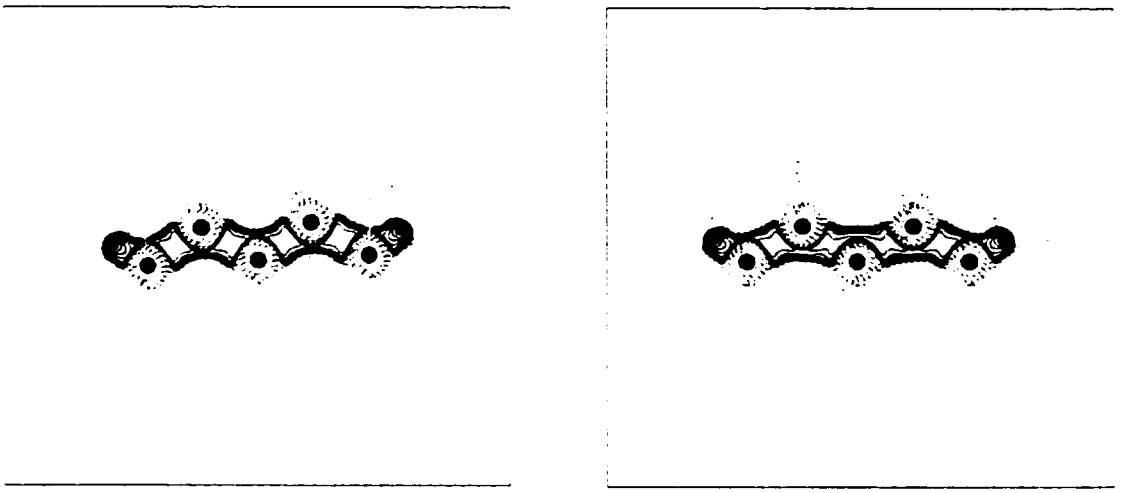

X^1A_1 $X^1A_1 \rightarrow 1^1B_2$

What becomes clear from the emerging pattern is how upon excitation, the majority of electron density rearrangement occurs in the backbone of the oligosilane. There is little net transfer of density between the ligands and the backbone (about 0.02 au on average), or even between the silyl and silylene groups (0.002 au, on average). In the excited state, each group appears to draw its valence density more closely to itself, resulting in a net loss of density at the Si-Si bond charge concentrations, and a net gain in density at the (3,-1) critical points between these concentrations. As Table 105 shows, the Si-H bond properties of heptasilane do not change appreciably with excitation, but the Si-Si bond properties do show a decrease in rho upon excitation, in particular the bonds closest to the middle of the molecule. As in the other oligosilanes of this series, there is also a substantial increase in the ellipticity of the Si-Si bonds of heptasilane upon excitation; given the nature of the electron density rearrangement within the backbone, an increase in ellipticity along the short axis of the molecular backbone is expected.

Table 105: Bond Data for States of Heptasilane

	r	r_c(Si)	% r_c(Si)	ρ_b	L(r)$_b$	ε
$X\ ^1A_1$						
Si1-Si2	4.4877	2.2398	49.91	0.0909	0.0355	0.0226
Si1-H'	2.7905	1.3545	48.54	0.1211	-0.0487	0.0297
Si1-H	2.7909	1.3544	48.53	0.1211	-0.0489	0.0288
Si3-Si4	4.4903	2.2465	50.03	0.0898	0.0344	0.0465
Si4-H	2.7963	1.3576	48.55	0.1196	-0.0491	0.0302
$X\ ^1A_1 \rightarrow 1\ ^1B_2$						
Si1-Si2	4.4878	2.2376	49.86	0.0872	0.0327	0.0745
Si1-H'	2.7904	1.3609	48.77	0.1202	-0.0441	0.0470
Si1-H	2.7906	1.3593	48.71	0.1212	-0.0437	0.0281
Si3-Si4	4.4902	2.2433	49.96	0.0789	0.0254	0.1970
Si4-H	2.7967	1.3617	48.69	0.1212	-0.0418	0.0112

As was described previously in the electron density section, one can express the VSCC of an atom in a molecule in terms of a tetrahedral structure, with maxima at the vertices, (3,-1) critical points at the edges, and (3,+1) critical points at the faces. For oligosilanes, the values of these L(r) critical points change little with chain length: the majority of the points are negative, indicating regions of electron depletion. As Table 105 shows, there is a marked change in the BCPs upon excitation. Clearly the critical points of L(r) change as well, as the contour plots indicate, and Figure 90 confirms.

Figure 90: Values of L(r) at (3,-3) and (3,-1) Critical Points for Ground State (left) and Excited State (right) Si_7H_{16}, Central Silicon.

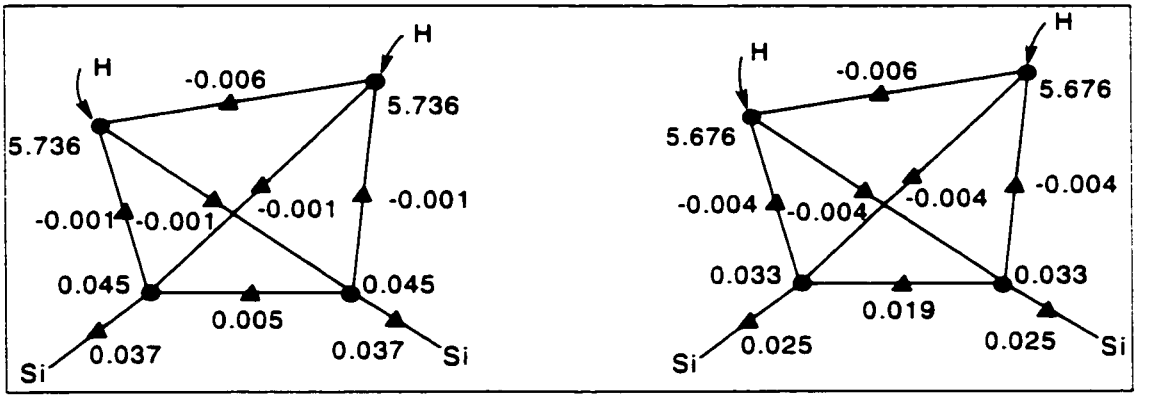

For the central silicon in heptasilane, one sees a marked change in the values of L(r) at some of the critical points of the VSCC. For the upper maxima, which coincide with the positions of the hydrogens, there is a relatively small decrease in the value: the (3,-1) critical point that links them does not change in value at all. The same can be said for the (3,-1) critical points that link the hydrogen maxima to the maxima that reside

in the Si-Si bond charge concentrations. Only three critical points show any appreciable change in value upon excitation. The maxima in the Si-Si bond charge concentrations, the (3,-1) critical points that connect the VSCC tetrahedral structures, and the (3,-1) critical points that form the edge between these maxima within a tetrahedron. One observes a reduction in the value of L(r) and rho in the critical points that link the tetrahedra; these can be called vicinal critical points. At the same time, one sees an increase in L(r) and rho in what can be described as a geminal critical point, as it links two maxima within the VSCC of the same silicon. One can consider the change in these points as a correlation with the Sandorfy model, where these critical points correspond to the resonance interactions between the sp^3 basis functions in the model. As expected from the electron density work seen previously, the value of L(r) at these geminal and vicinal critical points do not change with chain length in the ground state. As Figure 91 shows, however, there is a marked change in the critical points of the excited state.

Figure 91: Values of L(r) for Silyl Geminal and Vicinal Critical Points in L(r) Density of Oligosilanes

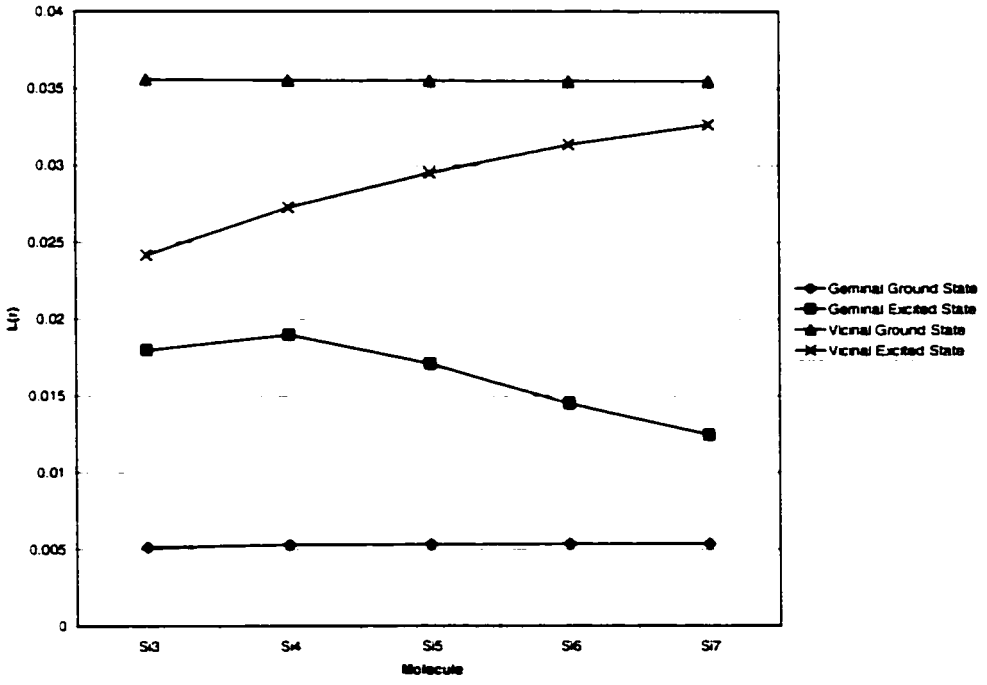

This graph shows the changes in L(r) of the geminal and vicinal critical points about the silyl silicon: the same trends are observed for the VSCCs of the other silicon atoms. The value of L(r) at each geminal and

vicinal critical point increases and decreases upon excitation respectively, but the gain or loss at each point decreases with chain length. The amount of L(r) increase in the geminal points is greater than the decrease from the vicinal points because there are also increases in L(r) at the maxima in the backbone, as well as the hydrogens. Since there is a decrease in L(r) from not only the vicinal critical points but also the maxima they are connected to, it makes more sense to discuss changes in the geminal points, which are the only points that show an increase in L(r) upon excitation. The net increase in L(r) in all the geminal points increases with chain length, as Figure 92 shows.

Figure 92: Net Increase in L(r) from All Geminal (3,-1) Critical Points in L(r) Density of Oligosilanes

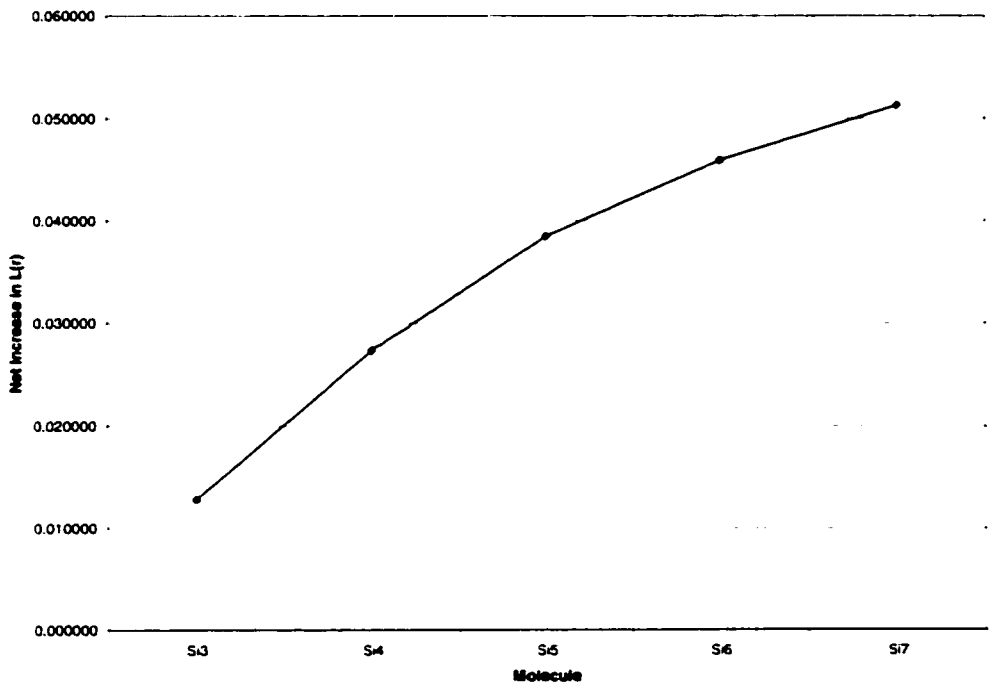

As the graph shows, the increase in L(r) in all the geminal points in the backbone is almost linear. If the increase at each point remained constant with chain length, this plot would be linear. As it is, there is a slight curvature to the graph. One would intuitively expect that the changes in L(r) within the backbone would require increasing amounts of energy for increases in L(r) at the geminal points. Figure 93 shows that for oligosilanes, the opposite is true: there is a nearly perfect linear relationship between the excitation energy and the net increase in L(r) at the geminal points in the backbone.

Figure 93: Net Increase in L(r) in Geminal (3,-1) Critical Points in L(r) Density for Oligosilanes versus Excitation Energy

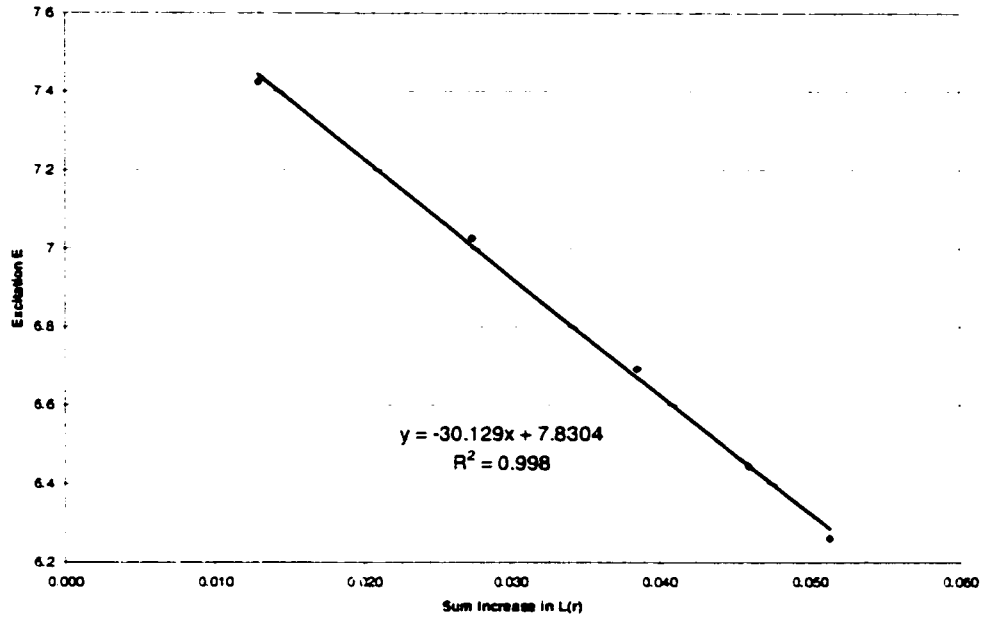

As the net change in L(r) at the geminal points increases, the excitation energy decreases. From this result, the idea of a bathochromic shift as a function of chain length becomes simple to understand: as one increases the chain length, the number of geminal points able to take on changes in L(r) also increases. Thus, the net change in L(r) at all the geminal points increases, and the excitation energy decreases accordingly. This idea has a basis in the local expression of the virial theorem, as described in Section 2.4.2 (Equation 60).

$$-\mathrm{L}(\mathbf{r}) = 2\mathrm{G}(\mathbf{r}) + V(\mathbf{r}) \tag{60}$$

The kinetic energy function G(r) will always be greater than zero, while the potential energy function V(r) will always be less than zero. For a given geminal point in the backbone of an oligosilane, G(r) remains constant in both the ground and excited states, but L(r) increases upon excitation, as a result of the increase in the electron density at the critical point. As a result, V(r) must decrease accordingly to maintain the equality of the expression. This decrease in V(r) corresponds to an increased stabilization of the potential energy of the molecule in the excited state: the greater this stabilization, the less energy required to rearrange the electron density in the backbone in order to reach the excited state.

6.2.1.5 Excited State Densities of Hydrocarbons

While this explains the bathochromic shift observed in polysilanes, there still remains the matter of why hydrocarbons do not exhibit the same behavior.

Figure 94: L(r) Contour Maps of Heptane, Ground and Excited State

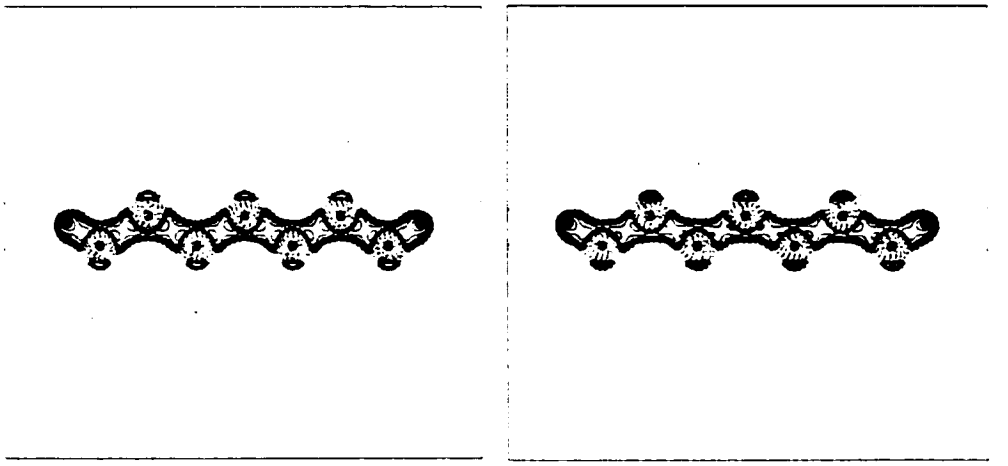

Figure 94 shows the L(r) contour maps of heptane, in the ground (left) and excited (right) states. From these maps, one can conclude that the mechanism of backbone rearrangement observed in oligosilanes is not exclusive to that class of molecules. This raises the issue of how to explain the lack of bathochromic shift in hydrocarbons when there is no difference in the excitation mechanism. Another look at the excitation energies shown in Table 99 shows that for the examples ethane and heptane, there is a decrease in the excitation energy, of 0.34 eV. This is a small difference, but it is still a bathochromic shift. It is thus proposed that the differences in photophysics of hydrocarbons and oligosilanes are not a matter of overall mechanism, but simply of degree.

Figure 95: Values of L(r) (3,-3) and (3,-1) Critical Points for Ground State (left) and Excited State (right) C_7H_{16}, Central Carbon.

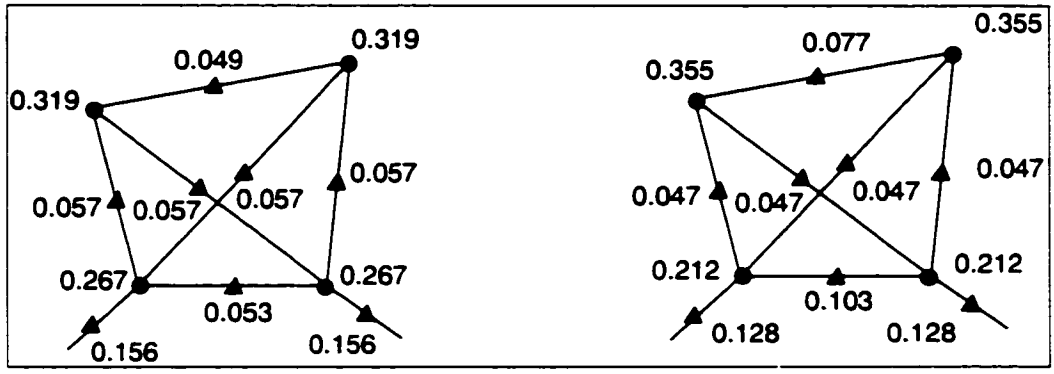

As Figure 95 illustrates, the values of L(r) at the critical points in the VSCC of carbon are considerably higher: the contour plots of L(r) of heptane show that there is a great deal of electron density in the valence region. The amount of electron density that shifts from the vicinal to the geminal points is also much higher, as Table 106 illustrates.

Table 106: Values of Rho at L(r) (3,-1) Critical Points Around Central Backbone Atom

	Geminal	Vicinal
C_7H_{16} gr. st.	0.203	0.253
C_7H_{16} exc. st.	0.222	0.228
Si_7H_{16} gr. st.	0.051	0.091
Si_7H_{16} exc. st.	0.066	0.079

The net density gained at the geminal points of heptane equals –0.120 au, a value higher than –0.050, the amount of density lost from the vicinal points of heptasilane, (the geminal points in heptane gain a total of 0.069 au of density, as compared to 0.055 au in heptasilane). Despite the fact that more density rearranges in these hydrocarbons upon excitation, any energy benefit gained by this rearrangement is much smaller than it is in oligosilanes. One could apply the same analysis as shown in Figure 93 to the equivalent hydrocarbons, to see if the gain in geminal density also follows a linear relationship with excitation energy. Figure 96 shows that there is a good relationship between excitation energy and the amount of electron density gained in the geminal points upon excitation. Application of the local expression of the virial theorem to hydrocarbon excitations has a similar effect, but with one important difference. The value of G(r) for a geminal point in a hydrocarbon is far greater than that of an oligosilane, 0.217 au versus 0.021 au, on average. Another difference is the relative magnitudes of the changes in L(r) and V(r) at a geminal

point. For oligosilanes, the two magnitudes values are nearly identical for all oligosilanes, as the G(r) remains nearly constant in both the ground and excited states. For hydrocarbons, however, G(r) decreases by about 3% in the excited state; thus, $V(r)$ is always smaller in magnitude than L(r), the ratio $V(r)/L(r)$ averaging about 0.7. This indicates that while the increase in electron density at the geminal points upon excitation is greater in hydrocarbons, the degree of stabilization of $V(r)$ per unit charge increase in the geminal points is not as great as that seen in the oligosilanes.

Figure 96: Net Increase in L(r) in Geminal (3,-1) Critical Points in L(r) Density for Hydrocarbons versus Excitation Energy

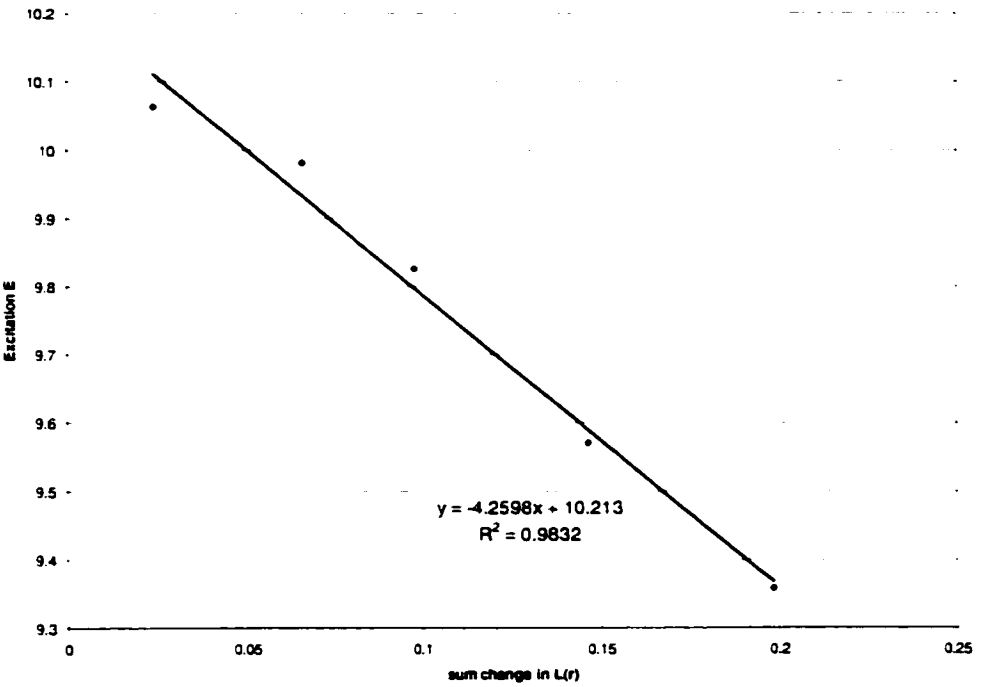

Figure 93 and Figure 96 provide excellent measures of the extent of stabilization of the excitation energy as a function of the net increase in L(r) at the geminal points. The slope of the graph in Figure 93 is –30.129 eV/au of L(r) density, as opposed to a slope of –4.2598 eV/au in Figure 96. This shows clearly that the extent of stabilization of the excitation energy per unit increase in L(r) for oligosilanes is far greater than that of hydrocarbons, which would result in a greater bathochromic shift as a function of chain length.

6.2.2 Silicon Torsion Study

The first analysis performed on this series of hexasilane conformers was to observe the molecular energy as a function of the torsion angle of the central Si-Si bond. Figure 97 shows that the molecular ground state energies do indeed follow the expected pattern; the molecular energy rises as the central torsion angle decreases from 180°, reaching a local maximum at 120°, where the disilyl groups eclipse the hydrogens on the central silicons. The energy then drops to a local minimum at 60° (the gauche staggered conformation) before rising to the maximum energy observed at 0°, the fully eclipsed geometry.

Figure 97: Molecular Energy of Si_6H_{14} as Function of Central Bond Torsion

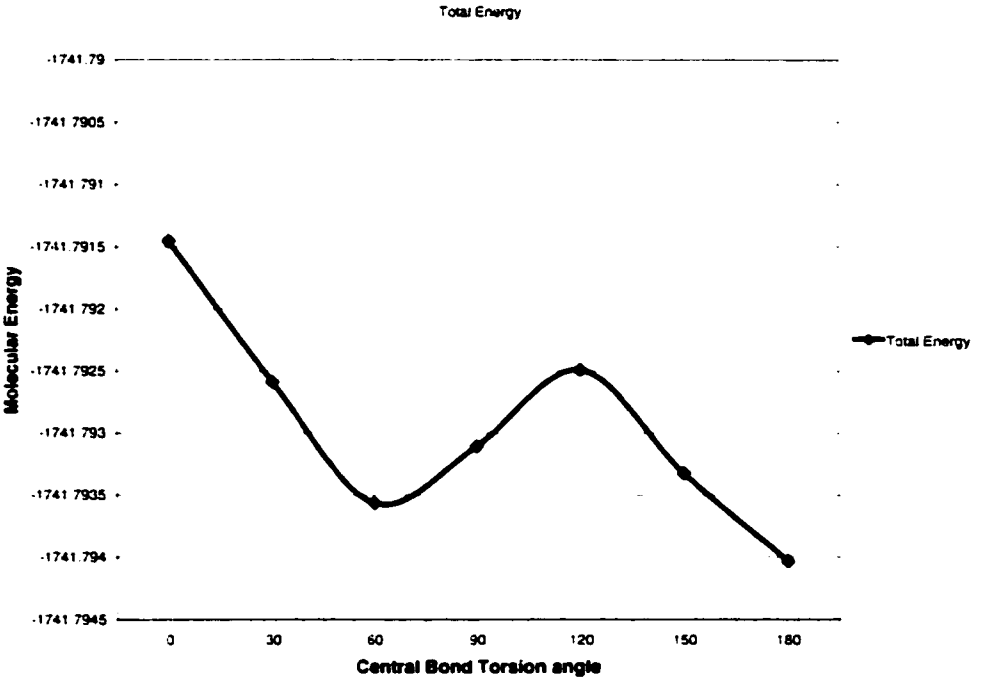

From this graph, one calculates a rotational barrier of 0.001 au, or 6.28 kcal/mol.

6.2.2.1 Transition Dipoles

What was unexpected in the analysis of this series was the nature of the excitations these conformers undergo. Table 107 shows the data for the two dominant excitations of the hexasilane conformers.

Table 107: Excited States of Si_6H_{14} Conformers

Torsion Angle	Energy (eV)	Transition dipole			Osc. Strength
		x	y	z	
0	6.9959	2.2558	-1.9170	0.0000	1.5020
30	6.8442	-2.0551	0.0000	0.0696	0.7090
	7.1144	-2.0424	0.0000	-0.0186	0.7271
60	6.8281	2.6496	0.0000	-0.0628	1.1750
	7.2782	-1.2088	0.0000	-0.0348	0.2608
90	6.6800	2.7755	0.0000	-0.0987	1.2623
	7.2848	0.8770	0.0000	0.1165	0.1397
120	6.4995	-2.9207	-0.1329	0.0000	1.3611
	7.1866	-0.9223	0.1809	0.0001	0.1555
150	6.4479	3.2223	0.1195	0.0000	1.6425
	7.2111	-0.4734	0.1544	0.0000	0.0438
180	6.4462	-3.3498	0.1046	0.0000	1.7738

Rather than a single dominant excitation as seen in the 180° conformer, there are two dominant excitations, both of the same symmetry. For the 0° and 180° conformers, the symmetry of the excited state is A_1 and B_u respectively, with the rest having a symmetry of A. Figure 98 shows the oscillator strengths of the first six excited states of each conformer.

Figure 98: Oscillator Strengths of Excitations of Si_6H_{14} Conformers

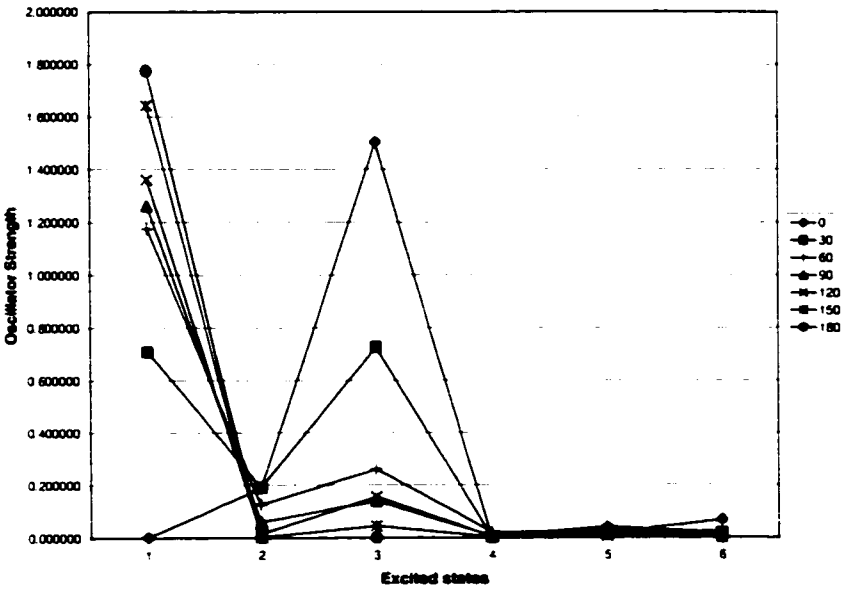

This graph shows that there is a distinct trend in the oscillator strengths of the first and third excited states as the central Si-Si bond is twisted, with the remaining excited states having negligible intensity. What is

not immediately clear is why this trend occurs, or even why more than one excited state should arise. A closer look at the first and third excited states of hexasilane show the specific trend that occurs as the central Si-Si bond is twisted. As Figure 99 shows, the first excited state, the one that dominates in the 180° conformation, gradually loses intensity as the torsion angle decreases, finally disappearing altogether at 0°. At the same time, the third excited state gains intensity, becoming the only dominant excitation at 0°. Of note is the small deviation at 120°, the same angle at which the local ground state energy becomes locally maximized as a result of the eclipse interaction. This implies that the steric interaction not only affects the ground state energy, but also the intensity of the excited state of the molecule.

Figure 99: Oscillator Strengths of First and Third Excited States vs Torsion Angle

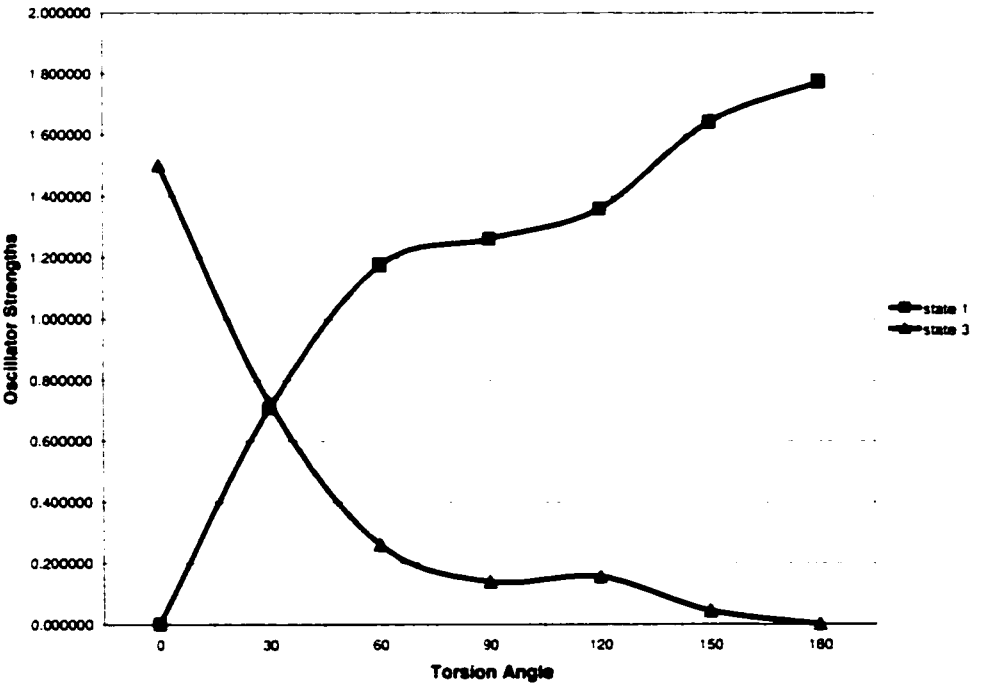

The third excited state is far more interesting; it experiences a local minimum at 120°, with the energy almost returning to the same level as it was at 180° before dropping to its minimum value at 0°. This seems to lend weight to the idea that the 120° steric interaction has a direct effect on the excited states and their intensity. Figure 100 shows the excitation energies themselves, and how they change with torsion angle. The first excited state shows a simple trend with the torsion angle: the excitation energy begins to rise

substantially at about 120°, then levels off at 60°. The third excited state shows a local minimum at 120°, then a local maximum at around 60°, before reaching its lowest value. It appears that the steric effect seen in the oscillator strengths affects the third excited state, but not the first.

Figure 100: Excitation Energies of First and Third Excited States vs Torsion Angle

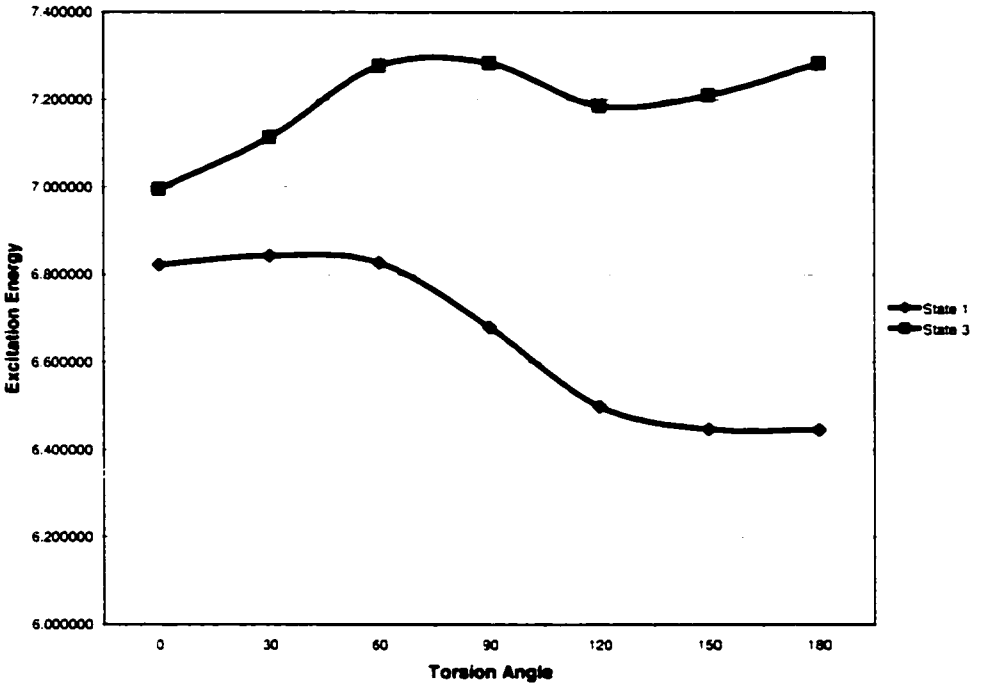

To understand what is happening, one must go back to the data obtained for the chain length study, specifically Table 102. A look at the excitation energy of tetrasilane (7.0248 eV) shows a remarkable similarity to the dominant excitation energy of the 0° conformer (6.9959 eV). Add to this the observation of the oscillator strength of tetrasilane; 0.8371 au, a value approximately half that of the 0° conformer oscillator strength. These facts lead to an important conclusion: twisting the central Si-Si bond in a polysilane containing *n* silicon atoms will produce an excitation equivalent to two polysilanes containing $(n/2)+1$ silicon atoms. This idea becomes reasonable when one takes into consideration the structure of L(r) of polysilanes. Hexasilane contains five Si-Si charge concentrations, whereas tetrasilane contains three. In the 180° conformer of hexasilane, an incoming photon will induce an oscillation along this string of charge concentrations: all five interact, since they all lie in a straight line. In the 0° conformation of hexasilane, the

maximum number of charge concentrations that can be lined up for interaction with a photon is three, the same number as that of tetrasilane. This lends strong support to the idea that it is these charge concentrations that are key to the excitation properties of polysilanes.

Table 108: Transition Data of Si_6H_{14} Conformers: State 1

Torsion Angle	$\mu_{nk}(\Omega)$ x	$\mu_{nk}(\Omega)$ y	$\mu_{nk}(\Omega)$ z	$\lvert\mu_{nk}\rvert(\Omega)$	$f_{nk}(\Omega)$
30					
$Si1H_3$	0.2364	0.0151	-0.0393	0.2883	0.0826
$Si2H_2$	0.2635	-0.1490	0.0560	0.3986	0.0915
$Si3H_2$	0.5338	0.0540	-0.0701	0.5601	0.1859
Total	2.0675	-0.1598	-0.1067	2.0764	0.7199
60					
$Si1H_3$	-0.3218	-0.0135	0.0224	0.3474	0.1427
$Si2H_2$	-0.3758	-0.0129	0.0131	0.4767	0.1664
$Si3H_2$	-0.6238	-0.0026	0.0040	0.6334	0.2758
Total	-2.6428	-0.0580	0.0791	2.6446	1.1698
90					
$Si1H_3$	-0.3223	-0.0881	-0.0407	0.3422	0.1467
$Si2H_2$	-0.4035	-0.1089	0.0509	0.5009	0.1848
$Si3H_2$	-0.6457	0.0554	0.0241	0.6671	0.2885
Total	-2.7430	-0.2832	0.0685	2.7584	1.2401
120					
$Si1H_3$	-0.3427	0.0362	0.0024	0.3637	0.1574
$Si2H_2$	-0.4483	-0.0723	-0.0585	0.5161	0.2079
$Si3H_2$	-0.6581	-0.0269	0.0457	0.6855	0.3046
Total	-2.8982	-0.1262	-0.0207	2.9010	1.3398
150					
$Si1H_3$	-0.3873	0.0412	-0.0018	0.3903	0.1965
$Si2H_2$	-0.5381	-0.0923	-0.0050	0.5594	0.2761
$Si3H_2$	-0.6876	-0.0128	-0.0006	0.6930	0.3507
Total	-3.2260	-0.1277	-0.0147	3.2285	1.6465
180					
$Si1H_3$	0.3983	0.0440	-0.0000	0.4007	0.2091
$Si2H_2$	0.5611	-0.0898	0.0000	0.5682	0.2975
$Si3H_2$	0.7096	-0.0140	0.0000	0.7098	0.3743
Total	3.3379	-0.1197	0.0000	3.3400	1.7618

These results give a strong argument for this idea, but it will be the group contributions to the oscillator strength and transition dipole, given in Table 108 and Table 109, that will confirm this hypothesis.

Table 109: Transition Data for Si_6H_{14} Conformers: State 3

Torsion Angle	$\mu_{nk}(\Omega)$ x	$\mu_{nk}(\Omega)$ y	$\mu_{nk}(\Omega)$ z	$\lvert\mu_{nk}\rvert(\Omega)$	$f_{nk}(\Omega)$
0					
$Si1H_3$	-0.2737	0.2113	-0.0000	0.4055	0.1761
$Si2H_2$	-0.3949	0.1676	0.0000	0.5528	0.2106
$Si3H_2$	-0.5309	0.5030	0.0000	0.7479	0.3711
Total	-2.3990	1.7637	0.0000	2.9776	1.5156
30					
$Si1H_3$	-0.2292	0.0468	0.0031	0.6713	0.0788
$Si2H_2$	-0.2551	-0.4876	0.0983	0.5619	0.1111
$Si3H_2$	-0.5259	0.1370	-0.0638	0.5715	0.1787
Total	-2.0202	-0.6076	0.0753	2.1110	0.7373
60					
$Si1H_3$	0.0987	0.0015	0.0786	0.2070	0.0215
$Si2H_2$	0.1519	-0.0653	-0.1179	0.2203	0.0325
$Si3H_2$	0.3515	0.0171	0.0507	0.3630	0.0756
Total	1.2043	-0.0933	0.0229	1.2081	0.2592
90					
$Si1H_3$	0.0286	0.0007	0.0343	0.3051	0.0055
$Si2H_2$	0.0834	0.1538	-0.0808	0.2292	0.0098
$Si3H_2$	0.3222	-0.0825	0.1350	0.3881	0.0545
Total	0.8683	0.1440	0.1770	0.8978	0.1396
120					
$Si1H_3$	-0.0726	-0.0171	-0.0205	0.5177	0.0113
$Si2H_2$	-0.1162	-0.0818	0.2300	0.4244	0.0229
$Si3H_2$	-0.2756	0.1206	-0.0648	0.3679	0.0447
Total	-0.9287	0.0433	0.2894	0.9737	0.1579
150					
$Si1H_3$	-0.0329	-0.0246	-0.0036	0.1287	0.0019
$Si2H_2$	-0.0433	-0.0282	-0.0074	0.0863	0.0026
$Si3H_2$	-0.1564	0.1451	0.0059	0.2815	0.0176
Total	-0.4651	0.1847	-0.0102	0.5006	0.0443

As these tables show, the trend observed in the oscillator strengths of the total conformers applies to the group oscillator strengths as well. Table 108 shows that the group oscillator strengths for the first excited state decrease as the torsion angle decreases, but increase with decreasing torsion angle for the third excited state, as shown in Table 109. A plot of the silyl oscillator strengths versus the torsion angle for both states is given in Figure 101.

Figure 101: Silyl Group Oscillator Strengths vs Torsion Angle

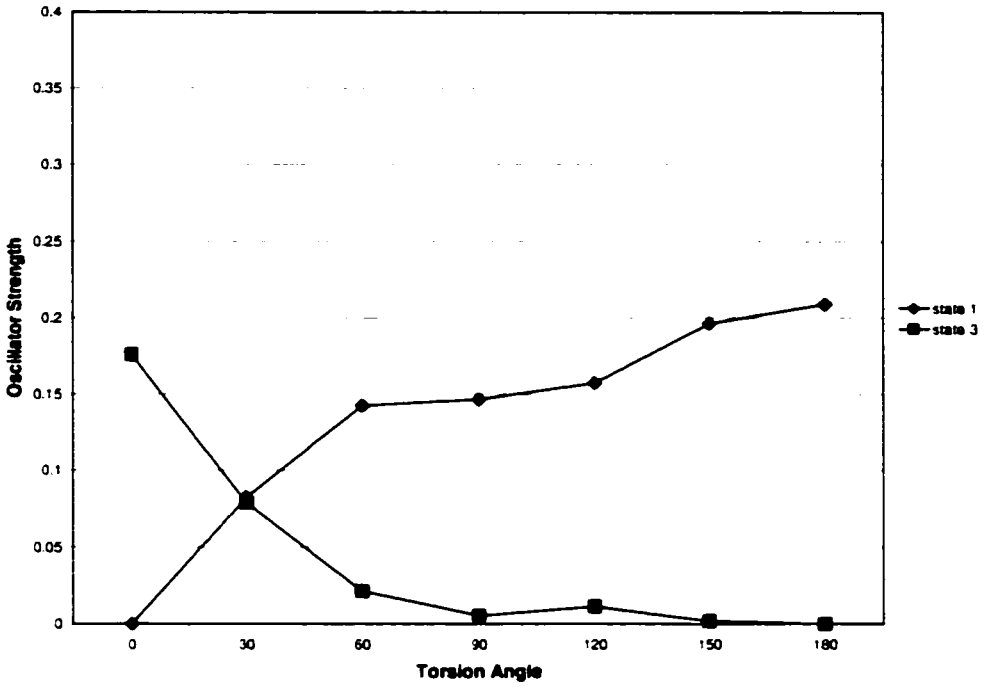

As with the total oscillator strengths shown in Figure 99, the first excited state loses intensity, while the third excited state gains intensity. Reference to Table 103 gives the oscillator strength of the silyl group in tetrasilane to be 0.1925 au, a value slightly higher than that of the silyl group in the 0° conformation of hexasilane. Thus, as the torsion angle decreases, the hexasilane excitation loses intensity, and a new 'tetrasilane' excitation becomes dominant, not only for the molecule as a whole, but for the groups as well. This argument is further strengthened by Figure 102, which shows the change in oscillator strength for an α-silylene group as a function of torsion angle. While the trend is no different to that seen in Figure 101, what is important is that the 0° conformer oscillator strength is much lower than that of the 180° conformer.

Figure 102: α-Silylene Group Oscillator Strengths vs Torsion Angle

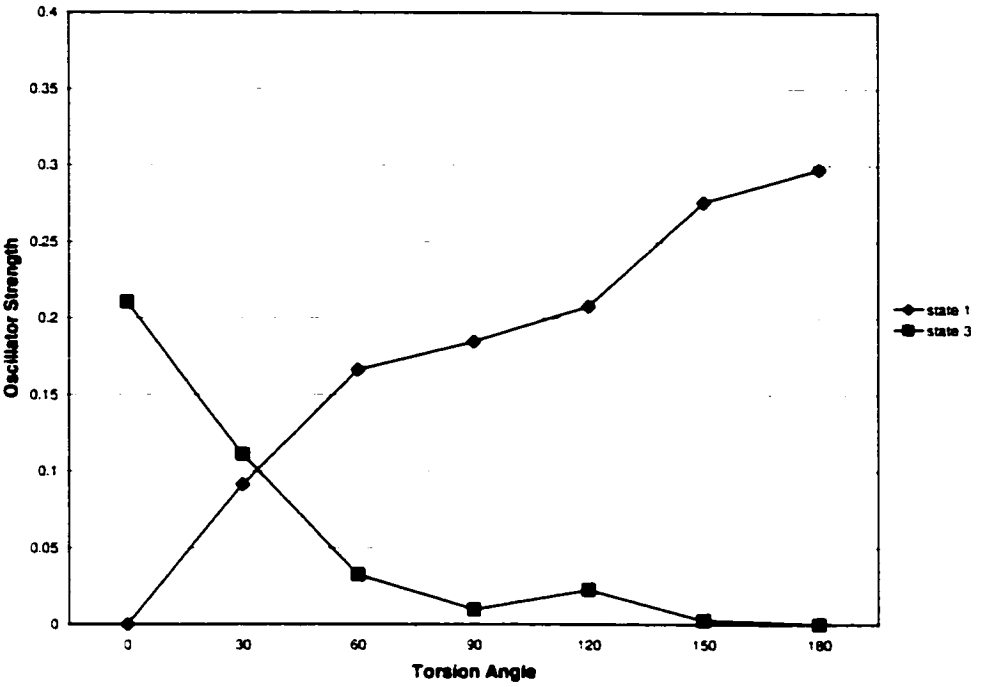

The oscillator strength of the internal silylene group in tetrasilane is 0.2291 au, a value in close agreement to the 0° conformer α-silylene group oscillator strength of 0.2106 au. This shows conclusively that the third excited state is effectively a tetrasilane-like excitation, which gains dominance as the torsion angle decreases.

Figure 103 shows a trend which does not appear to fit what has been observed so far. Rather than the third excited state of the internal silylene group increasing to about the same amount as the α-silylene group, the 0° conformer oscillator strength is nearly equal to that of the 180° conformer. An explanation for this can be developed from the arguments made earlier concerning the number of charge concentrations involved in the 0° conformer excitation. If three of the five charge concentrations are involved to create a doubly strong tetrasilane-like excitation, then there must be some overlap concerning the central charge concentration for each of these tetrasilane-like excitations. If one adds together the oscillator strengths of the silyl and silylene groups in tetrasilane, one ends up with a value of 0.4216 au, a value not far from the value of 0.3711 au for the internal silylene group of the 0° conformer.

Figure 103: Internal Silylene Group Oscillator Strengths vs Torsion Angle

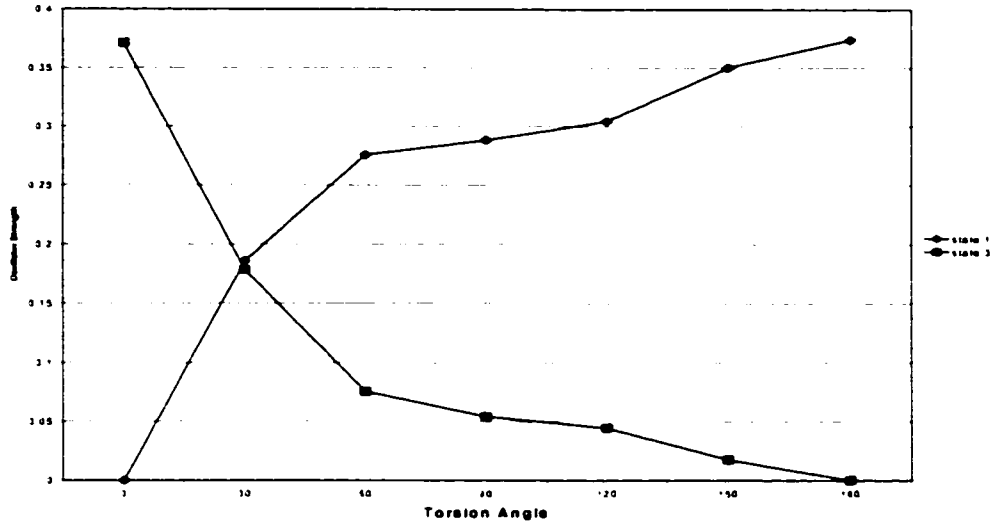

A final point about these oscillator strengths is the fact that while the first excited state shows a gradual loss in intensity as the torsion angle decreases, the third excited state still remains quite weak until 60°, where it undergoes a dramatic increase in intensity. A possible reason for this is the relative stability of each excited state: the chain length studies performed showed that the group transition dipoles were highly coherent, all pointing in the same direction. It seems logical then, that a weak molecular transition would have incoherent group transition dipoles. In general, oscillator strengths tend to have a much lower sensitivity to changes in environment than do transition dipoles, as was seen in Figure 77 and Figure 78. The same is true for the torsion study: it is very difficult to gauge how the dipole directions relate to the molecular framework for each excited state. Fortunately, graphical software is such that these vectors can be easily visualized within the context of the molecular framework they represent. The following pictures were created using author-developed software, which shows the direction and relative magnitude of each group transition dipole moment, centered on each silicon atom. Only select examples will be used to illustrate this point, namely the excited states of the 0°, 30°, 150° and 180° conformers.

Figure 104: Vector Map of Transition Dipoles in 0° Conformation, State 3

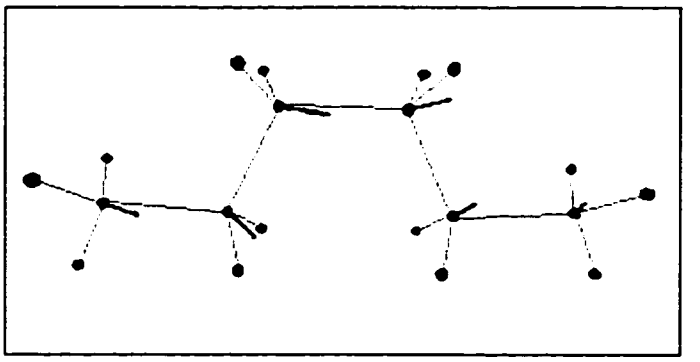

Figure 104 shows the direction of the group transition dipoles for the 0° conformer. Unlike the chain length study, which showed the transition dipoles to be perpendicular to the plane of the group, these dipoles tend to be more parallel to the group plane. This picture gives the impression that rather than pointing along each half of the backbone as expected, the transition dipole points perpendicular to it. While this gives a molecular dipole that points in the expected direction, it shows that the group contributions are of a different type.

Figure 105: Vector Maps of Transition Dipoles of 30° Conformer, States 1 (left) and 3 (right)

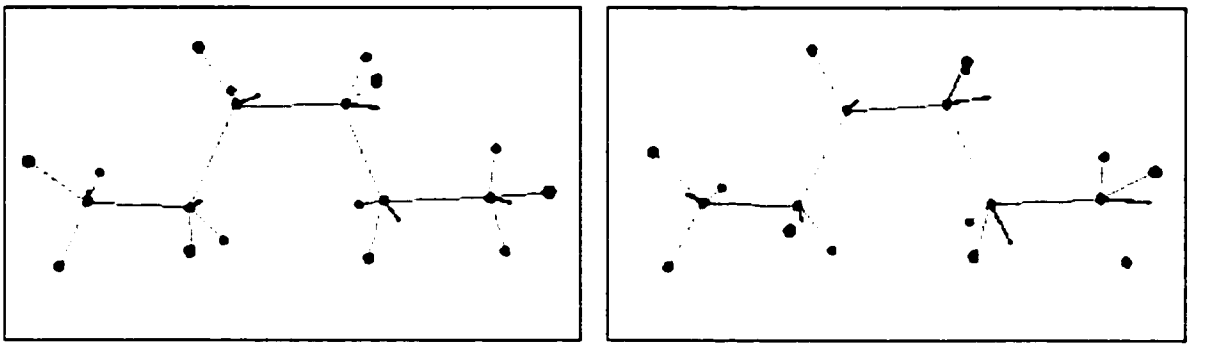

The 30° conformer, shown in Figure 105, shows both the first and third excited states, and their transition dipoles. The first exited state, shown on the left, already has dipoles pointing perpendicular to the group planes, as expected. The third excited state has some dipoles pointing parallel to their group planes, though some start to deviate. This can be looked at as a result of the gradual destabilization and weakening of this excited state, as the torsion angle increases.

Figure 106: Vector Maps of Transition Dipoles of 150° Conformer, States 1 (left) and 3 (right)

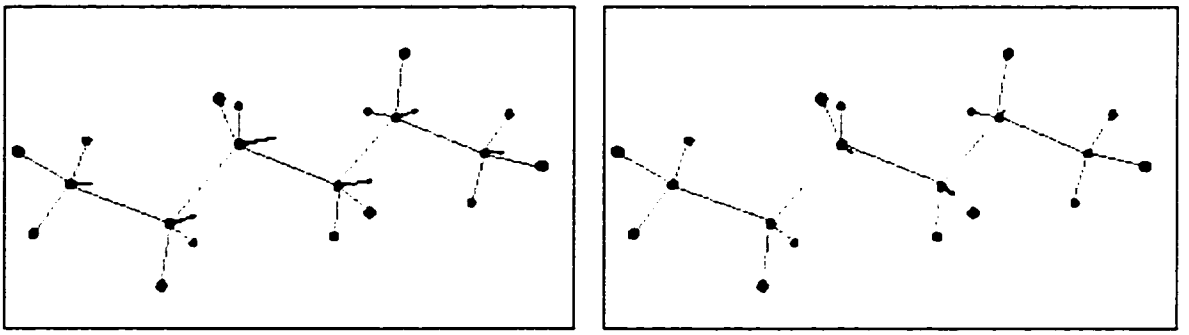

The 150° conformer, shown in Figure 106, shows how weak the third excited state (on the right) has become at this point relative to the first. The dipoles themselves are barely discernible, and show no pattern of direction at all. Figure 107 shows the first excited state dipoles of the 180° conformation, which, like the other species examined in the chain length study, all point in the same direction: perpendicular to the silylene group, and along the molecular backbone.

Figure 107: Vector Map of Transition Dipole of 180° Conformer, State 1

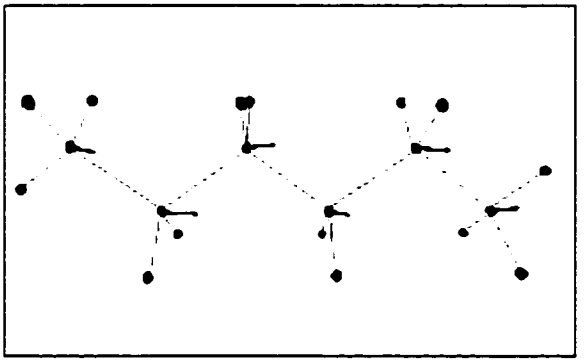

These pictures show that the two excited states in question are indeed very different. The first excited state is in fact the same one observed in the chain length study, with group dipoles that remain true with respect to the expected direction as well as magnitude. The third excited state, however, is more complicated. While the oscillator strength data indicates a tetrasilane-like transition, the group dipoles are in fact parallel to the group planes, rather than perpendicular. This does make sense, in terms of the excitations taking place. If the third excited state was in fact a simple combination of two tetrasilane excitations pointing along each half of the backbone, then the dipoles would be perpendicular to the group planes for that

excitation as well. This would make both excitations indistinguishable, so the dipoles point in the only direction left available. Clearly this third excited state dipole direction is far less stable than the first excited state dipole, as shown by the loss of coherence of the groups as the torsion angle increased: this is understandable, since this direction is perpendicular to the local string of charge concentrations present. It is only for the 0° conformer that this pattern is energetically favorable: the first excited state becomes much more intense, and thus more probable, even at low torsion angles.

6.2.2.2 Transition Densities

While the transition density data, in particular the oscillator strengths, reveal a great deal about the nature of the excitations of these conformers, the contour plots of the transition densities prove to be far easier to visualize. Only the 0°, 30°, 150° and 180° conformer plots will be shown, as these will provide an adequate idea of the trends that take place.

Figure 108: Transition Density Contour Plot of 0° Conformer, State 3

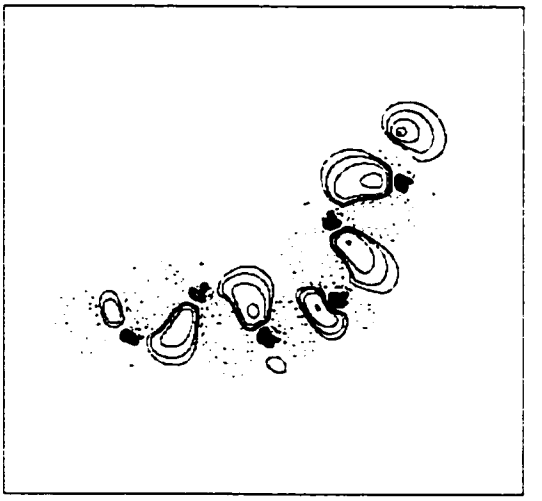

The 0° conformer plot, shown in Figure 108, shows how the transition density adapts to the bond torsion. Of particular note is the central Si-Si bond region, where the lobes are considerably smaller than the rest of the molecule, which looks quite similar to the structures observed in the chain length study. The inference from this is that the lobes in this central region are partially cancelled, implying overlap of two smaller transition densities. Another possibility is that the central bond looks similar to the transition density of disilane, with a net loss of density at the central Si-Si bond, and a separation of the electronic structure of

the two halves of the molecule.

Figure 109: Transition Density Contour Plots of 30° Conformer, State 1 (left) and State 3 (right)

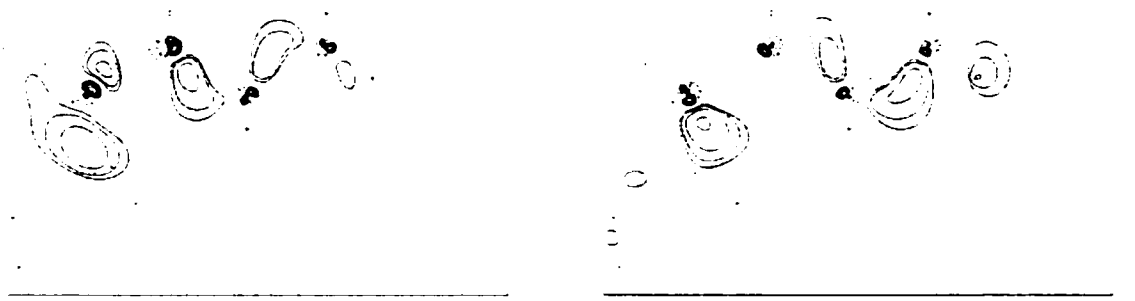

The 30° conformer, shown in Figure 109, provides the first opportunity to examine the differences between two excited states, the weak first excited state (on the left) and the stronger third excited state (on the right). The first excited state contour looks quite similar in structure to the 0° conformer, with the small lobes in the central bond region. The third excited state, by contrast, has only one lobe in this region, which is connected to the adjacent lobe of the next bond. This implies a connection between the charge concentrations that form the Si-Si bonds there. The 150° conformer, shown in Figure 110, shows yet different structures in the transition density. The first excited state (left) looks much more like the transition densities seen in the chain length studies, with the lobes of the central Si-Si bond region having that same recognized shape. The third excited state (right) is completely unlike the 30° conformer: the lobes in the central bond region are transverse to what is seen in the chain length studies, and the other bond regions only have single lobes. This implies that the transition dipole is pointing in a completely different direction from what has been seen in earlier studies, and that the groups within are no longer behaving in the 'standard' manner.

Figure 110: Transition Density Contour Plots of 150° Conformer, State 1 (left) and State 3 (right)

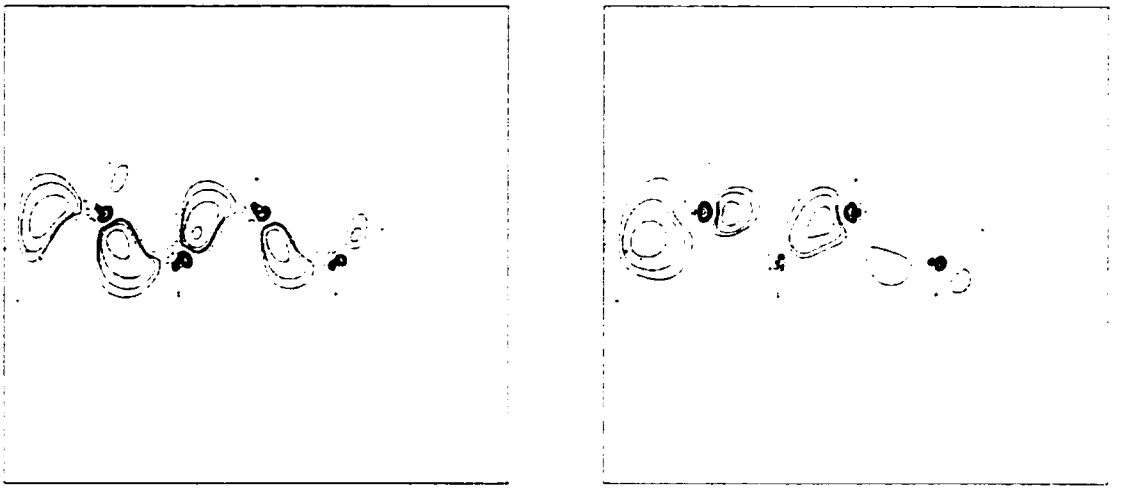

The last contour plot is that of the 180° conformer, shown in Figure 111. This transition density looks like the others seen in the chain length study, confirming the expected behavior of the transition dipoles in this conformer.

Figure 111: Transition Density Contour Plot of 180° Conformer, State 1

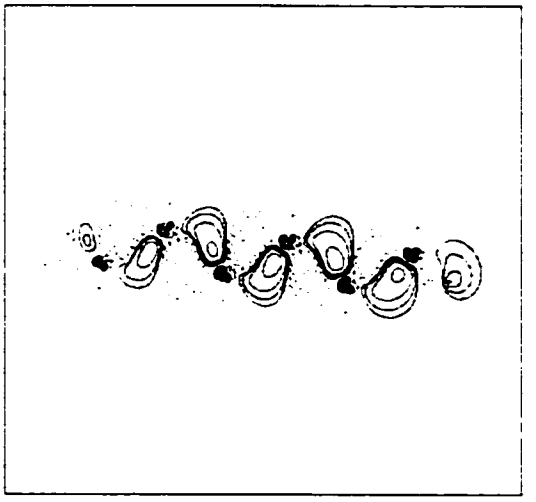

These contour maps indicate something that the previous transition dipole data hinted at, that while the first excited state is similar to that seen in the chain length studies, the third excited state is quite different. Given the relative intensities and energies of the two states with respect to torsion angle, it is clear that the third excited state is not a normal one for hexasilane. As the torsion angle increases, the first excited state adopts a 'stable' transition density structure, while the third excited state becomes increasingly unstable.

6.2.2.3 Excited State Properties

The changes in molecular properties as a result of excitation provide an excellent picture of how the torsion angle affects the way the density rearranges, as well as providing insight into the character of each excited state. Table 110 provides information about the ground state properties of the different conformers of hexasilane. For the purposes of the quadrupole moments, the long axis of the molecule is along the *z*-axis, and the short axis along the y-axis. The first important feature of this table is the insensitivity of the group populations and volumes to the torsion angle, in particular the central silylene groups. This is reasonable, as the barrier to bond rotation is relatively small, and only minor changes to the molecular geometry and the electron density would result.

Table 110: Atomic Properties of Si_6H_{14} Conformers: Ground State

Torsion Angle	N(Ω)	Q_{xx}(Ω)	Q_{yy}(Ω)	Q_{zz}(Ω)	v(Ω)
0					
$Si1H_3$	16.9827	1.2118	0.0030	-1.2147	357.69
$Si2H_2$	16.0200	2.7210	-0.5618	-2.1591	297.58
$Si3H_2$	15.9985	2.6579	-0.4638	-2.1941	293.25
30					
$Si1H_3$	16.9835	1.1485	1.2188	-2.3673	357.99
$Si2H_2$	16.0197	2.6055	-0.6825	-1.923	298.92
$Si3H_2$	16.0009	2.3386	-0.7181	-1.6205	293.47
60					
$Si1H_3$	16.9821	0.9618	1.2188	-2.1806	357.81
$Si2H_2$	16.0119	2.1259	-0.0769	-2.049	293.64
$Si3H_2$	16.0027	1.7039	-0.1103	-1.5936	293.84
90					
$Si1H_3$	16.9847	0.5973	1.2332	-1.8305	358.09
$Si2H_2$	16.0131	0.8186	0.9375	-1.756	294.89
$Si3H_2$	16.0031	0.9650	0.7318	-1.6968	294.13
120					
$Si1H_3$	16.9864	1.2304	0.4023	-1.6326	358.12
$Si2H_2$	16.0082	1.7664	0.2082	-1.9745	294.46
$Si3H_2$	16.0044	1.7514	0.1670	-1.9814	294.27
150					
$Si1H_3$	16.9872	1.2197	0.2647	-1.4844	358.23
$Si2H_2$	16.0078	2.4095	-0.1938	-2.2156	294.55
$Si3H_2$	16.0046	2.4879	-0.3536	-2.1342	294.06
180					
$Si1H_3$	16.9868	1.2288	0.1722	-1.401	357.95
$Si2H_2$	16.0079	2.7132	-0.4105	-2.3117	294.06
$Si3H_2$	16.0045	2.6817	-0.4754	-2.2063	293.87

The quadrupole moment shows the same polarization along the long axis of the molecule, as expected; the minor polarizations along the y-axis are due to the orientation changes needed to keep the long axis of the molecule lying along the z-axis.

Table 111 contains the excited state integration data of those conformers that yield strong intensities in the first excited state; all trends for this state will be discussed in terms of decreasing torsion angle or decreasing transition intensity. It is remarkable that the volume increase is still very low for the excitation, and that the small volume increases do not change appreciably with torsion angle. This indicates the same kind of excitation as seen in the chain length study, where electron density is rearranging in the backbone of the molecule, with little contribution from the ligands. As with the other molecules calculated in that study, a small amount of density moves from the central groups to the silyl groups in the 180° conformer of hexasilane.

Table 111: Changes in Atomic Properties of Si_6H_{14} Conformers Upon Excitation: State 1

Torsion Angle	$\Delta N(\Omega)$	$\Delta Q_{xx}(\Omega)$	$\Delta Q_{yy}(\Omega)$	$\Delta Q_{zz}(\Omega)$	$\Delta v(\Omega)$
30					
$Si1H_3$	-0.0642	-0.2127	-0.2327	0.4454	-1.04
$Si2H_2$	-0.0228	-0.5139	0.1445	0.3694	1.64
$Si3H_2$	0.0852	-2.0010	-0.0463	2.0473	15.38
60					
$Si1H_3$	-0.0274	-0.2437	-0.2556	0.4993	3.73
$Si2H_2$	-0.0119	-0.4711	0.0923	0.3788	28.24
$Si3H_2$	0.0411	-1.8566	-0.0148	1.8714	8.91
90					
$Si1H_3$	-0.0251	-0.3276	-0.1850	0.5126	2.71
$Si2H_2$	-0.0070	-1.2000	0.0888	1.1111	2.96
$Si3H_2$	0.0002	-2.5720	0.2701	2.3018	8.86
120					
$Si1H_3$	-0.0231	-0.1542	-0.4151	0.5692	2.63
$Si2H_2$	0.0076	0.2502	-1.5873	1.3369	3.23
$Si3H_2$	0.0173	0.3090	-2.9847	2.7386	9.23
150					
$Si1H_3$	-0.0105	-0.1322	-0.4972	0.6294	3.19
$Si2H_2$	0.0024	0.2558	-1.9300	1.6742	3.00
$Si3H_2$	0.0039	0.3152	-2.9735	2.6582	6.98
180					
$Si1H_3$	0.0067	-0.0428	-0.6272	0.6701	4.76
$Si2H_2$	-0.0004	0.2522	-2.1053	1.8621	3.85
$Si3H_2$	-0.0043	0.3095	-2.9218	2.6123	5.18

As the torsion angle decreases, however, the opposite trend occurs. There is an increasing buildup of density at the central silylene groups, to the point where both the silyl and α-silylene groups are losing density to the central silylene groups. As the torsion angle decreases, the silyl group population changes are very small, about +0.01 au at 180°, and increase to about -0.07 au at 30°. Another observation is that of the volumes: as the torsion angle decreases, the volume of the central silylene group increases, with a sharp rise at 30°. The α-silylene group volume remains fairly constant with torsion angle, with a sharp increase at 60° and a return to a similar volume at 30°. The silyl group volume actually decreases with torsion angle, with a volume at 30° that is smaller than the ground state. It is the quadrupole moments, however, that show the most dramatic changes. As Table 110 showed, the polarization of the density of each silicon lies along the *z*-axis or long axis of the molecule. This remains true for the silyl group in the first excited state: as seen in the ground state, this polarization increases with decreasing torsion angle. For the α-silylene groups, a much different trend occurs. As the torsion angle decreases, the polarization of the silicon changes direction, from along the y-axis, as expected from the observations made in the chain length study, to along the *z*-axis. The internal silylene group shows the most change in the quadrupole moment, with the polarization lying along the y-axis in the 180° conformer, shifting to the x-axis at 90°, and then back to the y-axis at 30°, with intermediate changes at 60°. Clearly, there are important changes in the rearrangement of electron density upon excitation as the torsion angle decreases.

Table 112: Changes in Atomic Properties of Si_6H_{14} Conformers Upon Excitation: State 3

Torsion Angle	$\Delta N(\Omega)$	$\Delta Q_{xx}(\Omega)$	$\Delta Q_{yy}(\Omega)$	$\Delta Q_{zz}(\Omega)$	$\Delta v(\Omega)$
0					
$Si1H_3$	-0.0276	-0.1338	0.3828	-0.2491	4.21
$Si2H_2$	0.0047	0.3573	-0.1641	-0.1933	3.95
$Si3H_2$	0.0283	-0.0147	-1.1007	1.1154	7.95
30					
$Si1H_3$	-0.0775	-0.1578	-0.4061	0.5639	0.00
$Si2H_2$	0.0043	0.1401	-0.4256	0.2855	5.20
$Si3H_2$	0.0700	-0.2266	-0.8558	1.0824	14.93
60					
$Si1H_3$	-0.0882	-0.1332	-0.4065	0.5397	-1.68
$Si2H_2$	0.0505	-0.2649	-0.4497	0.7145	11.52
$Si3H_2$	0.0484	-0.3478	-0.6317	0.9795	11.68
90					
$Si1H_3$	-0.1116	-0.0936	-0.4505	0.5441	-2.40
$Si2H_2$	0.0660	-0.0623	-0.5946	0.6569	11.26
$Si3H_2$	0.0456	-0.5810	-0.4360	1.0170	14.29
120					
$Si1H_3$	-0.1355	-0.4480	-0.1334	0.5812	-2.53
$Si2H_2$	0.0514	-0.6935	-0.1278	0.8212	12.95
$Si3H_2$	0.0873	-0.2913	-1.1971	1.5514	23.20
150					
$Si1H_3$	-0.1400	-0.4670	-0.0542	0.5212	-4.11
$Si2H_2$	0.0775	-1.4050	-0.1099	1.5148	14.91
$Si3H_2$	0.0630	-0.5411	-0.9928	1.5339	18.28

These results imply that there is minimal rearrangement of the silyl density at any torsion angle, and that the α-silylene group density becomes decreasingly rearranged as the torsion angle decreases, becoming more like the density in the ground state. Only the internal silylene groups show rearrangement at all torsion angles, with the density polarization shifting from the y to the x-axis and back, being more a factor of molecular geometry than anything else.

Table 112 shows the changes in those conformers that yield strong intensities in the third excited state. The group population changes are much larger than those observed in the first excited state. For these results, it is easier to discuss them in terms of increasing torsion angle, which is the direction in which this transition loses intensity. At the 0° conformer, the silyl group population is slightly lower than that of the ground state, and decreases in population as the torsion angle increases, about 0.1 au. Both the α-silylene and internal silylene groups show a small increase in population with increasing torsion angle, indicating that most of the density shift in this excited state comes from the silyl group. What is important to note is

how the populations change for both excited states relative to the ground state. As was seen previously, the change in silyl population changes was small for the first excited state, about +0.01 au to -0.06 au with decreasing torsion angle. For the third excited state, the silyl population change starts at -0.03 au at 0°, and increases with increasing torsion angle to -0.14 au at 150°. The volume changes are more drastic in the third excited state as well: the silyl volume decreases with increasing torsion angle, actually becoming smaller than the ground state volume. The volumes of both types of silylene groups increase, in agreement with the population changes observed. The quadrupole moments show some trends similar to that of the first excited state. The silyl group polarization remains pointed along the z-axis for all torsion angles, and decreases with increasing torsion angle. The α-silylene group behaves the same way, in contrast to the first excited state, which showed a shift in the direction of polarization with torsion angle change. The internal silylene group remains for the most part polarized along the y or short axis, shifting to the z-axis at 90° and back to the y-axis at 120°. Unlike the first excited state, the extent of rearrangement in the molecule does not change much with torsion angle, according to the quadrupole moments, even though there are more substantial changes in population and volume. Analysis of the atomic populations of these groups shows an important difference between the third excited state and the first excited state. Unlike the first excited state, the populations of the hydrogen ligands change appreciably in the third excited state, as the volume changes imply. The third excited state sees an increasing shift of density into the hydrogens as the torsion angle increases. This explains why there is such a difference in group populations in the third excited state as a function of torsion, even though the polarizations of the silicons do not change direction.

Figure 112 shows the total amount of electron density that shifts from the ligands to the backbone for both excited states, as a function of the torsion angle.

Figure 112: Total Change in Population Upon Excitation, in Silicon Backbone and in Ligands, vs Torsion Angle, in Si_6H_{14}

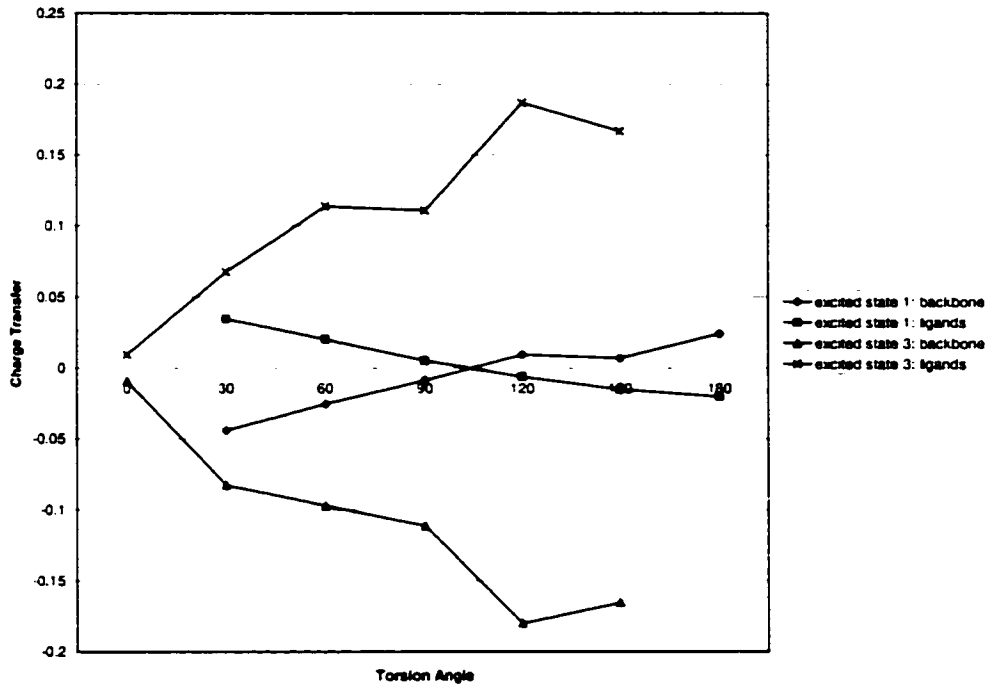

The graph shows that for the first excited state, there is a small net transfer of density from the ligands to the backbone in the 180°, in agreement with the chain length studies. As the torsion angle decreases, however, that density transfer decreases, eventually resulting in a net transfer of density from the backbone to the ligands. For the third excited state, there is already a small net transfer of density from the backbone to the ligands; as the torsion angle increases, this transfer grows dramatically, reaching a 17-fold increase in the 150° conformation. Though the net loss/gain of electron density should result in mirror images of the graphs, integration error results in slight deviations in the charge transfer plots.

6.2.2.4 Excited State Densities

The contour plots of the electron densities of the ground states and excited states of these conformers help to illustrate the overall picture of how the electron density redistributes itself upon excitation. Figure 113 and Figure 115 contain the rho and L(r) contour plots for the 0° and 30° conformers of hexasilane, respectively. For the purposes of this discussion, only the contour plots of the 0°, 30°, 150° and 180° conformers will be studied in detail, as these will be adequate to discuss the overall trends.

L(r) of the 0° conformer, shown in Figure 113, shows an interesting structure; on either side of the central Si-Si bond are two geminal points that are spatially close together. Any buildup of density between the charge concentrations would cause a great deal of density to build up in this one position, which would be an energetically unfavorable situation.

Figure 113: Ground State Contour Plot of 0° Conformer

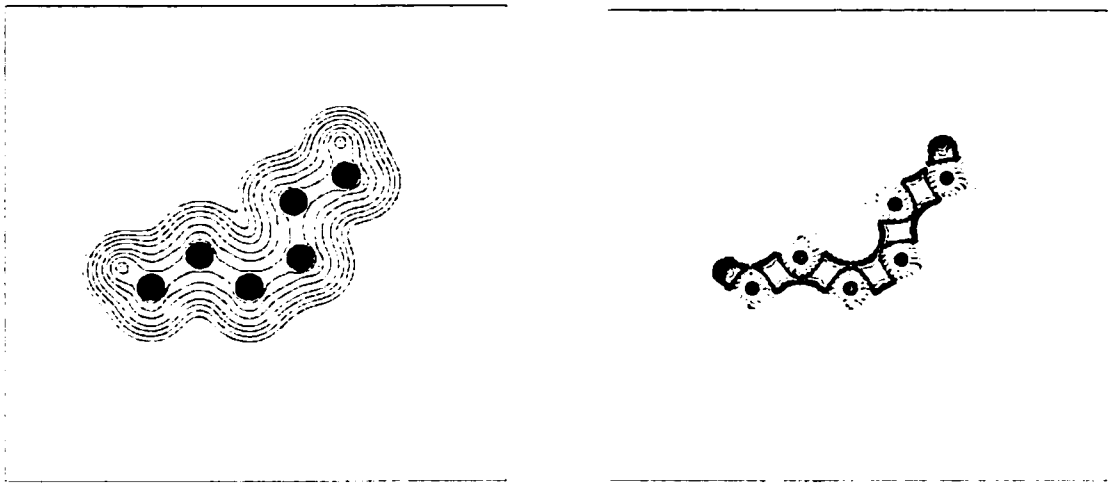

Figure 114 shows the contour plot for the third excited state of the 0° conformation.

Figure 114: Contour Plot of 0° Conformer, Excited State 3

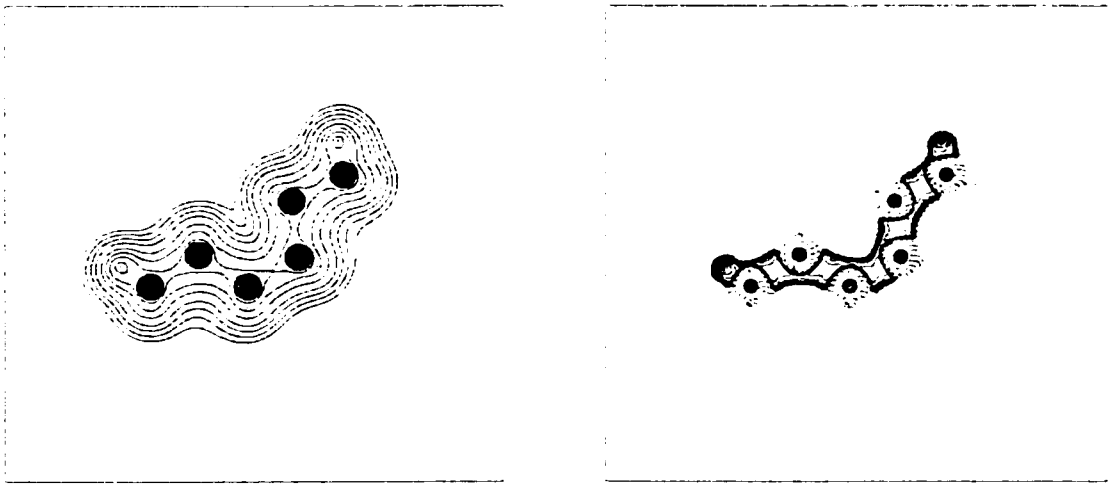

As implied by the integration data, the central Si-Si bond loses the most density, with the amount of vicinal density lost decreasing as one proceeds towards the ends of the molecule. The geminal points on either side of the central Si-Si bond do not appear to be as large as those near the ends. This can be explained through

the integration data, which shows an increase in ligand population in the third excited state of this conformer, as previously described. Rather than shift into the geminal positions, the density lost from the central vicinal points moves to the ligands instead.

Figure 115: Ground State Contour Plot of 30° Conformer

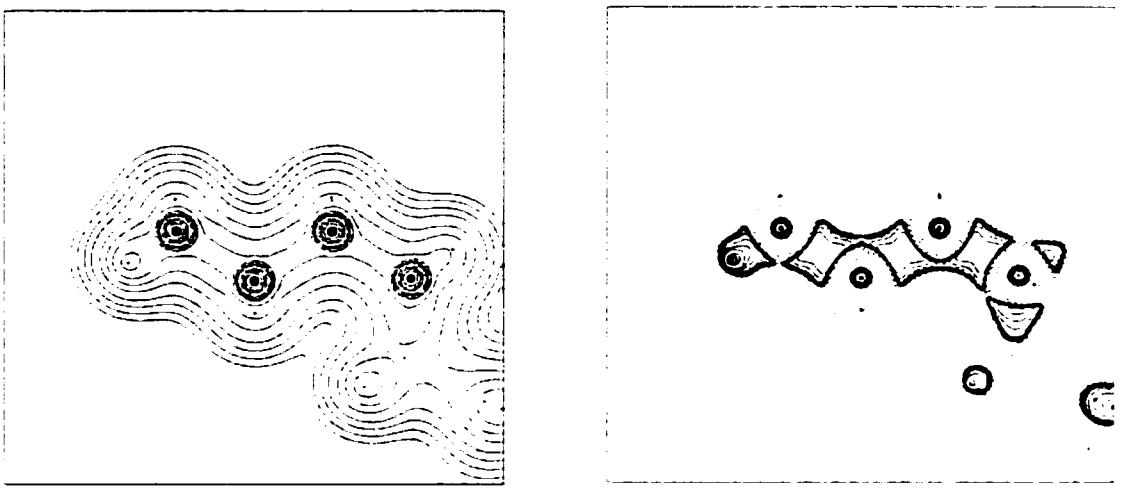

Figure 115 shows the contour plot of the 30° conformer. The plane selected contains only four of the six silicons, so as to show the changes in the bonds between them. Despite the change in the central bond angle, the Si-Si bonds remain quite similar topologically. The first excited state for this conformation (Figure 116) shows some buildup in the geminal positions, and corresponding loss of density within the vicinal charge concentrations. It is interesting to note that the central charge concentration seems to have undergone the greatest loss, and that the loss of density at the vicinal points decreases towards the end of the molecule, even though the two geminal points look quite similar. The fact that the internal silylene groups gain density upon excitation can be explained by the fact that some of the density gained from the vicinal points moved to the internal silylene group hydrogens.

Figure 116: Contour Plot of 30° Conformer, Excited State 1

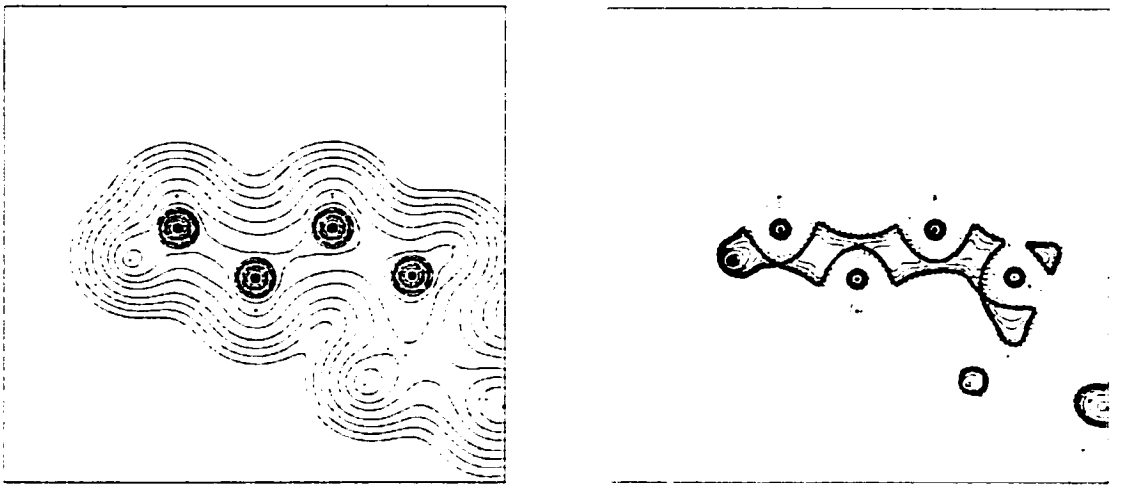

The third excited state, shown in Figure 117, is comparable in structure to the contour plots of the first excited state. Atomic and group populations indicate that the amount of electron density that rearranges in both cases is quite similar; seeing that the key changes that occur at the vicinal and geminal points will require quantitative measurements at the L(r) critical points, which will be shown later.

Figure 117: Contour Plot of 30° Conformer, Excited State 3

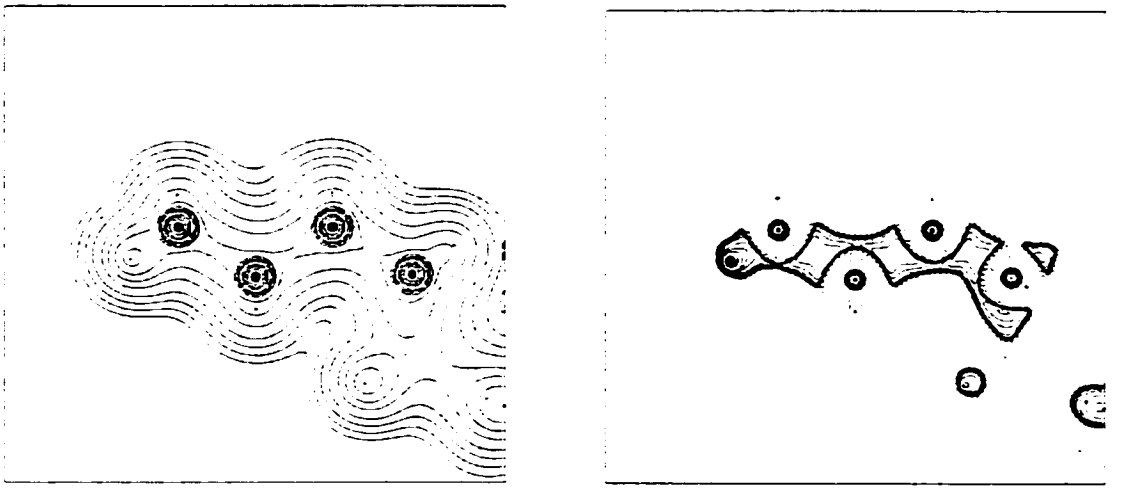

The 150° conformer shows the differences between the first and third excited states much more clearly. Figure 118 shows the rho and L(r) contour plots of this conformer in the ground state. Much like the other conformers presented, this one shows little change in bonding as a result of the torsion angle. This would be expected of a species only 30° short of a fully staggered conformation.

Figure 118: Contour Plot of 150° Conformer, Ground State

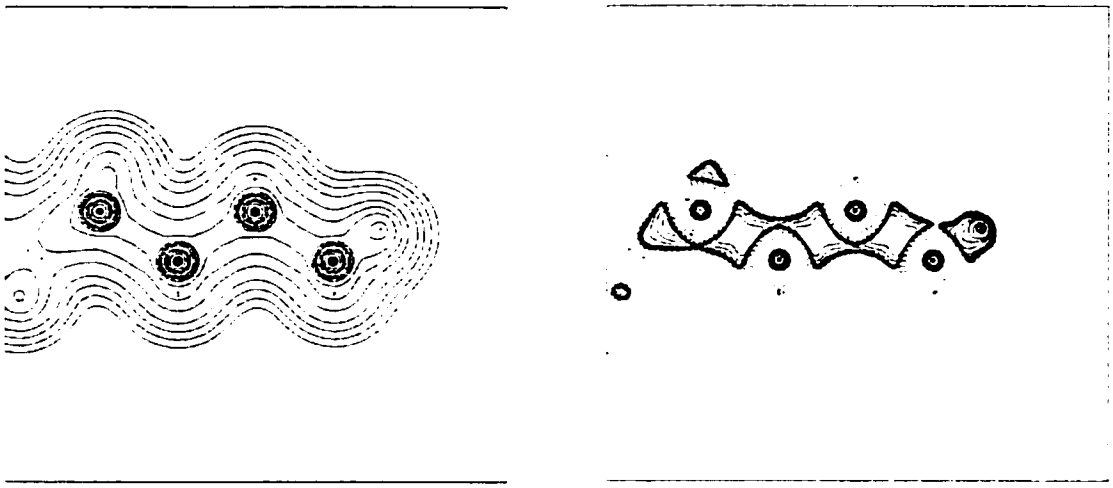

The first excited state of the conformer, shown in Figure 119, illustrates how the density redistributes upon excitation. The vicinal charge concentration between the silyl and α-silylene groups shows no discernible loss of density, while the vicinal charge concentrations between both types of silylene groups show far greater density loss. There is also a substantial increase in the density at the geminal positions; overall, the 150° conformer is behaving much like the 180° conformer in the first excited state.

Figure 119: Contour Plot of 150° Conformer, First Excited State

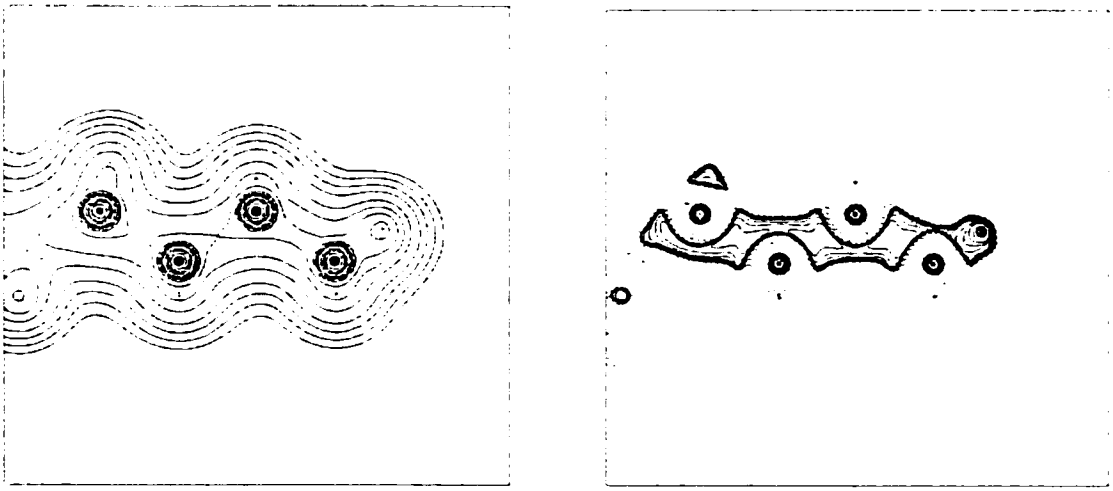

The third excited state, shown in Figure 120, tells a much different story. All three vicinal charge concentrations present show little sign of depletion, and the only area that has lost density is the in-plane hydrogen. Given that the populations of both types of silylene groups increase on excitation, and that the

majority of increase is on the hydrogens, it can be seen that the backbone density is playing a far smaller role in density rearrangement in the third excited state of this conformer.

Figure 120: Contour Plot of 150° Conformer, Third Excited State

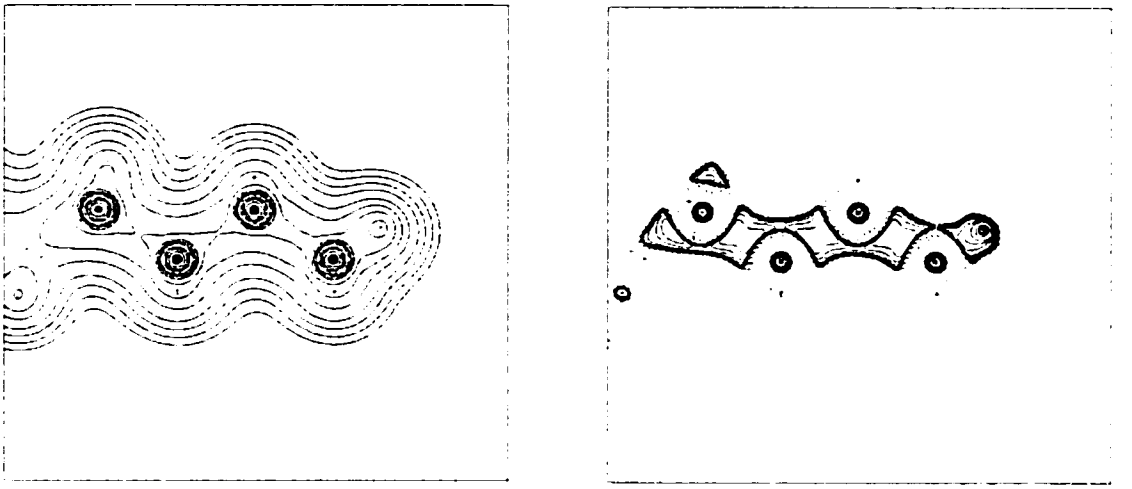

The final conformer to be studied is the 180° conformer. As Figure 121 shows, the ground state looks no different from the other species shown in the chain length study.

Figure 121: Contour Plot of 180° Conformer, Ground State

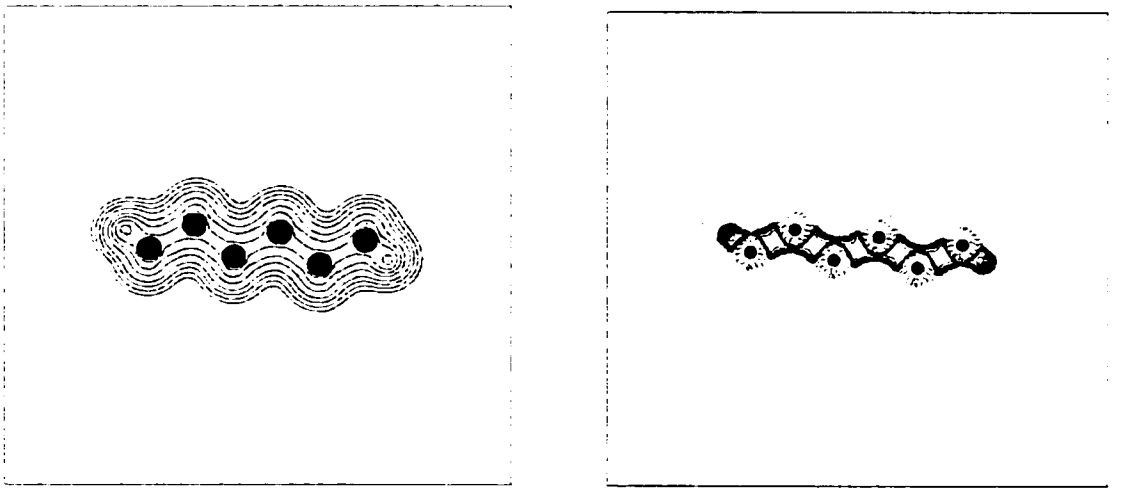

Figure 122 shows the 180° conformer in the first excited state, the only dominant excitation for this species. As seen in the chain length study, there is the observed rearrangement of the backbone density, with the five vicinal charge concentrations losing density, and the four geminal points gaining density.

Figure 122: Contour Plot of 180° Conformer, First Excited State

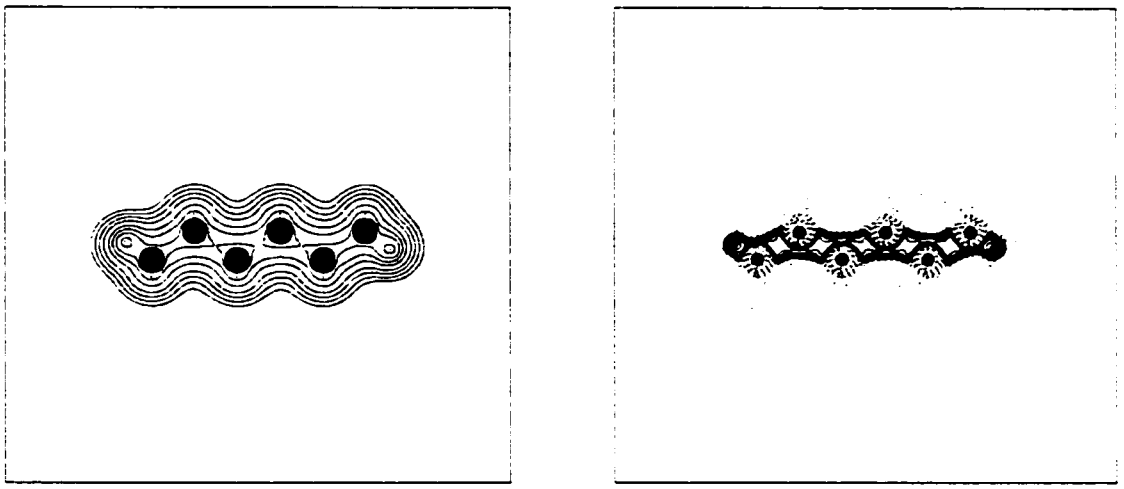

While the contour plots reveal much about the way the electron density rearranges for both excited states, a more quantitative discussion is required to explain what is occurring. The following are graphs of rho at the various vicinal and geminal (3,-1) critical points of L(r) of different conformers. The value of rho at these critical points was used, as it is easier to show the changes in the trends; the trends shown here are the same as those seen in the values of L(r).

Figure 123 : Electron Density at Vicinal (3,-1) Critical Points in L(r) for Different Conformers of Si_6H_{14}, Ground State

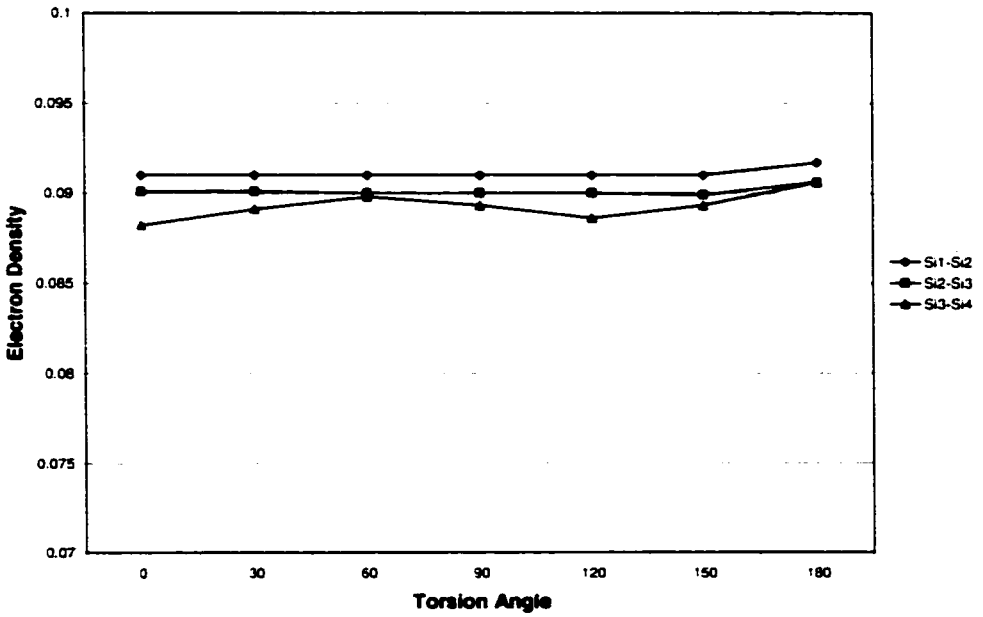

As Figure 123 shows, the values of electron density at these vicinal critical points in L(r), which coincide with the Si-Si BCP positions, show little change in value with torsion angle. The exception to this is the vicinal point for the central Si-Si bond itself, which follows the same pattern observed in the molecular energies of Figure 97. As the molecule enters an eclipsed geometry, the central Si-Si BCP loses density.

Figure 124: Electron Density at Vicinal (3,-1) Critical Points in L(r) for Different Conformers of Si_6H_{14}, First Excited State

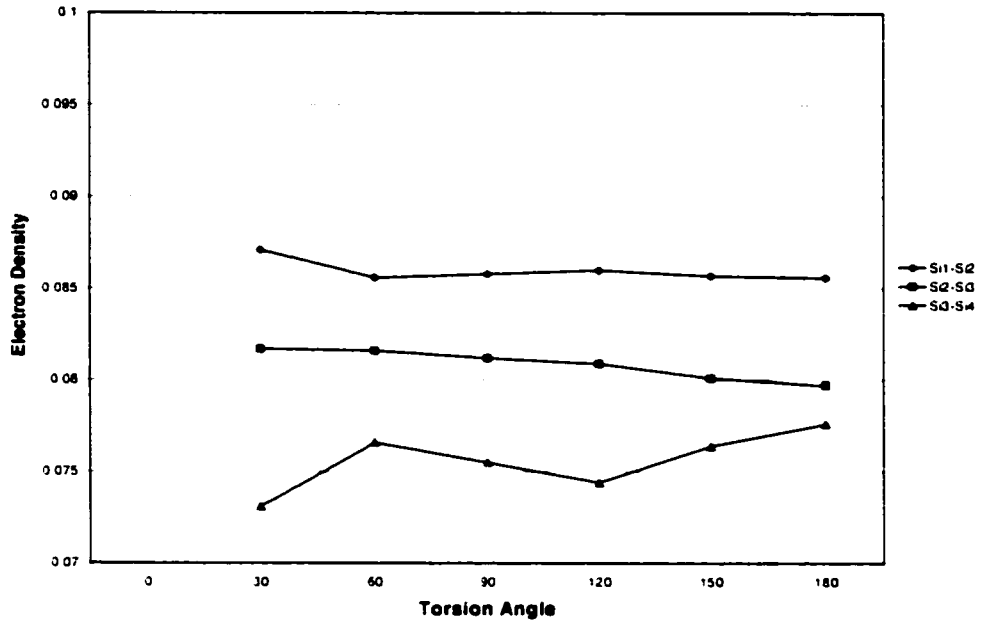

Upon excitation to the first excited state, one sees a marked decrease in the magnitude of rho at these vicinal points, as expected from the results of the chain length study (Figure 124). As the torsion angle (and thus transition intensity) decreases, one can see that the silyl-α-silylene and α-silylene-internal silylene vicinal points gain density. Meanwhile, the central vicinal point, while following the same pattern observed in Figure 123, loses density overall. As the integration results implied, there seems to be an increased localization of the rearrangement of density in the backbone, where the central vicinal point appears to take on an increasing load of the density rearrangement.

Figure 125: Electron Density at Vicinal (3,-1) Critical Points in L(r) for Different Conformers of Si_6H_{14}, Third Excited State

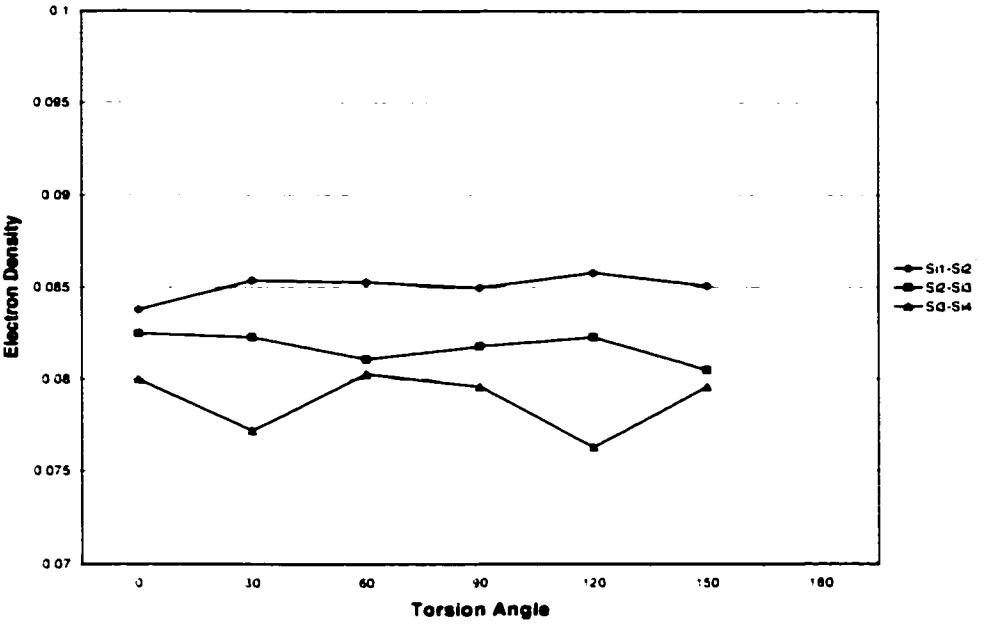

The third excited state, shown in Figure 125, shows a much different pattern. The silyl-α-silylene vicinal point shows no significant change with increasing torsion angle (decreased intensity in the third excited state), while the α-silylene-internal silylene vicinal point shows a very slight decrease, and the central vicinal point also shows little or no overall change. As the atomic integration data of this excited state indicated, one observes increased electron density transfer to the hydrogen ligands with increased torsion angle. This implies a lesser role on the part of the backbone density.

Figure 126 shows the values of rho at the (3,-1) geminal points in L(r) of the ground state hexasilane conformers. There are two types of geminal points in hexasilane, one that lies between the silyl and internal silylene group silicons, and one that lies between the α-silylene group silicons. For the purposes of the graphs, the former shall be called an 'end' geminal point, and the latter, an 'internal' geminal point.

Figure 126: Electron Density at Geminal (3,-1) Critical Points in L(r) for Different Conformers of Si_6H_{14}, Ground State

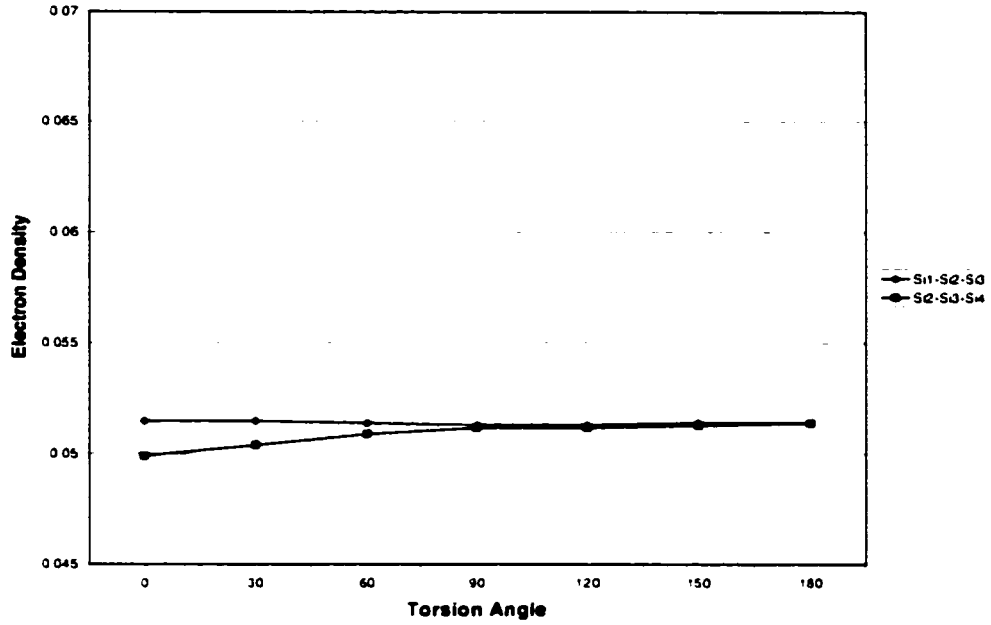

The end geminal point remains unchanged with torsion angle, while the internal geminal point decreases slightly with decreasing torsion angle. This effect can be explained by considering that both internal geminal points are being brought into close proximity, and there should be some increased electron-electron repulsion as a result. Figure 127 shows the change in these geminal points with torsion angle in the first and third excited states. As torsion angle decreases, both the end and internal geminal points lose density. The end geminal point has less density than the internal geminal point, and loses density at a slower rate. Thus, for the first excited state, the amount of density gained at the geminal points decreases as the torsion angle decreases. For the third excited state, a similar trend occurs. As the intensity of the transition decreases (this time with increasing torsion angle), the amount of density gained in the geminal points upon excitation decreases, though the trend is not as smooth as that of the first excited state.

Figure 127: Electron Density at Geminal (3,-1) Critical Points in L(r) for Different Conformers of Si_6H_{14} Excited States

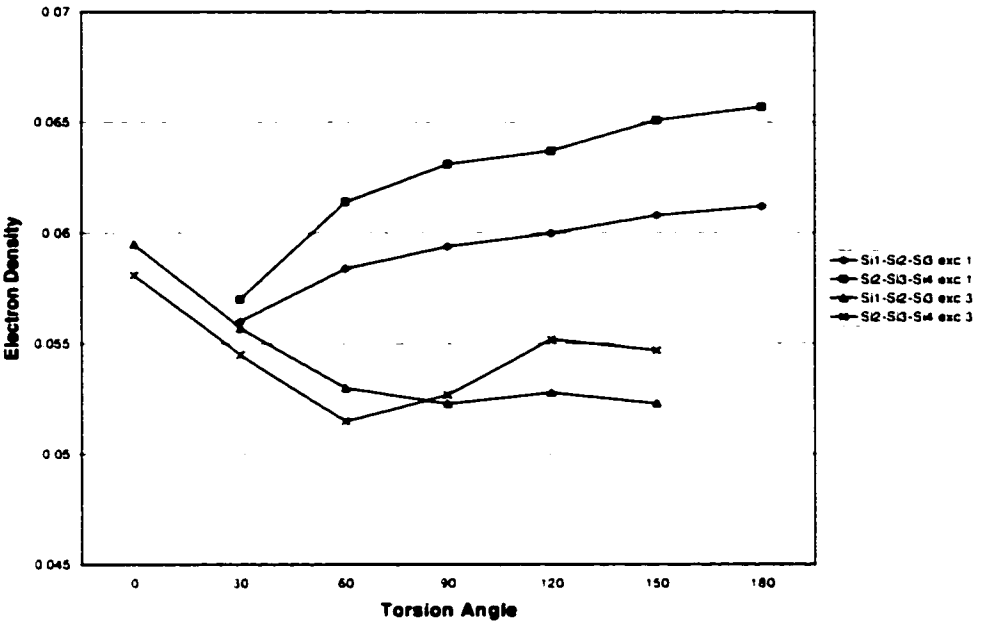

The chain length study showed a simple linear relationship between the net movement of electron density from the backbone vicinal (3,-1) critical points to the backbone geminal (3,-1) critical points in L(r) and the excitation energy; the more density that shifted from the vicinal to the geminal domains for a given excitation, the lower the excitation energy became. From the results shown in the previous figures, and Figure 112, there is a fundamental change in the way density rearranges upon excitation, when the backbone contains a torsional 'kink'. The outermost vicinal points show a small decrease in loss upon excitation as the torsion angle decreases, while the central vicinal point shows an increase in loss. This indicates less participation from the vicinal domains outside the torsion, with most of the loss coming from the central vicinal point. The geminal points show a net decrease in gained density upon excitation as the torsion angle decreased, confirming the vicinal point results. Finally, Figure 112 shows that as the torsion angle decreases, more density shifts from the backbone to the hydrogen ligands upon excitation, which explains where the density was moving to, if not to the geminal points. This leads back to the idea originally proposed for explaining the tendency of the Sandorfy model to underestimate excitation energies of polysilanes. When a torsion kink occurs, density shifts from the backbone to the ligands in the vicinity of

the kink, effectively disrupting the amount of backbone density that can participate in the rearrangement. Thus, for a given conformationally staggered section of polysilane, the number of charge concentrations within it denote the effective length of the group in terms of excitation energy. At the positions of the backbone kinks, the rearrangement of density involves the ligands of those silylene groups involved at the backbone kink, effectively 'capping' the electron density rearrangement at those points.

6.3 Model Proposition: The Moderated Backbone Rearrangement Model of Excitation

From the calculations performed on the transition density of oligosilanes, and the excited state densities, one obtains a definite pattern of behavior for the excitations. The majority of the excitation occurs within the backbone of the molecule, where the Si-Si bond charge concentrations in L(r) form a string of diffuse density in the staggered conformation. Upon excitation, the L(r) density rearranges, with the charge concentrations in the backbone showing a decrease in L(r), and the points between them showing an increase in L(r). The charge concentrations can be represented by the (3,-1) critical points at their center, and are called vicinal critical points, while the (3,-1) critical points that link these charge concentrations within the backbone are called geminal critical points. The net changes in L(r) at the vicinal and geminal points are a function of chain length. This implies that when electronic excitation occurs, there is a net moderation of the molecular energy increase as a result of this rearrangement. Figure 93 shows that there is an inverse linear relationship between the net increase in L(r) at the geminal points and the excitation energy. A model is proposed to explain this behavior, based on the computational results of this thesis: the Moderated Backbone Rearrangement Model of Excitation.

As illustrated in the local expression of the virial theorem (Equation 60), any increase in L(r) must result in a corresponding decrease in the potential energy function $V(r)$ to maintain the equality of the expression, provided that the kinetic energy function G(r) remains constant. Changes in $V(r)$ represent the stabilization or destabilization of the potential energy of the molecule; if $V(r)$ decreases, then the energy of the molecule will also decrease, etc. Thus, provided that G(r) remains constant during some change in the electronic structure of a molecule, the net change in L(r) can be related directly to the change in the energy of the molecule.

When a photon approaches a saturated long-chain molecule, its oscillating electric field perturbs the

density of the molecule's backbone, inducing an oscillating transition dipole. The magnitude of this dipole depends on how tightly bound the backbone density is. For a hydrocarbon, the backbone density is so tightly bound that little or no polarization can occur: the induced transition dipole is very small, as is the intensity of the excitation. For an oligosilane, the diffuse, loosely-bound backbone density is easily polarized. It has been observed that each silyl and silylene group in the molecule contributes a standard amount to the induced transition dipole, resulting in an intense excitation that increases linearly with chain length.

Upon absorption of the photon, the electronic structure of the molecule changes. As Figure 90 shows, when an oligosilane shifts to an excited state, the majority of the critical points in the L(r) density show marked decreases in their L(r) values, especially in the backbone, while the G(r) density remains unchanged. This results in a net destabilization of the potential energy of the molecule, as required by the local expression of the virial theorem, and a net increase in the molecular energy. Thus, the change in L(r) upon absorption of the photon energy results in an increase of molecular energy, the difference in molecular energy before and after the photon absorption being the energy of excitation. The geminal points in the backbone, however, show an increase in L(r) upon excitation, which would result in a local stabilization of the potential energy. The net increase in L(r) at the geminal points serves to moderate the increase in molecular energy, making it less than what it would be if these geminal points were not present. As the chain length of the oligosilane increases, so do the number of geminal points, and as Figure 92 illustrates, so does the net increase in L(r) at the geminal points. Thus, the bathochromic shift observed in oligosilanes is explained by the increased moderation of the excitation energy through the greater net increase in L(r) at the geminal points. The graph shown in Figure 93 would provide a convenient set of parameters for describing the bathochromic shift with chain length, in terms of this geminal point moderation. The intercept of the graph (7.8304 eV) would represent the Unmoderated Excitation Energy for the excitations of a given symmetry found in a class of molecules, such as Si_nH_{2n+2}. The slope of the graph (-30.129 eV/au) would represent a Moderation Coefficient, which describes how much the excitation energy decreases with net increase in L(r) at the geminal points.

Despite the fact that hydrocarbons are considered not to experience a bathochromic shift as a function

of chain length, this model can be applied to the excited states of hydrocarbons as well, provided that some important differences between hydrocarbons and oligosilanes are considered. The first difference is that unlike oligosilanes, there are much larger absolute decreases in L(r) at the vicinal points and maxima in the backbone, as indicated in Figure 95. A greater net decrease in L(r) means a greater increase in molecular energy. As illustrated in Section 6.2 of this thesis, hydrocarbons as a whole have much higher excitation energies then their corresponding oligosilanes. The second important difference is the nature of G(r) in hydrocarbons. Unlike oligosilanes, the value of G(r) at a given point decreases somewhat upon excitation. Using the local expression of the virial theorem, this means that any increase in L(r) will correspond to a smaller decrease in $V(r)$. In terms of the moderation of the excitation energy by the geminal points in the backbone of a hydrocarbon, this moderation will be much smaller than that seen in an oligosilane, resulting in a much smaller bathochromic shift with respect to increasing chain length. These ideas are reinforced by the proposed Unmoderated Excitation Energy and Moderation Coefficient terms for hydrocarbons, shown in Figure 96, with values of 10.213 eV and –4.2598 eV/au, respectively. The Unmoderated Excitation Energy of C_nH_{2n+2} is much higher than that of Si_nH_{2n+2}, and its Moderation Coefficient is much smaller, in agreement with the proposed model concepts.

The matter of conformational dependence on the excitation energy is explained through the results of the torsional studies. It was found that when a silicon-silicon bond is twisted, the backbone density in the vicinity no longer shifts from the vicinal charge concentrations to the geminal points, but to the ligands instead. This disrupts the rearrangement of density in the backbone, limiting the excitation to the number of silicon atoms that are in an all-staggered conformational section of the backbone. This reduces the degree of moderation of a polysilane's excitation energy, resulting in an excitation energy higher than expected from the total chain length.

6.4 Comparison with Other Work

The majority of theoretical work involving the excited states of polysilanes has made use of MO-based models to explain the bathochromic shift that occurs with increasing chain length. Preliminary work made use of simple valence band structures similar to the Hückel models described earlier[165]. These calculations did reasonably well in estimating the orbital energies of short chain species, but showed increasing error

with chain length, as the model did not take into account details such as torsional dependence. Other research made use of this same Hückel-type model to relate excitation energies of polysilanes to the size of the ligands[95]. This work does a reasonably good job of explaining the conformational dependence factor in polysilane excitation; bulkier ligands serve to conformationally lock the polysilane in an all-trans conformation, lowering the excitation energy. Another approach to better understanding the mechanism of excitation involved the use of ionization potentials[163]. The linear relationship found between ionization potential and excitation energy indicated that it is the HOMO energy that changes most dramatically with chain length and conformation, allowing one to estimate excitation energy based on calculations of ionization potentials derived from valence effective Hamiltonian techniques[45], or electron propagator theory[96]. These methods provide excellent agreement to experimental excitation energies, but do not satisfactorily explain the mechanism by which the bathochromic shift occurs, beyond arguments based on the spatial shapes of the HOMO and LUMO orbitals. Attempts to incorporate torsional dependence involved treating a polysilane as a one-dimensional semi-conductor, using Koopman ionization potentials to determine the extent of delocalization in kinked polysilane structures[166], in turn using orbital modelling systems which treat the polysilane as a crystal[167]. These studies show the decrease in ionization potential with chain length, and that the inclusion of a backbone kink results in an increase in ionization potential, the size of which depends on its position in the backbone[168]. Whether obtained by computation or experiment[43,92], discussing excitation energies in terms of ionization potentials only serves to relate excitation to orbital energy, and does not provide any explanation concerning a mechanism of delocalization or conjugation.

Among the best-known work in the field of oligosilane photophysics and spectroscopy is that of Josef Michl[97], who has contributed much to the current models used in describing and predicting the excited states of oligosilanes and polysilanes. Of particular importance is the Ladder model[96], which takes into consideration the all-important conformational dependence on electronic excitation[169]. As explained in the introduction, the Sandorfy model uses the sp^3-hybridized orbitals to determine the excitation energy of the HOMO-LUMO gap. Other research that uses the parameters derived from this model apply them to simple equations relating excitation energy to chain length, often adjusting said parameters to better fit

experimental trends[62]. To account for the torsion dependence, Michl incorporated into the determinant another resonance term, $\beta_{1,4}$, which, when combined with the Coulomb integral α and the resonance integrals β_{vic} and β_{gem}, provide more accurate values for the orbital energies. These models, while simple to understand and effective for excitation energy calculations, cannot describe whether or not the excitation is localized to a small group of atoms within the molecule or delocalized over the entire molecule, as has been previously explained. Determining the atomic contributions to the molecular excitation is also important for the conformational dependence. Michl himself addresses this issue in the paper referenced above, by describing the changes in orbital energies fitted through the Ladder model when one splits a polysilane chain in two smaller sections. The results he describes provide a compelling argument, but extreme caution must be taken in their interpretation. The Coulomb and resonance integral values derived in Michl's work also stem from fittings to photoelectron spectra of oligosilanes, which give the experimental orbital energies[170], as well as *ab initio* calculations. As a result, however, one does not know whether one is dealing with a ground state or excited state property with these models. This makes it impossible to interpret these results in the context of a property density, and thus impossible to partition the results in terms of contributions of functional groups or sections of polysilane. Very little discussion is made outside this thesis about the use of oscillator strengths in determining the extent of delocalization in polysilane excitations. Work involving experimental UV spectra of trisilane and tetrasilane[93], and conformationally locked tetrasilanes[98], make passing reference to the changes in calculated oscillator strengths of the excited states of tetrasilane as a function of Si-Si bond torsion angle. This work shows the same pattern of change with torsion angle as shown in this thesis, with a strong excitation losing intensity in favor of another excitation as the torsion angle decreases. Michl acknowledges that the large changes in oscillator strengths are significant, and that the UV spectra should be interpreted in terms of conformationally dependent transition intensities rather than transition energies. He then goes on to interpret this phenomenon in terms of avoided state crossings[171], attributing the changes in oscillator strength to the fact that only σ-σ^* excitations show intense transitions. The change from an all-staggered conformation to an anti conformation results in the symmetry of the excitation changing to π-π^*, which has no intensity. At

intermediate torsion angles, there is sharing of the oscillator strength between the high energy 0° excited state and the lower energy 180° excited state. No mention, however, is made of the excitation energy and oscillator strength of trisilane in relation to the tetrasilane calculations, which may show the same trend observed in the research of this thesis. A high level CASSCF calculation was performed, making direct comparisons with the work done in this thesis impossible. The best one can do is to note the fact that the ratio of oscillator strengths of the tetrasilane 180° and 0° conformers calculated in the paper (2.8) are reasonably close to the ratio of the oscillator strength of tetrasilane and trisilane calculated in this thesis (2.97). This author has shown that MO symmetry arguments are unnecessary for explaining the changes in excitation as a result of bond torsion, and that the transition density and its properties provide a simple description for the behavior of oligosilane species. Other work by Michl has addressed the issue of localization of the excitation in excited states where the geometry has relaxed[172]. Short chain oligosilanes show to have nearly identical fluorescence spectra: it is proposed by Michl that this is due to localization of the excitation within a single bond in the backbone, which stretches by nearly half its ground state length and gains considerable zwitterionic character[173]. As the chain length increases, the fluorescence behaves more as a vertical excitation with delocalization along the backbone. As all of the work in Chapter 6 involves vertical excitations, a requirement for determining the transition density, no comment can be made in relation to the aforementioned work.

A large body of other work has been devoted to the photochemistry of oligosilanes, which has sought to provide theoretical explanations for the rearrangements that are observed[53]. The majority of these works cite the inclusion of 4s and 3d orbitals in the excited state orbitals, implying a sizable increase in the volume of the excited state species: this contradicts the work shown in this thesis. It has been shown that the use of contour maps of the excited state density provides a much clearer picture of what is happening to the density of these species upon excitation. Rather than a diffusion of the valence density overall, the density in the backbone region rearranges, causing a net decrease in the Si-Si bond densities, and a net movement of density toward the ends of the molecule. These excited states are clearly in a position to undergo chemical rearrangement, either by radical scission of the Si-Si bond, or silylene extrusion. The question of which mechanism would be dominant in polysilanes would make for interesting future work.

7 Conclusions

Over the last few years, the research included in the thesis has taken several exciting new directions, culminating in the development of a new technique for analyzing the excited states of molecules. It is hoped that this groundbreaking work will continue to expand, to cover a variety of new systems, along with the discovery of new applications. The following is a summary of the work and discoveries made in this thesis.

7.1 Number Density

In general, Section 4.1 of this thesis illustrates the significant differences in the properties of carbon and the analogous silicon species. While exhibiting properties similar to carbon, such as coordination, the population and bond properties of silanes are more akin to metals, making silicon more like a metal in its properties.

The C-X bond was shown to have distinct properties, as well as having a relatively high covalency for most elements X, the exceptions being those elements with a significantly lower electronegativity, such as lithium. Those elements commonly bonded to carbon, such as hydrogen, nitrogen, oxygen, and carbon itself, form bonds with high BCP density, and high covalency, as indicated by positive L(r) values. In these cases, rho is at least 0.2 au. Third-row elements tend to form weaker bonds, with more ionic character; surprisingly, the element with the highest value of rho in the C-X bond, and most covalency, is sulfur. Double bonds to carbon also have high density at the BCP, especially with the commonly bonded elements listed above, while the third-row elements prove nearly as ionic as the appropriate singly-bonded species, as well as having BCP rho values only slightly higher.

The Si-X bond differs considerably from this. The BCP rho value as a whole is much lower, indicating a great deal less density involved in the bond itself. Further, nearly all of the Si-X bonds have negative L(r) values, indicating a high degree of ionic character within the bond. When combined with the low rho values, one can conclude that the Si-X bond contains a high degree of ionic character. The Si-X

double bond also contains a high degree of ionic character, as well as a very low value of rho. In fact, the Si=O bond cannot really be considered a double bond, given its low ellipticity, and is more like a zwitterionic system.

Population analyses of these systems reveal similar information as the bond studies. Carbon based compounds tend to retain most of the valence density on carbon. Depending on the electronegativity of X, carbon can bear either a positive or negative charge, but never ranges much past ±0.7 au in the context of this research. The charge on the hydrogen bonded to carbon is equally notable. At about –0.05 au, it becomes clear that the C-H bond is highly covalent in nature, and the population goes far to explain the relatively low reactivity of hydrocarbons. The populations of the corresponding silicon species are much different; it is clear from the uniformly large positive charge on silicon that most of the valence density is lost to the atoms that are bonded to silicon. Even the silyl anion and corresponding molecules bear a positive charge on silicon, which correlates well with the high polarity and low rho value observed in Si-X bonds. Any doubts as to the validity of these numbers need only look at the contour maps of these species, in particular the laplacian. Carbon-based compounds contain a great deal of charge concentration in the valence region of carbon, which correlates with its relatively small charge. With silicon, there is very little density in the valence region at all, with large diffuse charge concentrations on the bonded atoms. The hydrogens bonded to silicon are nearly hydridic in nature, with charges averaging about –0.7 au. This value increases with the co-ordination around silicon, along with an increase in the ionic character of the Si-H bond. Silicon, rather than losing or gaining charge with increased co-ordination, shows little change in population or energy, with the excess charge of the molecule being taken up evenly by all the ligands instead.

From the large body of theoretical research involving various population analyses on carbon and silicon species, it becomes clear that all of these MO techniques grossly underestimate the charge separation that occurs. Silicon is given a small positive charge at best, while the bonded hydrogens average around –0.1 au. Such a result does not make sense, given the high reactivity observed in the Si-H bond. The charge on fluorine, a highly labile ligand in silanes, is given a charge of about –0.5 au. It is very difficult to believe that an element with low electronegativity such as silicon could successfully retain nearly half the

valence density of the most electronegative element in the periodic table. This reinforces the point that MO-based methods do not produce populations that correlate well with qualitative experimental results.

Numerous experimental results have established the transferability of the methyl and methylene group in hydrocarbons. One can predict the energy of a hydrocarbon simply by adding up the energies of the corresponding groups, obtaining results with very high accuracy. This makes these groups additive as well. These results are reproducible theoretically, except that rather than being perfectly transferable, these groups exhibit compensatory transferability. This means that the methyl gains some density compared to the standard value, and the α-methylene group loses the same amount of density, with the internal methylenes approaching the standard values of energy and population expected. Remarkably, this compensatory effect not only conserves the charge, but the energy as well. A question that arose early in this thesis work was, does this same additivity apply to polysilanes? Polysilanes, unlike their hydrocarbon counterparts, undergo strong electronic excitations, with a bathochromic shift as a function of chain length. This behavior has been termed 'σ-conjugation', and numerous models have been developed to try and explain the mechanism. It was thought that perhaps this conjugation would reveal itself in the number density properties, and that an oligosilane would not show the same additivity that hydrocarbons do. The calculations showed that silyl and silylene groups in oligosilanes are in fact as additive and transferable as hydrocarbons, with an important difference. While the 'end-effect' of the methyl group only affects the adjacent α-methylene, the silyl group's effects are longer reaching, causing both the α- and β-silylene groups to deviate from standard value, surprisingly by the same amount. In terms of bond data and population data, there is no discernible difference in the group properties as the oligosilane chain length increases, unlike π-conjugated systems, where the π-bond density is distributed between all the C-C bonds.

7.2 Pair Density

The pair density is a simple idea: it measures the extent to which electron density is localized within a region of space, causing the partial condensation of electron pairs within the molecule. By integrating this density over atomic basins, one can gain a direct measure of how much of an atoms' density remains localized within the atomic basin, and how much is shared with other atoms, an excellent definition of

delocalization.

The simple M-X systems studied previously with respect to the number density were studied again, this time with respect to the pair density. In the C-X species, the percentage localization of valence carbon electron density on carbon averages about 50%, with the remainder distributed onto the other adjacent atoms as a function of their relative electronegativities. As expected, the percentage localization of X valence density on X is a function of electronegativity. As X becomes more electronegative, it holds more valence density, resulting in an increasingly negative charge, density which is not shared with other atoms. Silicon based species show this trend as well: the percentage of silicon valence density localized on silicon averages only about 15%, with the remaining density being shared with both the bonded element X and the silyl hydrogens. While atomic localization indices for silicon are very low, the localization index for the silyl group is rather high, and does not change appreciably with the electronegativity of X, unlike the methyl group. This is because most of the valence density of the silyl group is tied up in the hydrogens, leaving little valence density for X to share. Pair density integrations provide not only localization indices, but also a form of bond order, which measures the extent to which the electron density of two atoms is shared between them. The values obtained for carbon based species match rather well with the bond orders associated with Lewis structures, averaging around one for the C-H and C-C bonds. The value tends to decrease if there is a large difference in electronegativity between the two atoms. Doubly bonded carbon species do not in fact have a bond order of two, though it comes close at about 1.8. Bond orders of double bonds are much more sensitive to the electronegativity difference than single bonds, a logical conclusion given the more diffuse nature of the π-bond density. Silicon species have much smaller bond orders, averaging about 0.4 for Si-X single bond systems, and 0.8 for doubly bonded systems. This too makes sense, given the reduced valence density in silicon, density that tends to accumulate in the bonded atoms, rather than be shared. Increasing the coordination around silicon causes an increase in the localization of the ligand density on the ligands, and a decrease in the bond order, as expected from the number density results.

The concept of additivity in hydrocarbons need not be limited to number density properties: the pair density should be additive as well, which it is. Both localization indices and bond orders remain constant

for hydrocarbons of varying length, showing that the quality of additivity can be extended to any property. Whether this property extends to oligosilanes then becomes the major issue. Since these molecules exhibit properties associated with delocalization, a property such as the pair density should show trends conducive to delocalization. The results of studying the pair densities of oligosilanes are twofold. Firstly, the localization indices and bond orders of oligosilanes are additive, just as with hydrocarbons. This indicated that the electron density was not delocalized in the context of the pair density, with no change in localization as a function of chain length. The other, more striking result came with comparing the localization indices of methyl and silyl groups, and methylene and silylene groups. It was found that the valence density of the silyl group is more localized than that of the methyl group, by several percent. The conclusion made was that in terms of the number and pair densities, polysilanes are not delocalized. The next problem became to find out what property was delocalized, and in what context delocalization should therefore be explained.

7.3 Transition Density

The transition density is an odd property, as it not something that can be observed experimentally. It is the molecule's reaction to an absorbed photon, whose oscillating electric field causes sympathetic oscillations in the electron density of the molecule. This induces what is called a transition dipole, a property that in turn controls the magnitude of the oscillator strength, a measurable property that is directly related to the extinction coefficient of an electronic transition. These properties, like any other, can be partitioned into their atomic contributions: if the majority of a molecule's oscillator strength comes from one or two atoms out of many, then the excitation must be localized to those atoms. If all the atoms or groups in a molecule make a significant contribution to the excitation, then one would have a sound definition for delocalization, one that uses the context of electronic transition properties.

The measure and partitioning of the transition density broke new ground in theoretical research. The first application of the software that would perform these calculations involved the Rydberg-like transitions of formaldehyde and ammonia. As was expected, the carbonyl group of formaldehyde behaved as a chromophore, with over 70% of the transition coming from this group. Ammonia behaved similarly, with close to 70% of the transition coming from the nitrogen for the $n \rightarrow p_z$ transition. The change in density

upon excitation was equally informative. The excitation of a non-bonding electron to the 3s, $3p_z$ and $3p_y$ orbitals was readily apparent in the excited state contour maps of both formaldehyde and ammonia, along with the changes in atomic populations. Overall, the study revealed some interesting characteristics in these excitations.

The primary reason for developing this software was to apply it to oligosilanes, in hope of finding a correlation between transition densities and the bathochromic shift. Initial excited state calculations showed a clear trend in excitation energy versus oligosilane chain length, as well as oscillator strength. This showed that the decrease in excitation energy and increase in extinction coefficient observed experimentally was reproducible computationally. A surprising trend was observed in the oscillator strengths of the oligosilane series, from trisilane on: there is a near perfect linear relationship between oscillator strength and chain length, implying additivity in this property as well. Unlike the pair density, additivity would go far to explaining the delocalization observed in oligosilanes, as it implies that each group contributes to the excitation, rather than one chromophore in the molecule. Partitioning the transition density by silyl and silylene group led to an exciting discovery. The transition dipole and oscillator strength are transferable, with standard values for the silyl, α-silylene and silylene groups. This explains the increase in extinction coefficient with chain length, as each group contributes a set amount: the more silylene groups present, the larger the molecular value. The transition dipoles also helped to explain the suspected origin of the transition itself. A contour map of the laplacian of an oligosilane shows a string of charge concentrations sitting at the Si-Si bond positions, charge concentrations that show some interaction, rather than being completely isolated from each other. It was suspected that this density was what the incoming photon was interacting with, inducing a dipole that ran along the length of the backbone. The vectors of the group transition dipoles confirmed this prediction, with all the vectors running parallel to the string of charge concentration. The only remaining issue was the bathochromic shift itself, and why the energy of the excitation should decrease with chain length. The answer to this lay in the changes in the backbone density upon excitation. BCP analysis showed that the Si-Si bonds lost considerable density in the excited state, which was confirmed by the analysis of the atomic properties of the excited state, compared to the ground state. It was found that there was little transfer of electron density between groups or even between silicons

and their ligands, even though the quadrupole moments showed considerable reorganization of the electron density. Contour maps of L(r) of the excited state and analysis of the critical points of L(r) showed that electron density was rearranging almost exclusively within the backbone. Density that accumulated in the vicinal charge concentrations between bonded silicons shifted to the geminal points between the concentrations. The more surprising discovery was that there was a direct correlation between the net increase in L(r) at the geminal (3,-1) critical points in the L(r) density function and the excitation energy: the greater the increase in L(r) at these points upon excitation, the lower the excitation energy. This led to the proposal of the Moderated Backbone Rearrangement Model of Excitation, which treats the geminal points in the backbone as moderators of the excitation energy of the oligosilane: the more geminal points present in the backbone of a polysilane, the lower the excitation energy. This model represents a significant forward in the understanding of oligosilane photospectra. While the MO-based models described in Section 6.4 provide very accurate methods of predicting the excitation energies of polysilanes, they fail to explain the mechanism behind it. The ability to partition the transition probability into atomic contributions provided clear evidence that polysilanes are in fact conjugated systems, without having to rely on MO manipulation. The Moderated Backbone Rearrangement Model of Excitation reveals, in a concise, non-arbitrary manner, why these species experience a bathochromic shift with increased chain length.

An important feature of polysilane excitation is what is known as conformational dependence. It was found that predicted excitation energies were always lower than experimental results, and that with the addition of very bulky ligands, the energy of a polysilane of known chain length could be lowered to approach that of theory. It was surmised that the torsion angle of a given Si-Si bond disrupted the delocalization, and that an observed excitation energy was the sum of the excitations coming from the staggered sections of the molecule. This idea fitted into the proposed model, as it meant that an excitation would only work with those charge concentrations that lay in a straight line. To test this, a series of hexasilane conformers were studied, where the central Si-Si bond was twisted from 0° to 180°. The general results proved very promising; as the torsion angle decreased, the dominant excitation gained energy and lost intensity, and a second excitation began to dominate. In the 0° conformer, this excited state had approximately the same energy as tetrasilane, with about double the intensity. This reinforced the proposed

theory about the charge concentrations, for with the 0° conformer, a maximum of three charge concentrations could be aligned, the same number as that found in tetrasilane. The dependence of excitation intensities as a function of torsion angle applied to the group oscillator strengths as well as that of the molecule, reinforcing the idea of a hexasilane-like transition giving way to a tetrasilane-like excitation. The excited state densities gave more intriguing results. It was found that for the excited state, the density shifted from the silicons in the bond being twisted to the bonded hydrogen ligands, rather than rearrange within the backbone, and that this shift in density to the ligands grew as the torsion angle decreased. This would explain why the energy of this excitation increases. Instead of having all the vicinal charge concentrations in the backbone involved in rearrangement, only those within the staggered section would be involved, with the rearrangement 'capped' at the bond kinks. Moving from oligosilanes to long-chain polysilanes, this kind of behavior would be unobservable, as the dynamic twisting of the backbone and the distribution of different staggered sections would result in a broad excitation spectra with no fine details observable.

7.4 Future Work

The proposed future work focuses mainly on the transition density studies, as this research is still in its infancy. The following studies are proposed:

- Excitation Properties as a Function of Ligands. It has been shown experimentally that the excitation energy of a polysilane decreases if the electronegativity of the ligand attached to the silicon increases; oxygen versus carbon, for example. What is proposed is a study of the excitation properties of a series of oligosilanes of varying length. Each set of oligosilanes would bear ligands other than hydrogen, such as methyls, hydroxyls, and halogens. It is hoped that this study would lead to the discovery of standard excitation properties for dimethylsilylene or dihalosilylene groups, for example, or better still, a correlation between group oscillator strengths and the ligands attached to said groups. An end result of this study would involve the development of a table of standard group oscillator strengths and transition dipoles, enabling one to construct block polysilanes, and be able to predict their transition intensities[174]. In addition to this, the study would determine how the ligands affect the excitation energy, and what their contributions would be to the Moderated Backbone Rearrangement Model.

- Rings and Branches. It has been observed that while the existing MO–based models can accurately predict the excitation energies of long chain polysilanes, these models fail for cyclopolysilanes and branched polysilanes. The excitation energies of cyclic species tend to increase with ring size before reaching a maximum at about n = 8 and decreasing again. Clearly there is some ring strain factor that these models cannot account for, one that this new technique can hopefully deal with. Studying the excited state properties of these species should determine how ring strain affects any rearrangement of electron density that would occur in the molecule upon excitation. Branched systems tend to have higher excitation energies than single chain systems: these species not only contain silyl and silylene groups, but also SiH and Si groups. One of the drawbacks of the existing MO-based models is that they are all based on a single chain structure, and cannot account for the other groups present. Perhaps these groups disrupt the delocalization in a manner similar to torsional effects. A proposed study involves the study of cyclic systems of various sizes, along with branched oligosilanes, in the hopes of finding more standard groups to add to the list that would be created in the previously proposed study.
- Very Long Chain Studies. Experiment has shown that once any conjugated system reaches a certain length, the excitation energy reaches a lower limit. This limit is purely electronic in nature, and is independent of torsional dependence; for oligosilanes, this limit is reached at 18-22 units, depending on the ligands attached to the backbone. Atoms in Molecules clearly showed the backbone rearrangement that occurs upon excitation in oligosilanes, and could also show what occurs when polysilanes of this size and larger are excited.
- Chromophore Studies. Most of the proposed work focuses on polysilanes and delocalization; there remains a vast untapped source of research involving the excitation properties of chromophoric groups. One proposed task is the study of the carbonyl group in a variety of chemical environments, to observe the changes in this group's contribution to the excitation. This would include aliphatic and π-conjugated ketones, cyclic ketones of various sizes, aldehydes and carboxylic acids. The results could be compared to experimental results, to see how the theoretical changes correlate to experiment.

8 References

[1] Slater, J. C. *J. Chem. Phys.*, **1964**, *41*, 3199.

[2] Corey, J. Y. *The Chemistry of Organic Silicon Compounds;* John Wiley and Sons, University of Missouri-St. Louis, St. Louis, Missouri, **1989**, p 1.

[3] Bovey, L. F. *J. Chem. Phys.*, **1953**, *21*, 830.

[4] Cypryk, M.; Apeloig, Y. *Organomet.*, **1997**, *16*, 5938.

[5] a) Allan, H. C.; Pyler, E. K. *J. Chem. Phys.*, **1959**, *31*, 1062. b) *Tetrahedron* **1972**, *28*, 2147.

[6] a) Müller, T.; Apeloig, Y.; Hemme, I.; Klingebel, U.; Noltemeyer, M. *J. Organomet. Chem.*, **1995**, *494*, 133. b) Schmedake, T. A.; Haaf, M.; Apeloig, Y.; Muller, T.; Bukalow, S.; West, R. *J. Am. Chem. Soc.*, **1999**, *121*, 9479.

[7] Lide, D. R. *J. Chem. Phys.*, **1957**, *27*, 343.

[8] Gerry, M. C. L.; Less, R. M.; Winnewisser, G. *J. Mol. Spectrosc.*, **1976**, *61*, 231.

[9] Clark, N. W.; DeLucia, F. C. *J. Mol. Struct.*, **1976**, *32*, 29.

[10] Stolevik, R.; Postmyr, L. *J. Mol. Str.*, **1996**, *375*, 273.

[11] Kojima, T.; Breig, E. L.; Lin, C. C. *J. Chem. Phys.*, **1961**, *35*, 2139.

[12] Glidewell, C.; Pinder, P. M. ; Robiette, A. G. ; Sheldrick, G. M. *J. Chem. Soc., Dalton Trans.*, **1972**, 1402.

[13] Kojima, T.; Nishikawa, T. *J. Phys. Soc. Jpn.*, **1957**, *12*, 680.

[14] Almenningen, A.; Hedberg, K.; Seip, R. *Acta Chem. Scand.*, **1963**, *17*, 2264.

[15] Miller, S. L.; Aamodt, G.; Dousmanis, G.; Townes, C. H. *J. Chem. Phys.*, **1952**, *20*, 1112.

[16] Gundersen, G.; Mayo, R. A.; Rankin, D. W. H. *Acta Chem. Scand., Ser. A.*, **1984**, *38*, 579.

[17] Ebsworth, E. A. V.; Emeleus, H. J. *J. Chem. Soc.*, **1958**, 2150.

[18] Durig, J.; Flanagan, M. J.; Kalasinsky, V. F. *J. Chem. Phys.*, **1977**, *66*, 2775.

[19] Ebsworth, E. A. V. *Acc. Chem. Res.*, **1987**, *20*, 295.

[20] Pauling, L. *The Nature of the Chemical Bond*, 3rd ed.; Cornell University Press, Ithica, NY, **1960**, p. 93.

[21] Kuchitsu, K. *J. Am. Chem. Soc.*, **1966**, *44*, 906.

[22] Apeloig, Y. *The Chemistry of Organic Silicon Compounds:* John Wiley and Sons, Technion-Israel Institute of Technology, Haifa, Israel, **1989**, p 1.

[23] Helmer, B. J.; West, R.; Corriu, R. J. P.; Poirier, M.; Royo, G.; DeSaxce, A. *J. Organomet. Chem.*, **1983**, *251*, 295.

[24] Bassindale, A. R.; Taylor, P. G. *The Chemistry of Organic Silicon Compounds*, John Wiley and Sons, The Open University, Milton Keynes, UK, **1989**, p.839.

[25] Dewar, M. J. S.; Healy, E. *Orgaonmetallics*, **1982**, *1*, 1705.

[26] Golden, D. M.; Benson, S. W. *Chem. Rev.*, **1969**, *69*, 125.

[27] McMillen, D. R.; Golden, D. M. *Annu. Rev. Phys. Chem.*, **1982**, *11*, 493.

[28] Walsh, R.; *Acc. Chem. Res.*, **1981**, *14*, 246.

[29] Davidson, I. M. T.; Howard, A. V. *J. Chem. Soc., Faraday Trans.*, **1975**, *71*, 69.

[30] Cottrell, T. L. *Strengths of Chemical Bonds*, 2nd ed., Butterworths, London, **1958**.

[31] Saalfield, F. E.; Svec, H. J. *Inorg. Chem.*, **1964**, *3*, 1442.

[32] Huheey, J. H. *Inorganic Chemistry*, 3rd ed., Harper and Row, New York, **1983**, Appendix E, p. A-29.

[33] Benson, S. W. *Thermochemical Kinetics*, 2nd ed., Wiley, New York, **1976**.

[34] Luke, B. T.; Pople, J. A.; Krogh,-Jespersen, M.-B.; Apeloig, Y.; Karni, M.; Chandresekhar, J.; Schleyer, P. v. R. *J. Am. Chem. Soc.*, **1986**, *108*, 270.

[35] Shizuka, H.; Tanaka, H.; Okazaki, K.; Kato, M.; Watanabe, H.; Nagai, Y.; Ishikawa, M. *J. Chem. Soc., Chem. Commun.*, **1986**, 748.

[36] Douglas, J. E.; Rabinovitch, B. S.; Looney, F. S. *J. Chem. Phys.*, **1955**, *23*, 315.

[37] Olbrich, G.; Potzinger, P.; Reimann, B.; Walsh, R. *Organometallics*, **1984**, *3*, 1267.

[38] Corriu, R. J. P.; Guerin, C. *J. Organomet. Chem.*, **1980**, *74*, 1.

[39] Sommer, L. H.; Korte, W. D. *J. Am. Chem. Soc.*, **1967**, *89*, 5802.

[40] Sommer, L. H. *Intra-Sci. Chem Rep.*, **1973**, *7*, 1.

[41] McKinnie, B. G.; Bhacca, N. S.; Cartledge, F. K.; Fayssoux, J. *J. Org. Chem.*, **1976**, *41*, 1534.

[42] Kumada, M. *J. Organomet. Chem.*, **1975**, *100*, 127.

[43] Bock, H.; Ensslin, W.; Feher, F.; Freund, R. *J. Am. Chem. Soc.*, **1976**, *98*, 668.

[44] Hsiao, Y-L.; Waymouth, R. M. *J. Am. Chem. Soc.*, **1994**, *116*, 9779.

[45] Crespo, R.; Picqueras, M. C.; Orti, E.; Bredas, J. L. *Synth. Met.*, **1991**, *41*, 3457.

[46] Trefonas, P. III; West, R.; Miller, R. D.; Hofer, D. *J. Poly. Sci.: Poly. Lett. Ed.*, **1983**, *21*, 823.

[47] Miller, R. D.; Wallraff, G.; Clecak, N.; Sooriyakumaran, R.; Michl, J.; Karatsu, T.; Mckinley, A. J.; Klingensmith, K. A.; Downing, J. *Poly. Eng. And Sci.*, **1989**, *13*, 882.

[48] Hofer, D. C.; Miller, R. D.; Willson, C. G. *Proc. SPIE*, **1984**, *469*, 16.

[49] Steinmetz, M. G.; *Chem. Rev.*, **1995**, *95*, 1527.

[50] Michl, J.; Miller, R. D. *Chem. Rev.*, **1989**, *89*, 1359.

[51] McKinley, A. J.; Karatsu, T.; Wallraff, G. M.; Miller, R. D.; Sooriyakumaran, R.; Michl, J. *Organometallics*, **1988**, *7*, 2567.

[52] Halevi, E. A.; Winkelhofer, G.; Meisl, M.; Janoschek, R. *J. Organomet. Chem.*, **1985**, *294*, 151.

[53] Bott, S. G.; Marshall, P.; Wagenseller, P. E.; Wang, Y.; Conlin, R. T. *J. Organomet. Chem.*, **1995**, *499*, 11.

[54] Longuet-Higgins, H. C. *Advan. Chem. Phys.*, **1958**, *1*, 239.

[55] Coulson, C. A. *Valence*, 2nd ed. Oxford Univ. Press, New York, **1961**, Ch. 9.

[56] Pauling, L.; Wilson, E. B. Jr. *Introduction to Quantum Mechanics*, McGraw-Hill, New York, **1935**, Ch. 5.

[57] Hückel, E. *Z. Physik* **1931**, *70*, 204; *ibid.* **1931**, *72*, 310; *ibid.* **1932**, *76*, 628.

[58] Coulson, C. A. *Valence*, 2nd ed. Oxford Univ. Press, New York, **1961**, p. 79.

[59] Coulson, C. A. *Proc. Roy. Soc. (London)*, **1939**, *A169*, 413.

[60] Roothaan, C. C. J. *Rev. Mod. Phys.*, **1951**, *23*, 69.

[61] Musgrave, C. B.; Dasgupta, S.; Goddard, W. A. III. *J. Phys. Chem.*, **1995**, *99*, 13321.

[62] Walsh, C.; Burland, D. M.; Miller, R. D. *Chem. Phys. Lett.*, **1990**, *175*, 197.

[63] Salem, L. *The Molecular Orbital Theory of Conjugated Systems*, W. A. Benjamin, New York, **1966**.

[64] Rheingold, A. L. *Homoatomic Rings, Chains and Macromolecules of Main-Group Elements*. Elsevier, Amsterdam, **1977**.

[65] Sandorfy, C. *Can. J. Chem.*, **1955**, *33*, 1337.

[66] Balaji, V.; Michl, J. *Polyhedron*, **1991**, *10*, 1265.

[67] Plitt, H. S.; Michl, J. *Chem. Phys. Lett.*, **1992**, *198*, 400.

[68] Klingensmith, K. A.; Downing, J. W.; Miller, R. D.; Michl, J. *J. Am. Chem. Soc.*, **1986**, *108*, 7438.

[69] Mulliken, R. S. *J. Chim. Phys.*, **1949**, *46*, 497.

[70] Mulliken, R. S. *J. Chem. Phys.*, **1955**, *23*, 1833.

[71] Mulliken, R. S. *J. Chem. Phys.*, **1955**, *23*, 1841.

[72] Mulliken, R. S.; Ermler, W. C. *Diatomic Molecules: Results of Ab Initio Calculations*. Academic Press, New York, **1977**, pp 33-38.

[73] Mulliken, R. S. *J. Chem. Phys.*, **1962**, *36*, 3428.

[74] Collins, J. B.; Streitweiser, A. *J. Comput. Chem.*, **1980**, *1*, 81.

[75] Cho, S. G.; Rim, O. K; 1995, *Theochem*, **357**, 177.

[76] Mulliken, R. S., Politzer, P. *J. Chem. Phys.*, **1971**, *55*, 5135.

[77] Reed, A. E.; Weinstock, R. B.; Weinhold, F. *J. Chem. Phys*, **1985**, *83*, 735.

[78] Lowdin, P. O. *Phys. Rev.*, **1955**, *97*, 1474.

[79] Gronert, S.; Glaser, R.; Streitwieser, A. *J. Am. Chem. Soc.*, **1989**, *111*, 3111.

[80] Almenningen, A.; Bastiansen, O.; Ewing, V.; Hedberg, K.; Tratteberg, M. *Acta Chem. Scand.*, **1963**, *17*, 2455.

[81] Kimura, K.; Kubo, M. *J. Chem. Phys.*, **1959**, *30*, 151.

[82] Sommer, L. H.; Piettrusza, E. W.; Whitmore, F. C. *J. Am. Chem. Soc.*, **1946**, *68*, 2282.

[83] Beagley, B.; Conrad, A. R. *Trans. Faraday Soc.*, **1970**, *66*, 2740.

[84] Kwart, H.; King, K. G. *D-orbitals in the Chemistry of Silicon, Phosphorus and Sulfur*. Springer-Verlag, Berlin, **1977**.

[85] West, R.; Baney, R. H. *J. Am. Chem. Soc.*, **1959**, *81*, 6145.

[86] Pitt, C. G. *J. Organomet. Chem.*, **1973**, *61*, 49.

[87] Rempfer, B.; Oberhammer, H.; Auner, N. *J. Am. Chem. Soc.*, **1986**, *108*, 3893.

[88] Gillespie, R. J.; Johnson, S. A. *Inorg. Chem.* **1997**, *36*, 3031.

[89] Janes, N.; Oldfield, E. *J. Am. Chem. Soc.*, **1986**, *108*, 5743.

[90] Bassindale, A. R.; Glynn, S. J.; Taylor, P. G. *The Chemistry of Organic Silicon Compounds*, John Wiley and Sons, The Open University, Milton Keynes, UK, **1998**, p.355.

[91] Ogretir, C.; Csizmadia, I. G. *Computational Advances in Organic Chemistry: Molecular Structure and Reactivity*, Kluwer Academic Publishers, **1991**, pp. 323-354.

[92] Itoh, U.; Toyoshima, Y.; Onuki, H.; Washida, N.; Ibuki, T. *J. Chem. Phys.*, **1986**, *85*, 1867.

[93] Albinsson, B.; Teramae, H.; Plitt, H. S.; Goss, L. M.; Schmidbaur, H.; Michl, J. *J. Phys. Chem.*, **1996**, *100*, 8681.

[94] Sun, Y-P.; Hamada, Y.; Huang, L-M.; Maxka, J.; Hsiao, J-S.; West, R.; Michl, J. *J. Am. Chem. Soc.*, **1992**, *114*, 6301.

[95] Harrah, L. A.; Zeigler, J. M. *Macromol.*, **1987**, *20*, 601.

[96] Ortiz, J. V. *Macromol.*, **1993**, *26*, 2989.

[97] Miller, R. D.; Hofer, D.; Rabolt, J.; Fickes, G. N. *J. Am. Chem. Soc.*, **1985**, *107*, 2172.

[98] Imhof, R.; Teramame, H.; Michl, J. *Chem. Phys. Lett.*, **1997**, *270*, 500.

[99] Grev, R. S.; Schaefer, H. F. III *J. Am. Chem. Soc.*, **1987**, *109*, 6569.

[100] Ohshita, J.; Yoshitomi, T.; Ishikawa, M. *Organomet.*, **1994**, *13*, 3227.

[101] Schrödinger, E. *Ann. Phys.*, **1926**, *81*, 109.

[102] Bader, R. F. W. *Atoms in Molecules - A Quantum Theory*; Oxford University Press: Oxford, UK, **1990**.

[103] Gatti, C.; Fantucci, P.; Pacchioni, G. *Theor. Chim. Acta.*, **1987**, *72*, 433.

[104] Cao, W. L.; Gatti, C.; MacDougall, P. J.; Bader, R. F. W. *Chem. Phys. Lett.*, **1987**, *141*, 380.

[105] Bader, R. F. W. *Chem. Rev.*, **1991**, *91*, 893.

[106] Cremer, D.; Kraka, E. *Angew. Chem.*, **1984**, *23*, 627.

[107] Liu, G. H.; Parr, R. G. *J. Am. Chem. Soc.*, **1994**, *117*, 3179.

[108] Bader, R. F. W.; Nyugen-Dang, T. T. *Adv. Quantum Chem.*, **1981**, *14*, 63.

[109] Bader, R. F. W. *Phys. Rev. B.*, **1994**, *49*, 13348.

[110] Schwinger, J. *Phys. Rev.*, **1951**, *82*, 914.

[111] Bader, R. F. W.; Larouche, A.; Gatti, C.; Carroll, M. T.; MacDougall, P. J.; Wiberg, W. B. *J. Chem. Phys.*, **1987**, *87*, 1142.

[112] Bader, R. F. W. *Phys. Rev.*, **1994**, *B49*, 13348.

[113] Bader, R. F. W. *Can. J. Chem.* **1998**, *76*, 973.

[114] Gillespie, R. J.; Bayles, D.; Platts, J.; Heard, G. L.; Bader, R. F. W. *J. Phys. Chem.*, **1998**, *102*, 3407.

[115] Bader, R. F. W.; Heard, G. L. *J. Chem. Phys.*, **1999**, *111*, 8789.

[116] Bader, R. F. W.; Stephens, M. E. *J. Am. Chem. Soc.*, **1975**, *97*, 7391.

[117] Angyan, J. G.; Loos, M.; Mayer, I. *J. Phys. Chem.*, **1994**, *74*, 185.

[118] Bader, R. F. W.; Streitwieser, A.; Neuhaus, A.; Laidig, K. E.; Speers, P. *J. Am. Chem. Soc.*, **1996**, *118*, 4959.

[119] Bader, R. F. W.; Johnson, S.; Tang, T.-H.; Popelier, P. L. A. *J. Phys. Chem.*, **1996**, *100*, 15398.

[120] Gillespie, R. J.; Hargittai, I. *The VSEPR Model of Molecular Geometry*. Allyn and Bacon: Boston, MA, **1991**.

[121] Chang, R. *Basic Principles of Spectroscopy*, McGraw-Hill Book Co., New York, **1971**, p.19.

[122] Barrow, G. M. *Introduction to Molecular Spectroscopy*, McGraw-Hill Book Co. New York, **1962**, Ch. 4.

[123] Longuet-Higgins, H. C. *Proc. Roy. Soc. (London)*, **1956**, *A235*, 537.

[124] Schatz, G. C.; Ratner, M. A. *Quantum Mechanics in Chemistry*, Prentice Hall, Englewood Cliffs, New Jersey 07632, **1993**.

[125] Frisch, M. J.; Trucks, G. W.; Schlegel, H. B.; Gill, P. M. W.; Johnson, B. G.; Robb, M. A.; Cheeseman, J. R.; Keith, T.; Petersson, G. A.; Montgomery, J. A.; Raghavachari, K.; Al-Laham, M. A.; Zakrzewski, V. G.; Ortiz, J. V.; Forseman, J. B.; Cioslowski, J.; Stefanov, B. B.; Nanayakkara, A.; Challacombe, M.; Peng, C. Y.; Ayala, P. Y.; Chen, W.; Wong, M. W.; Andres, J. L.; Replogle, E. S.; Gomperts, R.; Martin, R. L.;

Fox, D. J.; Binkley, J. S.; Defrees, D. J.; Baker, J.; Stewart, J. P.; Head-Gordon, M.; Gonzalez, C.; Pople, J. A. GAUSSIAN 94, Revision E.2, Gaussian, Inc., Pittsburgh PA, **1995.**

[126] Hehre, W. J.; Radom, L.; Schleyer, P. v. R.; Pople, J. A. *Ab Initio Molecular Orbital Theory*, Wiley, New York, **1986**, Ch. 6.

[127] Biegler-König, F. W.; Bader, R. F. W.; Tang, T. H. *J. Comput. Chem.*, **1982**, *3*, 317.

[128] Forseman, J. B.; Head-Gordon, M.; Pople, J. A.; Frisch, M. J. *J. Phys. Chem.*, **1992**, *96*, 135.

[129] Schmidt, M. W.; Baldridge, K. K.; Boatz, J. A.; Elbert, S. T.; Gordon, M. S.; Jensen, J. J.; Koseki, S.; Matsunaga, N.; Nyugen, K. A.; Su, S.; Windus, T. L.; Dupuis, M.; Montgomery, J. A. *J. Comput. Chem.*, **1993**, *14*, 1347.

[130] Gordy, W.; Cook, R. L. *Microwave Molecular Spectra, Vol. 18*, Wiley, New York., **1984**, Ch. 6.

[131] Ingram, D. J. E. *Spectroscopy at Radio and Microwave Frequencies*, Butterworth, London, **1967**, Ch. 9.

[132] Bader, R. F. W.; Johnson, S.; Tang, T.-H.; Popelier, P. *J. Phys. Chem.*, **1996**, *100*, 15398.

[133] Dixon, R. E.; Streitwieser, A.; Laidig, K. E.; Bader, R. F. W.; Harder, S. *J. Phys. Chem.*, **1993**, *97*, 3728.

[134] Gatti, C.; MacDougall, P. J.; Bader, R. F. W. *J. Chem Phys.*, **1988**, *88*, 3792.

[135] Cargnoni, F.; Gatti, C.; Colombo, L. *Phys. Rev. B.*, **1998**, *57*, 170.

[136] Cargnoni, F.; Gatti, C.; May, E.; Narducci, D. *J. Chem. Phys.*, **2000**, *112*, 887.

[137] Carroll, M. T.; Cheeseman, J. R.; Osman, R.; Weinstein, H. *J. Phys. Chem.*, **1989**, *93*, 5120.

[138] Gillespie, R. J.; Bytheway, I.; DeWitte, R. S.; Bader, R. F. W. *Inorg. Chem.*, **1994**, *33*, 2115.

[139] Burgi, H. B.; Dunitz, J. D. *Acc. Chem. Res.*, **1983**, *16*, 153.

[140] Gordon, M. S.; Windus, T. L.; Burggraf, L. W.; Davis, L. P. *J. Am. Chem. Soc.*, **1990**, *112*, 7167.

[141] Shi, Z.; Boyd, R. J. *J. Am. Chem. Soc.*, **1990**, *112*, 6789.

[142] Gordon, M. S.; Carroll, M. T.; Jansen, J. H.; Davis, L. P.; Burggraf, L. W.; Guldry, R. M. *Organomet.*, **1991**, *10*, 2657.

[143] Gordon, M. S.; Packwood, T. J.; Carroll, M. T.; Boatz, J. A. *J. Phys. Chem.*, **1991**, *95*, 4332.

[144] Boyd, R. J.; Shi, Z. *J. Phys. Chem.*, **1991**, *95*, 4698

[145] Sommer, L. H. *Stereochemistry, Mechanism and Silicon: an Introduction to the Dynamic Stereochemistry and Reaction Mechanisms of Silicon Centers*. McGraw-Hill, New York, **1975**.

[146] Keith, T. A.; Bader, R. F. W. *J. Chem. Phys.*, **1992**, *96*, 3447.

[147] Bader, R. F. W.; Bayles, D. *J. Phys. Chem. A*, **2000**, *104*, 5579.

[148] Bader, R. F. W.; Martín, F. J. *Can. J. Chem.* **1998**, *76*, 284.

[149] Bader, R. F. W.; Keith, T. A.; Gough, K. M.; Laidig, K. E. *Molec. Phys.*, **1992**, *75*, 1167.

[150] Wiberg, K. B.; Bader, R. F. W.; Lau, C. D. H. *J. Am. Chem. Soc.*, **1987**, *109*, 1001.

[151] Benson, S. W.; Cruickshank, F. R.; Golden, D. M.; Haugen, G. R.; O'Neal, H. E.; Rodgers, A. S.; Shaw, R.; Walsh, R. *Chem. Rev.* **1969**, *69*, 279.

[152] Kopp, H. 1855, as reported in Glasstone, S. *Textbook of Physical Chemistry*, 2nd ed. p. 525. Van Nostrand, New York, **1946**.

[153] Henrichsen, G. *Wied. Ann.* **1888**, *34*, 186.

[154] Pascal, P. *Ann. Chim.Phys.* **1910**, *19*, 5. Pascal, P.; Gallais, F.; Labarre, S. F. *Acad. Sci.* **1961**, *252*, 2644.

[155] Rossini, F. D. *J. Res. Natl. Bur. Stand.* **1931**, *6*, 37; **1931**, *7*, 329; **1934**, *13*, 21. Prossen, E. J.; Johnson, W. H.; Rossini, F. D. *ibid.* **1946**, *37*, 51.

[156] Bader, R. F. W.; Popelier, P. L. A.; Keith, T. A. *Angew. Chem., Int. Ed. Engl.* **1994**, *33*, 620.

[157] Bader, R. F. W.; Martín, F. J. *Can. J. Chem.* **1998**, *76*, 284.

[158] Bader, R. F. W.; Bayles, D.; Heard, G. L. *J. Chem. Phys.* **2000**, *112*, 10095.

[159] Rianda, R.; Frueholz, R. P.; Goddard, W. A. III *Chem. Phys.* **1977**, *19*, 131.

[160] Hachey, R. J.; Bruna, P. J.; Grein, F. *J. Phys. Chem.*, **1995**, *99*, 8050.

[161] Bader, R. F. W.; Carroll, M. T.; Cheeseman, J. R.; Chang, C. *J. Am. Chem. Soc.*, **1987**, *109*, 7968.

[162] Runau, R.; Peyerimhoff, S. D.; Buenker, R. J. *J. Mol. Spect.* **1977**, *68*, 253.

[163] Pitt, C. G.; Bursey, M. M.; Rogerson, P. F. *J. Am. Chem. Soc.*, **1970**, *92*, 519.

[164] Bigelow, R. W. *Chem. Phys. Lett.*, **1986**, *126*, 63.

[165] Nelson, J. T.; Pietro, W. J. *J. Phys. Chem.*, **1988**, *92*, 1365.

[166] Matsumoto, N.; Teramae, H. *J. Am. Chem. Soc.*, **1991**, *113*, 4481.

[167] Teramae, H.; Takeda, K. *J. Am. Chem. Soc.*, **1989**, *111*, 1281.

[168] Teramae, H.; Matsumoto, N. *Solid State Commun.* **1996**, *99*, 917.

[169] Plitt, H. S.; Downing, J. W.; Raymond, M. K.; Balaji, V.; Michl, J. *J. Chem. Soc., Faraday, Trans.*, **1994**, *90*, 1653.

[170] Herman, A.; Dreczewski, B.; Wojnowski, W. *Chem. Phys.*, **1985**, *98*, 475.

[171] Teramae, H.; Michl, J. *Mol. Cryst. Liq. Cryst.* **1994**, *256*, 149.

[172]Teramae, H.; Michl, J. *Chem. Phys. Lett.*, **1997**, *276*, 127.

[173] Plitt, H. S.; Balaji, V.; Michl, J. *Chem. Phys. Lett.*, **1993**, *213*, 158.

[174] Thorne, J. R. G.; Hochstrasser, R. M.; Zeigler, J. M.; Tilgner, A.; Trommsdorff, H. P.; French, R. H.; Fagan, P. J.; Miller, R. D. *Mol. Cryst. Liq. Cryst.* **1992**, *216*, 13.